Spatiotemporal variability in dissolved organic matter composition and its relationship to photochemical reactivity

By

Stephanie Marie Berg

A dissertation submitted in partial fulfillment of

the requirements for the degree of

Doctor of Philosophy

(Environmental Chemistry and Technology Program)

at the

UNIVERSITY OF WISCONSIN-MADISON

2021

Date of final oral examination: 04/29/2021

The dissertation is approved by the following members of the Final Oral Committee:
Christina K. Remucal, Associate Professor, Civil and Environmental Engineering
Matthew Ginder-Vogel, Associate Professor, Civil and Environmental Engineering
James P. Hurley, Professor, Civil and Environmental Engineering
Katherine D. McMahon, Professor, Civil and Environmental Engineering
Joel A. Pedersen, Professor, Soil Science

Abstract

Spatiotemporal variability in dissolved organic matter composition and its relationship to photochemical reactivity

By

Stephanie Marie Berg

Doctor of Philosophy – Environmental Chemistry and Technology Program

University of Wisconsin – Madison

Associate Professor Christina K. Remucal

Dissolved organic matter (DOM) is a ubiquitous group of biologically derived organic molecules found in all natural waters. DOM makes up a substantial amount of the carbon stored in surface waters, and its original sources include allochthonous, or terrestrial, inputs as well as autochthonous, or aquatic, inputs. It is primarily made of up small (i.e., < 800 Da) molecules including combinations of carbon, hydrogen, oxygen, nitrogen, and sulfur, along with trace amounts of other elements. Furthermore, it undergoes a variety of chemical and biological transformations in the environment which adds further complexity to its composition. Importantly, the composition of DOM dictates its reactivity in a variety of chemical processes which work together to affect the fate of many contaminants in aquatic systems.

Concentrations and composition of dissolved carbon show high amounts of spatial and seasonal variability in the tributaries of Lake Michigan and relate to land cover types in the surrounding watershed. Multiple linear regressions show that concentrations of dissolved organic carbon ([DOC]) are most strongly related to the presence of wetland land cover. Additionally [DOC] is highest in the fall season. Concentrations of inorganic carbon ([DIC]) approximated via

alkalinity measurements, are more related to surrounding urban land cover and show no seasonal dependence. [DIC] is also related to the presence of carbonate bedrock underlying the watershed. Ultraviolet-visible spectroscopy (UV-Vis) shows that DOM is more aromatic and larger in size in watersheds with more surrounding wetland land cover. Overall, spatial variability exceeds that of seasonal variability for concentrations of dissolved carbon and composition of DOM. However, seasonal variation has a larger effect on composition than either concentration term indicating that environmental processing has profound effects on DOM composition in the tributaries.

Lake stratification and resulting redox conditions within water columns affect [DOC] and DOM composition. Samples collected from May to November within the water column of Lake Mendota in Madison, Wisconsin, USA show variability in DOM composition at the bulk level using UV-Vis spectroscopy and at the molecular level using Fourier transform-ion cyclotron resonance mass spectrometry (FT-ICR MS). At the surface and throughout the water column, DOM becomes more oxidized throughout the sampling period. At the surface of the lake, this can be primarily attributed to photochemical reactions. Within the water column, DOM is larger, more aromatic, and more oxidized near the bottom of the lake when the lake is stratified. However, differences in DOM composition with depth are much smaller than the observed temporal variability.

When DOM absorbs light, it produces a suite of highly reactive photochemically produced reactive intermediates (PPRI) including excited triplet state DOM (^{3}DOM), excited singlet state oxygen ($^1O_2$), and radicals such as hydroxyl radical ($^{\bullet}$OH). PPRI are of interest because they can react to degrade many persistent organic contaminants in surface waters. They can also react to alter the composition and bioavailability of the existing DOM pool. Samples collected from the St. Louis River in Minnesota, USA show that highly saturated DOM produce ^{3}DOM and $^1O_2$ more

efficiently while oxygenated, polyphenolic-like DOM produce •OH more efficiently. This difference in PPRI precursors suggests that unlike $^1O_2$, •OH may not form via ^{3}DOM which has important implications for predicting its formation in surface waters.

To determine if relationships between DOM composition and PPRI formation observed in the St. Louis River are universal, a diverse group of surface waters are considered including dystrophic bogs, a mesotrophic lake, oligotrophic lakes, eutrophic lakes, and rivers all in rural, urban, and agricultural land. Additionally, thirteen wastewater effluent samples are analyzed from five different wastewater treatment plants. Quantum yields for formation of $^1O_2$ and •OH are both related to molecular composition of DOM. For rural and wastewater samples, largely separate pools of DOM are positively related to $^1O_2$ and •OH while for urban and agriculture an overlapping pool is positively related. Electron donating capacity (EDC) is included as a potential predictor variable of photochemical reactivity. In these samples, it is positively related to specific ultraviolet absorbance at 254 nm ($SUVA_{254}$) for all sample types. It is also related to DOM molecular composition with positive relationships observed for lignin-like DOM for natural waters, but not related to DOM molecular composition in clear ways in wastewater effluents. EDC shows a negative correlation to $^1O_2$ but no relationship to •OH. Overall, •OH formation remains difficult to predict in diverse natural waters.

Acknowledgements

There are so many people in my life who made it possible for me to complete this dissertation including my friends, family, mentors, and teachers along the way. I would likely to acknowledge many, though not all, of those people here.

To my advisor Christy Remucal, thank you for your incredible mentoring over the past 5 years. I have had a wonderful time in graduate school and contribute that completely to the healthy environment you foster in your lab. I learned how to navigate academia from you. Your willingness to allow me to tag along with you at conferences and introduce me to your colleagues was so valuable and I am incredibly grateful. Lastly, thank you for caring about me as a person as well as a scientist.

I would also like to thank the other members of my dissertation committee including Matt Ginder-Vogel, Jim Hurley, Trina McMahon, and Joel Pedersen. I appreciate the feedback you all have given me over the years on my preliminary defense, seminars, manuscript drafts, and now this dissertation. To Jim, a special thank you for fostering a positive environment in the Environmental Chemistry and Technology program and for always accepting my late seminar feedback questionnaires.

To all the past and present members of the Water Science and Engineering Laboratory. A special thanks to Remucal Lab alumni Megan McConville and Andrew Maizel for their peer mentoring when I first joined the lab. I am lucky to have Sarah Balgooyen, Devon Bulman, and Emma Trainer as the very best of friends. I am thankful for the friendship of Madeleine Mathews and Lily Schact who always cared about my wellbeing and introduced me to my husband in a round-a-bout way. Finally, a special thanks to Amber White and Marissa Kneer for their thoughtful discussions, and Reid Milstead for all of his pranks. I would also like to acknowledge the WSEL

staff members Chris Worley and James Lazarcik for analytical troubleshooting and for making sure we were always set up to succeed. Finally, a special shoutout to Sue Pustina for disentangling all of my reimbursement requests and all of our chats over the years.

I think my prior education prepared me well for graduate school, and I would like to acknowledge those who contributed most to that. The biggest thank you goes to my undergraduate advisor Kris Wammer who taught me how to do research and made me love environmental chemistry. You have always been the strongest voice encouraging me to pursue my career goals even when life got in the way. To my chemistry cohort Danielle Webb, Joe Jaye, Brian Bustrom, and John Kummer, I never would have turned in all my homework or attended seminar without your reminders. I had the most fun majoring in chemistry with you all. Finally, a special thank you to my high school chemistry teach Heidi Haugen who taught me that stoichiometry is fun and to my middle school science teacher Andre Johnson who taught me how to think critically.

I am grateful for my family and for the friends I consider family. To my parents who have always believed in me and encourage me to keep going. To my sister Katie Berg who finds humor in everything and keeps me in check. To Laini Cossette, who is the greatest friend, college roommate, and study partner I could ever have asked for. Finally, to my best friend Ellie Vanasse, whose opinion I value over all others, and who I would not have become the same person without.

Lastly, I am so grateful for my husband Alex Kocher who I met and married while in graduate school. I could not ask for a more supportive person to spend my life with. I am incredibly thankful for the sacrifices you have made for me already, and I promise to always put our marriage first.

Table of Contents

List of Figures

List of Tables

Chapter 1

Introduction

1.1 Motivation

This dissertation considers how the composition of dissolved organic matter (DOM) varies in time and space and how this variation affects its photochemical reactivity. DOM represents a significant pool of carbon in aquatic ecosystems therefore any processes that affect DOM affect the broader carbon cycle of our planet. DOM composition is determined by its source and by the extent of subsequent processing in the environment. Changes in DOM composition with time and space alter its reactivity in numerous processes, including the photochemical reactions considered in this dissertation.

Land cover is a major factor that determines the initial source, and therefore composition, of DOM. However, few studies consider concentrations of dissolved organic carbon ([DOC]), concentrations of dissolved inorganic carbon ([DIC]), and DOM composition simultaneously. This is noteworthy because this limitation does not allow temporal and spatial variability to be compared directly which represents a significant knowledge gap in the field of DOM in the environment. We evaluate the variability of all dissolved forms of carbon in tributaries of the Great Lakes to determine how land cover and temporal variability influence both DOM and DIC.

Reactions occurring within aquatic ecosystems produce, degrade, and alter carbon concentration and composition. While broad understanding exists about formation and oxidation of DOM in the environment, little is known about the relative contributions of mechanisms contributing to the observed changes. For example, only a few evaluations of DOM composition

as a function of depth in freshwaters have been made and observed changes in DOM composition transformation at the surfaces of waters is often attributed to a variety of processes.

Finally, the amount and composition of DOM in surface waters affects its reactivity towards a variety of processes including photochemical reactions. When DOM absorbs sunlight, it forms a collection of photochemically produced reactive intermediates (PPRI) which are highly reactive in many contexts. Many relationships have been made between DOM composition and PPRI formation. However, limited information exists about the relationship between PPRI formation and DOM composition at the molecular level. In particular, predictions about the formation of hydroxyl radical ($^{\bullet}OH$) or other hydroxylating species have been elusive in the literature to date. Here, we apply bulk and molecular level characterization of DOM from diverse sources and compare relationships to PPRI including triplet DOM (^3DOM), singlet oxygen ($^1O_2$) and hydroxyl radical ($^{\bullet}OH$). Results are discussed in the context of potential mechanisms for $^{\bullet}OH$ formation, which are much less understood than the other PPRI discussed within.

1.2 Characterization of Dissolved Organic Matter

DOM consists of mostly carbon, hydrogen and oxygen, with contributions from heteroatoms including nitrogen, sulfur, phosphorus, and halogens.[1,2] The size of DOM is small and updated measurements of molecular weight show the majority of DOM is < 800 Da,[3] although hydrophobic interactions have complicated estimations of size with earlier overpredictions.[4] Predominant classes of compounds include heteropolysaccharides, carboxyl-rich alicyclic molecules (CRAM), and aromatic compounds.

Analytical techniques to characterize DOM composition are complicated by the fact that DOM consists of thousands of structurally similar formulas which are not separable by chromatographic

techniques. Nonetheless, characterization of its composition remains vitally important to understand its functions, reactivity, and fate in natural and engineered environments. Several articles have been written summarizing characterization techniques.[5,6]

1.2.1 Concentration of DOM

The concentration of dissolved organic matter ([DOC]) is commonly quantified through the complete oxidation of DOM with subsequent detection of the product CO_2. The contribution of carbonate species originally present in the sample is subtracted out by quantifying the CO_2 measured when acid and no oxidizer is used. Other estimates of [DOC] have been made via UV-Vis spectroscopy using total absorbance values.[7] [DOC] is commonly reported and is an important water quality parameter, but it offers no information about DOM composition and thus reactivity in the environment.

1.2.2 Optical Properties

Ultraviolet-visible absorbance (UV-Vis) is one of the most common techniques for measuring bulk characteristics of DOM. DOM absorbs the most at short wavelengths and absorbance decreases exponentially with wavelength (**Figure 1.1**).[8] Despite similar overall shapes of spectra, much compositional information can be gained. Spectral slope indices such as the absorbance at 250 nm divided by the absorbance at 365 nm (E_2:E_3) are inversely proportional to molecular weight.[8,9] The molar absorptivity at 254 and 280 nm ($SUVA_{254}$ and $SUVA_{280}$, respectively) is positively correlated to aromaticity using ^{13}C NMR.[4,10] Values of SUVA have also been related to indices of molecular weight including positive relationships to molecular weight measured by size exclusion chromatography,[4,11] susceptibility to coagulation,[12] and gel permeation

chromatography.[13] Optical relationships show that aromaticity and molecular weight are generally inversely proportional to one another.[7,14]

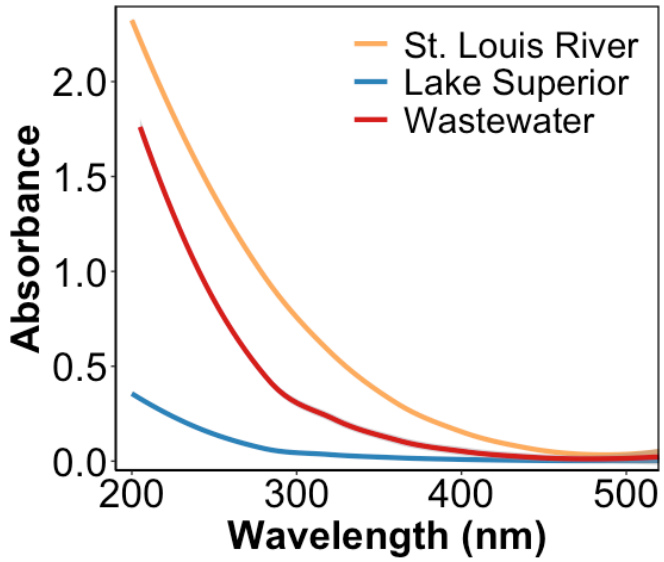

Figure 1.1. Representative ultraviolet-visible absorbance spectra collected in the St. Louis River, on the shore of Lake Superior, and final wastewater effluent from a wastewater treatment plant in Duluth, Minnesota.

Excitation-emission matrix (EEM) fluorescence spectroscopy provides further information about the optical properties of DOM. Some simple indices have been developed[15] and shown to be related to DOM compositional information including a negative relationship between the fluorescence index and aromaticity of DOM.[16] Fluorescence spectroscopy has also been shown to be a useful technique to detect the presence of aromatic moieties within DOM.[17] Parallel factor analysis (PARAFAC) reduces EEM components to quantify subsets of chemical groups (e.g., protein-like and humic-like fractions).[18,19] However, one limitation to PARAFAC modelling is that it assumes absorbance based on the superposition of chromophores.[20]

Many efforts have been made to determine the major functional groups within DOM giving rise to optical properties. Borohydride reduction is commonly employed towards these efforts

because this treatment results in the selective reduction of ketone and aldehyde groups within DOM structures. Subsequent reduction results in decreased absorbance providing evidence that these structures give rise to much of the overall DOM absorption of light.[21–23]

No substantial amounts of compounds known to be present within DOM can account for the amount of light absorbed by DOM solution at long wavelengths (i.e., >350 nm). Therefore, other photophysical models besides simple superposition of individual chromophores have been proposed to account for this light absorbance, including the formation of charge transfer states.[23–25] Evidence for these species include observations of decreased absorbance at longer wavelengths made after selectively destructing chromophores using shorter wavelength lasers.[25] Additionally, the selective reduction of proposed acceptor groups including aromatic carbonyl groups also results in unexpected loss of absorbance at long wavelengths.[22] Lasty, the monotonic decrease in absorbance at higher wavelengths in addition to decreases in photochemical quantum yields at higher excitation wavelengths is evidence against individual chromophores giving rise to DOM optical properties.[26–34]

While charge transfer states can explain observed long-wavelength absorbance of DOM, other observations are inconsistent with their formation. Most notably, DOM absorbance and fluorescence has no detectable dependence on temperature or solvent polarity and viscosity.[35] Furthermore, distinct distributions of fluorophore lifetimes measured by time resolved fluorescence spectroscopy yield evidence that superposition of individual chromophores likely do not explain DOM optical properties.[36] It is beyond the scope of this dissertation to engage in this debate, but UV-Vis and fluorescence spectroscopy represent common methods for DOM characterization, and therefore it is important to recognize relevant limitations.

1.2.3 Redox Activity of DOM

Redox activity of DOM, such electron donating capacity (EDC) and accepting capacity (EAC), can be quantified by methods such as direct electrochemical reduction,[37] mediated electrochemical reduction and oxidation,[37] cyclic voltammetry,[38] and spectroscopic assays of electron shuttle molecules.[39] Phenols and quinones are key redox active moieties within DOM. Phenolic content, measured via titrations, has been positively correlated to EDC in numerous studies,[40–42] while quinones are likely the predominate electron accepting moieties in DOM.[43,44] Measurements of redox activity made using cyclic voltammetry detect three distinct redox groups. Just two of these groups show reversible redox character, providing evidence that there is likely a non-quinone based structure contributing to the reactivity[37,45] which may be attributable to heteroatom-containing functional groups.[45,46]

Relationships have been drawn between DOM composition and redox activity. For example, studies have measured higher EDC in terrestrial DOM than aquatic DOM.[39] Higher EDC values are also observed in DOM from natural environments compared to DOM from wastewater effluents.[47] There is also evidence that the specific molecules giving rise to EDC is different between natural waters and effluents as one study saw the most electron donating moieties in the higher molecular weight fractions for natural organic matter but lower molecular weight fractions for effluent organic matter.[47] Relationships have been drawn to composition including positive relationships between EDC and aromaticity measured by UV-vis spectroscopy[47] and ^{13}C NMR[40] and negative relationships between EAC and aromaticity measured by ^{13}C NMR. Interestingly, the slopes of these relationships are the same for terrestrial and aquatic isolates for EAC but different slopes were observed for the relationship with EDC possibly indicating differences in the groups giving rise to redox behavior in each class of DOM.[40]

1.2.4 High-Resolution Mass Spectrometry

Additional molecular information can be gained about DOM composition using ultrahigh-resolution mass spectrometry including Fourier transform-ion cyclotron resonance mass spectrometry (FT-ICR MS) and Orbitrap mass spectrometry.[48,49] In the case of most natural waters, DOM is typically extracted via solid phase extraction prior to mass spectrometry analysis.[50] While no stationary phase is able to capture all of the carbon, styrene-divinylbenzene copolymer (PPL) sorbents have been shown to have relatively good recovery (i.e., >60%) and capture a representative portion of the DOM.[51–54] Electrospray ionization is the most common method of ionization used although others have been compared and contrasted including atmospheric pressure chemical ionization and atmospheric pressure photo ionization.[1,55] Positive and negative mode capture complimentary, but unique pools within DOM.[1,56] Negative mode is used most commonly because carboxylates and other acidic functional groups deprotonate readily. However, positive mode may be used to specifically consider basic moieties such as nitrogen-containing functional groups.[56] Overall, soft ionization methods are most successful because data interpretation is based on exact masses of parent ions alone (e.g., no fragmentation).[57]

The resulting data are assigned to formula masses based on mass accuracy. Most commonly, raw data signatures are matched using exact masses by comparing their masses with a list of potential formulas is compiled using known information about DOM in general.[58–60] For example, the ubiquity of homologous series (i.e., CH_2 groups or substitution between CH_4 and O) have been leveraged to aid in formulas matching.[57] While most labs use in-house programs for formula matches, publicly available software have been developed.[61]

Results of formula matches can be visualized on van Krevelen diagrams[62] or related to some bulk reactivity metric and then plotted on van Krevelen diagrams, and bulk weighted averages for

some indices are computed (**Figure 1.2**).[63] Comparisons among mass spectrometers have shown that relative trends of formulas matches among DOM types are identified consistently, but parameters such as oxygenation and average molecular weight can vary depending on instrument settings.[64]

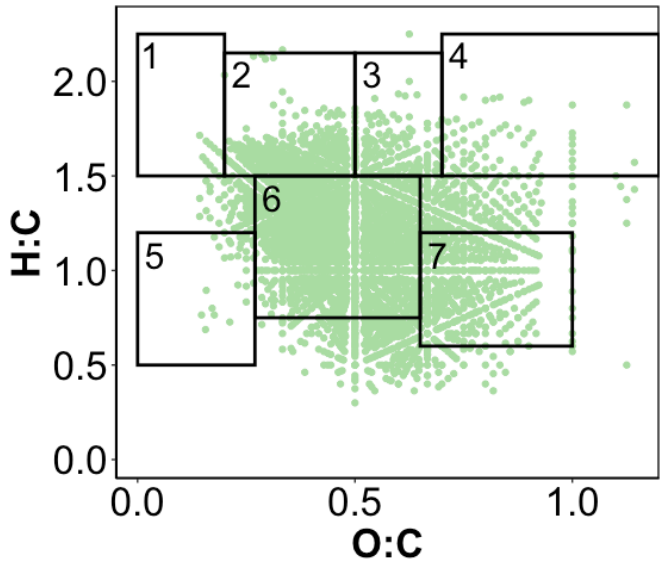

Figure 1.2. Example van Krevelen diagram of a sample taken from Sparkling Lake in northern Wisconsin. Boxes on the plot correspond to 1) lipid-, 2) protein-, 3) aminosugar-, 4) carbohydrate, 5) condensed hydrocarbon-, 6) lignin-, and 7) tannin-like formulas.[5]

Verification of formulas identified by high-resolution mass spectrometry have been made using other analytical techniques. For example, % S-containing formulas identified with FT-ICR MS were linearly correlated with S-content detected X-ray absorption spectroscopy.[65] Relative molecular weights have also been verified by size exclusion chromatography.[66] Additionally, mass spectral properties have been related to other compositional parameters. For example, $SUVA_{254}$ can be positively correlated to formulas with high O:C molecular ratios[67] and low H:C ratios (i.e., < 1).[68] $SUVA_{254}$ is also positively related to aromaticity as measured by FT-ICR MS[66] and ^{13}C NMR.[10] Some spectral slope ratios including E_2:E_3 and $S_{275\text{-}600}$ can be positively correlated to relatively saturated (i.e., H:C > 1) formulas as well.[68]

1.3 Sources of DOM

DOM source is a major factor in determining its concentration and composition. Autochthonous DOM is derived from microbes within the water column and is especially enriched in aliphatic and carbohydrate material.[69] In contrast, allochthonous DOM is primarily derived from terrestrial plants and contains more lignin- and tannin-like material.[66] DOM in aquatic systems is typically a mixture of both autochthonous and allochthonous sources and its composition is further altered by environmental processing. For example, observations of lower $SUVA_{254}$ in lakes compared to their tributaries are attributable to the longer water retention times in lakes and subsequent extent of environmental processessing.[70,71]

Land use in the surrounding watershed plays a major role in determining [DOC] and DOM composition in natural systems.[72] By far, the most reliable predictor of [DOC], which is a measurement of the quantity of organic carbon, is the amount of wetland in the surrounding watershed.[73–84] Other land cover types have also been correlated to [DOC] but with much more variability among studies. For example, both positive and negative relationships have been observed between [DOC] and the amount of agricultural land,[85–87] urban land,[87–90] and forests[81,85,87] in a watershed. Of course, the conflicting relationships are not evidence of error, but rather an indication of the diverse effects land cover can have on DOM in aquatic systems. Each study also varies in the number of samples collected, diversity of watersheds considered in the study, and model construction.

In terms of composition, wetlands again show the strongest relationships with the amount of wetlands being correlated with more allochthonous inputs of organic matter using spectroscopic indices.[82,85,91,92] Other land cover types have also been correlated to more allochthonous DOM including agricultural land[85,87] and forests.[87,91] In contrast, autochthonous DOM has been

positively related to the percentages of forest,[93] urban,[13,87,90,94] and agricultural land within a watershed.[86]

The composition of wastewater is distinct from other natural sources. High-resolution mass spectral data shows it mostly consists of lipid- and protein- like formulas.[56,95] Wastewater-impacted DOM includes enriched amounts of heteroatom-containing formulas, especially N and S.[56] In fact, increased N-containing formulas have been identified in septic-impacted ground water.[96]

1.4 Transformation of DOM Composition in the Environment

Despite the original source of DOM, its composition can be further altered in the environment. Transformation of DOM in the environment proceeds through a variety of processes and rates of these processes are dependent of DOM composition. Some molecules, including carboxyl-rich alicyclic molecules (CRAM), have been shown to be especially refractory in the environment.[97] CRAM can be identified with a combination of high resolution mass spectral and NMR spectroscopy analysis.[97]

1.4.1 Photodegradation of DOM

Photodegradation can result in complete oxidation of DOM to CO_2[98–104] and release of inorganic nutrients in sunlit surface waters including ammonium,[99,105] nitrate,[106] phosphate,[99] and sulfate.[100,107] Sunlight can also alter the composition of DOM without resulting in complete mineralization in a process known as partial photooxidation. Although this process is frequently overlooked in carbon models, partial oxidation of DOM yielding organic products may be underestimated by four times.[108]

Compounds within DOM that can be degraded by sunlight include aldehyde and ketone groups, carboxyl groups, and aromatics.[109,110] Many S-containing formulas have also been shown to be particularly photolabile.[111,112] Other metrics, such as double bond equivalents minus oxygen (DBE-O) values greater than 9,[113] or H:C formulas < 1[114] have been used to be successful in denoting formulas as photolabile. Formulas formed include generally more oxidized compounds[98,108,115,116] including CRAM,[108] some carboxylic acids,[117,118] phenols,[103] and carbohydrates,[109] as well as aliphatic compounds.[109] While accumulation of carboxylates have been observed, there is also evidence of decarboxylation reactions.[109] Therefore, while some trends of photochemically altered DOM may be universal, others depend on original DOM composition and the mechanism of the degradation.

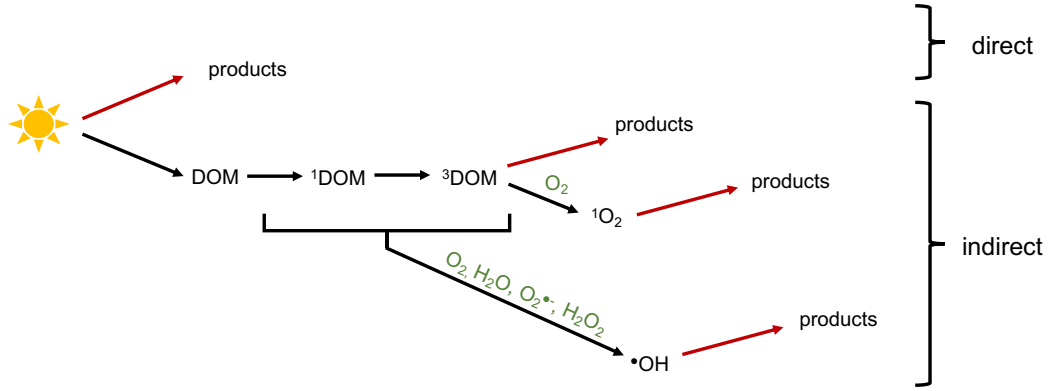

Figure 1.3. Schematic showing pathways of direct and indirect photodegradation. Indirect photodegradation involves reactions with PPRI including ^{3}DOM, $^1O_2$, and •OH.

The change in optical properties following either sunlight or laboratory irradiation are largely consistent across studies. Overall, general loss of absolute absorbance is observed,[101,103,105,119–124] as well as $SUVA_{280}$.[125] Additionally, numerous metrics measuring DOM molecular weight have shown overall decreases during irradiation including measurements made by FT-ICR MS[109] and UV-Vis absorbance spectral slopes.[104,125] The ability of photochemistry to alter DOM composition has been shown in lab irradiation experiments to result in similar DOM types to those found in the

epilimnion of arctic lakes.[126] Successful attempts have been made to model photobleaching in surface waters and overall, temperature and exposure history were predicting variables in these models.[127]

Photochemical alteration of DOM can occur directly through destruction of chromophores within DOM. It may also occur indirectly through reactions with photochemically produced reactive intermediates (PPRI) which are excited state species and radicals such as triplet excited state DOM (^{3}DOM), singlet excited state oxygen ($^1O_2$) and hydroxyl radical ($^{\bullet}$OH) among others, are formed during irradiation of DOM (**Figure 1.3**).[128] Evidence exists that ^{3}DOM can oxidize some DOM including carboxylic acid structures.[129] Photodegradation via $^1O_2$ and $^{\bullet}$OH have also been proposed.[130] However, a few studies show the reaction with $^1O_2$ may be minimal.[130,131] Furthermore, while DOM acts as a sink for $^{\bullet}$OH [132] resulting in transform of DOM composition,[133–135] it is unlikely to contribute to mineralization.[136]

1.4.2 Microbial Alteration of DOM

Microbial activity can affect both [DOC] and DOM composition with the result often depending on original DOM composition. Importantly, microbial alteration includes a combination of microbial degradation of organic matter leading to complete mineralization to inorganic forms or transformation to organic products, as well as microbial production of DOM via carbon fixation. Fresh DOM, including from newly degraded allochthonous material or DOM from melting glaciers has shown to be relatively bioavailable.[137] Furthermore, protein-like DOM has also been described as particularly labile as measured by fluorescence spectroscopy[138–140] and FT-ICR MS.[141–143] Several observations of readily bioavailable formulas point to those with high H:C values[144,145] as well as both low[146] and high[147] O:C ratios. Preferential consumption of smaller,

less aromatic, and N-containing DOM has been observed.[139,148] Much like photochemistry, microbial alteration also ultimately depends on initial DOM composition,[149,150] and other water chemistry parameters including dissolved oxygen.[151]

Microbially-produced DOM is structurally different than terrestrial or older forms of DOM. This DOM may have low $SUVA_{254}$ values,[152] increased N-content,[150,153] increased polysaccharide content,[154] and overall higher O:C ratios compared to terrestrial DOM.[146] Overall lower apparent molecular weight is observed.[147]

1.4.3 Simultaneous Photochemical- and Biological Degradation of DOM

While photochemical and biological alteration of DOM are often considered independently, it is important to note that both occur simultaneous in the environment and thus each affects the other rate. Some studies have concluded that photochemical alteration[153] explains DOM variability in a given system while other conclude microbial alteration is the major transformation process.[155] Ultimately, this depends on many factors and will continue to be difficult to compare because the two processes are inherently related to one other.

Following irradiation, both increases and decreases in bioavailability of the DOM have been observed which is likely a result of differences in original DOM composition and the microbial community.[103,105,118,156] Some variability in the literature may also be due to differences in reaction time and whether or not microbial communities have had time to evolve to use the available carbon source.[98] Overall, irradiation of terrestrial DOM increases bacterial use as more complex DOM is degraded to more bioavailable forms,[99,117,118,157] while irradiation of aquatic DOM decreases bacterial use as particularly labile substances are reacted away.[118] Furthermore, some microbially-

produced DOM is structurally similar to photoreactive compounds possibly creating a cycle of formulas with fast turnover.[158]

1.4.4 Sorption and Desorption Processes Affect Composition

Physical properties such as sorption and desorption and precipitation can also affect the composition of the DOM detected in the corresponding aqueous phase. For example, the sorption onto iron oxides, particularly ferrihydrite,[159] has been shown to remove DOM from the dissolved phase[160–163] and preferentially DOM that is terrestrially-dervied,[164,165] larger,[159] or carboxylate-rich.[163] In fact, decreases in [DOC] at oxic-anoxic interfaces have been observed in porewaters.[166] Incubations with porewaters conducted in anoxic conditions have shown the accumulation of tannin-like DOM.[167,168] Potentially, the dissolution of iron oxides in reducing conditions releases the tannin-like DOM that had preferentially precipitated.[167] Many studies have also evaluated DOM composition in porewater and have found that this DOM is overall larger, less oxygenated, more unsaturated, enriched in polyphenolic compounds,[164,169,170] and enriched in N and S as compared to water near the bottom of the water column.[65,167,169,171] Thus, changing redox conditions can result in the dissolution of this type of DOM in the hypolimnion of lakes.

1.4.5 DOM Variability Within Water Bodies

The competing processes of photodegradation, microbial degradation and production, and sorption can lead to variability of DOM with time. For example, DOM composition can vary within the water column of individual water bodies such as lakes. Stratification of lakes can have profound effects on DOM composition temporally and as a function of depth. In one boreal lake, the highest weighted averages of O:C ratios ($O:C_w$) were observed at the bottom lake in April, but

by June the surface had higher O:C_w ratios as measured by FT-ICR MS.[172] It is possible that this observation is due to photooxidation occurring at the surface of the lake. In fact, formulas with high O:C ratios have bene positively correlated to water residence times in a lake in Sweden,[114] and increases in O:C_w, weighted average of double bond equivalents (DBE_w), and a modified calculation of aromaticity index (AI_{mod}) detected by high-resolution mass spectrometry increased from May to March of the following year in a eutrophic lake in China.[173] Variability in changes in amounts of N-containing DOM formulas in eutrophic lakes have been observed in summer months with both increases[174] and decreases[69] reported for a eutrophic lakes. DOM transformation at the surface of stratified lakes[158] and arctic surface waters[153] have been attributed primarily to photochemical reactions.

1.5 Photochemical Reactivity of DOM

Upon absorption of sunlight, DOM produces a collection PPRI including triplet excited state DOM (^{3}DOM), singlet excited state oxygen ($^1O_2$), hydroxyl radical ($^{\bullet}OH$) and other hydroxylating species, superoxide radical anion ($O_2^{\bullet-}$), hydrogen peroxide (H_2O_2), carbonate radical anion ($CO_3^{2\bullet}$), and hydrated electron ($e^-_{hydrated}$). These species are noteworthy because they can react to degrade many persistent organic contaminants in surface waters (**Figure 1.3**). They can also be leveraged in some UV-based advanced oxidation processes to degrade contaminants,[175–178] as well as some bacteria and viruses during water treatment.[179–181] Besides contaminants, PPRI also react to degrade and transform DOM itself which has implications for microbial utilization of the DOM, as well as the global carbon cycle generally.[182]

Predicting indirect photolysis rates of contaminants requires quantification of PPRI generated when DOM is exposed to sunlight. However, the detection of PPRI is complicated by the fact that

many are too short-lived to be amenable to traditional analytical techniques. Instead, many PPRI are commonly measured indirectly through reaction with probe compounds.[183] The energy- and electron- transfer reactivity of ^{3}DOM are often measured through reaction with sorbic acid[184] and 2,4,6-trimethylphenol,[185] respectively. $^1O_2$ is quantified by it reaction with furfuryl alcohol, while $^{\bullet}$OH and hydroxylating capacity can be quantified using terephthalic acid.[186,187] $^1O_2$ can also be measured directly using phosphorescence.[188] Quantum yields for formation of each PPRI refer to the efficiency of the reaction or the number of PPRI produced per photon of light absorbed. They are commonly calculated via comparisons to chemical actinometers such as *p*-nitroanisole/pyridine solutions, which are well-studied chemicals used to quantify light intensity.[189]

While experiments have not been conducted for every organic contaminant detected in surface waters, some general conclusions can be drawn about PPRI and contaminant photodegradation. Additionally, several reviews have been published on the topic including reviews on indirect photolysis of pharmaceuticals[190,191] and pesticides.[192] Some contaminants, such as fludioxonil[193] and some fluoroquinone antibiotics,[194] degrade faster through direct photolysis (e.g., absorption of sunlight break bonds to degrade the contaminant); therefore, the presence of DOM actually inhibits their degradation (**Figure 1.3**).[195,196] Contaminants with phenol or aniline groups and specifically acetaminophen,[197] isoflavones,[198] phenylurea herbicides,[199] and 17α-ethynylestradiol[200] have been shown to be susceptible to oxidation by ^{3}DOM.[201,202] $^1O_2$ has been shown to react with fludioxonil,[193] dichloroacetamide safeners,[203] thiol- groups at high pH,[204] benzotriazoles,[205] isoflavones,[198] and niclosamide.[206] $^{\bullet}$OH is known to react with dichloroacetamide safeners,[203] thiol-groups at low pH,[204] benzotriazoles,[205] alachlor,[207] ionic liquids,[208] and 17α-ethylestradiol.[200]

$CO_3^{2\bullet-}$ is a more selective PPRI but is reactive towards aromatic amine and S-containing contaminants[209] and has also been implicated in the degradation of a cyanotoxin.[210]

Perhaps even more valuable than individual contaminant degradation studies are those that develop relationships between contaminant structure and degradation rates. Relationships have been developed that show that N-containing contaminant degradation rates by both ^{3}DOM and $CO_3^{2\bullet-}$ can be predicted by one electron oxidation potentials.[211] Furthermore, electron donating and withdrawing groups affect the rates of pyrroles with ^{3}DOM.[193] Relationships have also been developed and shown to predict phenol and phenolate degradation via ^{3}DOM, $^1O_2$, and $CO_3^{2\bullet-}$ using one electron oxidation potentials.[212] Degradation of phenols and anilines by ^{3}DOM have been modeled well by oxidation potential and OH bond dissociation energy, respectively.[213]

Importantly, photodegradation rates in the field depend on many more factors than laboratory conditions (e.g., cloud cover, canopy cover, and residence times) and slower than expected photodegradation rates are often observed.[214,215] Other complexities that need to be addressed include the need for accurately extrapolate results to polychromatic sunlight conditions.[216] Furthermore, there is a need to identify products of photochemical degradation as reactions with most PPRI do not result in mineralization of the contaminant and therefore both increases and decreases in toxicity of solution mixtures following irradiation have been observed.[217–219] In fact, the photodegradation products of some contaminants, including dienone and trienone steroids, revert back to parent products in environmental conditionals and thus probably should not be considered degradation products at all.[218,219] While this is not an exhaustive list of the contaminant photodegradation literature, it serves to demonstrate how understanding PPRI formation in natural waters is vitally important to the goal of predicting contaminant fate in the environment.

1.5.1 Triplet DOM (^{3}DOM)

Upon absorption of light, DOM can enter into its singlet excited state (^{1}DOM).[220] These species are relatively short-lived (e.g., 100 picoseconds) with most undergoing internal conversion back to their ground state and others emitting a photon of light and fluorescing back to ground state.[20] However, a fraction of these species undergo intersystem crossing to enter into a triplet excited state (^{3}DOM).[220] ^{3}DOM has much longer lifetimes and therefore undergoes a wider variety of reactions.[30] The predominant quencher of ^{3}DOM is oxygen (O_2), but ^{3}DOM can also react with other organics including DOM or contaminants via energy-[221] or electron- transfer processes.[222,223]

Measurements of steady-state concentrations and quantum yields for formation of ^{3}DOM are commonly made through use of kinetic probe molecules which react selectively and with known rate constants. The isomerization of sorbic acid can quantify energy transfer ability of ^{3}DOM.[184] However, the energy needed for this isomerization is 250 kJ mol^{-1}. Most triplet energies are estimated to range from 170 – 300 kJ mol^{-1} and therefore sorbic acid isomerization is only able to capture the top 59% of ^{3}DOM.[220,224] 2,4,6-Trimethylphenol (TMP) has been used to quantify the electron-transfer ability of ^{3}DOM. Often, quantum yield coefficients (f_{TMP}) are commonly reported rather than quantum yields for this probe so as to avoid the need to estimate deactivation rate constants with DOM. While absolute values between f_{TMP} and quantum yields (Φ_{3DOM}) are different, they generally follow the same trend and the Φ_{3DOM} notation will be used throughout this section.[225] TMP likely captures a much larger percent of the ^{3}DOM pool.[225] However, since this probe degrades through a radical cation intermediate which can undergo reduction by DOM back to the parent probe,[202,225–230] other electron transfer probes have been proposed including *N*-cyclopropylanilines whose rings are opened following oxidation by ^{3}DOM making the reaction irreversible.[202] Evidence exists that the reduction of the radical cation intermediate is due to

phenolic moieties since ozonation of the DOM, which preferentially destroys phenolic groups, decreases the inhibitory effect.[231] Generally, steady-state concentrations measured in whole waters range on the order of femtomolar – picomolar and quantum yields 10^{-3} – 10^{-2}.[220]

Because DOM is a diverse group of organic molecules, so too is ^{3}DOM. Much effort has been put in to determine the structures in DOM most likely to give rise to the ^{3}DOM population. Decreases in ^{3}DOM after selective reduction of aromatic ketones by borohydride reduction are evidence that these groups are a dominant precursor to ^{3}DOM.[232] However, some formation of ^{3}DOM is still observed even after reduction meaning that other groups must also contribute to the ^{3}DOM pool.[232]

The role of DOM composition in the formation of ^{3}DOM varies in the environment. Overall autochthonous DOM consistently has higher quantum yields than allochthonous DOM.[66] Wastewater effluents have especially high Φ_{3DOM}.[71,225,228] Surrounding land cover also has an effect. For example, Φ_{3DOM} were found to increase moving from watersheds dominated by rock < meadows < trees land cover.[233] Another study found that Φ_{3DOM} varies as a function of surrounding land cover with values increasing from forest < croplands < wetlands.[234] Because DOM composition varies between seasons,[80,235–241] so too does Φ_{3DOM}. While seasonal variability of Φ_{3DOM} has not been considered extensively in the literature, observations of Φ_{3DOM} increasing from spring to fall in prairie pothole wetlands have been made.[239] Water chemistry parameters can also affect observations of ^{3}DOM. For example, increases in $[^3DOM]_{ss}$ were observed with increases halide concentrations[242,243] and attributed to a decrease in ^{3}DOM rate of decay.[243]

Many relationships between Φ_{3DOM} and DOM compositional parameters have been made. The most common observation is that DOM that is smaller in molecular weight has higher Φ_{3DOM}. This has been demonstrated using the optical property E_2:E_3,[66,71,234,239,244–249] as well as using

coagulation to reduce molecular weight.[250] Negative Φ_{3DOM} correlations to measurements in aromaticity, such as $SUVA_{254}$, are also commonly reported.[71,234,248] Negative relationships to EDC[244] have been observed and are likely due to increased redox activity quenching ^{3}DOM. Several studies have correlated Φ_{3DOM} high-resolution MS data with observations including positive relationships to formulas with high H:C ratios.[71,227,245]

1.5.2 Singlet Oxygen ($^1O_2$)

$^1O_2$ is formed during the irradiation of natural waters via energy transfer from ^{3}DOM to O_2.[251–253] Lifetimes are on the order of microseconds[254] with steady-state concentrations around tens of picomolar. Quantum yields for the formation of $^1O_2$ (Φ_{1O2}) decrease with increasing excitation wavelength[28–30,255] and range from $8 \times 10^{-3} - 1.6 \times 10^{-2}$.[255] Because ^{3}DOM is a direct precursor to $^1O_2$, the same functional groups in DOM giving rise to ^{3}DOM also give rise to $^1O_2$. As observed with ^{3}DOM, borohydride reduction of aromatic ketones and aldehydes decreases Φ_{1O2}.[30]

$^1O_2$ reacts with electron-rich function groups including double bonds in [2+2] cycloaddition reactions.[256] Reactions products include endoperoxides and ring-opened products.[254,257] Sinks of $^1O_2$ include electron donators within the DOM pool resulting in the production of $O_2^{\bullet-}$ and subsequently H_2O_2,[130,258] although the extent of this reaction may be insignificant in the environment.[41,131] $^1O_2$ can also react with tertiary aliphatic amines via energy transfer reactions.[254]

Variability in Φ_{1O2} exists and is associated with the composition of DOM. Like Φ_{3DOM}, Φ_{1O2} are also higher in autochthonous DOM than allochthonous DOM.[66] Wastewater has been shown to have especially high Φ_{1O2}.[71,225,228,259] Observations of Φ_{1O2} increasing from spring to fall have also been made.[239]

Many relationships have been made between DOM composition and the formation of $^1O_2$ and mirror those observed for ^{3}DOM. For example, negative correlations between Φ_{1O2} and molecular weight using optical properties have been made,[30,66,259–261,71,125,239,244,246–249] including among black carbon[262,263] and wastewater samples[228] and for molecular weight using size fractionation[66,259] or coagulation.[250] Negative relationships to aromaticity based on $SUVA_{254}$ values have also been made.[71248] Φ_{1O2} shows negative relationships to EDC likely because of ^{3}DOM quenching by redox capacity of DOM.[125,244] Relationships have also been made to high-resolution mass spectrometry data and include positive correlations to formulas with high H:C ratios, which is similar to the relationships observed for ^{3}DOM.[71,245]

1.5.3 Hydroxyl Radical (•OH)

•OH is produced during the irradiation of surface waters. Irradiation of nitrate and nitrite can produce •OH,[132,264–266] as well as some photo-Fenton processes,[267,268] but these reactions cannot account for all of the observed •OH produced in many systems.[269] Steady-state concentrations of •OH during irradiation of whole waters are generally lower than those of ^{3}DOM and $^1O_2$ and are in the attomolar range (i.e., 10^{-18} – 10^{-16}). Quantum yields vary by several orders of magnitude between 10^{-6} – 10^{-3}.

Terephthalic acid is the most common probe common used to measure •OH in aquatic photochemistry but other compounds have been compared and contrasted.[186,270,271] Some probes, such as terephthalic acid, cannot differentiate between free •OH and other hydroxylating species and evidence exists that both are formed during irradiation of DOM.[272–275] Because the vast majority of the DOM photochemistry literature makes no attempt to differentiate between the two, the discussion here will also group them together unless otherwise noted.

Formation of •OH varies in the environment. Lower •OH formation rates have been observed in rivers as compared to lakes.[276] $\Phi_{\bullet OH}$ has been shown to be especially high in wastewater effluent.[277] DOM with relatively high polyphenolic-like structures also have high $\Phi_{\bullet OH}$.[71,278] Water chemistry parameters may also play a role. For example, decreases in $\Phi_{\bullet OH}$ have been observed with increasing halide concentration.[242]

Evidence exists that multiple mechanisms lead to •OH formation. Both an H_2O_2-dependent and H_2O_2-independent pathway for •OH formation have been proposed.[275] The H_2O_2-dependent mechanism likely involves direct photolysis of photochemically produced H_2O_2. H_2O_2 production can occur through $O_2^{-\bullet}$ dismutation previously formed via O_2 reduction.[131,279] However, observed •OH formation in anoxic conditions provides evidence of an O_2-independent pathway that does not involve $O_2^{-\bullet}$ intermediates.[269,278] In the H_2O_2-independent pathway, H-atom abstraction by water has been hypothesized[274,280] and lack of •OH formation in experiments conducted in acetonitrile show •OH formation does need water.[278] While differentiating between the two mechanisms has been elusive, there is evidence via catalase addition experiments that a combination of both mechanisms may occur.[275] In fact, quantum yields for •OH formation show different wavelength dependence in oxic and anoxic conditions.[269] ^{1}DOM, ^{3}DOM, DOM charge transfer states, and exciplexes between water and excited state DOM have all been proposed as precursors to both of these mechanisms.[125,260,273,279] Higher $\Phi_{\bullet OH}$ in oxic waters may be taken to mean that the O_2-dependent pathway dominants in sunlit surface waters.[269]

Efforts have been made to relate $\Phi_{\bullet OH}$ to properties of DOM composition. However, much more variability exists in these relationships than those developed for either ^{3}DOM or $^1O_2$. Molecular weight has been negatively related to $\Phi_{\bullet OH}$ using optical properties,[246,248,249] ultrafiltration,[281] and coaugulation.[250] A parameter similar to $\Phi_{\bullet OH}$, carbon normalized $[\bullet OH]_{ss}$, is

positively related to aromaticity and negatively related to molecular weight of DOM using optical properties.[276] Aromaticity estimated by $SUVA_{254}$ has been shown to be negatively related to $\Phi_{\bullet OH}$ in some studies[248] or not related in others.[71]

Sinks of $^{\bullet}OH$ in environmental waters include DOM and carbonate species, although under typical environmental conditions DOM is likely the dominant sink.[132] $^{\bullet}OH$ reacts quickly with organic molecules with slight dependence on temperature and organic composition.[280,282–286] $^{\bullet}OH$ reacts lignin-like DOM to form CRAM molecules which are highly recalcitrant in the environment.[135] Reactions have also been shown to produce both reduced and saturated formulas.[133]

1.5.4 Superoxide Radical Anion ($O_2^{\bullet-}$)

Although superoxide radical anion is not very reactive with organic compounds, it contributes to contaminant and DOM transformations by serving as a precursor to $^{\bullet}OH$. $O_2^{\bullet-}$ forms as a result of redox reactions and specifically reduction of O_2.[131,287] Precursors likely include reducing agents among DOM,[41,131,287–291] although ^1DOM[41] and $e^-_{hydrated}$ have also been proposed.[253] A few studies specifically rule out formation via other PPRI including ^3DOM[41,292] and $^1O_2$ reaction with DOM.[41,131] Formation through reduction of O_2 by charge transfer states of DOM has been proposed based on the fact that phenolic groups within DOM are positively related to both formation and decay rates of $O_2^{\bullet-}$ during irradiation.[41] In fact, $O_2^{\bullet-}$ has been shown to react with DOM which may produce a DOM reducing agent ($DOM^{\bullet-}$)[290] that could potentially go on to regenerate $O_2^{\bullet-}$. This mechanism is consistent with excited states of DOM, but specifically not ^3DOM, leading to $O_2^{\bullet-}$ formation.[41]

1.5.5 Hydrogen Peroxide (H_2O_2)

H_2O_2 is formed during irradiation of natural waters and is related to $O_2^{\bullet-}$ formation.[293,294] $O_2^{\bullet-}$ is easily reduced to H_2O_2 under environmental conditions.[41] H_2O_2 has been observed following $^1O_2$ reaction with DOM[130] but this pathway is expected to be minimal in environmental conditions.[260,294] Unlike ^{3}DOM and $^1O_2$, borohydride reduction does not decrease quantum yield for H_2O_2 formation (Φ_{H2O2}), which suggests that triplet aromatic ketones and aldehydes do not contribute to H_2O_2 formation.[294]

Production of H_2O_2 depends on DOM composition. Positive correlations have been made to increasing aromaticity measured via ^{13}C NMR,[295] molecular weight measured optically,[125,260] and to measurements of EDC.[125] Likewise, rates of H_2O_2 production increase with addition of phenolic compounds to DOM solution.[294]

1.6 Relationships Between PPRI

Understanding the relationships between different PPRI can yield evidence about their formation mechanisms. For example, the production of ^{3}DOM and $^1O_2$ are correlated based on the fact that ^{3}DOM a direct precursor to $^1O_2$.[66,71,225,228,244–246,249] Some exceptions to this general trend exist such as increases in Φ_{1O2} but decreases in Φ_{3DOM} following photooxidation experiments.[125] Also, for black carbon specifically, evidence for a separate pool of DOM forming ^{3}DOM compared to $^1O_2$ exists.[263]

Relationships between $^{\bullet}$OH, $O_2^{\bullet-}$, and H_2O_2 with other PPRI vary in the literature. Opposite trends between ^{3}DOM and $^{\bullet}$OH,[71] $^1O_2$ and $^{\bullet}$OH,[71] and $^1O_2$ and H_2O_2 have been reported.[260] In contrast, trends in the same direction have been observed for ^{3}DOM and $^{\bullet}$OH.[246] Observations of no trends between ^{3}DOM and $^{\bullet}$OH as well as $^1O_2$ and $^{\bullet}$OH have also been reported.[71,249]

Another method for evaluating relationships between PPRI formation is to alter the DOM composition in some way, and then measure resulting quantum yield for PPRI formation. Some treatments have had the same effect on all PPRI. For example, increasing chlorine dosage in a UV/HOCl advanced oxidation process led to increases in Φ_{3DOM}, Φ_{1O2}, and $\Phi_{\bullet OH}$.[248] Similarly, coagulation treatment also resulted in increases in Φ_{3DOM}, Φ_{1O2}, and $\Phi_{\bullet OH}$.[250] However, in other cases divergent trends are observed. Increasing halide concentrations led to increases in Φ_{3DOM} and Φ_{1O2} but decreases for $\Phi_{\bullet OH}$.[242] Following photooxidation experiments, Φ_{1O2} increased while quantum yields for Φ_{3DOM}, Φ_{H2O2}, and $\Phi_{\bullet OH}$ decreased.[125] Clearly, it is not yet possible to $\Phi_{\bullet OH}$ in diverse samples or during treatment processes.

1.7 Identified Research Needs

Both the concentration and composition of DOM influence its reactivity, yet many studies that quantify these properties are limited in scale and it is unclear what factors ultimately determine the quantity and quality of DOM. Specifically, a systematic study including measurements of [DOC], [DIC], and composition as a function of both land cover and season is lacking. As a result, no direct comparisons of the effect land cover versus season of sample collection have on the three parameters listed above have been made. Additionally, as land use continues due to wetland destruction and urbanization, studies considering wide ranges of land cover in a given geographic area are needed.

In addition to original DOM source, processing of DOM in the environment also drastically affects composition in the environment. In particular, long residence times at the surface of stratified lakes result in extensive processing of DOM. Both photochemical and microbial alteration work to control DOM composition in surface waters. However, traditional analytical

techniques make it hard to disentangle the two processes. Furthermore, stratified lakes experience steep redox gradients which are expected to alter DOM composition due to divisions in microbial metabolism, precipitation and dissolution reactions, as well as distinct transformation pathways in hypo- and epilimnion due to prolonged periods of unmixed layers. In the literature, DOM transformation at the surface of lakes has been considered but the contribution of specific mechanisms is not well understood. Furthermore, reports of DOM composition as a function of depth and redox state are lacking in the literature.

Finally, the composition of DOM controls its reactivity towards numerous processes including photochemical reactivity. An understanding of the ability of DOM to produce PPRI is a prerequisite to predicting contaminant fate in environmental surface waters. While many relationships have been drawn between PPRI formation and bulk composition, very few have been drawn to molecular composition and specifically none between formation of $^{\bullet}OH$ and DOM molecular composition. This is of particular interest because $^{\bullet}OH$ is reactive towards the widest variety of contaminants and its dominant mechanism for formation is still under debate. Therefore, relationships between its formation and DOM composition are not easy to predict and may yield mechanistic information which would be of interest to the broader aquatic chemistry field.

1.8 Research Objectives

A brief overview of the research chapters found in this dissertation are included in this section. Chapters 2 – 5 are the main research articles prepared for publication. Chapters 2 and 3 focus on DOM composition in tributaries of Lake Michigan and in Lake Mendota, respectively, and include discussions on how DOM source and subsequent environmental processing affect its composition. Chapters 4 and 5 consider the dependence of DOM photochemical reactivity on

DOM composition. Bulk and molecular characterization of DOM are included in both studies. Finally, Chapter 6 includes a summary of the presented work as well as suggestions for future work based on the results of these studies.

In Chapter 2, measurements of [DOC], [DIC], and DOM composition via UV-Vis spectroscopy (e.g., E_2:E_3 and $SUVA_{254}$ measurements) are presented for > 100 tributaries that drain in Lake Michigan. These samples were collected once in all four seasons. Multiple linear regressions were developed to determine the predictive ability of surrounding land cover in the watershed and season of sample collection on each of the four parameters. For [DIC], geologic information about the underlying bedrock was also considered in the model. The scale of this study allowed for the direct comparison between spatial and seasonal variability for each parameter.

Chapter 3 provides a detailed analysis of DOM composition in Lake Mendota during ice-off conditions. Samples include both integrated epilimnion samples and depth-discrete samples collected during stratification. [DOC] and UV-vis measurements are presented for all samples and FT-ICR MS data is available for a subset of the depth-discrete samples. At the surface, correlations between mass spectrometry data and both chlorophyll and light intensity allow for the comparison of photo- and bio- transformation. Measurements throughout the water column allow the composition of DOM as a function of depth to be evaluated.

Relationships between DOM composition and photochemical reactivity for samples collected throughout the St. Louis River and Estuary in Minnesota and Wisconsin are presented in Chapter 4. Composition of the DOM is analyzed via UV-vis spectroscopy and FT-ICR MS and results are related to PPRI formation during irradiation. Differences in relationships between PPRI and DOM composition are interpreted in terms of mechanisms for PPRI formation.

Finally, Chapter 5 is an extension of the work presented in Chapter 4. Here, sample collection is expanded to include rural, agricultural, and urban watersheds with samples collected from lakes, rivers, and agricultural ditches to test whether the trends observed in Chapter 4 are universal in more diverse DOM sources. Additionally, 13 samples from five different wastewater treatment plants are included allowing for both the comparison of wastewater effluents to natural waters as well as comparisons among effluents from treatment plants receiving different source water and employing different treatments. The additional characterization technique of electron donating capacity is presented for this study and used as a potential predictor of photochemical reactivity. Lastly, the large data set compiled for this study allowed for the development of multiple linear regression models to predict quantum yields for PPRI formation.

In Chapter 6, a brief summary is provided of the previous 4 research chapters. Broad conclusions are drawn outstanding questions are outlines. A subsection of this chapter details suggestions for future work.

1.9 References

(1) Hertkorn, N.; Frommberger, M.; Witt, M.; Koch, B. P.; Schmitt-Kopplin, P.; Perdue, E. M. Natural organic matter and the event horizon of mass spectrometry. *Anal. Chem.* **2008**, *80*, 8908–8919.

(2) Gribble, G. W. The diversity of naturally produced organohalogens. *Chemosphere* **2003**, *52* (2), 289–297.

(3) McAdams, B. C.; Aiken, G. R.; McKnight, D. M.; Arnold, W. A.; Chin, Y. P. High pressure size exclusion chromatography (HPSEC) determination of dissolved organic matter molecular weight revisited: Accounting for changes in stationary phases, analytical standards, and isolation methods. *Environ. Sci. Technol.* **2018**, *52* (2), 722–730.

(4) Chin, Y. P.; Alken, G.; O'Loughlin, E. Molecular weight, polydispersity, and spectroscopic properties of aquatic humic substances. *Environ. Sci. Technol.* **1994**, *28* (11), 1853–1858.

(5) Minor, E. C.; Swenson, M. M.; Mattson, B. M.; Oyler, A. R. Structural characterization of dissolved organic matter: A review of current techniques for isolation and analysis. *Environ. Sci. Process. Impacts* **2014**, *16*, 2064–2079.

(6) Nebbioso, A. Molecular characterization of dissolved organic matter (DOM): A critical review. *Anal. Bioanal. Chem*. **2013**, *405*, 109–124.

(7) Fichot, C. G.; Benner, R. A novel method to estimate DOC concentrations from CDOM absorption coefficients in coastal waters. *Geophys. Res. Lett.* **2011**, *38* (3), 1–5.
(8) Helms, J. R.; Stubbins, A.; Ritchie, J. D.; Minor, E. C.; Kieber, D. J.; Mopper, K. Absorption spectral slopes and slope ratios as indicators of molecular weight, source, and photobleaching of chromophoric dissolved organic matter. *Limnol. Oceanogr.* **2008**, *53* (3), 955–968.
(9) Dalzell, B. J.; Minor, E. C.; Mopper, K. M. Photodegradation of estuarine dissolved organic matter: A multi-method assessment of DOM transformation. *Org. Geochem.* **2009**, *40* (2), 243–257.
(10) Weishaar, J.; Aiken, G.; Bergamaschi, B.; Fram, M.; Fujii, R.; Mopper, K. Evaluation of specific ultra-violet absorbance as an indicator of the chemical content of dissolved organic carbon. *Environ. Sci. Technol.* **2003**, *37* (20), 4702–4708.
(11) Nguyen, H. V. M.; Hur, J. Tracing the sources of refractory dissolved organic matter in a large artificial lake using multiple analytical tools. *Chemosphere* **2011**, *85* (5), 782–789.
(12) Korshin, G.; Chow, C. W. K.; Fabris, R.; Drikas, M. Absorbance spectroscopy-based examination of effects of coagulation on the reactivity of fractions of natural organic matter with varying apparent molecular weights. *Water Res.* **2009**, *43* (6), 1541–1548.
(13) Chen, H.; Liao, Z. L.; Gu, X. Y.; Xie, J. Q.; Li, H. Z.; Zhang, J. Anthropogenic influences of paved runoff and sanitary sewage on the dissolved organic matter quality of wet weather overflows: An excitation-emission matrix parallel factor analysis assessment. *Environ. Sci. Technol.* **2017**, *51* (3), 1157–1167.
(14) Jiang, T.; Wang, D.; Meng, B.; Chi, J.; Laudon, H.; Liu, J. The concentrations and characteristics of dissolved organic matter in high-latitude lakes determine its ambient reducing capacity. *Water Res.* **2020**, *169*, 115217.
(15) Coble, P. G. Characterization of marine and terrestrial DOM in seawater using excitation-emission matrix spectroscopy. *Mar. Chem.* **1996**, *51*, 325-346.
(16) McKnight, D. M.; Boyer, E. W.; Westerhoff, P. K.; Doran, P. T.; Kulbe, T.; Andersen, D. T. Spectrofluorometric characterization of dissolved organic matter for indication of precursor organic material and aromaticity. *Limnol. Oceanogr.* **2001**, *46* (1), 38–48.
(17) Cory, R. M.; McKnight, D. M. Fluorescence spectroscopy reveals ubiquitous presence of oxidized and reduced quinones in dissolved organic matter. *Environ. Sci. Technol.* **2005**, *39* (21), 8142–8149.
(18) Murphy, K. R.; Stedmon, C. A.; Graeber, D.; Bro, R. Fluorescence spectroscopy and multi-way techniques. PARAFAC. *Anal. Methods*. **2013**, *5* (23), 6557–6566.
(19) Stedmon, Colin A.; Bro, R. Characterizing dissolved organic matter fluorescence with parallel factor analysis: A tutorial. *Limnol. Oceanogr. Methods* **2008**, *6*, 572–579.
(20) McKay, G. Emerging investigator series: Critical review of photophysical models for the optical and photochemical properties of dissolved organic matter. *Environ. Sci. Process. Impacts* **2020**, *22* (5), 1139–1165.
(21) Schendorf, T. M.; Del Vecchio, R.; Bianca, M.; Blough, N. V. Combined effects of pH and borohydride reduction on optical properties of humic substances (HS): A comparison of optical models. *Environ. Sci. Technol.* **2019**, *53* (11), 6310–6319.
(22) Ma, J.; Del Vecchio, R.; Golanoski, K. S.; Boyle, E. S.; Blough, N. V. Optical properties of humic substances and CDOM: effects of borohydride reduction. *Environ. Sci. Technol.* **2010**, *44* (14), 5395–5402.

(23) Del Vecchio, R.; Schendorf, T. M.; Blough, N. V. Contribution of quinones and ketones/aldehydes to the optical properties of humic substances (HS) and chromophoric dissolved organic matter (CDOM). *Environ. Sci. Technol.* **2017**, *51* (23), 13624–13632.
(24) Boyle, E. S.; Guerriero, N.; Thiallet, A.; Del Vecchio, R.; Blough, N. V. Optical properties of humic substances and CDOM: Relation to structure. *Environ. Sci. Technol.* **2009**, *43* (7),
(25) Del Vecchio, R.; Blough, N. V. On the origin of the optical properties of humic substances. *Environ. Sci. Technol.* **2004**, *38* (14), 3885–3891.
(26) Sharpless, C. M.; Blough, N. V. The importance of charge-transfer interactions in determining chromophoric dissolved organic matter (CDOM) optical and photochemical properties. *Environ. Sci.: Process. and Impacts,* **2014**, *16* (4), 654–671.
(27) B. Partanen, S.; R. Erickson, P.; E. Latch, D.; J. Moor, K.; McNeill, K. Dissolved organic matter singlet oxygen quantum yields: Evaluation using time-resolved singlet oxygen phosphorescence. *Environ. Sci. Technol.* **2020**, *54* (6), 3316–3324.
(28) Haag, W. R.; Hoign, J.; Gassman, E.; Braun, A. M. Singlet oxygen in surface waters-Part II: Quantum yields of its production by some natural humic materials as a function of wavelength. **1984**, *13* (6), 641–650.
(29) Halladja, S.; Ter Halle, A.; Aguer, J. P.; Boulkamh, A.; Richard, C. Inhibition of humic substances mediated photooxygenation of furfuryl alcohol by 2,4,6-trimethylphenol. Evidence for reactivity of the phenol with humic triplet excited states. *Environ. Sci. Technol.* **2007**, *41* (17), 6066–6073.
(30) Sharpless, C. M. Lifetimes of triplet dissolved natural organic matter (DOM) and the effect of $NaBH_4$ reduction on singlet oxygen quantum yields: Implications for DOM photophysics. *Environ. Sci. Technol.* **2012**, *46* (8), 4466–4473.
(31) Qian, J.; Mopper, K.; Kieber, D. J. Photochemical production of the hydroxyl radical in antarctic waters. *Deep. Res. Part I Oceanogr. Res. Pap.* **2001**, *48* (3), 741–759.
(32) Powers, L. C.; Miller, W. L. Apparent quantum efficiency spectra for superoxide photoproduction and its formation of hydrogen peroxide in natural waters. *Front. Mar. Sci.* **2016**, *3*, 1–9.
(33) Kieber, D. J.; Miller, G. W.; Neale, P. J.; Mopper, K. Wavelength and temperature-dependent apparent quantum yields for photochemical formation of hydrogen peroxide in seawater. *Environ. Sci. Process. Impacts* **2014**, *16* (4), 777–791.
(34) Thomas-Smith, T. E.; Blough, N. V. Photoproduction of hydrated electron from constituents of natural waters. *Environ. Sci. Technol.* **2001**, *35* (13), 2721–2726.
(35) McKay, G.; Korak, J. A.; Erickson, P. R.; Latch, D. E.; McNeill, K.; Rosario-Ortiz, F. L. The case against charge transfer interactions in dissolved organic matter photophysics. *Environ. Sci. Technol.* **2018**, *52* (2), 406–414.
(36) Chen, Y.; Liu, J.; Zhang, X.; Blough, N. V. Time-resolved fluorescence spectra of untreated and sodium borohydride-reduced chromophoric dissolved organic matter. *Environ. Sci. Technol.* **2020**, *54* (19), 12109–12118.
(37) Aeschbacher, M.; Sander, M.; Schwarzenbach, R. P. Novel electrochemical approach to assess the redox properties of humic substances. *Environ. Sci. Technol.* **2010**, *44* (1), 87–93.
(38) Aeschbacher, M.; Vergari, D.; Schwarzenbach, R. P.; Sander, M. Electrochemical analysis of proton and electron transfer equilibria of the reducible moieties in humic acids. *Environ. Sci. Technol.* **2011**, *45* (19), 8385–8394.

(39) Walpen, N.; Houska, J.; Salhi, E.; Sander, M.; von Gunten, U. Quantification of the electron donating capacity and UV absorbance of dissolved organic matter during ozonation of secondary wastewater effluent by an assay and an automated analyzer. *Water Res.* **2020**, *185*, 116235.

(40) Aeschbacher, M.; Graf, C.; Schwarzenbach, R. P.; Sander, M. Antioxidant properties of humic substances. *Environ. Sci. Technol.* **2012**, *46* (9), 4916–4925.

(41) Ma, J.; Nie, J.; Zhou, H.; Wang, H.; Lian, L.; Yan, S.; Song, W. Kinetic consideration of photochemical formation and decay of superoxide radical in dissolved organic matter solutions. *Environ. Sci. Technol.* **2020**, *54* (6), 3199–3208.

(42) Walpen, N.; Schroth, M. H.; Sander, M. Quantification of phenolic antioxidant moieties in dissolved organic matter by flow-injection analysis with electrochemical detection. *Environ. Sci. Technol.* **2016**, *50* (12), 6423–6432.

(43) Nurmi, J. T.; Tratnyek, P. G. Electrochemical properties of natural organic matter (NOM), fractions of NOM, and model biogeochemical electron shuttles. *Environ. Sci. Technol.* **2002**, *36* (4), 617–624.

(44) Scott, D. T.; Mcknight, D. M.; Blunt-Harris, E. L.; Kolesar, S. E.; Lovley, D. R. Quinone moieties act as electron acceptors in the reduction of humic substances by humics-reducing microorganisms. *Environ. Sci. Technol.* **1998**, *32* (19), 2984–2989.

(45) Ratasuk, N.; Nanny, M. A. Characterization and quantification of reversible redox sites in humic substances. *Environ. Sci. Technol.* **2007**, *41* (22), 7844–7850.

(46) Fimmen, R. L.; Cory, R. M.; Chin, Y. P.; Trouts, T. D.; McKnight, D. M. Probing the oxidation-reduction properties of terrestrially and microbially derived dissolved organic Matter. *Geochim. Cosmochim. Acta* **2007**, *71* (12), 3003–3015.

(47) Wu, Q. Y.; Zhou, T. H.; Du, Y.; Ye, B.; Wang, W. L.; Hu, H. Y. Characterizing the molecular weight distribution of dissolved organic matter by measuring the contents of electron-donating moieties, UV absorbance, and fluorescence intensity. *Environ. Int.* **2020**, *137*, 105570.

(48) Hawkes, J. A.; Dittmar, T.; Patriarca, C.; Tranvik, L.; Bergquist, J. Evaluation of the orbitrap mass spectrometer for the molecular fingerprinting analysis of natural dissolved organic matter. *Anal. Chem.* **2016**, *88* (15), 7698–7704.

(49) Remucal, C. K.; Cory, R. M.; Sander, M.; McNeill, K. Low molecular weight components in an aquatic humic substance as characterized by membrane dialysis and Orbitrap mass spectrometry. *Environ. Sci. Technol.* **2012**, *46* (17), 9350–9359.

(50) Dittmar, T.; Koch, B.; Hertkorn, N.; and Kattner, T. A simple and efficient method for the solid-phase extraction of dissolved organic matter (SPE-DOM) from seawater. *Limnol. Oceanogr. Methods,* **2008**, *6*, 230–235.

(51) Li, Y.; Harir, M.; Lucio, M.; Gonsior, M.; Koch, B. P.; Schmitt-Kopplin, P.; Hertkorn, N. Comprehensive structure-selective characterization of dissolved organic matter by reducing molecular complexity and increasing analytical dimensions. *Water Res.* **2016**, *106*, 477–487.

(52) Li, Y.; Harir, M.; Uhl, J.; Kanawati, B.; Lucio, M.; Smirnov, K. S.; Koch, B. P.; Schmitt-Kopplin, P.; Hertkorn, N. How representative are dissolved organic matter (DOM) extracts? A comprehensive study of sorbent selectivity for DOM isolation. *Water Res.* **2017**, *116*, 316–323.

(53) Raeke, J.; Lechtenfeld, O. J.; Wagner, M.; Herzsprung, P.; Reemtsma, T. Selectivity of solid phase extraction of freshwater dissolved organic matter and its effect on ultrahigh resolution mass spectra. *Environ. Sci. Process. Impacts* **2016**, *18* (7), 918–927.

(54) Yang, K.; Zhang, Y.; Dong, Y.; Li, W. Selectivity of solid phase extraction for dissolved organic matter in the hypersaline Da Qaidam Lake, China. *Environ. Sci. Process. Impacts* **2017**, *19* (11), 1374–1386.

(55) Sleighter, R. L.; Hatcher, P. G. The application of electrospray ionization coupled to ultrahigh resolution mass spectrometry for the molecular characterization of natural organic matter. *Journal of Mass Spectrom*. **2007**, *42* (5), 559–574.

(56) Maizel, A. C.; Remucal, C. K. The effect of advanced secondary municipal wastewater treatment on the molecular composition of dissolved organic matter. *Water Res.* **2017**, *122*, 42–52.

(57) Stenson, A. C.; Marshall, A. G.; Cooper, W. T. Exact masses and chemical formulas of individual Suwannee River fulvic acids from ultrahigh resolution electrospray ionization Fourier transform ion cyclotron resonance Mass Spectra. *Anal. Chem.* **2003**, *75* (6), 1275–1284.

(58) Herzsprung, P.; Hertkorn, N.; Von Tumpling, W.; Harir, M.; Friese, K.; Schmitt-Kopplin, P. Understanding molecular formula assignment of Fourier transform ion cyclotron resonance mass spectrometry data of natural organic matter from a chemical point of view. *Anal. Bioanal. Chem.* **2014**, *406* (30), 7977–7987.

(59) Herzsprung, P.; Hertkorn, N.; Von Tümpling, W.; Harir, M.; Friese, K.; Schmitt-Kopplin, P. Molecular formula assignment for dissolved organic matter (DOM) using high-field FT-ICR-MS: Chemical perspective and validation of sulphur-rich organic components (CHOS) in pit lake samples. *Anal. Bioanal. Chem.* **2016**, *408* (10), 2461–2469.

(60) Koch, B. P.; Dittmar, T.; Witt, M.; Kattner, G. Fundamentals of molecular formula assignment to ultrahigh resolution mass data of natural organic matter. *Anal. Chem.* **2007**, *79* (4), 1758–1763.

(61) Tolić, N.; Liu, Y.; Liyu, A.; Shen, Y.; Tfaily, M. M.; Kujawinski, E. B.; Longnecker, K.; Kuo, L. J.; Robinson, E. W.; Paša-Tolić, L.; Hess, N. J. Formularity: Software for automated formula assignment of natural and other organic matter from ultrahigh-resolution mass spectra. *Anal. Chem.* **2017**, *89* (23), 12659–12665.

(62) Kim, S.; Kramer, R. W.; Hatcher, P. G. Graphical method for analysis of ultrahigh-resolution broadband mass spectra of natural organic matter, the van Krevelen diagram. *Anal. Chem.* **2003**, *75* (20), 5336–5344.

(63) Koch, B. P.; Dittmar, T. From mass to structure: An aromaticity index for high-resolution mass data of natural organic matter. *Rapid Commun. Mass Spectrom.* **2006**, *20* (5), 926–932.

(64) Hawkes, J. A.; D'Andrilli, J.; Agar, J. N.; Barrow, M. P.; Berg, S. M.; Catalán, N.; Chen, H.; Chu, R. K.; Cole, R. B.; Dittmar, T.; Gavard, R.; Gleixner, G.; Hatcher, P. G.; He, C.; Hess, N. J.; Hutchins, R. H. S.; Ijaz, A.; Jones, H. E.; Kew, W.; Khaksari, M.; Palacio Lozano, D. C.; Lv, J.; Mazzoleni, L. R.; Noriega-Ortega, B. E.; Osterholz, H.; Radoman, N.; Remucal, C. K.; Schmitt, N. D.; Schum, S. K.; Shi, Q.; Simon, C.; Singer, G.; Sleighter, R. L.; Stubbins, A.; Thomas, M. J.; Tolic, N.; Zhang, S.; Zito, P.; Podgorski, D. C. An international laboratory comparison of dissolved organic matter composition by high resolution mass spectrometry: Are we getting the same answer? *Limnol. Oceanogr. Methods* **2020**, *18* (6), 235-258.

(65) Poulin, B. A.; Ryan, J. N.; Nagy, K. L.; Stubbins, A.; Dittmar, T.; Orem, W.; Krabbenhoft, D. P.; Aiken, G. R. Spatial dependence of reduced sulfur in Everglades dissolved organic matter controlled by sulfate enrichment. *Environ. Sci. Technol.* **2017**, *51* (7), 3630–3639.

(66) Maizel, A. C.; Remucal, C. K. Molecular composition and photochemical reactivity of size-fractionated dissolved organic matter. *Environ. Sci. Technol.* **2017**, *51* (4), 2113–2123.

(67) Waggoner, D. C.; Chen, H.; Willoughby, A. S.; Hatcher, P. G. Formation of black carbon-like and alicyclic aliphatic compounds by hydroxyl radical initiated degradation of lignin. *Org. Geochem.* **2015**, *82*, 69–76.

(68) Kellerman, A. M.; Kothawala, D. N.; Dittmar, T.; Tranvik, L. J. Persistence of dissolved organic matter in lakes related to its molecular characteristics. *Nat. Geosci.* **2015**, *8* (6), 454–457.

(69) Brown, A.; McKnight, D. M.; Chin, Y. P.; Roberts, E. C.; Uhle, M. Chemical characterization of dissolved organic material in Pony Lake, a saline coastal pond in antarctica. *Mar. Chemistry*, **2004**, *89*, 327–337.

(70) A. M. Worms, I.; E. Chmiel, H.; Traber, J.; Tofield-Pasche, N.; I. Slaveykova, V. Dissolved organic matter and associated trace metal dynamics from river to lake, under ice-covered and ice-free conditions. *Environ. Sci. Technol.* **2019**, *53* (24), 14134–14143.

(71) Berg, S. M.; T. Whiting, Q.; A. Herrli, J.; Winkels, R.; H. Wammer, K.; K. Remucal, C. The role of dissolved organic matter composition in determining photochemical reactivity at the molecular level. *Environ. Sci. Technol.* **2019**, *53* (20), 11725–11734.

(72) Alan Roebuck, J.; Seidel, M.; Dittmar, T.; Jaffé, R. Controls of land use and the river continuum concept on dissolved organic matter composition in an anthropogenically disturbed subtropical watershed. *Environ. Sci. Technol.* **2019**, *54* (1), 195–206.

(73) Cawley, K. M.; Campbell, J.; Zwilling, M.; Jaffé, R. Evaluation of forest disturbance legacy effects on dissolved organic matter characteristics in streams at the Hubbard Brook Experimental Forest, New Hampshire. *Aquat. Sci.* **2014**, *76* (4), 611–622.

(74) Clark, M. J.; Cresser, M. S.; Smart, R.; Chapman, P. J.; Edwards, A. C. The Influence of Catchment Characteristics on the Seasonality of Carbon and Nitrogen Species Concentrations in Upland Rivers of Northern Scotland. *Biogeochem,* **2004**, *68*, 1-19.

(75) Palviainen, M.; Lauren, A.; Launiainen, S.; Piirainen, S. Predicting the export and concntrations of organic carbon, nitrogen and phosphorus in boreal lakes by catchment characterististics and land use: A practical approach. *AMBIO A J. Hum. Environ.* **2016**, *45* (8).

(76) Xenopoulos, M. A.; Lodge, D. M.; Frentress, J.; Kreps, T. A.; Bridgham, S. D.; Grossman, E.; Jackson, C. J. Regional comparisons of watershed determinants of dissolved organic carbon in temperate lakes from the Upper Great Lakes Region and selected regions globally. *Limnol. Ocean.* **2003**, *48* (6), 2321–2334.

(77) Dalmagro, H. J.; Johnson, M. S.; de Musis, C. R.; Lathuillière, M. J.; Graesser, J.; Pinto-Júnior, O. B.; Couto, E. G. Spatial patterns of DOC concentration and DOM optical properties in a Brazilian tropical river-wetland system. *J. Geophys. Res. Biogeosciences* **2017**, *122* (8), 1883–1902.

(78) Dillon, P. J.; Molot, L. A. Effect of landscape form on export of dissolved organic carbon, iron, and phosphorus from forested stream catchments. *Water Resour. Res.* **1997**, *33* (11), 2591–2600.

(79) Eckhardt, B. W.; Moore, T. W. Controls on dissolved organic carbon concentrations in streams, Southern Quebec. *J. Fish. Aquaa. Sci.* **1990**, *47* (8), 1537-1544.

(80) Flint, S. A.; McDowell, W. H. Effects of headwater wetlands on dissolved nitrogen and dissolved organic carbon concentrations in a buburban New Hampshire watershed. *Freshw. Sci.* **2015**, *34* (2), 456–471.
(81) Frost, P. C.; Larson, J. H.; Johnston, C. A.; Young, K. C.; Maurice, P. A.; Lamberti, G. A.; Bridgham, S. D. Landscape predictors of stream dissolved organic matter concentration and physicochemistry in a Lake Superior river watershed. *Aquat. Sci.* **2006**, *68* (1), 40–51.
(82) Hanley, K. W.; Wollheim, W. M.; Salisbury, J.; Huntington, T.; Aiken, G. Controls on dissolved organic carbon quantity and chemical character in temperate rivers of North America. *Global Biogeochem. Cycles* **2013**, *27* (2), 492–504.
(83) Kortelainen, P.; Saukkonen, S. Organic vs. minerogenic acidity in headwater streams in Finland. *Water, Air, Soil Pollut.* **1995**, *85* (2), 559–564.
(84) Mattsson, T.; Kortelainen, P.; Räike, A. Export of DOM from boreal catchments: Impacts of land use cover and climate. *Biogeochemistry* **2005**, *76* (2), 373–394.
(85) Graeber, D.; Gelbrecht, J.; Pusch, M. T.; Anlanger, C.; von Schiller, D. Agriculture has changed the amount and composition of dissolved organic matter in central European headwater streams. *Sci. Total Environ.* **2012**, *438*, 435–446.
(86) Shang, P.; Lu, Y. H.; Du, Y. X.; Jaffé, R.; Findlay, R. H.; Wynn, A. Climatic and watershed controls of dissolved organic matter variation in streams across a gradient of agricultural land use. *Sci. Total Environ.* **2018**, *612*, 1442–1453.
(87) McElmurry, S. P.; Long, D. T.; Voice, T. C. Stormwater dissolved organic matter: influence of land cover and environmental factors. *Environ. Sci. Technol.* **2014**, *48* (1), 45–53.
(88) Aitkenhead-Peterson, J. A.; Steele, M. K.; Nahar, N.; Santhy, K. Dissolved organic carbon and nitrogen in urban and rural watersheds of south-Central Texas: Land use and land management influences. *Biogeochemistry* **2009**, *96* (1), 119–129.
(89) Alvarez-Cobelas, M.; Angeler, D. G.; Sánchez-Carrillo, S.; Almendros, G. A worldwide view of organic carbon export from catchments. *Biogeochemistry* **2012**, *107* (1–3), 275–293.
(90) Hosen, J. D.; McDonough, O. T.; Febria, C. M.; Palmer, M. A. Dissolved organic matter quality and bioavailability changes across an urbanization gradient in headwater streams. *Environ. Sci. Technol.* **2014**, *48* (14), 7817–7824.
(91) Singh, S.; Dash, P.; Silwal, S.; Feng, G.; Adeli, A.; Moorhead, R. J. Influence of land use and land cover on the spatial variability of dissolved organic matter in multiple aquatic environments. *Environ. Sci. Pollut. Res.* **2017**, *24* (16), 14124–14141.
(92) Williams, C. J.; Yamashita, Y.; Wilson, H. F.; Jaffe, R.; Xenopoulos, M. A. Unraveling the role of land use and microbial activity in shaping dissolved organic matter characteristics in stream ecosystems. *Limnol. Oceanogr.* **2010**, *55* (3), 1159–1171.
(93) Heinz, M.; Graeber, D.; Zak, D.; Zwirnmann, E.; Gelbrecht, J.; Pusch, M. T. Comparison of organic matter composition in agricultural versus forest affected headwaters with special emphasis on organic nitrogen. *Environ. Sci. Technol.* **2015**, *49* (4), 2081–2090.
(94) Lu, Y. H.; Bauer, J. E.; Canuel, E. A.; Chambers, R. M.; Yamashita, Y.; Jaffé, R.; Barrett, A. Effects of land use on sources and ages of inorganic and organic carbon in temperate headwater streams. *Biogeochemistry* **2014**, *119* (1–3), 275–292.
(95) Gonsior, M.; Zwartjes, M.; Cooper, W. J.; Song, W.; Ishida, K. P.; Tseng, L. Y.; Jeung, M. K.; Rosso, D.; Hertkorn, N.; Schmitt-Kopplin, P. Molecular characterization of effluent

organic matter identified by ultrahigh resolution mass spectrometry. *Water Res.* **2011**, *45* (9), 2943–2953.

(96) Arnold, W. A.; Longnecker, K.; Kroeger, K. D.; Kujawinski, E. B. Molecular signature of organic nitrogen in septic-impacted groundwater. *Environ. Sci. Process. Impacts* **2014**, *16* (10), 2400–2407.

(97) Hertkorn, N.; Benner, R.; Frommberger, M.; Schmitt-Kopplin, P.; Witt, M.; Kaiser, K.; Kettrup, A.; Hedges, J. I. Characterization of a major refractory component of marine dissolved organic matter. *Geochim. Cosmochim. Acta* **2006**, *70* (12), 2990–3010.

(98) Cory, R. M.; Kling, G. W.; Stanley, E.; Del Giorgio, P. Interactions between sunlight and microorganisms influence dissolved organic matter degradation along the aquatic continuum. *Limnol. Oceanogr. Lett.* **2018**, *3*, 102–116.

(99) Moran, M. A.; Zepp, R. G. Role of photoreactions in the formation of biologically labile compounds from dissolved organic matter. *Limnol. Oceanogr.* **1997**, *42* (6), 1307–1316.

(100) Ossola, R.; Clerc, B.; McNeill, K. Mechanistic insights into dissolved organic sulfur photomineralization through the study of cysteine sulfinic Acid. *Environ. Sci. Technol.* **2020**, *54* (20), 13066–13076.

(101) Brinkmann, T.; Sartorius, D.; Frimmel, F. H. Photobleaching of humic rich dissolved organic matter. *Aquat. Sci.* **2003**, *65* (4), 415–424.

(102) Granéli, W.; Lindell, M.; Tranvik, L. Photo-oxidative production of dissolved inorganic carbon in lakes of different humic content. *Limnol. Oceanogr.* **1996**, *41* (4), 698–706.

(103) Judd, K. E.; Crump, B. C.; Kling, G. W. Bacterial responses in activity and community composition to photo-oxidation of dissolved organic matter from soil and surface waters. *Aquat. Sci.* **2007**, *69* (1), 96–107.

(104) Moran, M. A.; Sheldon, W. M.; Zepp, R. G. Carbon loss and optical property changes during long-term photochemical and biological degradation of estuarine dissolved organic matter. *Limnol. Oceanogr.* **2000**, *45* (6), 1254–1264.

(105) Lønborg, C.; Nieto-Cid, M.; Hernando-Morales, V.; Hernández-Ruiz, M.; Teira, E.; Álvarez-Salgado, X. A. Photochemical alteration of dissolved organic matter and the subsequent effects on bacterial carbon cycling and diversity. *FEMS Microbiol. Ecol.* **2016**, *92* (5), 1-13.

(106) Bushaw, K. L.; Zepp, R. B.; Tarr, M. A.; Schulz-Jander, D.; Bourbonniere, R. A.; Hudson, R. E.; Miller, William L.; Bronk, D. A.; Moran, M. A. Photochemical release of biologically available nitrogen from aquatic dissolved organic matter. *Lett. to Nat.* **1996**, *381*, 404–407.

(107) Ossola, R.; Tolu, J.; Clerc, B.; R. Erickson, P.; H. E. Winkel, L.; McNeill, K. Photochemical production of sulfate and methanesulfonic acid from dissolved organic sulfur. *Environ. Sci. Technol.* **2019**, *53* (22), 13191–13200.

(108) Ward, C. P.; Cory, R. M. Assessing the prevalence, products, and pathways of dissolved organic matter partial photo-oxidation in arctic surface waters. *Environ. Sci. Process. Impacts* **2020**, *22* (5), 1214–1223.

(109) Ward, C. P.; Cory, R. M. Complete and partial photo-oxidation of dissolved organic matter draining permafrost soils. *Environ. Sci. Technol.* **2016**, *50* (7), 3545–3553.

(110) Minor, E. C.; Dalzell, B. J.; Stubbins, A.; Mopper, K. Evaluating the photoalteration of estuarine dissolved organic matter using direct temperature-resolved mass spectrometry and UV-visible spectroscopy. *Aquat. Sci.* **2007**, *69* (4), 440–455.

(111) Herzsprung, P.; Hertkorn, N.; Friese, K.; Schmitt-Kopplin, P. Photochemical degradation of natural organic sulfur compounds (CHOS) from iron-rich mine pit lake pore waters - an initial understanding from evaluation of single-elemental formulae using ultra high-resolution mass spectrometry. *Rapid Commun. Mass Spectrom.* **2010**, *24* (19), 2909–2924.
(112) Gomez-Saez, G. V.; Pohlabeln, A. M.; Stubbins, A.; Marsay, C. M.; Dittmar, T. Photochemical alteration of dissolved organic sulfur from sulfidic porewater. *Environ. Sci. Technol.* **2017**, *51* (24), 14144–14154.
(113) Gonsior, M.; Peake, B. M.; Cooper, W. T.; Podgorski, D.; D'Andrilli, J.; Cooper, W. J. Photochemically induced changes in dissolved organic matter identified by ultrahigh resolution Fourier transform ion cyclotron resonance mass spectrometry. *Environ. Sci. Technol.* **2009**, *43* (3), 698–703.
(114) Kellerman, A. M.; Dittmar, T.; Kothawala, D. N.; Tranvik, L. J. Chemodiversity of dissolved organic matter in lakes driven by climate and dydrology. *Nat. Commun.* **2014**, *5*, 1-8.
(115) Ward, C. P.; Sleighter, R. L.; Hatcher, P. G.; Cory, R. M. Insights into the complete and partial photooxidation of black carbon in surface waters. *Environ. Sci. Process. Impacts* **2014**, *16* (4), 721–731.
(116) Gonsior, M.; Schmitt-Kopplin, P.; Bastviken, D. Depth-dependent molecular composition and photo-reactivity of dissolved organic matter in a boreal lake under winter and summer conditions. *Biogeosciences* **2013**, *10* (11), 6945–6956.
(117) Bertilsson, S.; Tranvik, L. J. Photochemically produced carboxylic acids as substrates for freshwater bacterioplankton. *Limnol. Oceanogr.* **1998**, *43* (5), 885–895.
(118) Tranvik, L. J.; Bertilsson, S. Contrasting effects of solar UV radiation on dissolved organic sources for bacterial growth. *Ecol. Lett.* **2001**, *4* (5), 458–463.
(119) Müller, R. A.; Kothawala, D. N.; Podgrajsek, E.; Sahlée, E.; Koehler, B.; Tranvik, L. J.; Weyhenmeyer, G. A. Hourly, daily, and seasonal variability in the absorption spectra of chromophoric dissolved organic matter in a eutrophic, humic lake. *J. Geophys. Res. G Biogeosciences* **2014**, *119* (10), 1985–1998.
(120) Bittar, T. B.; Stubbins, A.; Vieira, A. A. H.; Mopper, K. Characterization and photodegradation of dissolved organic matter (DOM) from a tropical lake and its dominant primary producer, the cyanobacteria *Microcystis aeruginosa*. *Mar. Chem.* **2015**, *177*, 205–217.
(121) Gao, H. Factors influencing photoreactions of dissolved organic matter in a coastal river of the southeastern United States. *Environ. Sci. Technol.* **1998**, *32*, 2940–2946.
(122) Helms, J. R.; Stubbins, A.; Perdue, E. M.; Green, N. W.; Chen, H.; Mopper, K. Photochemical bleaching of oceanic dissolved organic matter and its effect on absorption spectral slope and fluorescence. *Mar. Chem.* **2013**, *155*, 81–91.
(123) Helms, J. R.; Mao, J.; Stubbins, A.; Schmidt-Rohr, K.; Spencer, R. G. M.; Hernes, P. J.; Mopper, K. Loss of optical and molecular indicators of terrigenous dissolved organic matter during long-term photobleaching. *Aquat. Sci.* **2014**, *76* (3), 353–373.
(124) Hur, J.; Jung, K. Y.; Jung, Y. M. Characterization of spectral responses of humic substances upon UV irradiation using two-dimensional correlation spectroscopy. *Water Res.* **2011**, *45* (9), 2965–2974.
(125) Sharpless, C. M.; Aeschbacher, M.; Page, S. E.; Wenk, J.; Sander, M.; McNeill, K. Photooxidation-induced changes in optical, electrochemical, and photochemical properties of humic substances. *Environ. Sci. Technol.* **2014**, *48* (5), 2688–2696.

(126) Cory, R. M.; Harrold, K. H.; Neilson, B. T.; Kling, G. W. Controls on dissolved organic matter (DOM) degradation in a headwater stream: The influence of photochemical and hydrological conditions in determining light-limitation or substrate-limitation of photo-degradation. *Biogeosciences* **2015**, *12* (22), 6669–6685.
(127) Zhu, X.; L. Miller, W.; G. Fichot, C. Simple method to determine the apparent quantum yield matrix of CDOM photobleaching in natural waters. *Environ. Sci. Technol.* **2020**, *54* (21), 14096–14106.
(128) Aguer, J.-P.; Richard, C. Reactive species produced on irradiation at 365 nm of aqueous solutions of humic acids. *Photochem. Photobiol. A.* **1996**, *93*, 193-198.
(129) Zhao, L.; Chen, H.; Lu, X.; Lin, H.; Christensen, G. A.; Pierce, E. M.; Gu, B. Contrasting effects of dissolved organic matter on mercury methylation by *Geobacter sulfurreducens* PCA and *Desulfovibrio desulfuricans* ND132. *Environ. Sci. Technol.* **2017**, *51*, 10468-10475.
(130) Cory, R. M.; Cotner, J. B.; Mcneill, K. Quantifying interactions between singlet oxygen and aquatic fulvic acids. *Environ. Sci. Technol.* **2009**, *43* (3), 718–723.
(131) Garg, S.; Rose, A. L.; Waite, T. D. Photochemical production of superoxide and hydrogen peroxide from natural organic matter. *Geochim. Cosmochim. Acta* **2011**, *75* (15), 4310–4320.
(132) Brezonik, Patrick L.; Fulkerson-Brekken, J. Nitrate-induced photolysis in natural waters: Controls on concentrations of hydroxyl radical photo-intermediates by natural scavenging agents. *Environ. Sci. Technol.* **1998**, *32*, 3004–3010.
(133) Remucal, C. K.; Salhi, E.; Walpen, N.; von Gunten, U. Molecular-level transformation of dissolved organic matter during oxidation by ozone and hydroxyl radical. *Environ. Sci. Technol.* **2020**, *54* (16), 10351-10360.
(134) Waggoner, D. C.; Hatcher, P. G. Hydroxyl radical alteration of HPLC fractionated lignin: Formation of new compounds from terrestrial organic matter. *Org. Geochem.* **2017**, *113*, 315–325.
(135) Waggoner, D. C.; Wozniak, A. S.; Cory, R. M.; Hatcher, P. G. The role of reactive oxygen species in the degradation of lignin derived dissolved organic matter. *Geochim. Cosmochim. Acta* **2017**, *208*, 171–184.
(136) Goldstone, J. V.; Pullin, M. J.; Bertilsson, S.; Voelker, B. M. Reactions of hydroxyl radical with humic substances: Bleaching, mineralization, and production of bioavailable carbon substrates. *Environ. Sci. Technol.* **2002**, *36* (3), 364–372.
(137) Singer, G. A.; Fasching, C.; Wilhelm, L.; Niggemann, J.; Steier, P.; Dittmar, T.; Battin, T. J. Biogeochemically diverse organic matter in alpine glaciers and its downstream fate. *Nat. Geosci.* **2012**, *5* (10), 710–714.
(138) Cory, R. M.; Kaplan, L. A. Biological lability of streamwater fluorescent dissolved organic matter. *Limnol. Oceanogr.* **2012**, *57* (5), 1347–1360.
(139) Bai, L.; Cao, C.; Wang, C.; Xu, H.; Zhang, H.; Slaveykova, V. I.; Jiang, H. Toward quantitative understanding of the bioavailability of dissolved organic matter in freshwater lake during cyanobacteria blooming. *Environ. Sci. Technol.* **2017**, *51* (11), 6018–6026.
(140) Feng, L.; Xu, J.; Kang, S.; Li, X.; Li, Y.; Jiang, B.; Shi, Q. Chemical composition of microbe-derived dissolved organic matter in cryoconite in Tibetan Plateau glaciers: Insights from Fourier transform ion cyclotron resonance mass spectrometry analysis. *Environ. Sci. Technol.* **2016**, *50* (24), 13215–13223.

(141) Lusk, M. G.; Toor, G. S. Dissolved organic nitrogen in urban streams: biodegradability and molecular composition studies. *Water Res.* **2016**, *96*, 225–235.
(142) Lusk, M. G.; Toor, G. S. Biodegradability and molecular composition of dissolved organic nitrogen in urban stormwater runoff and outflow water from a stormwater retention pond. *Environ. Sci. Technol.* **2016**, *50* (7), 3391–3398.
(143) Mangal, V.; Stock, N. L.; Guéguen, C. Molecular characterization of phytoplankton dissolved organic matter (DOM) and sulfur components using high resolution Orbitrap mass spectrometry. *Anal. Bioanal. Chem.* **2016**, *408* (7), 1891–1900.
(144) Sleighter, R. L.; Cory, R. M.; Kaplan, L. A.; Abdulla, H. A. N.; Hatcher, P. G. A coupled geochemical and biogeochemical approach to characterize the bioreactivity of dissolved organic matter from a headwater stream. *J. Geophys. Res. G Biogeosciences* **2014**, *119* (8), 1520–1537.
(145) D'Andrilli, J.; Cooper, W. T.; Foreman, C. M.; Marshall, A. G. An ultrahigh-resolution mass spectrometry index to estimate natural organic matter lability. *Rapid Commun. Mass Spectrom.* **2015**, *29* (24), 2385–2401.
(146) Kamjunke, N.; von Tümpling, W.; Hertkorn, N.; Harir, M.; Schmitt-Kopplin, P.; Norf, H.; Weitere, M.; Herzsprung, P. A new approach for evaluating transformations of dissolved organic matter (DOM) via high-resolution mass spectrometry and relating it to bacterial activity. *Water Res.* **2017**, *123*, 513–523.
(147) Kim, S.; Kaplan, L. A.; Hatcher, P. G.; Marshall, A. G.; Rodgers, R. P.; Wu, Z. Biodegradable dissolved organic matter in a temperate and a tropical stream determined from ultra-high resolution mass spectrometry. *Limnol. Ocean.* **2006**, *51* (2), 1054–1063.
(148) Logue, J. B.; Stedmon, C. A.; Kellerman, A. M.; Nielsen, N. J.; Andersson, A. F.; Laudon, H.; Lindström, E. S.; Kritzberg, E. S. Experimental insights into the importance of aquatic bacterial community composition to the degradation of dissolved organic matter. *ISME J.* **2016**, *10* (3), 533–545.
(149) D'Andrilli, J.; Junker, J. R.; Smith, H. J.; Scholl, E. A.; Foreman, C. M. DOM composition alters ecosystem function during microbial processing of isolated sources. *Biogeochemistry* **2019**, *142* (2), 281–298.
(150) Hertkorn, N.; Claus, H.; Schmitt-Kopplin, P.; Perdue, E. M.; Filip, Z. Utilization and transformation of aquatic humic substances by autochthonous microorganisms. *Environ. Sci. Technol.* **2002**, *36* (20), 4334–4345.
(151) Bastviken, D.; Persson, L.; Odham, G.; Tranvik, L. Degradation of dissolved organic matter in oxic and anoxic lake water. *Limnol. Oceanogr.* **2004**, *49*, 109-116.
(152) Henderson, R. K.; Baker, A.; Parsons, S. A.; Jefferson, B. Characterisation of algogenic organic matter extracted from cyanobacteria, green algae and diatoms. *Water Res.* **2008**, *42* (13), 3435–3445.
(153) Cory, R. M.; McKnight, D. M.; Chin, Y. P.; Miller, P.; Jaros, C. L. Chemical characteristics of fulvic acids from arctic surface waters: Microbial contributions and photochemical transformations. *J. Geophys. Res. Biogeosciences* **2007**, *112* (4).
(154) Aluwihare, L. I.; Repeta, D. J. A Comparison of the chemical characteristics of oceanic DOM and extracellular DOM produced by marine algae. *Mar. Ecol.* **1999**, *186*, 105-117.
(155) Bowen, J. C.; Kaplan, L. A.; Cory, R. M. Photodegradation disproportionately impacts biodegradation of semi-labile DOM in streams. *Limnol. Oceanogr.* **2020**, *65* (1), 13–26.

(156) Reader, H. E.; Miller, W. L. The efficiency and spectral photon dose dependence of photochemically induced changes to the bioavailability of dissolved organic carbon. *Limnol. Oceanogr.* **2014**, *59* (1), 182–194.
(157) Cory, R. M.; Crump, B. C.; Dobkowski, J. A.; Kling, G. W. Surface exposure to sunlight stimulates CO_2 release from permafrost soil carbon in the arctic. *Proc. Natl. Acad.* **2013**, *110* (9), 3429–3434.
(158) Herzsprung, P.; Wentzky, V.; Kamjunke, N.; Von Tümpling, W.; Wilske, C.; Friese, K.; Boehrer, B.; Reemtsma, T.; Rinke, K.; Lechtenfeld, O. J. Improved understanding of dissolved organic matter processing in freshwater using complementary experimental and machine learning approaches. *Environ. Sci. Technol.* **2020**, *54* (21), 13556–13565.
(159) Lv, J.; Zhang, S.; Wang, S.; Luo, L.; Cao, D.; Christie, P. Molecular-scale investigation with ESI-FT-ICR-MS on fractionation of dissolved organic matter induced by adsorption on iron oxyhydroxides. *Environ. Sci. Technol.* **2016**, *50* (5), 2328–2336.
(160) Wang, Z.; Lv, J.; Zhang, S.; Christie, P.; Zhang, S. Interfacial molecular fractionation on ferrihydrite reduces the photochemical reactivity of dissolved organic matter. *Environ. Sci. Technol.* **2021**, *55* (3), 1769–1778.
(161) Lalonde, K.; Mucci, A.; Ouellet, A.; Gélinas, Y. Preservation of organic matter in s ediments promoted by iron. *Nature* **2012**, *483* (7388), 198–200.
(162) Liao, P.; Li, W.; Jiang, Y.; Wu, J.; Yuan, S.; Fortner, J. D.; Giammar, D. E. Formation, aggregation, and deposition dynamics of NOM-iron colloids at anoxic-oxic interfaces. *Environ. Sci. Technol.* **2017**, *51* (21), 12235–12245.
(163) Linkhorst, A.; Dittmar, T.; Waska, H. Molecular fractionation of dissolved organic matter in a shallow subterranean estuary: The role of the iron curtain. *Environ. Sci. Technol.* **2017**, *51* (3), 1312–1320.
(164) Dadi, T.; Harir, M.; Hertkorn, N.; Koschorreck, M.; Schmitt-Kopplin, P.; Herzsprung, P. Redox conditions affect dissolved organic carbon quality in stratified freshwaters. *Environ. Sci. Technol.* **2017**, *51* (23), 13705–13713.
(165) Riedel, T.; Zak, D.; Biester, H.; Dittmar, T. Iron traps terrestrially derived dissolved organic matter at redox interfaces. *Proc. Natl. Acad.* **2013**, *110* (25), 10101–10105.
(166) Fu, P.; Wu, F.; Liu, C. Q.; Wei, Z.; Bai, Y.; Liao, H. Spectroscopic characterization and molecular weight distribution of dissolved organic matter in sediment porewaters from Lake Erhai, southwest China. *Biogeochemistry* **2006**, *81* (2), 179–189.
(167) Valle, J.; Gonsior, M.; Harir, M.; Enrich-Prast, A.; Schmitt-Kopplin, P.; Bastviken, D.; Conrad, R.; Hertkorn, N. Extensive processing of sediment pore water dissolved organic matter during anoxic incubation as observed by high-field mass spectrometry (FTICR-MS). *Water Res.* **2018**, *129*, 252–263.
(168) Yang, L.; Choi, J. H.; Hur, J. Benthic flux of dissolved organic matter from lake sediment at different redox conditions and the possible effects of biogeochemical processes. *Water Res.* **2014**, *61*, 97–107.
(169) Valle, J.; Harir, M.; Gonsior, M.; Enrich-Prast, A.; Schmitt-Kopplin, P.; Bastviken, D.; Hertkorn, N. Molecular differences between water column and sediment pore water SPE-DOM in ten Swedish boreal Lakes. *Water Res.* **2020**, *170*, 115320.
(170) Walpen, N.; Getzinger, G. J.; Schroth, M. H.; Sander, M. Electron-donating phenolic and electron-accepting quinone moieties in peat dissolved organic matter: quantities and redox transformations in the context of peat biogeochemistry. *Environ. Sci. Technol.* **2018**, *52* (9), 5236–5245.

(171) Schmidt, F.; P. Koch, B.; Elvert, M.; Schmidt, G.; Witt, M.; Hinrichs, K.-U. Diagenetic transformation of dissolved organic nitrogen compounds under contrasting sedimentary redox conditions in the Black Sea. *Environ. Sci. Technol.* **2011**, *45* (12), 5223–5229.
(172) Bracchini, L.; Dattilo, A. M.; Hull, V.; Loiselle, S. A.; Martini, S.; Rossi, C.; Santinelli, C.; Seritti, A. The bio-optical properties of CDOM as descriptor of lake stratification. *J. Photochem. Photobiol. B Biol.* **2006**, *85* (2), 145–149.
(173) Yuthawong, V.; Kasuga, I.; Kurisu, F.; Furumai, H. Application of Orbitrap mass spectrometry to investigate seasonal variations of dissolved organic matter composition in a eutrophic lake in Japan. *Environ. Sci. Water Res. Technol.* **2020**.
(174) Zhang, F.; Harir, M.; Moritz, F.; Zhang, J.; Witting, M.; Wu, Y.; Schmitt-Kopplin, P.; Fekete, A.; Gaspar, A.; Hertkorn, N. Molecular and structural characterization of dissolved organic matter during and post cyanobacterial bloom in Taihu by combination of NMR spectroscopy and FTICR mass spectrometry. *Water Res.* **2014**, *57*, 280–294.
(175) Guo, K.; Wu, Z.; Shang, C.; Yao, B.; Hou, S.; Yang, X.; Song, W.; Fang, J. Radical chemistry and structural relationships of PPCP degradation by UV/chlorine treatment in simulated drinking water. *Environ. Sci. Technol.* **2017**, *51* (18), 10431–10439.
(176) Lian, L.; Yao, B.; Hou, S.; Fang, J.; Yan, S.; Song, W. Kinetic study of hydroxyl and sulfate radical-mediated oxidation of pharmaceuticals in wastewater effluents. *Environ. Sci. Technol.* **2017**, *51* (5), 2954–2962.
(177) Huber, M. M.; Canonica, S.; Park, G. Y.; Von Gunten, U. Oxidation of pharmaceuticals during ozonation and advanced oxidation processes. *Environ. Sci. Technol.* **2003**, *37* (5), 1016–1024.
(178) Chuang, Y. H.; Chen, S.; Chinn, C. J.; Mitch, W. A. Comparing the UV/monochloramine and UV/free chlorine advanced oxidation processes (AOPs) to the UV/hydrogen peroxide AOP under scenarios relevant to potable reuse. *Environ. Sci. Technol.* **2017**, *51* (23), 13859–13868.
(179) Silverman, A. I.; Peterson, B. M.; Boehm, A. B.; McNeill, K.; Nelson, K. L. Sunlight inactivation of human viruses and bacteriophages in coastal waters containing natural photosensitizers. *Environ. Sci. Technol.* **2013**, *47* (4), 1870–1878.
(180) Kohn, T.; Nelson, K. L. Sunlight-mediated inactivation of MS2 coliphage via exogenous singlet oxygen produced by sensitizers in natural waters. *Environ. Sci. Technol.* **2007**, *41* (1), 192–197.
(181) Loeb, S.; Li, C.; Kim, J. H. Solar photothermal disinfection using broadband-light absorbing gold nanoparticles and carbon black. *Environ. Sci. Technol.* **2018**, *52* (1), 205–213.
(182) Ward, C. P.; Nalven, S. G.; Crump, B. C.; Kling, G. W.; Cory, R. M. Photochemical alteration of organic carbon draining permafrost soils shifts microbial metabolic pathways and stimultes respiration. *Nat. Commun.* **2017**, 1–7.
(183) Rosario-Ortiz, F. L.; Canonica, S. Probe compounds to assess the photochemical activity of dissolved organic matter. *Environ. Sci. Technol*. **2016**, *50* (23), 12532–12547.
(184) Grebel, J. E.; Pignatello, J. J.; Mitch, W. A. Sorbic acid as a quantitative probe for the formation, scavenging and steady-state concentrations of the triplet-excited state of organic compounds. *Water Res.* **2011**, *45* (19), 6535–6544.
(185) Canonica, S.; Freiburghaus, M. Electron-rich phenols for probing the photochemical reactivity of freshwaters. *Environ. Sci. Technol.* **2001**, *35* (4), 690–695.

(186) Page, S. E.; Arnold, W. A.; McNeill, K. Terephthalate as a probe for photochemically generated hydroxyl radical. *J. Environ. Monit.* **2010**, *12* (9), 1658–1665.
(187) Peller, J. R.; Mezyk, S. P.; McKay, G.; Watson, E. Hydroxyl radical probes for the comparison of secondary treated wastewaters. In *Water Reclamation and Sustainability*; Elsevier Inc., 2014; pp 247–263.
(188) Erickson, P. R.; Moor, K. J.; Werner, J. J.; Latch, D. E.; Arnold, W. A.; McNeill, K. Singlet oxygen phosphorescence as a probe for triplet-state dissolved organic matter reactivity. *Environ. Sci. Technol.* **2018**, *52* (16), 9170–9178.
(189) Laszakovits, J. R.; Berg, S. M.; Anderson, B. G.; O'Brien, J. E.; Wammer, K. H.; Sharpless, C. M. *p*-Nitroanisole/pyridine and *p*-nitroacetophenone/pyridine actinometers revisited: Quantum yield in comparison to ferrioxalate. *Environ. Sci. Technol. Lett.* **2017**, *4* (1), 11–14.
(190) Boreen, A. L.; Arnold, W. A.; McNeill, K. Photodegradation of pharmaceuticals in the aquatic environment: A review. *Aquat. Sci*. **2003**, 65, 320–341.
(191) Yan, S.; Song, W. Photo-transformation of pharmaceutically active compounds in the aqueous environment: A review. *Environmen. Sci.: Processes and Impacts*. **2014,** *16,* 697–720.
(192) Remucal, C. K. The role of indirect photochemical degradation in the environmental fate of pesticides: A review. *Environ. Sci.: Processes and Impacts*. 2014, *16*, 628–653.
(193) Apell, J. N.; C. Pflug, N.; McNeill, K. Photodegradation of fludioxonil and other pyrroles: The importance of indirect photodegradation for understanding environmental fate and photoproduct formation. *Environ. Sci. Technol.* **2019**, *53* (19), 11240–11250.
(194) Wammer, K. H.; Korte, A. R.; Lundeen, R. A.; Sundberg, J. E.; McNeill, K.; Arnold, W. A. Direct photochemistry of three fluoroquinolone antibacterials: norfloxacin, ofloxacin, and enrofloxacin. *Water Res.* **2013**, *47* (1), 439–448.
(195) Yuan, C.; Tebes-Stevens, C.; J. Weber, E. Reaction library to predict direct photochemical transformation products of environmental organic contaminants in sunlit aquatic systems. *Environ. Sci. Technol.* **2020**, *54* (12), 7271–7279.
(196) Janssen, E. M. L.; Erickson, P. R.; McNeill, K. Dual roles of dissolved organic matter as sensitizer and quencher in the photooxidation of tryptophan. *Environ. Sci. Technol.* **2014**, *48* (9), 4916–4924.
(197) Li, Y.; Pan, Y.; Lian, L.; Yan, S.; Song, W.; Yang, X. Photosensitized degradation of acetaminophen in natural organic matter solutions: The role of triplet states and oxygen. *Water Res.* **2017**, *109*, 266–273.
(198) Felcyn, J. R.; Davis, J. C. C.; Tran, L. H.; Berude, J. C.; Latch, D. E. Aquatic photochemistry of isoflavone phytoestrogens: Degradation kinetics and pathways. *Environ. Sci. Technol.* **2012**, *46* (12), 6698–6704.
(199) Canonica, S.; Hellrung, B.; Müller, P.; Wirz, J. Aqueous oxidation of phenylurea herbicides by triplet aromatic ketones. *Environ. Sci. Technol.* **2006**, *40* (21), 6636–6641.
(200) Ren, D.; Huang, B.; Bi, T.; Xiong, D.; Pan, X. Effects of pH and dissolved oxygen on the photodegradation of 17α-ethynylestradiol in dissolved humic acid solution. *Environ. Sci. Process. Impacts* **2016**, *18* (1), 78–86.
(201) Leresche, F.; Ludvíková, L.; Heger, D.; von Gunten, U.; Canonica, S. Quenching of an aniline radical cation by dissolved organic matter and phenols: A laser flash photolysis study. *Environ. Sci. Technol.* **2020**, *54* (23), 15057–15065.

(202) Pflug, N. C.; Schmitt, M.; McNeill, K. Development of N-cyclopropylanilines to probe the oxidative properties of triplet-state photosensitizers. *Environ. Sci. Technol.* **2019**, *53* (9), 4813–4822.
(203) Kral, A. E.; C. Pflug, N.; E. McFadden, M.; H. LeFevre, G.; D. Sivey, J.; M. Cwiertny, D. Photochemical transformations of dichloroacetamide safeners. *Environ. Sci. Technol.* **2019**, *53* (12), 6738–6746.
(204) Chu, C.; Stamatelatos, D.; McNeill, K. Aquatic indirect photochemical transformations of natural peptidic thiols: Impact of thiol properties, solution pH, solution salinity and metal ions. *Environ. Sci. Process. Impacts* **2017**, *19* (12), 1518–1527.
(205) Janssen, E. M. L.; Marron, E.; McNeill, K. Aquatic photochemical kinetics of benzotriazole and structurally related compounds. *Environ. Sci. Process. Impacts* **2015**, *17* (5), 939–946.
(206) McConville, M. B.; Mezyk, S. P.; Remucal, C. K. Indirect photodegradation of the lampricides TFM and niclosamide. *Environ. Sci. Process. Impacts* **2017**, *19* (8), 1028–1039.
(207) Miller, P. L.; Chin, Y. P. Indirect photolysis promoted by natural and engineered wetland water constituents: Processes leading to alachlor degradation. *Environ. Sci. Technol.* **2005**, *39* (12), 4454–4462.
(208) Pati, S. G.; Arnold, W. A. Photochemical transformation of four ionic liquid cation structures in aqueous solution. *Environ. Sci. Technol.* **2017**, *51* (20), 11780–11787.
(209) Huang, J.; Mabury, S. A. A new method for measuring carbonate radical reactivity toward pesticides. *Environ. Toxicol. Chem.* **2000**, *19* (6), 1501–1507.
(210) Hao, Z.; Ma, J.; Miao, C.; Song, Y.; Lian, L.; Yan, S.; Song, W. Carbonate radical oxidation of cylindrospermopsin (cyanotoxin): Kinetic studies and mechanistic consideration. *Environ. Sci. Technol.* **2020**, *54,* (16), 10118-10127.
(211) Arnold, W. A. One electron oxidation potential as a predictor of rate constants of N-containing compounds with carbonate radical and triplet excited state organic matter. *Environ. Sci. Process. Impacts* **2014**, *16* (4), 832–838.
(212) Arnold, W. A.; Oueis, Y.; O'Connor, M.; Rinaman, J. E.; Taggart, M. G.; McCarthy, R. E.; Foster, K. A.; Latch, D. E. QSARs for phenols and phenolates: oxidation potential as a predictor of reaction rate constants with photochemically produced oxidants. *Environ. Sci. Process. Impacts* **2017**, *19* (3), 324–338.
(213) Erickson, P. R.; Walpen, N.; Guerard, J. J.; Eustis, S. N.; Arey, J. S.; McNeill, K. Controlling factors in the rates of oxidation of anilines and phenols by triplet methylene blue in aqueous solution. *J. Phys. Chem. A* **2015**, *119* (13), 3233–3243.
(214) McConville, M. B.; Cohen, N. M.; Nowicki, S. M.; Lantz, S. R.; Hixson, J. L.; Ward, A. S.; Remucal, C. K. A field analysis of lampricide photodegradation in Great Lakes tributaries. *Environ. Sci. Process. Impacts* **2017**, *19* (7), 891–900.
(215) C. Scholes, R.; F. King, J.; A. Mitch, W.; L. Sedlak, D. Transformation of trace organic contaminants from reverse osmosis concentrate by open-water unit-process wetlands with and without ozone pretreatment. *Environ. Sci. Technol.* **2020**, *54* (24), 16176–16185.
(216) Vione, D. The modelling of surface-water photoreactions made easier: Introducing the concept of 'equivalent monochromatic wavelengths.' *Water Res.* **2021**, *190*, 116675.
(217) Albanese, K. A.; Lanno, R. P.; Hadad, C. M.; Chin, Y. P. Photolysis- and dissolved organic matter-induced toxicity of triclocarban to Daphnia Magna. *Environ. Sci. Technol. Lett.* **2017**, *4* (11), 457–462.

(218) Pflug, N. C.; Hankard, M. K.; Berg, S. M.; O'Connor, M.; Gloer, J. B.; Kolodziej, E. P.; Cwiertny, D. M.; Wammer, K. H. Environmental photochemistry of dienogest: phototransformation to estrogenic products and increased environmental persistence via reversible photohydration. *Environ. Sci. Process. Impacts* **2017**, *19* (11), 1414–1426.
(219) Wammer, K. H.; Anderson, K. C.; Erickson, P. R.; Kliegman, S.; Moffatt, M. E.; Berg, S. M.; Heitzman, J. A.; Pflug, N. C.; McNeill, K.; Martinovic-Weigelt, D.; Abagyan, R.; Cwiertny, D. M.; Kolodziej, E. P. Environmental photochemistry of altrenogest: Photoisomerization to a bioactive product with increased environmental persistence via reversible photohydration. *Environ. Sci. Technol.* **2016**, *50* (14), 7480–7488.
(220) McNeill, K.; Canonica, S. Triplet state dissolved organic matter in aquatic photochemistry: Reaction mechanisms, substrate scope, and photophysical properties. *Environ. Sci. Process. Impacts* **2016**, *18* (11), 1381–1399.
(221) Zepp, Richard G.; Schlotzhauer, Patricia F.; Sink, M. R. Photosensitized transformations involving electronic energy transfer in natural waters: Role of humic substances. *Environ. Sci. Technol.* **1985**, *19*, 74–81.
(222) Canonica, S. Oxidation of aquatic organic contaminants induced by excited triplet states. *Chimia (Aarau).* **2007**, *61* (10), 641–644.
(223) Canonica, S.; Hellrung, B.; Wirz, J. Oxidation of phenols by triplet aromatic ketones in aqueous solution. *J. Phys. Chem. A* **2000**, *104* (6), 1226–1232.
(224) Schmitt, M.; Moor, K. J.; Erickson, P. R.; McNeill, K. Sorbic acid as a triplet probe: Reactivity of oxidizing triplets in dissolved organic matter by direct observation of aromatic amine oxidation. *Environ. Sci. Technol.* **2019**, *53* (14), 8087–8096.
(225) Maizel, A. C.; Remucal, C. K. The effect of probe choice and solution conditions on the apparent photoreactivity of dissolved organic matter. *Environ. Sci. Process. Impacts* **2017**, *19* (8), 1040–1050.
(226) Canonica, S.; Laubscher, H. U. Inhibitory effect of dissolved organic matter on triplet-induced oxidation of aquatic contaminants. *Photochem. Photobiol. Sci.* **2008**, *7* (5), 547–551.
(227) McCabe, A. J.; Arnold, W. A. Reactivity of triplet excited states of dissolved natural organic matter in stormflow from mixed-use watersheds. *Environ. Sci. Technol.* **2017**, *51* (17), 9718–9728.
(228) O'Connor, M.; Helal, S. R.; Latch, D. E.; Arnold, W. A. Quantifying photo-production of triplet excited states and singlet oxygen from effluent organic matter. *Water Res.* **2019**, *156*, 23–33.
(229) Wenk, J.; Von Gunten, U.; Canonica, S. Effect of dissolved organic matter on the transformation of contaminants induced by excited triplet states and the hydroxyl radical. *Environ. Sci. Technol.* **2011**, *45* (4), 1334–1340.
(230) Wenk, J.; Eustis, S. N.; McNeill, K.; Canonica, S. Quenching of excited triplet states by dissolved natural organic matter. *Environ. Sci. Technol.* **2013**, *47* (22), 12802–12810.
(231) Wenk, J.; Aeschbacher, M.; Sander, M.; Gunten, U. Von; Canonica, S. Photosensitizing and inhibitory effects of ozonated dissolved organic matter on triplet-induced contaminant transformation. *Environ. Sci. Technol.* **2015**, *49* (14), 8541–8549.
(232) Golanoski, K. S.; Fang, S.; Del Vecchio, R.; Blough, N. V. Investigating the mechanism of phenol photooxidation by humic substances. *Environ. Sci. Technol.* **2012**, *46* (7), 3912–3920.

(233) De Laurentiis, E.; Minella, M.; Maurino, V.; Minero, C.; Brigante, M.; Mailhot, G.; Vione, D. Photochemical production of organic matter triplet states in water samples from mountain lakes, located below or above the tree line. *Chemosphere* **2012**, *88* (10), 1208–1213.

(234) McCabe, A. J.; Arnold, W. A. Multiple linear regression models to predict the formation efficiency of triplet excited states of dissolved organic matter in temperate wetlands. *Limnol. Oceanogr.* **2018**, *63* (5), 1992–2014.

(235) Aulló-Maestro, M. E.; Hunter, P.; Spyrakos, E.; Mercatoris, P.; Kovács, A.; Horváth, H.; Preston, T.; Présing, M.; Palenzuela, J. T.; Tyler, A. Spatio-seasonal variability of chromophoric dissolved organic matter absorption and responses to photobleaching in a large shallow temperate lake. *Biogeosciences* **2017**, *14* (5), 1215–1233.

(236) Dawson, J. J. C.; Tetzlaff, D.; Speed, M.; Hrachowitz, M.; Soulsby, C. Seasonal controls on DOC dynamics in nested upland catchments in NE Scotland. *Hydrol. Process.* **2011**, *25* (10), 1647–1658.

(237) Liu, W.; Xu, X.; McGoff, N. M.; Eaton, J. M.; Leahy, P.; Foley, N.; Kiely, G. Spatial and seasonal variation of dissolved organic carbon (DOC) concentrations in Irish streams: Importance of soil and topography characteristics. *Environ. Manage.* **2014**, *53* (5), 959–967.

(238) Mattsson, T.; Kortelainen, P.; Räike, A.; Lepistö, A.; Thomas, D. N. Spatial and temporal variability of organic C and N concentrations and export from 30 boreal rivers induced by land use and climate. *Sci. Total Environ.* **2015**, *508*, 145–154.

(239) McCabe, A. J.; Arnold, W. A. Seasonal and spatial variabilities in the water chemistry of prairie pothole wetlands influence the photoproduction of reactive intermediates. *Chemosphere* **2016**, *155*, 640–647.

(240) Mulholland, P. J.; Hill, W. R. Seasonal patterns in streamwater nutrient and dissolved organic carbon concentrations: Separating catchment flow path and in-stream effects. *Water Resour. Res.* **1997**, *33* (6), 1297–1306.

(241) Oni, S. K.; Futter, M. N.; Molot, L. A.; Dillon, P. J. Adjacent catchments with similar patterns of land use and climate have markedly different dissolved organic carbon concentration and runoff dynamics. *Hydrol. Process.* **2014**, *28* (3), 1436–1449.

(242) Glover, C. M.; Rosario-Ortiz, F. L. Impact of halides on the photoproduction of reactive intermediates from organic matter. *Environ. Sci. Technol.* **2013**, *47* (24), 13949–13956.

(243) Parker, K. M.; Pignatello, J. J.; Mitch, W. A. Influence of ionic strength on triplet-state natural organic matter loss by energy transfer and electron transfer pathways. *Environ. Sci. Technol.* **2013**, *47* (19), 10987–10994.

(244) Zhou, Y.; Cheng, F.; He, D.; Zhang, Y.; Qu, J.; Yang, X.; Chen, J.; Peijnenburg, W. J. G. M. Effect of UV / chlorine treatment on photophysical and photochemical properties of dissolved organic matter. **2021**, *Water Res*.*192*, 1–9.

(245) Bodhipaksha, L. C.; Sharpless, C. M.; Chin, Y.-P.; Sander, M.; K. Langston, W.; A. MacKay, A. Triplet photochemistry of effluent and natural organic matter in whole water and isolates from effluent-receiving rivers. *Environ. Sci. Technol.* **2015**, *49* (6), 3453–3463.

(246) Maizel, A. C.; Li, J.; Remucal, C. K. Relationships between dissolved organic matter composition and photochemistry in lakes of diverse trophic status. *Environ. Sci. Technol.* **2017**, *51* (17), 9624–9632.

(247) McKay, G.; Huang, W.; Romera-Castillo, C.; Crouch, J. E.; Rosario-Ortiz, F. L.; Jaffé, R. Predicting reactive intermediate quantum yields from dissolved organic matter photolysis

using optical properties and antioxidant capacity. *Environ. Sci. Technol.* **2017**, *51* (10), 5404–5413.

(248) Zhou, H.; Lian, L.; Yan, S.; Song, W. Insights into the photo-induced formation of reactive intermediates from effluent organic matter: The role of chemical constituents. *Water Res.* **2017**, *112*, 120–128.

(249) Wasswa, J.; Driscoll, C. T.; Zeng, T. Photochemical characterization of surface waters from lakes in the Adirondack region of New York. *Environ. Sci. Technol.* **2020**, *54* (17), 10654–

(250) McKay, G.; Couch, K. D.; Mezyk, S. P.; Rosario-Ortiz, F. L. Investigation of the coupled effects of molecular weight and charge-transfer interactions on the optical and photochemical properties of dissolved organic matter. *Environ. Sci. Technol.* **2016**, *50* (15), 8093–8102.

(251) Haag, W. R.; Hoigné, J. Singlet oxygen in surface waters. 3. Photochemical formation and steady-state concentrations in various types of waters. *Environ. Sci. Technol.* **1986**, *20* (4), 341–348.

(252) Zepp, Richard G.; Solfe, N. Lee; Baughman, G. L.; Hollis, R. C. Singlet oxygen in natural waters. *Nature* **1977**, *267*, 421–428.

(253) Bruccolerl, A.; Pant, B. C.; Sharma, D. K.; Langford'qt, C. H. Evaluation of Primary Photoproduct Quantum Yields in Fulvic Acid. *Environ. Sci. Technol.* **1993***, 27*, 889-894.

(254) Ossola, R.; Martin Jönsson, O.; Moor, K.; McNeill, K. Singlet oxygen quantum yields in environmental waters. *Chem. Rev.* **2021**, *in print.*

(255) B. Partanen, S.; R. Erickson, P.; E. Latch, D.; J. Moor, K.; McNeill, K. Dissolved organic matter singlet oxygen quantum yields: Evaluation using time-resolved singlet oxygen phosphorescence. *Environ. Sci. Technol.* **2020**, *54* (6), 3316–3324.

(256) Jaramillo, M.; A. Joens, J.; E. O'Shea, K. Fundamental studies of the singlet oxygen reactions with the potent marine toxin domoic acid. *Environ. Sci. Technol.* **2020**, *54* (10), 6073–6081.

(257) Tratnyek, P. G.; Hoigné, J. Photo-oxidation of 2,4,6-trimethylphenol in aqueous laboratory solutions and natural waters: Kinetics of reaction with singlet oxygen. *Photochem. Photobiol. A Chem* **1994**, *84*, 153–160.

(258) Cory, R. M.; McNeill, K.; Cotner, J. P.; Amado, A.; Purcell, J. M.; Marshall, A. G. Singlet oxygen in the coupled photochemical and biochemical oxidation of dissolved organic matter. *Environ. Sci. Technol.* **2010**, *44* (10), 3683–3689.

(259) Mostafa, S.; Rosario-Ortiz, F. L. Singlet oxygen formation from wastewater organic matter. *Environ. Sci. Technol.* **2013**, *47* (15), 8179–8186.

(260) Dalrymple, R. M.; Carfagno, A. K.; Sharpless, C. M. Correlations between dissolved organic matter optical properties and quantum yields of singlet oxygen and hydrogen peroxide. *Environ. Sci. Technol.* **2010**, *44* (15), 5824–5829.

(261) Leresche, F.; McKay, G.; Kurtz, T.; Von Gunten, U.; Canonica, S.; Rosario-Ortiz, F. L. Effects of ozone on the photochemical and photophysical properties of dissolved organic matter. *Environ. Sci. Technol.* **2019**, *53* (10), 5622–5632.

(262) Du, Z.; He, Y.; Fan, J.; Fu, H.; Zheng, S.; Xu, Z.; Qu, X.; Kong, A.; Zhu, D. Predicting apparent singlet oxygen quantum yields of dissolved black carbon and humic substances using spectroscopic indices. *Chemosphere* **2018**, *194*, 405–413.

(263) Wang, H.; Zhou, H.; Ma, J.; Nie, J.; Yan, S.; Song, W. Triplet photochemistry of dissolved black carbon and its effects on the photochemical formation of reactive oxygen species. *Environ. Sci. Technol.* **2020**, *54,* 4903-4911.
(264) Haag, W. R.; Hoign, J. Photo-sensitized oxidation in natural water via ˙OH radicals. *Chemosphere* **1985**, *14*, 1659–1671.
(265) Benedict, K. B.; McFall, A. S.; Anastasio, C. Quantum yield of nitrite from the photolysis of aqueous nitrate above 300 nm. *Environ. Sci. Technol.* **2017**, *51* (8), 4387–4395.
(266) Mack, J.; Bolton, J. R. Photochemistry of nitrite and nitrate in aqueous solution: A review. *Photochem. Photobiol. A.* **1999**, 128, 1-13.
(267) Southworth, B. A.; Voelker, B. M. Hydroxyl radical production via the photo-Fenton reaction in the presence of fulvic acid. *Environ. Sci. Technol.* **2003**, *37* (6), 1130–1136.
(268) Vermilyea, A. W.; Voelker, B. M. Photo-Fenton reaction at near neutral pH. *Environ. Sci. Technol.* **2009**, *43* (18), 6927–6933.
(269) Vaughan, P. P.; Blough, N. V. Photochemical formation of hydroxyl radical by constituents of natural waters. *Environ. Sci. Technol.* **1998**, *32* (19), 2947–2953.
(270) Jing, Y.; Chaplin, B. P. Mechanistic study of the validity of using hydroxyl radical probes to characterize electrochemical advanced oxidation processes. *Environ. Sci. Technol.* **2017**, *51* (4), 2355–2365.
(271) Vione, D.; Ponzo, M.; Bagnus, D.; Maurino, V.; Minero, C.; Carlotti, M. E. Comparison of different probe molecules for the quantification of hydroxyl radicals in aqueous solution. *Environ. Chem. Lett.* **2010**, *8* (1), 95–100.
(272) Algeria, A. E.; Ferrez, A.; Santiago, G.; Sepulveda, E. F. W. Photochemistry of water-soluble quinones. Production of hydroxyl radical, singlet oxygen, and the superoxide ion. *J. Photochem. Photobiol. A* **1999**, *127*, 57–65.
(273) Gan, D.; Jia, M.; Vaughan, P. P.; Falvey, D. E.; Blough, N. V. Aqueous photochemistry of methyl-benzoquinone. *J. Phys. Chem. A* **2008**, *112* (13), 2803–2812.
(274) Pochon, A.; Vaughan, P. P.; Gan, D.; Vath, P.; Blough, N. V.; Falvey, D. E. Photochemical oxidation of water by 2-methyl-1,4-benzoquinone: Evidence against the formation of free hydroxyl radical. *J. Phys. Chem. A* **2002**, *106* (12), 2889–2894.
(275) Page, S. E.; Arnold, W. A.; McNeill, K. Assessing the contribution of free hydroxyl radical in organic matter-sensitized photohydroxylation reactions. *Environ. Sci. Technol.* **2011**, *45* (7), 2818–2825.
(276) Xu, H.; Li, Y.; Liu, J.; Du, H.; Du, Y.; Su, Y.; Jiang, H. Photogeneration and steady-state concentration of hydroxyl radical in river and lake waters along middle-lower Yangtze Region, China. *Water Res.* **2020**, *176*, 115774.
(277) Dong, M. M.; Rosario-Ortiz, F. L. Photochemical formation of hydroxyl radical from effluent organic matter. *Environ. Sci. Technol.* **2012**, *46* (7), 3788–3794.
(278) Sun, L.; Qian, J.; Blough, N. V.; Mopper, K. Insights into the photoproduction sites of hydroxyl radicals by dissolved organic matter in natural waters. *Environ. Sci. Technol. Lett.* **2015**, *2* (12), 352–356.
(279) McKay, G.; Rosario-Ortiz, F. L. Temperature dependence of the photochemical formation of hydroxyl radical from dissolved organic matter. *Environ. Sci. Technol.* **2015**, *49* (7), 4147–4154.
(280) Vione, D.; Falletti, G.; Maurino, V.; Minero, C.; Pelizzetti, E.; Malandrino, M.; Ajassa, R.; Olariu, R. I.; Arsene, C. Sources and sinks of hydroxyl radicals upon irradiation of natural water samples. *Environ. Sci. Technol.* **2006**, *40* (12), 3775–3781.

(281) Lee, E.; Glover, C. M.; Rosario-Ortiz, F. L. Photochemical formation of hydroxyl radical from effluent organic matter: Role of composition. *Environ. Sci. Technol.* **2013**, *47* (21), 12073–12080.

(282) Buxton, G. V; Greenstock, C. L.; Helman, W. P.; Ross, A. B. Critical review of rate constants for reactions of hydrated electrons, hydrogen atoms, and hydroxyl radical (OH/O-) in aqueous solutions. *J. Phys. Chem. Ref. Data* **1988**, *117*, 513–886.

(283) Appiani, E.; Page, S. E.; McNeill, K. On the use of hydroxyl radical kinetics to assess the number-average molecular weight of dissolved organic matter. *Environ. Sci. Technol.* **2014**, *48* (20), 11794–11802.

(284) McKay, G.; Dong, M. M.; Kleinman, J. L.; Mezyk, S. P.; Rosario-Ortiz, F. L. Temperature dependence of the reaction between the hydroxyl radical and organic matter. *Environ. Sci. Technol.* **2011**, *45* (16), 6932–6937.

(285) Dong, M. M.; Mezyk, S. P.; Rosario-Ortiz, F. L. Reactivity of effluent organic matter (EfOM) with hydroxyl radical as a function of molecular weight. *Environ. Sci. Technol.* **2010**, *44* (15), 5714–5720.

(286) Page, S. E.; Logan, J. R.; Cory, R. M.; McNeill, K. Evidence for dissolved organic matter as the primary source and sink of photochemically produced hydroxyl radical in arctic surface waters. *Environ. Sci. Process. Impacts* **2014**, *16* (4), 807–822.

(287) Frimmel, F. H.; Bauer, H.; Putzlen, J.; Murasecco, P.; Braun, A. M. Laser flash photolysis of dissolved aquatic humic material and the sensitized production of singlet oxygen. *Environ. Sci. Technol.* **1987**, *21* (6), 541–545.

(288) Chen, Y.; Zhang, X.; Feng, S. Contribution of the excited triplet state of humic acid and superoxide radical anion to generation and elimination of phenoxyl radical. *Environ. Sci. Technol.* **2018**, *52* (15), 8283–8291.

(289) Garg, S.; Rose, A. L.; David Waite, T. Production of reactive oxygen species on photolysis of dilute aqueous quinone solutions. *Photochem. Photobiol.* **2007**, *83*, 904–913.

(290) Ma, J.; Zhou, H.; Yan, S.; Song, W. Kinetics studies and mechanistic considerations on the reactions of superoxide radical ions with dissolved organic matter. *Water Res.* **2019**, *149*, 56–64.

(291) Zhang, Y.; V. Blough, N. Photoproduction of one-electron reducing intermediates by chromophoric dissolved organic matter (CDOM): Relation to $O_2^{\bullet-}$ and H_2O_2 photoproduction and CDOM photooxidation. *Environ. Sci. Technol.* **2016**, *50* (20), 11008–11015.

(292) Zhang, Y.; Del Vecchio, R.; Blough, N. V. Investigating the mechanism of hydrogen peroxide photoproduction by humic substances. *Environ. Sci. Technol.* **2012**, *46* (21), 11836–11843.

(293) Cooper, W. J.; Zlka, R. G.; Petasne, R. G.; Plane, J. M. C. Photochemical formation of H_2O_2 in natural waters exposed to sunlight. *Environ. Sci. Technol.* 1**988**, *22*, 1156-1160.

(294) Zhang, D.; Yan, S.; Song, W. Photochemically induced formation of reactive oxygen species (ROS) from effluent organic matter. *Environ. Sci. Technol.* **2014**, *48* (21), 12645–12653.

(295) Fujii, M.; Otani, E. Photochemical generation and decay kinetics of superoxide and hydrogen peroxide in the presence of standard humic and fulvic acids. *Water Res.* **2017**, *123*, 642–654.

(296) O. Sunday, M.; Takeda, K.; Sakugawa, H. Singlet oxygen photogeneration in coastal seawater: Prospect of large-scale modeling in seawater surface and its environmental significance. *Environ. Sci. Technol.* **2020**, *54* (10), 6125–6133.
(297) Chen, Y.; M Hozalski, R.; G Olmanson, L.; P Page, B.; C Finlay, J.; Brezonik, P.; A. Arnold, W. Prediction of photochemically produced reactive intermediates in surface waters via satellite remote sensing. *Environ. Sci. Technol.* **2020**, *54* (11), 6671-6681.

Chapter 2

Seasonal and spatial variability of dissolved carbon concentration and composition in Lake Michigan tributaries

2.1 Details on Collaboration

Chapter 2 is a collaboration between Stephanie Berg, Christina Remucal, Megan McConville, Robert Mooney, and Peter McIntyre. R.M. collected the samples and developed the models. M.M. and S.B. performed the analyses. S.B. wrote the manuscript with input from all coauthors.

2.2 Abstract

Dissolved organic matter (DOM) is a complex mixture of many compounds, and its composition dictates numerous reactions in the environment. Large lakes and marine coastlines receive DOM from watersheds that differ widely in their land cover, with potential implications for both the quantity and composition of carbon inputs. Seasonal variation in DOM quantity and composition may also differ among tributaries and be mediated by land cover. Here, we quantify spatial (i.e., among tributary) and temporal (i.e., among season) variation in DOM concentration, DOM composition based on ultraviolet-visible spectroscopy, and alkalinity across 101 tributaries of Lake Michigan, one of the world's largest lakes. Wetland land cover has the largest effect on DOM, producing high concentrations of DOM that is more aromatic and larger in apparent molecular weight. Seasonal variation is also pronounced, with concentrations and aromaticity of DOM peaking in fall across most tributaries. Watershed lithology and land cover both affect

inorganic carbon chemistry; alkalinity is associated with the geography of carbonate bedrock and is enhanced in urbanized watersheds. Watershed land cover has a larger affect than season on all four carbon parameters. However, seasonal variation is especially important for DOM composition. This disparity suggests that environmental processing of DOM within river channels mediates its composition more than its concentrations. Considering the wide range of land cover and lithology around Lake Michigan and other large water bodies, accounting for both spatial and temporal dynamics is essential for understanding controls on DOM delivery.

2.3 Introduction

Dissolved forms of carbon represent a significant portion of the global carbon pool.[1] Dissolved inorganic carbon (DIC), which exists as carbonate species in water, exchanges with carbon dioxide in the atmosphere and can be converted to and from dissolved organic matter (DOM) through a variety of processes.[2,3] DOM is a mixture of biologically-derived molecules that are diverse in their molecular composition, size, and properties. The composition of DOM depends on its original source (i.e., allochthonous inputs of terrestrial plant matter *versus* autochthonous material from algae and microbes) as well as processing via chemical[4] or biological reactions.[5] Anthropogenic pollution such as from leaching from impervious surfaces or wastewater discharge can further diversify DOM composition.[6,7]

DOM plays many key roles in aquatic environments, such as fueling microbial metabolism[2,8] and absorbing ultraviolet light entering the water.[9] It also mediates reactions that affect the fate of metals and organic contaminants through physical, chemical, and biological processes.[10–12] For example, DOM in surface waters can both decrease and enhance photochemical reactions that degrade persistent chemicals.[13] Importantly, the composition of DOM affects the rates and extent

of many of these reactions.[14,15] The composition of DOM also represents an important component of water quality as a whole. DOM in drinking water sources can be problematic because reactions with disinfectants such as chlorine and chloramine form toxic by-products.[16] Evidence shows these reactions are selective and the composition of DOM in source water affects by-product formation.[17]

Despite being among the largest lakes on Earth,[18] the Laurentian Great Lakes (hereafter Great Lakes) are strongly influenced by inflows of nutrients and carbon from tributaries.[19] Moreover, vast differences among tributaries in watershed land cover, discharge, and chemistry can create substantial differences in loads along the coastline of large lakes and seas.[20,21] Indeed, the observed spatial heterogeneity of nearshore nutrients and microbial metabolism within the Great Lakes is at least partially attributable to disparities in tributary inputs.[19,22] Recent work has addressed both spatial and temporal variation in tributary loading of nutrients across many Great Lakes tributaries revealing that small watersheds can have outsized influence on nearshore chemistry.[20,21] In contrast, variation in the quantity and composition of dissolved carbon inputs has received less attention across the spectrum of land cover, bedrock geology, and seasonal dynamics.

The concentration of dissolved organic carbon ([DOC]) is much more commonly reported in surface waters than measurements of its composition or concentrations of inorganic carbon. For example, previous research reports [DOC] in studies that take place over multiple years,[23,24] as a result of spatial variability,[25,26] as a function of season,[27] or variability due to a changing climate.[28–30] However, only a subset of existing [DOC] studies also include measurements of DOM composition (**Table A.1**).[31] While these studies provide useful data, an understanding of the variability in DOM composition across a wide spatial scale is critical for assessing its environmental reactivity.

Here we use ultraviolet-visible (UV-vis) spectroscopy to characterize DOM composition in tributaries of the Great Lakes. This technique is simple and inexpensive compared to other methods,[32] allowing us to consider differences in DOM composition across our entire data set. Additionally, UV-vis spectroscopy is the most commonly used technique for evaluating DOM composition and makes our results easily comparable to other studies.[33] Furthermore, the development of relationships between more complex DOM characterization (e.g., high-resolution mass spectrometry and nuclear magnetic resonance spectroscopy) and UV-vis measurements make UV-vis analysis even more informative.[34,35]

Here we evaluate patterns of both concentrations and composition of dissolved carbon reaching Lake Michigan during each season from 101 tributaries spanning its >2,000 km circumference, likely making the relationships discovered in this study more applicable to other sites. Our primary objectives are to test how land cover and seasonality give rise to spatiotemporal heterogeneity in DOM and to investigate how land cover, seasonality, and lithography affect alkalinity. We hypothesize that land cover influences concentrations of both organic and inorganic carbon as well as DOM composition, while alkalinity will additionally be affected by geology. These tributaries drain watersheds of vastly different size and land cover, so by sampling seasonally we can evaluate whether land cover effects override major swings in discharge, temperature, and carbon inputs to control both the quantity and composition of DOM. Our goal is to use these broad gradients in watershed context and seasonal conditions to disentangle the drivers of DOM composition from [DOC] and alkalinity, thereby yielding generalizable insights.

2.4 Materials and Methods

2.4.1 Materials and Sample Collection

Tributaries surrounding Lake Michigan were sampled in July (n = 97), and October (n = 99) of 2016 and January (n = 63) and March (n = 99) of 2017. The number of tributaries sampled during each season varied due to shifts in accessibility (e.g., ice cover during January). Surface water was collected at the road crossing closest to the mouth using bridge sampling methods.[36] Samples were immediately filtered through 0.45 μm nylon filters and stored in amber glass vials at 4 ºC. All chemical analyses were performed within one month of sample collection except where noted.

All glassware was combusted at 450 ºC for 8 hours to mineralize any trace amounts of organic carbon. Potassium hydrogen phthalate (ACS grade) and sulfuric acid (concentrated, ACS grade) were purchased from Fisher Scientific and used as received. All dilutions or blanks were prepared with ultra-pure water from a Milli-Q water purification system maintained at 18.2 MΩ cm.

2.4.2 Analytical Techniques

A Shimadzu total organic carbon analyzer was used to measure [DOC]. Each sample was injected four times and the results of the last three injections were averaged after confirming that the coefficient of variance was less than 10% for each sample. Alkalinity, which is a proxy for dissolved inorganic carbon concentration ([DIC]), was quantified by measuring the amount of 0.1 N H_2SO_4 required to reach an endpoint of pH 4.5 and is reported as $CaCO_3$ equivalents.[37] Ultraviolet-visible spectroscopy was used to measure the amount of light absorbed by the sample from 200 – 800 nm. A Shimadzu 2401PC recording spectrophotometer was used and spectra were

collected in 1 nm intervals. Water samples were referenced to ultra-pure water with absorbance from 700 – 800 nm subtracted. Samples whose absorbance values exceeded 1.5 at any wavelength were diluted with ultra-pure water. E_2:E_3 was calculated as the ratio of the absorbance at 250 nm to the absorbance at 365 nm and is inversely proportional to direct measurements of average molecular weight.[38] $SUVA_{254}$ (specific ultraviolet absorbance at 254 nm) was calculated by dividing the absorbance at 254 nm by the concentration of dissolved organic carbon. $SUVA_{254}$ is positively correlated to the aromaticity of DOM measured by nuclear magnetic resonance spectroscopy.[39]

It was necessary to rerun a subset of [DOC] samples that had been collected in the spring due to instrument malfunction. These samples had been frozen and thawed. To determine the effects of freezing and thawing on DOM analysis, 15 samples that had been successfully analyzed for both [DOC] and UV-vis spectroscopy in the spring were rerun after freezing and thawing and compared to their original values. A linear regression was performed that was then applied to the samples that only had their concentrations quantified after freezing and thawing. Further details and a demonstration of no preferential loss of carbon or change in optical properties is included in **Appendix A.1**.

2.4.3 Data Analysis

We determined the watershed area, % agricultural, % barren, % herbaceous, % forest, % shrubland, % urban, and % wetland for each of the 101 tributaries in the study with the Great Lakes Aquatic Habitat Framework (GLAHF).[18] A multiple linear regression (MLR) model was fitted to variation in each of our four carbon parameters: [DOC], alkalinity, $SUVA_{254}$, and E_2:E_3. Prior to any analysis, all values were $\log_{10}$ transformed to meet model assumptions. Each model included

terms for watershed area and three major land cover types (i.e., % agricultural, % urban, % wetland, which showed only modest collinearity and low variance inflation factors) as continuous independent variables, and the season of sample collection as a categorical independent variable. Only those tributaries that were sampled in all four seasons were included in this analysis (n = 56, 59, 55, and 53 for [DOC], E_2:E_3, $SUVA_{254}$, and alkalinity, respectively). Interactions were included to test whether effects of each land cover type varied with watershed area or season. Bayesian information criterion (BIC) was used to select a final reduced model for each carbon parameter.

Simple linear regressions of all data from each carbon parameter against every land cover type were used to make our results comparable to previous studies. We used Tukey's HSD to test for significant differences among seasons.

To specifically address the hypothesis that geology plays an important role in driving alkalinity in tributaries of Lake Michigan, we characterized the proportion of bedrock as carbonate using geological maps from the GLAHF.[40] We used MLR to test whether watershed area, season, and lithology have effects on alkalinity. We represented lithology using a binary classification of whether carbonate bedrock underlies >50% of the watershed. This simple approach was selected because most watersheds were made up of either predominantly carbonate or non-carbonate (e.g., shale, sandstone) bedrock.

To directly compare spatial and seasonal variations of each of the four carbon parameters, we calculated coefficients of variation for standard deviation of means from each season across all tributaries ($CV_{seasonal}$) and compared them to coefficients of variation for means of each tributary calculated across all four seasons ($CV_{spatial}$; **equations 1 and 2**). Further details of this calculation are described in **Appendix A.2**.

$CV_{spatial}$ = standard deviation of tributary means / mean of entire data set * 100 (**eq 2.1**)

$CV_{seasonal}$ = standard deviation of seasonal means / mean of entire data set * 100 (**eq 2.2**)

To prevent bias, only those tributaries that were sampled in all four seasons were included in this analysis.

2.5 Results and Discussion

2.5.1 Watershed Information

The watersheds surrounding Lake Michigan are diverse in terms of their size (3.1 km^2 to 16,469 km^2), predominant land cover, and geology. The three dominant types of land cover were urban (1.6 – 79.1%), agricultural (0 – 91.2%), and wetland (0.1 – 78.9%); forest (0.9 – 63.1%) and herbaceous (0 – 21.4%) were sometimes common, while barren (0 – 8.6%) and shrubland (0 – 6.1%) classes were always rare. Generally, watersheds with extensive wetlands are located around the northwestern part of Lake Michigan, while agriculture and urban land cover dominate the southern and eastern areas (**Figure 2.1**). Underlying bedrock includes crystalline igneous (0 – 38.3%), carbonate (0 – 100%), crystalline metamorphic (0 – 28.5%), iron formation (0 – 0.1%), sandstone (0 – 100%), shale (0 – 100%), and water (0 – 3.6%).

2.5.2 [DOC]

Dissolved organic carbon concentrations measured in the tributaries vary in space and by season. The mean [DOC] of the entire data set is 13.1 mg-C L^{-1} (n = 382). Generally, the highest [DOC] values are observed in the tributaries draining into the northwestern part of the lake (**Figure 2.1a**). Our DOC measurements fall within the ranges previously reported for tributaries of Lake Michigan[25,41] and other Great Lakes.[15,42]

Multiple linear regressions show that both land cover and the season of sample collection influence [DOC] in tributaries. Our reduced model includes terms for % agriculture, % urban, and % wetland in the watershed, as well as season (**Table A.2**). The % wetland in the watershed has the most significant positive effect on [DOC] (**Figure 2.1a**; **Table A.2**). Slope coefficients for urban and agricultural land cover are nearly an order of magnitude less than that of wetland land cover (**Table A.2**). The key contribution of wetland land cover to [DOC] is confirmed using simple linear regression; other land cover types were weakly negatively associated with [DOC] (**Figure A.3**). Watershed area is not a significant predictor of [DOC] across tributaries (**Table A.2**).

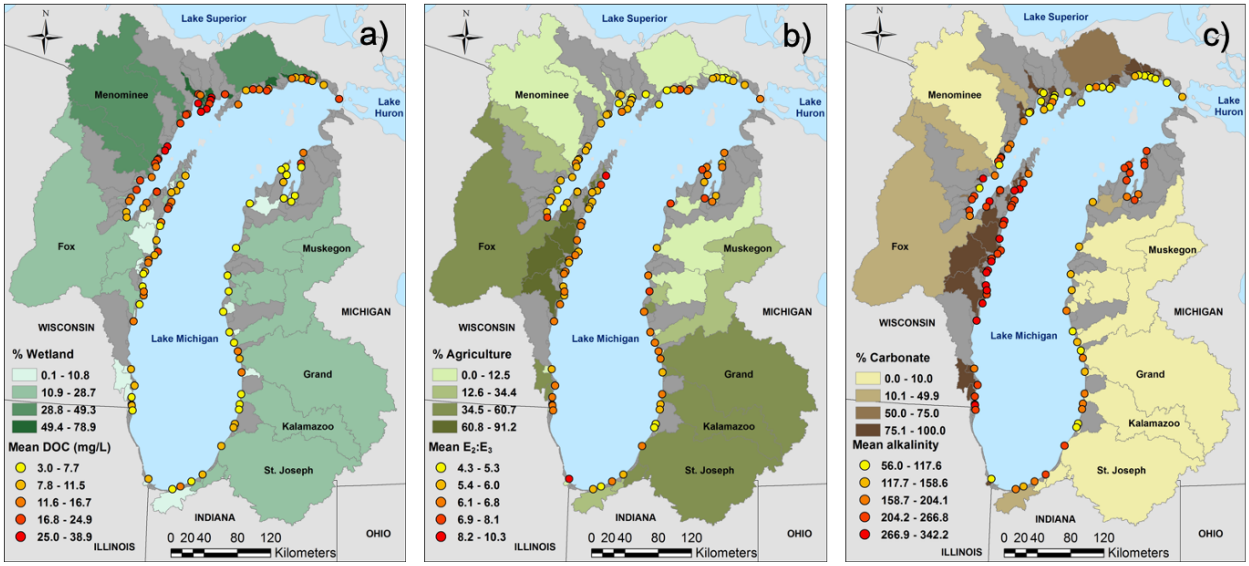

Figure 2.1. Maps of Lake Michigan tributaries and watersheds. Points represent tributaries sampled where the color corresponds to mean values of a) [DOC] in mg-C L^{-1}, b) E_2:E_3, and c) alkalinity in units of mg L^{-1} as $CaCO_3$ for all samples collected. Shading of the watersheds represents the % land cover of a) wetlands, b) agriculture, and c) % carbonate of the quaternary geology.

The primacy of wetlands as a source of DOM in watersheds is well established in the literature.[25,31,43–52] Water draining from wetlands draws upon carbon fixed in both terrestrial and aquatic ecosystems, and the slow rates of flow through saturated soils and shallow standing waters

allows ample opportunity for dissolution. There is less consensus about the role of other land cover types. We observe positive relationships between [DOC] and agriculture in the MLR model, in agreement with some studies[53,54] but not others.[41] Similarly, the positive relationship between [DOC] and urban land cover in our MLR models aligns with some earlier findings[6,55,56] but not others.[41] The MLR in this study does not consider forest land cover, but there is no obvious association of [DOC] with forest (**Figure A.3**). In other studies, % forest has been both positively[41] and negatively correlated to [DOC].[25,53]

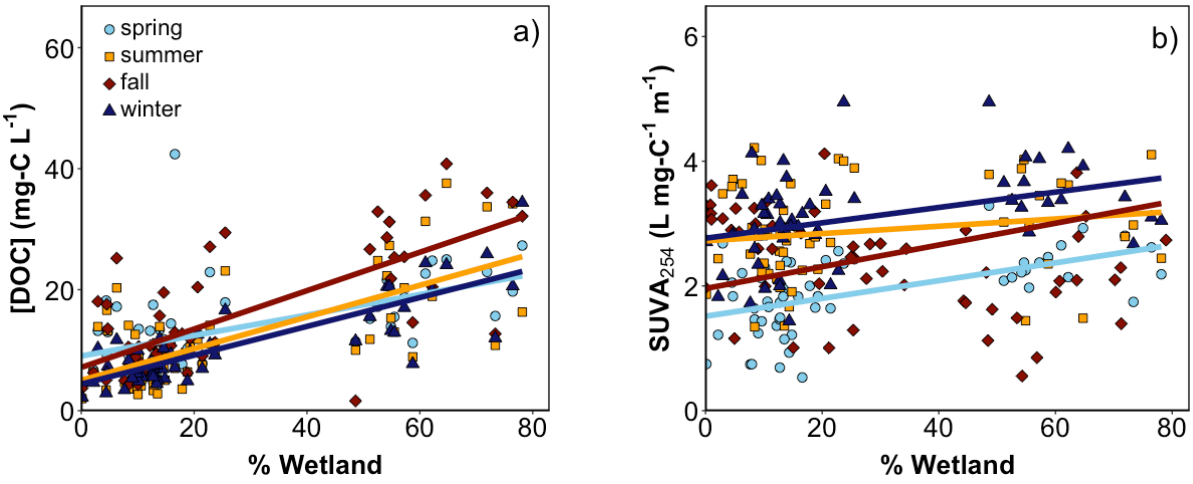

Figure 2.2. a) [DOC] and b) $SUVA_{254}$ versus % wetland in the watershed. Colors indicate season. Only tributaries sampled in all four seasons are included in this plot. Slopes, intercepts, and statistics for these plots are given in **Tables A.3** and **A.4**.

These inconsistencies across studies may be attributable to differences in sampling design, setting, and extent of comparisons (**Table A.1**). For example, McElmurry *et al.*[41] sampled surface runoff rather than stream channels. In addition, the types of statistics applied across data sets vary substantially with some groups using simple linear regressions[45,49,55] and others using MLR.[25,41,46–48,50–54,56] Even among the studies using MLR, the independent predictors tested and model selection methods vary widely (**Table A.1**).

Seasonality is also an important factor for [DOC]. Mean [DOC] in the tributaries increases in the order of winter < summer < spring < fall with values of 10.6, 11.9, 13.5, and 15.5 mg-C L^{-1}, respectively (**Figure 2.3a**; **Table A.9**). MLR, which accounts for many additional factors, indicates that [DOC] in the summer and winter is significantly lower than in fall (**Table A.2**). The different slopes of [DOC] among land cover types also affirm the importance of seasonality; the effect of wetlands was maximal in the fall compared to other seasons (**Figure 2.2a**).

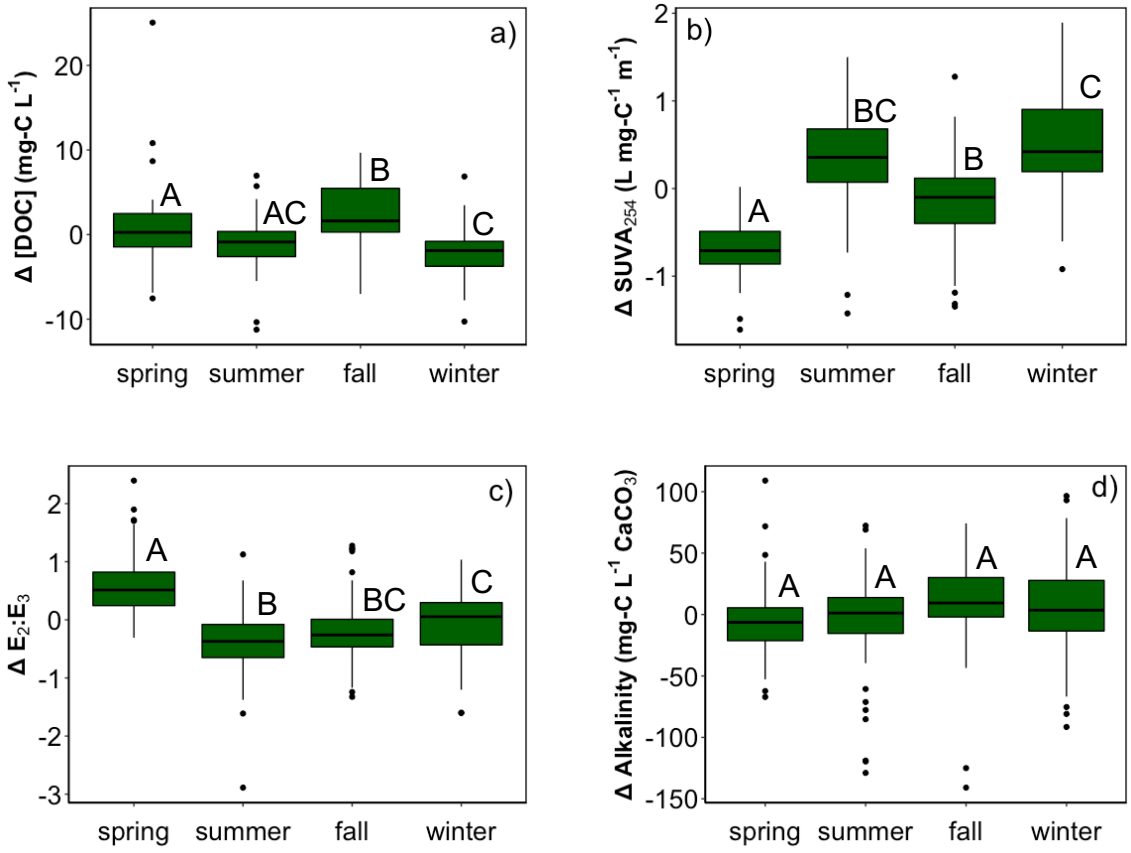

Figure 2.3. Differences (Δ) for a) [DOC], b) $SUVA_{254}$, c) E_2:E_3, and d) alkalinity. Only data from tributaries sampled in all four seasons are included. Letters indicate significant differences based on Tukey HSD comparisons.

Elevated [DOC] is frequently observed in the fall as organic compounds leach from leaf litter and other plant detritus in the water following the growing season.[26,27,50,57–61] The fall activities of fungi and bacteria may also contribute to releasing DOM into the water.[26] Increases

in the relative amount of terrestrial DOM is consistent with these hypotheses but cannot be assessed fully considering [DOC] alone. For example, the smaller amount of [DOC] observed in the winter samples may be consistent with either lower terrestrial inputs during this season or decreased microbial activity from autotrophs during the colder months.

2.5.3 DOM Composition

We observe a wide range of $SUVA_{254}$ values (0.35 to 4.95 L mg-C^{-1} m^{-1}) across Lake Michigan tributaries. The highest $SUVA_{254}$ values, which are indicative of terrestrially-derived DOM that has not been heavily processed,[39] are observed in tributaries draining into the northwest part of the lake, where wetland land cover dominates (**Figure A.4**). We also observe a wide range of E_2:E_3 values (3.6 to 12.0), where the upper end of the spectrum suggests either DOM originating from the aquatic ecosystem or heavily-processed terrestrially-derived molecules.[62] E_2:E_3 is highest the eastern and western sides of the lake (**Figure 2.1b**). In the remainder of this manuscript, we will refer to DOM composition as determined using optical parameters as proxies for aromaticity and molecular weight; no direct or molecular level analyses were performed.

The preferred MLR model for $SUVA_{254}$ includes season, % agriculture, % urban, and % wetland, along with interaction terms between the watershed area and both % urban and % wetland (**Table A.5**). Wetland has the strongest positive effects on $SUVA_{254}$ (**Figure 2.2b**; **Table A.5**). Interestingly, agricultural and urban land cover also lead to increased $SUVA_{254,}$ but the negative interaction terms indicate that these relationships become less important as the size of the watershed increases (**Table A.5**).

The strongest patterns in E_2:E_3 are attributable to seasonality, but wetland land cover and watershed size are significant correlates as well (**Table A.6**). E_2:E_3 increases with wetland

dominance, suggesting that DOM undergoes extensive processing upstream. There is also a significant negative interaction between wetlands and watershed area, which indicates that the influence of wetlands on E_2:E_3 is attenuated in large watersheds (**Figures A.7** and **A.8**; **Table A.6**).

$SUVA_{254}$ and E_2:E_3 are generally inversely proportional to one another,[63] and that is the case for Lake Michigan tributaries. When considered by land cover classes, the expected inverse relationship applied to all types except herbaceous land cover, which was uncommon in these watersheds (**Figures A.5** and **A.6**). This opposing relationship is not obvious considering the MLR results alone as the MLR for $SUVA_{254}$ and E_2:E_3 include different terms (**Tables A.5** and **A.6**). This result may be attributable to the fact that optical properties depend on both the source of the carbon and the extent of environmental processing of DOM.

Overall, the optical properties describing the composition of DOM show less spatial variability than [DOC]. The literature supports our observation that terrestrially-sourced DOM is consistently and positively correlated to % wetland using UV-vis spectroscopy[51] or fluorescence spectroscopy.[53,64,65] This observation is due to the large amount of plant-derived (i.e., allochthonous) carbon present in wetlands that is transferred into stream water. In addition, this organic carbon is fresh and therefore has had little opportunity to undergo environmental processing, which generally results in lower aromaticity.[66,67] Terrestrially-sourced DOM has also been correlated to other land cover types in the literature including % agriculture using UV-vis[41] and fluorescence spectroscopy,[53] as well as to % forest using UV-vis[41] and fluorescence spectroscopy.[65] Microbially-sourced (i.e., autochthonous) DOM or more environmentally processed DOM, which is represented with low $SUVA_{254}$ and high E_2:E_3 values in this study, has been correlated to % forest with fluorescence spectroscopy,[68] to % urban with both UV-vis[41] and fluorescence spectroscopy,[6,69,70], and to % agriculture with UV-vis spectroscopy (**Table A.1**).[54]

Seasonality has important effects on both $SUVA_{254}$ and $E_2:E_3$. Mean $SUVA_{254}$ values increase in order of spring < fall < summer < winter, with values of 1.98, 2.49, 2.95, and 3.10 L mg-C^{-1} m^{-1}, respectively (**Figure 2.3b**; **Table A.10**). The MLR for $SUVA_{254}$ similarly demonstrates that values in the spring are lowest and values in summer and winter are higher than those in the fall (**Table A.5**). Seasonal means for $E_2:E_3$ increase in order of summer < fall < winter < spring, with values of 5.70, 5.92, 6.02, and 6.71, respectively (**Figure 2.3c**; **Table A.11**). In the MLR, values in spring are lower than those in the fall (**Table A.6**).

Ours is among the first studies to analyze the seasonal dynamics of organic matter composition in parallel with concentration across a wide range of streams (**Table A.1**) and shows clear evidence of seasonal variation in DOM composition as well as concentrations. Previous reports of seasonal variation in DOM composition have been mixed, ranging from no effects observed using fluorescence spectroscopy,[68] to decreasing $SUVA_{254}$ over the warm months (i.e., spring to fall)[27,71],[27,72] increasing absorbance during the spring snowmelt,[73,74] and higher $E_2:E_3$ in the winter as compared to summer.[75] Most likely, these variable seasonal patterns are due to complex interactions between land cover and climatic seasonality.

The seasonal dynamics of DOM optical properties should reflect a combination of carbon sources, environmental processing of organic carbon, and dilution by hydrological fluctuations. High $SUVA_{254}$ values in the fall can be partially explained by leaching from newly-arrived leaf litter,[26] though only a modest proportion of watershed area in Lake Michigan tributaries is vegetated with deciduous trees. Conversely, we observe high $E_2:E_3$ and low $SUVA_{254}$ in the spring when new plant growth is only just starting in this region, leaving DOM pools dependent on older, more processed, forms of organic carbon. We also see the signature of microbial activity in the DOM composition proxies. Both heterotrophic respiration of DOM and autotrophic production of

DOM produces DOM with lower molecular weight (i.e., higher E_2:E_3) and lower aromaticity (i.e., lower $SUVA_{254}$),[26,76] and we see these shifts across most tributaries in the spring when terrestrial inputs are minimal but microbes are able to resume their activity under warming temperatures. Photobleaching also results in decreased $SUVA_{254}$ and increased E_2:E_3[38,42,57,62,74,77–79] and could be most influential around the time of our spring sampling when there is little canopy cover. However, if this were the primary driving factor, low $SUVA_{254}$ and high E_2:E_3 would also be expected in the winter in tributaries without ice cover. Our winter results are also interesting because both optical properties showed high values, which could reflect either the dominance of small, aromatic compounds or large compounds that are not aromatic. Since no new terrestrial inputs are expected during the winter, these compounds are likely either microbially-derived or other highly recalcitrant compounds.

2.5.4 Alkalinity

Alkalinity is a measurement for DIC because carbonate species are the main buffering components in natural waters.[80] In this study, alkalinity ranges from 11.6 to 468 mg L^{-1} as $CaCO_3$ L^{-1}, with a mean of 197 mg L^{-1} as $CaCO_3$. Alkalinity significantly correlates with certain land cover types (**Figure A.10**). The best MLR model includes terms for % agriculture, % urban, watershed area, and an interaction term between agriculture and watershed area (**Table A.7**). We observe the highest alkalinity values along the western side of Lake Michigan (**Figure 2.1c**), where urban land cover predominates and limestone beds are common.[81] The positive association between alkalinity and urban land cover may be augmented by weathering of concrete.[82]

In addition to the influence of land cover on alkalinity, bedrock lithology also plays a mediating role. Watersheds that are dominated by carbonate bedrock have significantly higher

alkalinity than those where shale and sandstone predominate (**Table A.8**), in keeping with previous findings.[83] We find a negative statistical interaction between watershed area, which generally increases alkalinity, and our binary carbonate variable, presumably resulting from the diversity of bedrock lithologies in large watersheds (**Figure 2.1c**). While it is clear that carbonate weathering is an important control on alkalinity in tributaries, especially in small watersheds, it would be ideal to have carbon isotope data to address other potential sources of alkalinity such as organic matter oxidation and gaseous CO_2.[84] Interestingly, there are some wetland-dominated watersheds located on the northern end of Lake Michigan that have high % watershed carbonate but low alkalinity (**Figure 2.1c**). These sites may support unusually high autotrophic growth (e.g., calcareous mosses) that draws down DIC, or have their limestone bedrock capped by sediment that limits dissolution and exchange with stream water.

The mean alkalinity increases in the order of spring < summer < winter < fall (**Figure 2.3d**; **Table A.12**). However, the best MRL model does not include seasonal effects, nor were pairwise differences statistically significant. This further suggests that geology, rather than land cover or seasonality, is the main driver of alkalinity (**Tables A.8** and **A.12**). The emergence of urban land cover as correlate of alkalinity is presumably attributable to the dissolution of concrete, which appears to have no strong seasonal signal. In addition, in the geology MLR, carbonate material is positively correlated to alkalinity which also does not change with season.

2.5.5 Spatial/Seasonal Comparison

One of the primary objectives of this study is to compare spatial versus seasonal variation in both concentration and composition of DOM and alkalinity in Lake Michigan tributaries. Our MLR models suggest that differences among watersheds land cover have the most predictable

effect on concentration parameters (i.e., [DOC] and alkalinity), while seasonality has more consistent influence on DOM composition (i.e., $SUVA_{254}$ and E_2:E_3). In fact, only seasonal effects were statistically significant for E_2:E_3 when complex interaction terms are excluded. To further partition dissolved carbon variation among watersheds and seasons, we compare coefficients of variation association with our spatial versus seasonal observations.

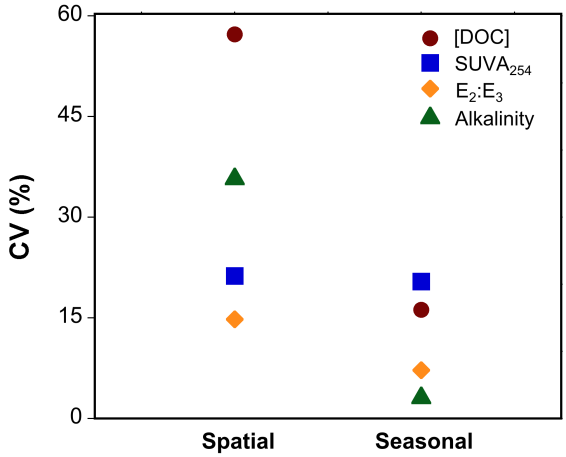

Figure 2.4. Coefficients of variation, $CV_{spatial}$ and $CV_{seasonal}$, for [DOC], alkalinity, $SUVA_{254}$, and E_2:E_3 measured in tributaries that were sampled in all four seasons.

For all four parameters tested, $CV_{spatial} > CV_{seasonal}$ (**Figure 2.4**). However, the difference in magnitude between spatial and seasonal CV is modest for the compositional parameters $SUVA_{254}$ and E_2:E_3. Thus, we infer that seasonal variation across sites creates almost as much variation in DOM composition as the myriad differences in watershed area, land cover, human population density, and other factors. In contrast, dissolved organic and inorganic carbon concentrations are primarily a reflection of disparities among watersheds, and show limited seasonal signal.

The differential partitioning of spatial and seasonal variation between carbon concentrations and composition is an important insight arising from our relatively comprehensive sampling approach and underscores the distinction between carbon sourcing and carbon processing. Contrasts in carbon source among watersheds are presumably stable across seasons, such that land cover and its correlates drive most variation in DOM concentrations, and bedrock lithology and urban concrete strongly influence alkalinity. We recognize that microbial and plant production of DOM varies widely throughout the year due to temperature, seasonal tissue senescence (e.g., leaf fall), water availability and flow paths, and other factors, so it is interesting that such temporal dynamics create only modest signals in [DOC].

The comparable magnitude of seasonal- and watershed-scale variation in DOM composition suggests that substantial temporal variation in the processing of DOM in aquatic environments is overlaid on seasonality of carbon inputs. Our optical proxies for the aromaticity and size of organic carbon molecules show clear seasonal variation that accords with differences in molecular weight and aromaticity. Although we have no data on process rates in these tributaries, the seasonal shifts in DOM composition are large enough to signify more than just fluctuations in the magnitude and source of inputs. A host of biological and chemical reactions convert DOM from one form to another, which would result in minor shifts in overall [DOC] but substantial changes in $SUVA_{254}$ and E_2:E_3. For instance, conversion of newly-leached allochthonous DOM transforms into more recalcitrant DOM is a well-recognized process that occurs primarily in the fall season. Our seasonal measurements across the tributaries suggests that such DOM processing produces a strong signature in the annual cycle of dissolved carbon availability and composition across the Lake Michigan basin.

2.6 Conclusions and Implications

We have documented extensive spatial and temporal variation in both concentration and composition of carbon forms across Lake Michigan tributaries. Our results show that land cover, lithology, and other differences among watersheds play a strong role in dictating both carbon concentrations and the optical properties of DOM, whereas seasonal dynamics affect the molecular composition of DOM more strongly than its abundance or alkalinity. By extending our sampling through all four seasons, we also detect complex interactions between watershed attributes and seasonality that will require further work to understand. Taken together, our extensive survey captures strong signals of both spatial and seasonal drivers of stream carbon dynamics, underscoring the fact that local-scale variation must be interpreted in light of both landscape and temporal context. Nonetheless, the parallel patterns of land cover and seasonal influences across so many discrete watersheds suggests a strong capacity for generalization within this geographic region.

As land cover and weather seasonality are shifting across the globe, there is a pressing need to understand the implications for carbon processing.[6] The dynamic and interactive effects of spatial (i.e., between watershed) and temporal (i.e., between season) factors documented in this study underscore the complexity of environmental controls on aquatic carbon, yet the strong signals of land cover and seasonal succession also offer hope for interpreting and predicting future carbon processing. Both land cover and climate are changing throughout much of the Great Lakes basin,[85,86] so corresponding changes in dissolved carbon concentrations and composition are to be expected. The strong influence of wetland areas on DOM are particularly noteworthy because these extensive, water-saturated environments are sensitive to climate change and local human activities. Ultimately, we must also consider the net effect of these changes on the Great Lakes

themselves, whose coastal ecosystems are strongly affected by the chemistry of inflowing tributaries.[21] Indeed, the seasonal swings in DOM concentrations documented here should be sufficient to measure by remote sensing, creating the possibility of higher-frequency observations than are feasible using extensive field surveys like ours. Integrating mechanistic perspectives and large-scale observational studies, whether in situ or remotely sensed, is a critical frontier in predicting the dynamics of dissolved carbon sources and processing across heterogenous landscapes like the Lake Michigan basin.

2.7 Acknowledgements

Authors declare no conflicts of interest. SMB was supported by NSF CBET (1802388). Additional funding for this work was provided by a Department of Interior Northeast Climate Adaptation Science Center graduate fellowship to RJM. Additional funds were provided to RJM through a UW-Madison Department of Zoology Graduate Fellowship. We also acknowledge Joseph Brunner and Gabrielle Campagnola for their assistance with data collection, and Lucas Gloege, Andrew Stevens, Thomas Shannon, and Joshua Kalman for their assistance with tributary sampling. Appendix A includes additional information about methods and model outputs.

2.8 References

(1) Cole, J. J.; Prairie, Y. T.; Caraco, N. F.; McDowell, W. H.; Tranvik, L. J.; Striegl, R. G.; Duarte, C. M.; Kortelainen, P.; Downing, J. A.; Middelburg, J. J.; Melack, J. Plumbing the global carbon cycle: Integrating inland waters into the terrestrial carbon budget. *Ecosystems* **2007**, *10* (1), 171–184.

(2) Ward, C. P.; Nalven, S. G.; Crump, B. C.; Kling, G. W.; Cory, R. M. Photochemical alteration of organic carbon draining permafrost soils shifts microbial metabolic pathways and stimulates respiration. *Nat. Commun.* **2017**, *8* (1), 1-8.

(3) Granéli, W.; Lindell, M.; Tranvik, L. Photo-oxidative production of dissolved inorganic carbon in lakes of different humic content. *Limnol. Oceanogr.* **1996**, *41* (4), 698–706.

(4) Gonsior, M.; Peake, B. M.; Cooper, W. T.; Podgorski, D.; D'Andrilli, J.; Cooper, W. J.

Photochemically induced changes in dissolved organic matter identified by ultrahigh resolution Fourier transform ion cyclotron resonance mass spectrometry. *Environ. Sci. Technol.* **2009**, *43* (3), 698–703.

(5) D'Andrilli, J.; Cooper, W. T.; Foreman, C. M.; Marshall, A. G. An ultrahigh-resolution mass spectrometry index to estimate natural organic matter lability. *Rapid Commun. Mass Spectrom.* **2015**, *29* (24), 2385–2401.

(6) Hosen, J. D.; McDonough, O. T.; Febria, C. M.; Palmer, M. A. Dissolved organic matter quality and bioavailability changes across an urbanization gradient in headwater streams. *Environ. Sci. Technol.* **2014**, *48* (14), 7817–7824.

(7) Bodhipaksha, L. C.; Sharpless, C. M.; Chin, Y. P.; MacKay, A. A. role of effluent organic matter in the photochemical degradation of compounds of wastewater origin. *Water Res.* **2017**, *110*, 170–179.

(8) Lovely, Derek R.; Coates, John D.; Blunt-Harris, Elizabeth L.; Phillips, Elizabeth J. P.; Woodward, J. C. Humic substances as electron acceptors for microbial respiration. *Lett. to Nature.* **1996**, *382*, 445–448.

(9) Steinberg, Deborah K.; Neson, Norman B.; Carlson, Craig A.; Prusak, A. C. Production of chromophoric dissolved organic matter (CDOM) in the open ocean by zooplankton and the colonial *Cyanobacterium trichodesmium* spp. *Mar. Ecol. Prog. Ser.* **2004**, *267*, 45–59.

(10) Raeke, J.; Lechtenfeld, O. J.; Seiwert, B.; Meier, T.; Riemenschneider, C.; Reemtsma, T. Photochemically induced bound residue formation of carbamazepine with dissolved organic matter. *Environ. Sci. Technol.* **2017**, *51* (10), 5523–5530.

(11) Aiken, G. R.; Hsu-Kim, H.; Ryan, J. N. Influence of dissolved organic matter on the environmental fate of metals, nanoparticles, and colloids. *Environ. Sci. Technol.* **2011**, *45* (8), 3196–3201.

(12) Zhao, L.; Chen, H.; Lu, X.; Lin, H.; Christensen, G. A.; Pierce, E. M.; Gu, B. Contrasting effects of dissolved organic matter on mercury methylation by *Geobacter sulfurreducens* PCA and *Desulfovibrio desulfuricans* ND132. *Environ. Sci. Technol.* **2017**, *51* (18), 10468-10475.

(13) Remucal, C. K. The role of indirect photochemical degradation in the environmental fate of pesticides: A review. *Environ. Sci.: Processes and Impacts*. **2014**, 16, 628–653.

(14) Maizel, A. C.; Li, J.; Remucal, C. K. Relationships between dissolved organic matter composition and photochemistry in lakes of diverse trophic status. *Environ. Sci. Technol.* **2017**, *51* (17), 9624–9632.

(15) Berg, S. M.; Whiting, Q. T.; Herrli, J. A.; Winkels, R.; Wammer, K. H.; Remucal, C. K. The role of dissolved organic matter composition in determining photochemical reactivity at the molecular level. *Environ. Sci. Technol.* **2019**.

(16) Bulman, D. M.; K. Remucal, C. Role of reactive halogen species in disinfection byproduct formation during chlorine photolysis. *Environ. Sci. Technol.* **2020**, *54* (15), 9629-9639.

(17) Lavonen, E. E.; Gonsior, M.; Tranvik, L. J.; Schmitt-Kopplin, P.; Köhler, S. J. Selective chlorination of natural organic matter: Identification of previously unknown disinfection byproducts. *Environ. Sci. Technol.* **2013**, *47* (5), 2264–2271.

(18) Forsyth, D. K.; Riseng, C. M.; Wehrly, K. E.; Mason, L. A.; Gaiot, J.; Hollenhorst, T.; Johnston, C. M.; Wyrzykowski, C.; Annis, G.; Castiglione, C.; Todd, K.; Robertson, M.; Infante, D. M.; Wang, L.; McKenna, J. E.; Whelan, G. The Great Lakes hydrography dataset: Consistent, binational watersheds for the Laurentian Great Lakes Basin. *J. Am. Water Resour. Assoc.* **2016**, *52* (5), 1068–1088.

(19) Marcarelli, A. M.; Coble, A. A.; Meingast, K. M.; Kane, E. S.; Brooks, C. N.; Buffam, I.; Green, S. A.; Huckins, C. J.; Toczydlowski, D.; Stottlemyer, R. Of small streams and Great Lakes: Integrating tributaries to understand the ecology and biogeochemistry of Lake Superior. *J. Am. Water Resour. Assoc.* **2019**, *55* (2), 442–458.
(20) Gloege, L.; McKinley, G. A.; Mooney, R. J.; Allan, J. D.; Diebel, M. W.; McIntyre, P. B. Lake hydrodynamics intensity the potential impact of watershed pollutants on coastal ecosystem services. *Environ. Res. Lett.* **2020**, *15,* 1–28.
(21) Mooney, R. J.; Stanley, E. H.; Rosenthal, W. C.; Esselman, P. C.; Kendall, A. D.; McIntyre, P. B. Outsized nutrient contributions from small tributaries to a Great Lake. *Proc. Natl. Acad. Sci.* **2020**, *117* (45), 28175–28182.
(22) Stephens, B. M.; Minor, E. C. DOM Characteristics along the continuum from river to receiving basin: A comparison of freshwater and saline transects. *Aquat. Sci.* **2010**, *72* (4), 403–417.
(23) Jane, S. F.; Winslow, L. A.; Remucal, C. K.; Rose, K. C. Long-term trends and synchrony in dissolved organic matter characteristics in Wisconsin, USA, Lakes: Quality, not quantity, is highly sensitive to climate. *J. Geophys. Res. Biogeosciences* **2017**, *122* (3), 546–561.
(24) Strock, K. E.; Theodore, N.; Gawley, W. G.; Ellsworth, A. C.; Saros, J. E. Increasing dissolved organic carbon concentrations in northern boreal lakes: Implications for lake water transparency and thermal structure. *J. Geophys. Res. Biogeosciences* **2017**, *122* (5), 1022–1035.
(25) Frost, P. C.; Larson, J. H.; Johnston, C. A.; Young, K. C.; Maurice, P. A.; Lamberti, G. A.; Bridgham, S. D. Landscape predictors of stream dissolved organic matter concentration and physicochemistry in a Lake Superior river watershed. *Aquat. Sci.* **2006**, *68* (1), 40–51.
(26) Mulholland, P. J.; Hill, W. R. Seasonal patterns in streamwater nutrient and dissolved organic carbon concentrations: Separating catchment flow path and in-stream effects. *Water Resour. Res.* **1997**, *33* (6), 1297–1306.
(27) McCabe, A. J.; Arnold, W. A. Seasonal and spatial variabilities in the water chemistry of prairie pothole wetlands influence the photoproduction of reactive intermediates. *Chemosphere* **2016**, *155*, 640–647.
(28) Weyhenmeyer, G. A.; Karlsson, J. Nonlinear response of dissolved organic carbon concentrations in boreal lakes to increasing temperatures. *Limnol. Oceanogr.* **2009**, *54* (6), 2513–2519.
(29) Freeman, C.; Fenner, N.; Ostle, N. J.; Kang, H.; Dowrick, D. J.; Reynolds, B.; Lock, M. A.; Sleep, D.; Hughes, S.; Hudson, J. Export of dissolved organic carbon from peatlands under elevated carbon dioxide levels. *Nature* **2004**, *430* (6996), 195–198.
(30) Schelker, J.; Eklöf, K.; Bishop, K.; Laudon, H. Effects of forestry operations on dissolved organic carbon concentrations and export in boreal first-order streams. *J. Geophys. Res. Biogeosciences* **2012**, *117* (1).
(31) Dalmagro, H. J.; Johnson, M. S.; de Musis, C. R.; Lathuillière, M. J.; Graesser, J.; Pinto-Júnior, O. B.; Couto, E. G. Spatial patterns of DOC concentration and DOM optical properties in a Brazilian tropical river-wetland system. *J. Geophys. Res. Biogeosciences* **2017**, *122* (8), 1883–1902.
(32) Minor, E. C.; Swenson, M. M.; Mattson, B. M.; Oyler, A. R. Structural characterization of dissolved organic matter: A review of current techniques for isolation and analysis. *Environ. Sci. Process. Impacts* **2014**, *16*, 2064–2079.
(33) Chin, Y. P.; Alken, G.; O'Loughlin, E. Molecular weight, polydispersity, and spectroscopic

properties of aquatic humic substances. *Environ. Sci. Technol.* **1994**, *28* (11), 1853–1858.
(34) Kellerman, A. M.; Kothawala, D. N.; Dittmar, T.; Tranvik, L. J. Persistence of dissolved organic matter in lakes related to its molecular characteristics. *Nat. Geosci.* **2015**, *8* (6), 454–457.
(35) Nebbioso, A.; Piccolo, A. Molecular characterization of dissolved organic matter (DOM): A critical review. *Anal. Bioanal. Chem*. **2013**, *405*, 109–124.
(36) Decker, C.; Simmons, K. Surface water sampling. *USEPA Publication.* **2013**, 1–22.
(37) Yakushev, E. Alkalinity. *Standard Methods for the Examination of Water and Wastewater*. **1999**.
(38) Helms, J. R.; Stubbins, A.; Ritchie, J. D.; Minor, E. C.; Kieber, D. J.; Mopper, K. Absorption spectral slopes and slope ratios as indicators of molecular weight, source, and photobleaching of chromophoric dissolved organic matter. *Limnol. Oceanogr.* **2008**, *53* (3), 955–968.
(39) Weishaar, J.; Aiken, G.; Bergamaschi, B.; Fram, M.; Fujii, R.; Mopper, K. Evaluation of specific ultra-violet absorbance as an indicator of the chemical content of dissolved organic carbon. *Environ. Sci. Technol.* **2003**, *37* (20), 4702–4708.
(40) Hu, Y.; Lu, Y. H.; Edmonds, J. W.; Liu, C.; Wang, S.; Das, O.; Liu, J.; Zheng, C. Hydrological and land use control of watershed exports of dissolved organic matter in a large arid river basin in northwestern China. *J. Geophys. Res. Biogeosciences* **2016**, *121* (2), 466–478.
(41) McElmurry, S. P.; Long, D. T.; Voice, T. C. Stormwater dissolved organic matter: Influence of land cover and environmental factors. *Environ. Sci. Technol.* **2014**, *48* (1), 45–53.
(42) Minor, E.; Stephens, B. Dissolved organic matter characteristics within the Lake Superior watershed. *Org. Geochem.* **2008**, *39* (11), 1489–1501.
(43) Kortelainen, P.; Saukkonen, S. Organic vs. minerogenic acidity in headwater streams in Finland. *Water, Air, Soil Pollut.* **1995**, *85* (2), 559–564.
(44) Palviainen, M.; Lauren, A.; Launiainen, S.; Piirainen, S. Predicting the export and concntrations of organic carbon, nitrogen and phosphorus in boreal lakes by catchment characterististics and land use: A practical approach. *AMBIO A J. Hum. Environ.* **2016**, *45* (8), 933-945.
(45) Cawley, K. M.; Campbell, J.; Zwilling, M.; Jaffé, R. Evaluation of forest disturbance legacy effects on dissolved organic matter characteristics in streams at the Hubbard Brook Experimental Forest, New Hampshire. *Aquat. Sci.* **2014**, *76* (4), 611–622.
(46) Clark, M. J.; Cresser, M. S.; Smart, R.; Chapman, P. J.; Edwards, A. C. The influence of catchment characteristics on the seasonality of carbon and nitrogen species concentrations in upland rivers of Northern Scotland. *Biogeochemistry*. **2004**l, *68*, 1-19.
(47) Dillon, P. J.; Molot, L. A. Effect of landscape form on export of dissolved organic carbon, iron, and phosphorus from forested stream catchments. *Water Resour. Res.* **1997**, *33* (11), 2591–2600.
(48) Mattsson, T.; Kortelainen, P.; Räike, A. Export of DOM from boreal catchments: Impacts of land use cover and climate. *Biogeochemistry* **2005**, *76* (2), 373–394.
(49) Eckhardt, B. W.; Moore, T. R. Controls on dissolved organic carbon concentrations in streams, Southern Quebec. *Can. J. Fish. Aquat. Sci.* **1990**, *47* (8), 1537–1544.
(50) Flint, S. A.; McDowell, W. H. Effects of headwater wetlands on dissolved nitrogen and dissolved organic carbon concentrations in a suburban New Hampshire watershed. *Freshw. Sci.* **2015**, *34* (2), 456–471.

(51) Hanley, K. W.; Wollheim, W. M.; Salisbury, J.; Huntington, T.; Aiken, G. Controls on dissolved organic carbon quantity and chemical character in temperate rivers of North America. *Global Biogeochem. Cycles* **2013**, *27* (2), 492–504.
(52) Xenopoulos, M. A.; Lodge, D. M.; Frentress, J.; Kreps, T. A.; Bridgham, S. D.; Grossman, E.; Jackson, C. J. Regional comparisons of watershed determinants of dissolved organic carbon in temperate lakes from the upper Great Lakes region and selected regions globally. *Limnol. Ocean.* **2003**, *48* (6), 2321–2334.
(53) Graeber, D.; Gelbrecht, J.; Pusch, M. T.; Anlanger, C.; von Schiller, D. Agriculture has changed the amount and composition of dissolved organic matter in central European headwater streams. *Sci. Total Environ.* **2012**, *438*, 435–446.
(54) Shang, P.; Lu, Y. H.; Du, Y. X.; Jaffé, R.; Findlay, R. H.; Wynn, A. Climatic and watershed controls of dissolved organic matter variation in streams across a gradient of agricultural land use. *Sci. Total Environ.* **2018**, *612*, 1442–1453.
(55) Aitkenhead-Peterson, J. A.; Steele, M. K.; Nahar, N.; Santhy, K. Dissolved organic carbon and nitrogen in urban and rural watersheds of south-central Texas: Land use and land management influences. *Biogeochemistry* **2009**, *96* (1), 119–129.
(56) Alvarez-Cobelas, M.; Angeler, D. G.; Sánchez-Carrillo, S.; Almendros, G. A worldwide view of organic carbon export from catchments. *Biogeochemistry* **2012**, *107* (1–3), 275–293.
(57) Aulló-Maestro, M. E.; Hunter, P.; Spyrakos, E.; Mercatoris, P.; Kovács, A.; Horváth, H.; Preston, T.; Présing, M.; Palenzuela, J. T.; Tyler, A. Spatio-seasonal variability of chromophoric dissolved organic matter absorption and responses to photobleaching in a large shallow temperate lake. *Biogeosciences* **2017**, *14* (5), 1215–1233.
(58) Dawson, J. J. C.; Tetzlaff, D.; Speed, M.; Hrachowitz, M.; Soulsby, C. Seasonal controls on DOC dynamics in nested upland catchments in NE Scotland. *Hydrol. Process.* **2011**, *25* (10), 1647–1658.
(59) Liu, W.; Xu, X.; McGoff, N. M.; Eaton, J. M.; Leahy, P.; Foley, N.; Kiely, G. Spatial and seasonal variation of dissolved organic carbon (DOC) concentrations in Irish streams: Importance of soil and topography characteristics. *Environ. Manage.* **2014**, *53* (5), 959–967.
(60) Mattsson, T.; Kortelainen, P.; Räike, A.; Lepistö, A.; Thomas, D. N. Spatial and temporal variability of organic C and N concentrations and export from 30 boreal rivers induced by land use and climate. *Sci. Total Environ.* **2015**, *508*, 145–154.
(61) Oni, S. K.; Futter, M. N.; Molot, L. A.; Dillon, P. J. Adjacent catchments with similar patterns of land use and climate have markedly different dissolved organic carbon concentration and runoff dynamics. *Hydrol. Process.* **2014**, *28* (3), 1436–1449.
(62) Helms, J. R.; Mao, J.; Stubbins, A.; Schmidt-Rohr, K.; Spencer, R. G. M.; Hernes, P. J.; Mopper, K. Loss of optical and molecular indicators of terrigenous dissolved organic matter during long-term photobleaching. *Aquat. Sci.* **2014**, *76* (3), 353–373.
(63) Fichot, C. G.; Benner, R. A novel method to estimate DOC concentrations from CDOM absorption coefficients in coastal waters. *Geophys. Res. Lett.* **2011**, *38* (3), 1–5.
(64) Williams, C. J.; Yamashita, Y.; Wilson, H. F.; Jaffe, R.; Xenopoulos, M. A. Unraveling the role of land use and microbial activity in shaping dissolved organic matter characteristics in stream ecosystems. *Limnol. Oceanogr.* **2010**, *55* (3), 1159–1171.
(65) Singh, S.; Dash, P.; Silwal, S.; Feng, G.; Adeli, A.; Moorhead, R. J. Influence of land use and land cover on the spatial variability of dissolved organic matter in multiple aquatic

environments. *Environ. Sci. Pollut. Res.* **2017**, *24* (16), 14124–14141.
(66) Helms, J. R.; Stubbins, A.; Perdue, E. M.; Green, N. W.; Chen, H.; Mopper, K. Photochemical bleaching of oceanic dissolved organic matter and its effect on absorption spectral slope and fluorescence. *Mar. Chem.* **2013**, *155*, 81–91.
(67) Minor, E. C.; Dalzell, B. J.; Stubbins, A.; Mopper, K. Evaluating the photoalteration of estuarine dissolved organic matter using direct temperature-resolved mass spectrometry and UV-visible spectroscopy. *Aquat. Sci.* **2007**, *69* (4), 440–455.
(68) Heinz, M.; Graeber, D.; Zak, D.; Zwirnmann, E.; Gelbrecht, J.; Pusch, M. T. Comparison of organic matter composition in agricultural versus forest affected headwaters with special emphasis on organic nitrogen. *Environ. Sci. Technol.* **2015**, *49* (4), 2081–2090.
(69) Chen, H.; Liao, Z. L.; Gu, X. Y.; Xie, J. Q.; Li, H. Z.; Zhang, J. Anthropogenic influences of paved runoff and sanitary sewage on the dissolved organic matter quality of wet weather overflows: An excitation-emission matrix parallel factor analysis assessment. *Environ. Sci. Technol.* **2017**, *51* (3), 1157–1167.
(70) Lu, Y. H.; Bauer, J. E.; Canuel, E. A.; Chambers, R. M.; Yamashita, Y.; Jaffé, R.; Barrett, A. Effects of land use on sources and ages of inorganic and organic carbon in temperate headwater streams. *Biogeochemistry* **2014**, *119* (1–3), 275–292.
(71) Müller, R. A.; Kothawala, D. N.; Podgrajsek, E.; Sahlée, E.; Koehler, B.; Tranvik, L. J.; Weyhenmeyer, G. A. Hourly, daily, and seasonal variability in the absorption spectra of chromophoric dissolved organic matter in a eutrophic, humic lake. *J. Geophys. Res. Biogeosciences.* **2014**, 1985–1998.
(73) Cao, X.; Aiken, G. R.; Spencer, R. G. M.; Butler, K.; Mao, J.; Schmidt-Rohr, K. Novel insights from NMR spectroscopy into seasonal changes in the composition of dissolved organic matter exported to the Bering Sea by the Yukon River. *Geochim. Cosmochim. Acta* **2016**, *181*, 72–88.
(74) Macdonald, M. J.; Minor, E. C. Photochemical degradation of dissolved organic matter from streams in the western Lake Superior watershed. *Aquat. Sci.* **2013**, *75* (4), 509–522.
(75) Yates, C. A.; Johnes, P. J.; Spencer, R. G. M. Assessing the drivers of dissolved organic matter export from two contrasting lowland catchments, U.K. *Sci. Total Environ.* **2016**, *569–570*, 1330–1340.
(76) Bai, L.; Cao, C.; Wang, C.; Xu, H.; Zhang, H.; Slaveykova, V. I.; Jiang, H.-L. Towards quantitative understanding of the bioavailability of dissolved organic matter in freshwater lake during cyanobacteria blooming. *Environ. Sci. Technol.* **2017**, *51*, 6018–6026.
(77) Brinkmann, T.; Sartorius, D.; Frimmel, F. H. Photobleaching of humic rich dissolved organic matter. *Aquat. Sci.* **2003**, *65* (4), 415–424.
(78) Cory, R. M.; McKnight, D. M.; Chin, Y. P.; Miller, P.; Jaros, C. L. Chemical characteristics of fulvic acids from arctic surface waters: Microbial contributions and photochemical transformations. *J. Geophys. Res. Biogeosciences* **2007**, *112* (4), 1–14.
(79) Vodacek, A.; Blough, N. V.; DeGrandpre, M. D.; Peltzer, E. T.; Nelson, R. K. Seasonal variation of CDOM and DOC in the Middle Atlantic Bight: Terrestrial inputs and photooxidation. *Limnol. Oceanogr.* **1997**, *42* (4), 674–686.
(80) Stumm, W. and Morgan. J. J. Aquatic Chemistry. Chemical Equilibria and Rates in Natural Waters. **1996**.
(81) Shedlock, R. J.; Wilcox, D. A.; Thompson, T. A.; Cohen, D. A. Interactions between ground water and wetlands, southern shore of Lake Michigan, USA. *J. Hydrol.* **1993**, *141*, 127–155.

(82) Kaushal, S. S.; Duan, S.; Doody, T. R.; Haq, S.; Smith, R. M.; Newcomer Johnson, T. A.; Newcomb, K. D.; Gorman, J.; Bowman, N.; Mayer, P. M.; Wood, K. L.; Belt, K. T.; Stack, W. P. Human-accelerated weathering increases salinization, major ions, and alkalinization in fresh water across land use. *Appl. Geochemistry* **2017**, *83*, 121–135.

(83) Mosher, J. J.; Klein, G. C.; Marshall, A. G.; Findlay, R. H. Influence of bedrock geology on dissolved organic matter quality in stream water. *Org. Geochem.* **2010**, *41* (11), 1177–1188.

(84) Aucour, A. M.; Sheppard, S. M. F.; Guyomar, O.; Wattelet, J. Use of ^{13}C to trace origin and cycling of inorganic carbon in the Rhone River system. *Chem. Geol.* **1999**, *159* (1–4), 87–105.

(85) Radeloff, V. C.; Nelson, E.; Plantinga, A. J.; Lewis, D. J.; Helmers, D.; Lawler, J. J.; Withey, J. C.; Beaudry, F.; Martinuzzi, S.; Butsic, V.; Lonsdorf, E.; White, D.; S., P. Economic-based projections of future land use in the conterminous United States under alternative policy scenarios. **2012**, *22* (3), 1036–1049.

(86) D'Orgeville, M.; Peltier, W. R.; Erler, A. R.; Gula, J. Climate change impacts on Great Lakes basin precipitation extremes. *J. Geophys. Res.* **2014**, *119* (18), 10799-10812.

Chapter 3

Spatial and temporal variability of dissolved organic matter molecules composition in a stratified eutrophic lake

3.1 Details on Collaboration

Chapter 3 is a collaboration between Stephanie Berg, Christina Remucal, Benjamin Peterson, and Katherine McMahon. Sample collection and water chemistry measurements were done by B.P. S.B. did the DOM analyses and wrote the manuscript with input from all authors.

3.2 Abstract

Dissolved organic matter (DOM) is a key component of the carbon cycle in aquatic ecosystems. It is an intermediate between organic carbon formed by primary producers and CO_2 produced through respiration. Its composition is an important factor that determines the routes by which it is ultimately mineralized. Here we evaluated DOM composition as a function of time and depth over five months in Lake Mendota, a highly productive, eutrophic lake that stratifies in warm months and is located in Madison, Wisconsin, USA. Dissolved organic carbon concentrations and optical properties are presented for 73 samples collected at a single location in the lake at varying depths within the water column from June to November. A subset of these samples were analyzed by Fourier transform-ion cyclotron resonance mass spectrometry (FT-ICR MS) to interrogate DOM composition at the molecular level. Over time, increases in more oxidized formulas are observed in both the epilimnion and hypolimnion. At the surface of the lake, correlations between DOM formulas and both chlorophyll concentrations and light intensity show that photochemical

reactions contribute to the observed oxidation of DOM. In the hypolimnion, redox conditions and interactions with sediments likely influence temporal compositional change. Our results show that DOM composition varies with depth with more highly oxidized formulas identified deeper in the water column. However, DOM composition varied more temporally than by location within the water column. This work has implications for climate change as DOM photooxidation in lakes represents an understudied flux of carbon dioxide to the atmosphere. Additionally, lake eutrophication is increasing due to warming global temperatures and this dataset yields detailed molecular information about DOM composition and processing in such lakes.

3.3 Introduction

Dissolved organic matter (DOM) is a ubiquitous, naturally occurring substance derived from plant and microbial residues that makes up a significant portion of all organic carbon on the globe.[1] DOM participates in many reactions in aquatic ecosystems. For example, DOM absorbs and blocks ultraviolet light in surface waters,[2] forming reactive species that can react with dissolved contaminants,[3–5] viruses,[6] or the DOM pool itself.[7] The presence of DOM also alters the solubility and availability of potentially harmful species, including toxic metals.[8,9] Importantly, the composition of DOM controls its reactivity in all of these processes.

DOM composition is driven by differences in source and in extent of environmental processing. However, differentiating between transformation processes is challenging because different processes may yield similar apparent trends and may occur simultaneously. Lakes are an ideal site to differentiate between DOM transformation and source because residence times can be quite long in large lakes thus allowing ample time for transformation to take place relative to fresh allochthonous inputs. Multiple processes are known to alter DOM composition in lakes including

photochemical transformation,[7] microbial transformation,[10] and other physical processes including sorption and dissolution from sediments or particulate phases.[11] Properties specific to particular lakes, such as trophic status, extent of stratification, redox state, and other geochemical parameters, likely also affect composition, although these topics are relatively understudied in DOM composition literature.

Here we analyze the composition of DOM via both ultraviolet-visible (UV-vis) spectroscopy and Fourier transform-ion cyclotron resonance mass spectrometry (FT-ICR MS) in eutrophic Lake Mendota, which is located in Madison, Wisconsin, USA. UV-vis spectroscopy is commonly used to calculate bulk properties including the ratio of absorbances at 250 nm to 365 nm (E_2:E_3) and the specific ultraviolet absorbance at 254 nm ($SUVA_{254}$).[12,13] This method is inexpensive and allows for a large number of samples to be analyzed. FT-ICR MS is a much more time and resource extensive approach but allows for molecular level characterization including weighted averages of H to C ($H:C_w$), O to C ($O:C_w$), and double bond equivalents (DBE_w). These results can be visualized on van Krevelen diagrams which fingerprint and give information about types of compound classes in samples.[14] Additionally, the presence of nitrogen and sulfur-containing formulas provide insight into the presence of heteroatoms in DOM.[15]

The thermal stratification Lake Mendota experiences in the summer and fall months allows for the distinct analysis of processes governing DOM transformation near the surface of the lake and near the bottom. Dissolved oxygen depletion in the bottom layer (i.e., hypolimnion) is driven by eutrophication due to excess nutrients originating mainly from agricultural runoff.[16] Dense and frequent cyanobacterial blooms ultimately deliver organic matter to the hypolimnion, creating strong biochemical oxygen demand. When oxygen becomes depleted at depth, often early in the summer, additional terminal electron acceptors become reduced causing build-up of products such

as Mn(II), Fe(II), and sulfide. The associated reduction processes are carried out by diverse microbes using DOM as a carbon and energy source.[17] Thus, hypolimnetic anoxia is expected to lead to temporal changes in DOM composition.

To investigate the transformation of DOM composition in lakes across space and time, we sampled a highly eutrophic temperate lake at the surface and as a function of depth from June to November in 2017. Physical and chemical properties of the lake were collected including temperature and concentrations of dissolved oxygen, manganese, iron, and sulfide to thoroughly describe extent of stratification and redox state. DOM is evaluated by its concentration, optical properties, and molecular structure using dissolved organic carbon (DOC) measurements, UV-vis spectroscopy, and ultrahigh-resolution mass spectrometry, respectively. This unique data set allows for the investigation into in-lake DOM transformation processes throughout the water column during open water conditions. Concurrent relationships to photo- and biotransformation markers are employed to enable a direct comparison between two potential transformation mechanisms at the surface.[18] We hypothesize that DOM transformation at the surface of the lake results primarily from photochemical reactions that result in overall oxidation while DOM composition throughout the water column depends on stratification status of the lake.

3.4 Materials and Methods

3.4.1 Sample Collection

All samples were collected from Lake Mendota (Madison, Wisconsin, USA), which is a highly eutrophic, temperate lake. This study site was chosen because it is part of the North Temperate Lakes Long-Term Ecological Research (NTL-LTER) program and therefore has a rich set of physical, chemical, and biological data publicly available.[19] The dominant water source is

from the Yahara River and the lake has a mean hydraulic residence time of 4.3 years.[16,20] Surrounding landcover is dominated by cropland and urban land (46.5% and 26.7%, respectively).[21]

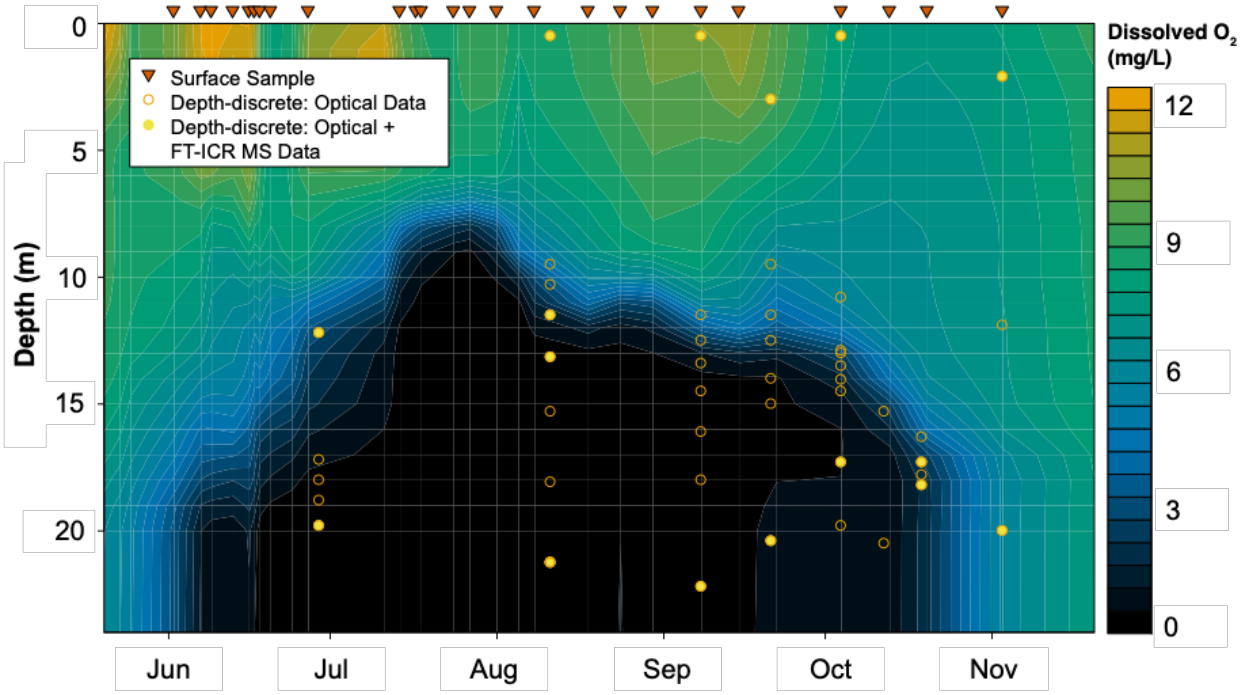

Figure 3.1. Dissolved oxygen (DO) profile heatmap for Lake Mendota for June – November 2017 based on DO measurements taken by the NTL-LTER research buoy. Points indicate sampling dates and depths of samples collected for DOM analysis.

All samples were collected near the NTL-LTER buoy (GPS coordinates: 43.09885, -89.40545), which is near the deepest location in the lake (https://lter.limnology.wisc.edu/data). Surface samples (n = 28) were taken as a composite of the top 12 m of the lake. The top 12 m can generally be considered as the epilimnion, but the location of the thermocline does vary throughout the sampling period (**Figure B.1**). Surface samples were collected approximately 1-2 times per week from June 2nd through November 3rd in 2017. Depth-discrete samples (n = 45) were collected 1-2 times per month at the exact depth listed as measured by a YSI Exo2 multiparameter sonde (YSI Incorporated, Yellow Springs, OH). All water samples were immediately filtered through a

0.22 μm pore-size PES filter and stored in glass bottles in the dark at °4 C. When necessary for analysis, dilutions for any of the analyses were made using ultrapure water (18.2 MΩ cm) obtained from a Milli-Q water purification system. A visual representation of a sample inventory for this study is provided in **Figure 3.1**.

3.4.1 Water Characterization

Geochemical measurements were performed on days when depth-discrete samples were taken and include temperature and concentrations of dissolved oxygen (DO), iron, manganese, and sulfide. Temperature and DO were measured using the YSI sonde. Dissolved concentrations (i.e., able to pass through a 0.45 μm filter) of iron and manganese were quantified by inductively coupled plasma-optical emission spectroscopy (ICP-OES) on a Varian Vista-MPX CCD ICP-OES. Sulfide was quantified spectrophotometrically using the Cline method.[22] Concentrations of chlorophyll, temperature, and DO on dates without sample collection were taken from the NTL-LTER database.[23]

Bulk DOM analyses, including measurements of concentration of dissolved organic carbon ([DOC]) and ultraviolet visible (UV-vis) spectra, were recorded for all surface and depth-discrete samples. [DOC] was measured on a Shimadzu total organic carbon analyzer, which was calibrated using known concentrations of potassium hydrogen phthalate as a standard (ACS grade) purchased from Fisher Scientific. Historical [DOC] measurements were obtained from the NTL-LTER database.[24] For a more accurate comparison to our surface samples, any historical measurements[24] that are made above 12 m on a single day were averaged together. The average [DOC] for each day occurring within the window of time included in our 2017 samples (87 - 241 days after ice-off) were plotted versus days since ice off of the given year. Slope directions were evaluated using

Kendall rank correlations with a 95% confidence interval. Historical sampling frequency depended on the year but was approximately monthly.

UV-vis spectra were collected via a Shimadzu 2401PC Recording Spectrophotometer with 1 nm intervals between 200 – 800 nm. All spectra were collected in 1 cm cuvettes, blank subtracted to Milli-Q water, and the average absorbance from 700 - 800 nm was also subtracted to correct for any light scattering. The optical property E_2:E_3 was calculated as the ratio of the absorbance at 250 nm to 365 nm and specific ultraviolet absorbance at 254 nm ($SUVA_{254}$) as the absorbance at 254 nm divided by [DOC].[12,13]

2.4.3 Mass Spectrometry Analysis

A subset of the depth-discrete samples was analyzed via Fourier transform-ion cyclotron resonance mass spectrometry. Sixteen samples were selected to span a variety of dates, depths, and observations of optical properties since previous work has demonstrated that changes in FT-ICR MS spectra correlate with optical parameters.[5,25–28] DOM was extracted via methods described elsewhere.[5,29] Mass spectra were collected using a SolariX XR 12 T FT-ICR mass spectrometer (Bruker) with a Triversa NanoMate sample delivery system (Advion) operating in negative mode with electrospray ionization. All *m/z* peaks with signal to noise > 3 were exported and considered for matching.

Raw data were linearly calibrated using known formulas commonly found in DOM as described previously.[25] Potential formula masses considered included $^{12}C_{1\text{-}100}{}^{13}C_{0\text{-}1}H_{1\text{-}100}O_{0\text{-}80}$ $N_{0\text{-}2}S_{0\text{-}1}P_{0\text{-}1}$. Combinations of heteroatoms allowed included $N_1S_0P_0$, $N_2S_0P_0$, $N_1S_1P_0$, $N_2S_1P_0$, $N_0S_1P_0$, and $N_0S_0P_1$ to limit the potential mass list while maximizing the numbers of formulas reliably matched. Identified formulas were required to have < 0.2 ppm error between the detected

mass and the actual mass of the formulas. Additionally, identified formulas were required to be part of a homologous series (+ CH_2 or CH_4 vs. O) with at least 3 members.[30] Weighted averages for bulk properties (i.e., $H:C_w$ and $O:C_w$) were calculated by adding values for individual formulas multiplied by their weighted intensities. Spearman rank analyses were used to compare relative formula intensities to location within the water column and bulk parameters such as $SUVA_{254}$ and $E_2:E_3$.

3.4.4 Solar Radiation Modelling

The "Simple Model of the Atmospheric Radiative Transfer of Sunshine" (SMARTS) was used to estimate irradiation at in Madison, WI (43.1097º N, 89.4206º W) at noon on August 11th, September 8th, September 21st, October 4th, and November 3rd of 2017. Intensities were summed from 280 – 500 nm.[31,32]

3.5 Results and Discussion

3.5.1 Lake Overview

In 2017, ice-off (i.e., the first date open water is observed on the lake) was declared for Lake Mendota on March 8th. Our first sample was collected on June 2nd, 87 days after ice-off. The lake was already thermally stratified by the date of our first sample (June 29th; **Figure B.1**) and mixed before the last depth-discrete sampling date (November 3rd; **Figure B.1**). [DOC] ranges from 4.12 – 7.07 mg-C L^{-1} in all samples collected during this study (**Table B.7**), which is within the range observed in the historical NTL-LTER database.[33] The optical properties $SUVA_{254}$ and $E_2:E_3$ range from 1.33 – 2.14 L mg-C^{-1} m^{-1} and 7.86 – 10.18, respectively (**Table B.7**). While there is no long-term UV-vis data set for Lake Mendota, the relatively low $SUVA_{254}$ and high $E_2:E_3$

values are indicative of DOM from autochthonous sources or allochthonous DOM that has undergone extensive environmental processing.[25]

3.5.1 Temporal Variation at the Surface

Integrated surface samples show DOM concentration and especially DOM composition vary over the sampling period. Although the temporal variation in [DOC] is not significant ($p = 0.30$; **Figure 3.2a**; **Table B.7**), a negative slope with time is observed. Decreasing [DOC] has also been observed historically in Lake Mendota over the same dates for 14 of the past 22 years between 1996 and 2017 but similarly without significant correlation (**Table B.8**). We observe a significant decrease in A_{254} over the sampling period ($p = 7.11 \times 10^{-3}$; **Figure 3.2b**; **Table B.7**). This means that the relative amount of light absorbing moieties in DOM are decreasing over time, but that this is not solely attributable to overall decreases in [DOC]. This shift DOM composition is supported by the observation that E_2:E_3 increases significantly ($p = 2.13 \times 10^{-8}$; **Figure 3.2d**; **Table B.7**), corresponding to a decrease in apparent molecular weight. However, no temporal trend exists for $SUVA_{254}$ likely because decreases in absorbance are cancelled out by variability in [DOC] (**Figure 3.2c**; **Table B.7**). Other studies have shown similar seasonal increases in E_2:E_3 as well as decreases in $SUVA_{254}$ in a eutrophic lake in Sweden[34] and in freshwaters in China.[35]

The increase in E_2:E_3 with time is consistent with both photooxidation and microbial alteration of DOM.[12,36,37] Autotrophic organisms living near the surface of the lake produce DOM molecules that are relatively simple and do not absorb light at long wavelengths (e.g. carboxylic acids, amino acids, and peptides).[10,38,39] In fact, incubations isolating DOM produced by phytoplankton show that the DOM is especially small in size,[40] and readily available to heterotrophic microbes.[41] In Lake Mendota, this DOM is unlikely to contribute to [DOC] because

it is so rapidly consumed. Alternatively, photochemical reactions can break down chromophoric DOM (generally of allochthonous origin) directly or form photochemically produced reactive intermediates (PPRI) that degrade DOM to form smaller DOM molecules that absorb less light.[12,42–49] Photooxidation can occur both completely to form carbonate species or incompletely to form more oxidized DOM and a combination of both is consistent with our observations. Both photochemical processes result in increases in E_2:E_3 and decreases in A_{254},[12,37,42–45,47–51] however only complete oxidation can result in [DOC] decreases. Since significant changes in [DOC] are not observed, neither autotrophic inputs nor complete oxidation to CO_2 are likely driving the observed differences in DOM composition. Instead incomplete oxidation is likely the dominant mechanism if photochemical reactions are responsible for the change in DOM composition observed in Lake Mendota.[12,51–56]

Further complicating the interpretation of changes in DOM composition is the fact that a combination of photochemical and microbial processes occur simultaneously, and our observations are likely the net results of a combination of the two. Thus, considering each process individually is likely an oversimplification. Both increases and decreases in measurements of bacterial growth have been observed as a result of photochemical alteration of DOM.[57,58] While this may be attributable to the original source of the DOM,[57] it also may be an artifact of the length of the experiment and whether or not microbial communities have been allowed time to adapt to the photoproduced DOM.[51] In Lake Mendota, the microbial community composition changes over the course of our sampling period and the diversity of communities increases with increasing time from the start of summer stratification,[59,60] but it is not known how the change in microbial community composition influences DOM cycling. It is not possible to distinguish between microbial and photochemical alteration of DOM solely based on bulk UV-vis measurements.

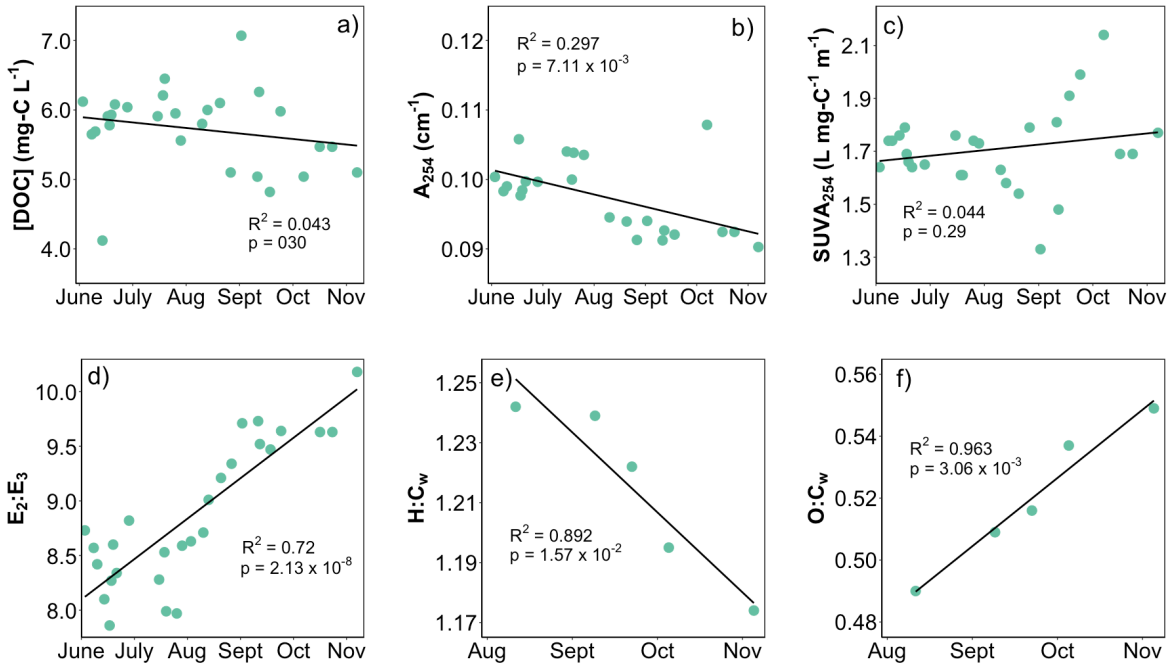

Figure 3.2. a) [DOC], b) $SUVA_{254}$, c) E_2:E_3, and d) A_{254} for integrated epilimnion samples and e) H:C_w and f) O:C_w of identified formulas detected by FT-ICR MS in the surface depth-discrete samples.

A subset of the depth-discrete samples analyzed by FT-ICR MS were collected from the epilimnion (n = 5) and can be used to evaluate changes in the molecular composition of DOM at the surface of the lake, providing more detailed information than bulk UV-vis spectroscopy measurements (**Figures B.5**, **B.8**, **B.10**, **B.12**, and **B.16**). H:C_w values of identified formulas range from 1.17 – 1.24 and decrease significantly over the course of the summer ($p = 1.56 \times 10^{-2}$; **Figure 3.2e**; **Table B.4**). This increase in aromaticity is accompanied by increases in O:C_w (range = 0.49 – 0.55; $p = 3.06 \times 10^{-3}$; **Figure 3.2f**). These ranges in weighted averages derived from FT-ICR MS data are consistent with DOM that is largely microbially-derived and/or has undergone extensive environmental processessing.[61,62] The large variation in these parameters, and particularly in O:C_w, is especially noteworthy given that the samples were taken from the same location in a single lake. In fact, the range in O:C_w in this study is approximately the same range observed across the entire

St. Louis River and Estuary which includes upstream samples dominated by terrestrial inputs and water from oligotrophic Lake Superior.[63] DBE_w and % CHO appear to increase while % N-containing and % S-containing formulas appear to decrease over the sampling period, but no significant trends are observed for the five samples ($p = 0.161$, 0.168, 0.111, and 0.157, respectively; **Figure B.18**).

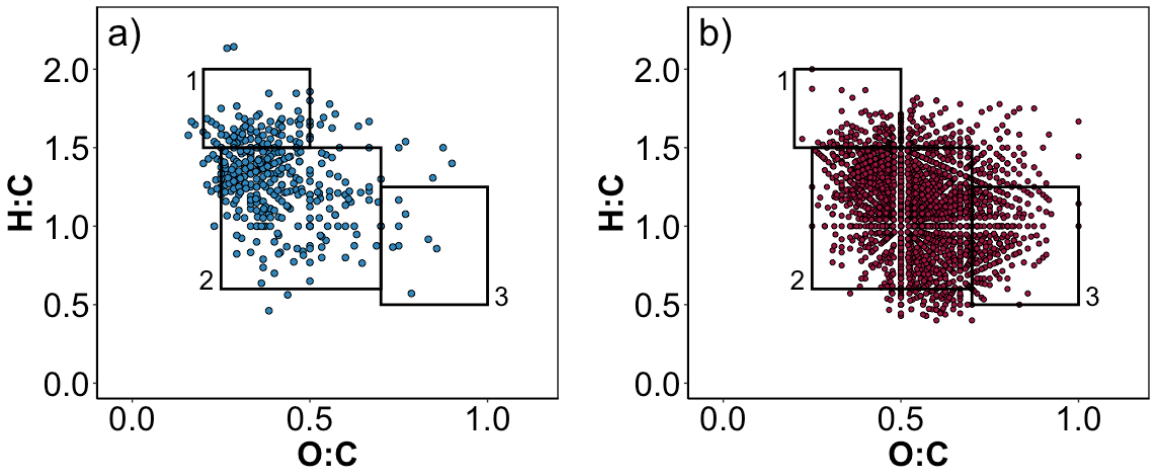

Figure 3.3. Formulas identified in at least four epilimnion samples that a) increase (rho > 0) or b) decrease (rho < 0) with time as determined by Spearman rank analysis. Boxes correspond to 1) protein-, 2) lignin- ,and 3) tannin-like formulas.[64]

Molecular data allows for temporal changes of individual identified formulas to be tracked. Note that this analysis only considers formulas detectable by FT-ICR MS; there is likely a large pool of highly bioavailable organic carbon that is rapidly produced and processed by microbes that is not detected by this technique. Lipid- and protein-like compounds show a net decrease over the course of the summer indicating their consumption rates are greater than production rates (**Figure 3.3a**). This results in the overall decrease in $H:C_w$ observed at the surface (**Figure 3.2e**). Formulas with high O:C and a range of H:C accumulate over our sampling period (**Figure 3.3b**; **Figure 3.2f**); these aromatic, tannin-like formulas result in the increase in $O:C_w$. Note that there is likely

a large pool of DOM we are not able to consider here due to its particularly fast consumption including both DOM produced by phytoplankton and potentially particularly labile photodegradation products.

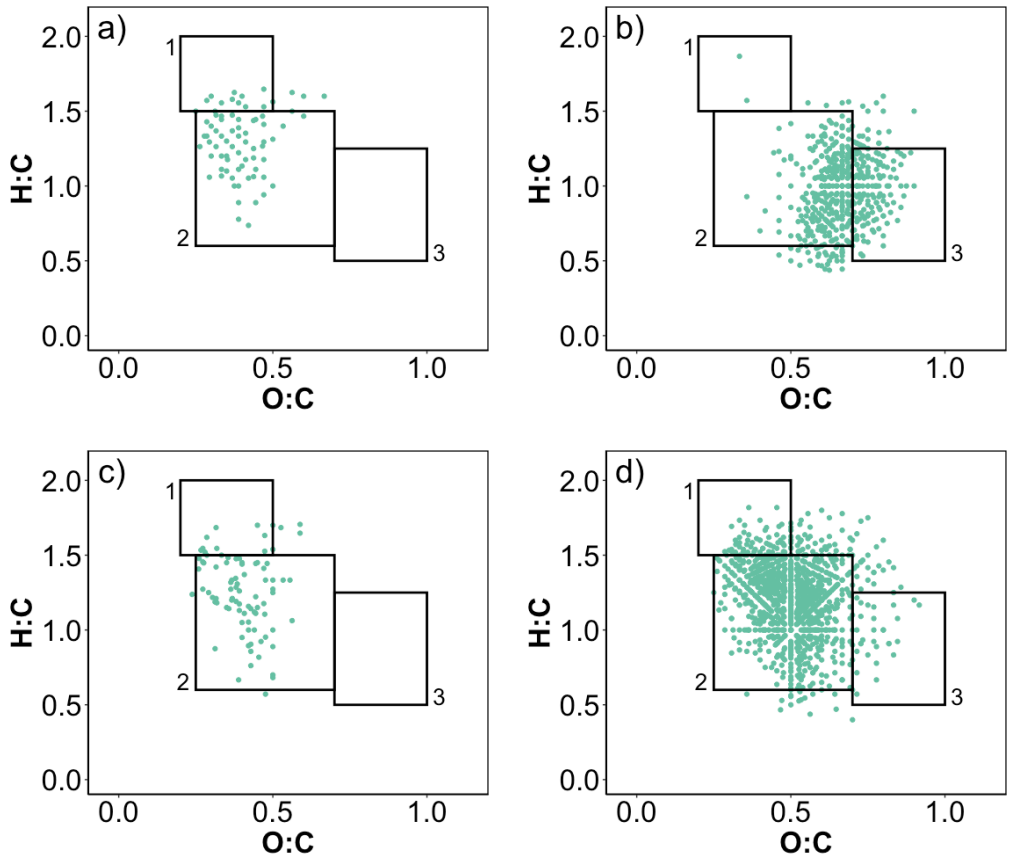

Figure 3.4. Identified formulas classified as a) photodegraded, b) photoproduct, c) microbially-degraded, and d) nonreactive based on correlations to chlorophyll concentrations and light intensity.[18] Only formulas identified in all five surface samples are considered. Boxes correspond to 1) protein-, 2) lignin-, and 3) tannin-like formulas.[64]

Microbial processing and photochemistry likely both alter DOM composition at the surface. Microbial processing includes both generally labile DOM production by phytoplankton and consumption by bacterioplankton. Phytoplankton are known to produce relatively simple molecules such as peptides and small carboxylic acids.[65] Although these small molecules are

outside the 200 – 800 *m/z* range of our method of FT-ICR MS method, high-resolution mass spectrometry has been used to study some other larger phytoplankton-derived DOM and shows that products that are detected are most similar to protein- and lipid-like compounds.[66] Furthermore, these formulas are especially bioavailable for consumption by heterotrophic microbes.[67] While the formulas that are degraded most quickly might never be detected because of rapid turnover and/or analytical limitations, the net decrease in highly saturated formulas is consistent with net consumption of these types of formulas (**Figure 3.3a**). This argument is similar to the marine carbon pump framework where observations of recalcitrant DOM accumulating in marine environments are made because the more labile DOM is consumed equally as fast as it is consumed.[68,69]

Our observations may also be explained by photochemical oxidation. DOM photolysis produces PPRI including singlet oxygen ($^1O_2$) and hydroxyl radical ($^{\bullet}OH$) that may react with phytoplankton-derived DOM via incomplete pathways that generate oxidized DOM.[70] $^1O_2$ is a selective oxidant that preferentially reacts with nucleophilic compounds and can be quenched by DOM.[71,72] $^{\bullet}OH$ also reacts quickly with aromatic rings via oxygen addition which could results in more oxidized products which is consistent with the observed increases in $O:C_w$ (**Figure 3.2f**) and the shift toward more oxidized lignin- and tannin-like formulas (**Figure 3.3b**).[28]

To differentiate between these two transformation mechanisms (e.g., microbial processing versus photo-altered DOM), we use a combination of correlations originally described in Herzprung *et al.*[18] to chlorophyll concentrations and solar radiation and to determine formulas produced and consumed by both microbial and photochemical processes, respectively (**Figure 3.4**; **Table B.3**). Only formulas identified in all surface samples are considered for this analysis and rho correlations are only included for those with $p < 0.05$. Values for chlorophyll concentrations

and light intensities on our sampling dates are listed in **Table B.3**. Formulas are classified into five reaction types including photodegraded compounds (n = 75), photoproducts (n = 494), microbially degraded compounds (n = 88), microbially derived products (n = 14), and nonreactive (n = 1060; **Figures 3.4** and **B.20**). The formulas classified as degraded decreased in their relative abundance while the formulas classified as products increased in their relative abundance.

Classified formulas fall within distinct regions of van Krevelen diagrams. Photodegraded compounds (**Figure 3.4a**) are depleted in O and are highly saturated. The large number of formulas classified as photoproducts have relatively high O:C ratios and fall within the tannin- and lignin-like regions of the diagram (**Figure 3.4b**), which supports the hypothesis that partial photochemical reactions are driving DOM composition changes at the surface. The accumulation of these formulas is noteworthy for several reasons. Specifically, these types of formulas are especially reactive in a wide variety of contexts including reactivity with chlorine[73] and ozone.[28] These formulas are also efficient at photochemically producing $^{\bullet}$OH, but not other PPRI like ^{3}DOM and $^{1}O_2$.[63]

In contrast to photochemical reactivity, a relatively small number of formulas detected by FT-ICR MS are found to be reactive towards biological consumption or transformation (**Figure 3.4c**; **Figure B.20**). However, we recognize that our sampling approach likely misses the most labile formulas which are consumed as quickly as they are produced and not part of the more recalcitrant DOM pool measured here. The formulas that are classified as microbially degraded (**Figure 3.4c**) are generally the same types that are classified as photodegraded (**Figure 3.4a**). Therefore, in Lake Mendota, photochemical reactions would likely make DOM less bio-available based on other incubation studies.[58,67] Collectively, this data set suggests that the DOM in Lake Mendota is mostly phytoplankton-derived or highly processed (i.e., refractory) based on low

$SUVA_{254}$ and high E_2:E_3 and H:C_w values, but that the DOM detected by FT-ICR MS is altered mainly through photochemical reactions over the course of our sampling period.

2.5.3 Variation with Depth

Geochemical and physiochemical parameters measured in the depth-discrete samples show that redox conditions are altered as Lake Mendota stratifies. Temperature and DO data indicate that Lake Mendota was stratified on every depth-discrete date except November 3rd (**Figures 3.5** and **Figures B22-B27**). Once stabilized, the thermocline is observed around 10 – 15 m into the water column (**Figure B.1**). Anoxia, as determined by DO measurements, is observed in the hypolimnion by the beginning of June and remains until the lake mixed in late-October (**Figure 3.1**). The presence of reduced forms of iron and manganese, as well as sulfide, indicate that alternative electron acceptors are used when DO is depleted (**Figure B.21-B.26**; **Table B.2**). Dissolved iron (11.4 – 114 μg L^{-1}) is detected in all samples in the hypolimnion except samples collected on November 3rd after the lake mixes. Concentrations of dissolved manganese range from 0 – 263 μg L^{-1}. Later in the season, manganese is observed at more shallow depths likely due to anoxic conditions existing near the thermocline. Sulfide is only detected when DO is depleted and concentrations increase later in the summer due to the consumption of other more thermodynamically favorable electron acceptors. Up to 5.4 mg L^{-1} of sulfide is measured (**Table B.2**). Once the lake is mixed in late October, Fe, Mn, and sulfide are not present above detection limits likely due to oxidation by O_2 and resorption to sediments.[74]

[DOC] varies within the water column when the lake is stratified but does not change consistently as a function of depth (**Figures 3.5c** and **Figures B.21-B26**). Sharp changes in [DOC] including decreases of around 2 mg-C L^{-1} over a meter, are observed around the thermocline when

the lake is stratified. This is noteworthy because the lowest [DOC] is observed right around the thermocline and where redox conditions change most rapidly and microbial activity is high (cite something – Ben would have the right one), leading to depleted labile DOM. DOM may also co-precipitate with redox active metals, likely manganese, to form particulates, and thus carbon in the dissolved phase decreases. In fact, spikes in particulate Mn are observed around the thermocline in this lake in the same year.[75] Changes in concentrations of DOM and metals due to complexation and precipitation reactions have been observed in other systems such as a creek bank[65] and an experimental drinking water treatment system.[66] In contrast, in November when the lake is mixed, [DOC] is constant with depth (**Figure 3.5c**).

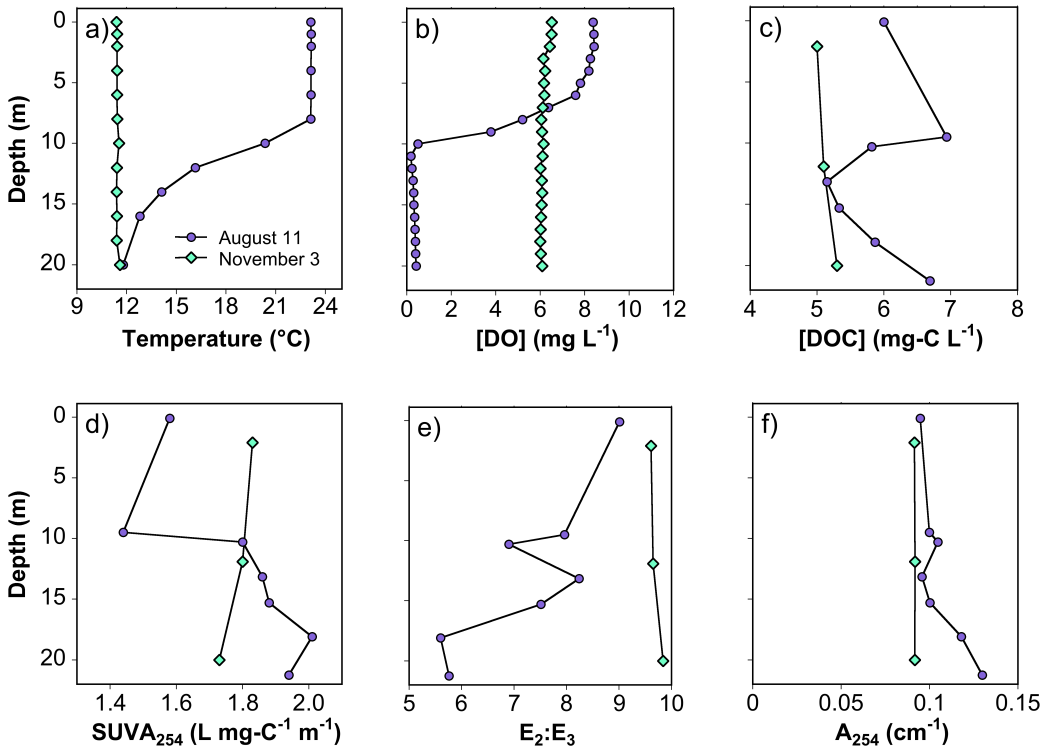

Figure 3.5. a) Temperature, b) [DO], c) [DOC], d) $SUVA_{254}$, e) E_2:E_3, and f) A_{254} measured during summer stratification (August 11th) and after fall turnover (November 3rd) at depth-discrete intervals.

Bulk DOM composition, as determined using optical measurements, also varies with depth. $SUVA_{254}$ is consistently lower and E_2:E_3 is consistently higher in the epilimnion compared to the hypolimnion when the lake is stratified (**Figures 3.5** and **B.21-B.26**). Similar evidence of DOM that is relatively more aromatic and higher in molecular weight being enriched in the hypolimnion has been observed and attributed to decreasing in aromaticity due to photobleaching at the surface of the artificial Lake Salto.[78] No variability in optical properties are observed after the lake has mixed (**Figures 3.5d-3.5f**). Interestingly, once the lake is mixed, values for $SUVA_{254}$ are in the middle of the range observed over the summer (**Figure 3.5d**). In contrast, values for E_2:E_3 are the highest of the season after the lake has mixed (**Figure 3.5e**). This is in agreement with the observations made at the surface of the lake that E_2:E_3 increases over the sampling period but $SUVA_{254}$ is constant (**Figure 3.2**).

Relative amounts of heteroatoms also vary with depth both when the lake is stratified and when it is mixed (**Figures 3.6a-3.6c**; **Tables B.5-B.6**). Ranges of % CHO, % N-containing, and % S-containing formulas vary from 38.7 – 49.9%. The percentage of CHO-only containing formulas decreases in the hypolimnion on each of the five days considered (**Figure 3.6a**), while the percentages of N- and S-containing formulas increase (**Figures 3.6b-3.6c**). The difference between heteroatom-containing formulas and CHO-only formulas is largest in the samples taken later in the season (i.e., October 4th and November 3rd), which suggests that the distribution of heteroatom-containing DOM does not depend on stratification since the lake is mixed on November 3rd.

The decrease in percentage of CHO-only formulas at the bottom of the lake is due to increases in heteroatom-containing formulas since the total number of formulas identified does not account for these differences (**Figure 3.6a; Table B.5-B.6**). Increases in S-containing formulas

may be due to nucleophilic attack by sulfide on DOM.[79–82] Under anoxic conditions, sulfide builds up and may have greater opportunity for this type of reaction (**Table B.2**). Linear correlations between concentrations of sulfide and % S-containing formulas have been reported previously.[81] Here, the highest % S-containing formulas are observed when higher concentrations of sulfide are detected, but the trend is not linear (**Figure B.27**). However, nucleophilic attack cannot be the only formation mechanism since a range of % S-containing formulas is observed even when no sulfide is detected, particularly at the surface of the lake. Additionally, the S-containing formulas observed in this data set preferentially fall within relatively saturated regions of the van Krevelen diagram which could be evidence of a biological pathway for their formation (**Figures B.3-B.17**).[80] In contrast, N-containing formulas make up approximately the same space on the van Krevelen diagrams as the DOM pool as a whole at all depths and therefore may be formed via abiotic addition of N-containing nucleophiles (**Figures B.3-B.17**).[80]

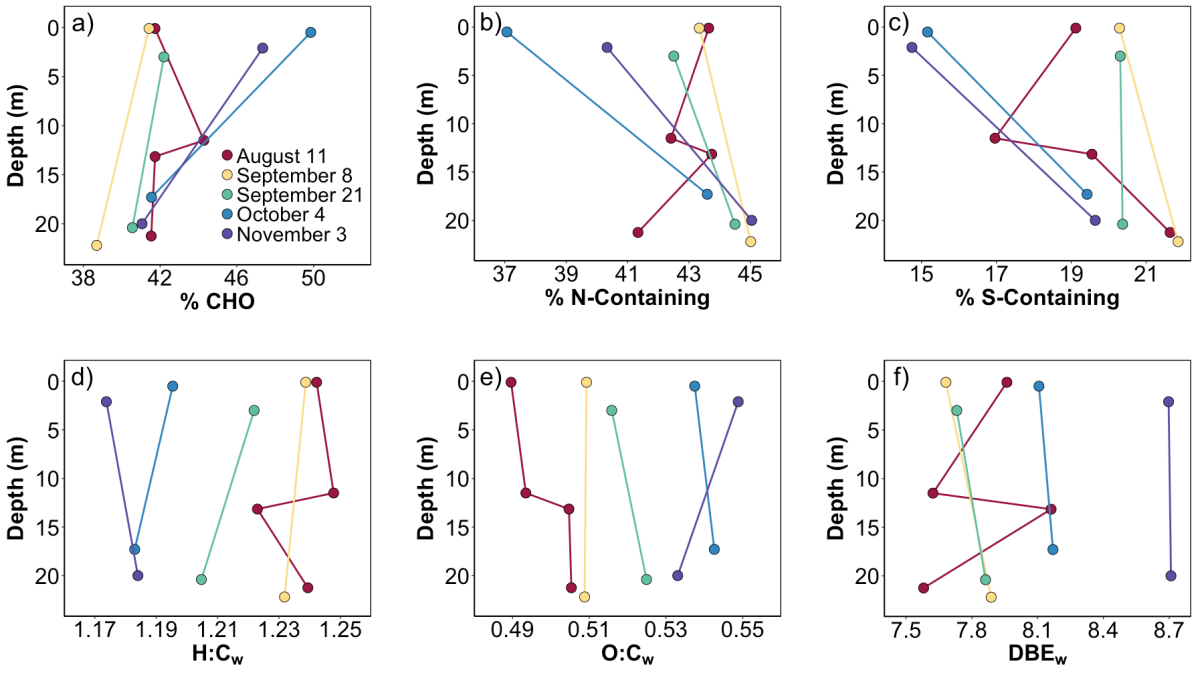

Figure 3.6. Variations in a) % CHO, b) % N-containing, c) % S-containing, d) H:C_w, e) O:C_w, and f) DBE_w of formulas identified by FT-ICR MS with depth. Only dates which have a sample collected from above and below the thermocline are included in this plot.

Changes in DOM molecular composition on individual days can be used to investigate how composition varies temporally and by depth when the lake is stratified and mixed. $H:C_w$ and $O:C_w$ vary by date much more than they vary by depth with $H:C_w$ values decreasing and $O:C_w$ values increasing over the sampling period (**Figures 3.6d-3.6e**; **Table B.4**). On each individual day when the lake is stratified, $H:C_w$ is higher in the epilimnion ($p = 0.049$) and $O:C_w$ appears higher in the hypolimnion although not statistically significant ($p = 0.0957$). On November 3rd, when the lake is mixed, the opposite trends are observed. This observation has also been made after a mixing event in a boreal lake in Switzerland.[83] DBE_w also appears to vary more temporally than spatially although less consistently than $H:C_w$ or $O:C_w$ (**Figure 3.6f**). Like the optical properties, changes in molecular composition are observed at the thermocline. Four samples were analyzed by FT-ICR MS on August 11th, including one sample above the thermocline (i.e., 11.5 m) and the sample immediately below the thermocline (i.e., 13.2 m). On this day, DOM sampled just below the thermocline has lower $H:C_w$ and higher $O:C_w$ and DBE_w than at any other location in the water column. In terms of heteroatoms, the percentages of % CHO-only and % N-containing formulas increase while the percent of % S-containing formulas decrease (**Figure 3.6**) near the thermocline. If co-precipitation of DOM with metals in the thermocline is responsible for loss of [DOC] as discussed above, these results suggest preferential removal of aromatic and S-containing DOM. Subsequent dissolution below the thermocline results in the increase of $O:C_w$ and decrease in $H:C_w$ at 12 m where [DO] is depleted. While this is only based on one sampling date, preferential removal of highly oxidized DOM has been observed with other metal oxides in a lake and in a water treatment system.[77,84]

Specific formulas identified within DOM by FT-ICR MS can be correlated to location within the water column and with bulk optical properties. These analyses are especially

informative because they allow for probing which individual molecular formulas are giving rise to the trends in weighted averages described above. Correlating relative intensities of formulas commonly identified in the depth-discrete samples shows that, in general, formulas with higher O:C ratios are enriched in the hypolimnion (**Figure 3.7**). There is also a slight dependence on the H:C ratio, where more aliphatic formulas are enriched near the surface of the lake. The same general pattern of correlations is observed for relative intensities correlated to DO (**Figure B.19**). However, it is important to note that there was only one sampling day where the DO was not dependent on depth (i.e., in November when the lake was mixed), so it is unclear whether or not this single day would be enough to disrupt the overall trend.

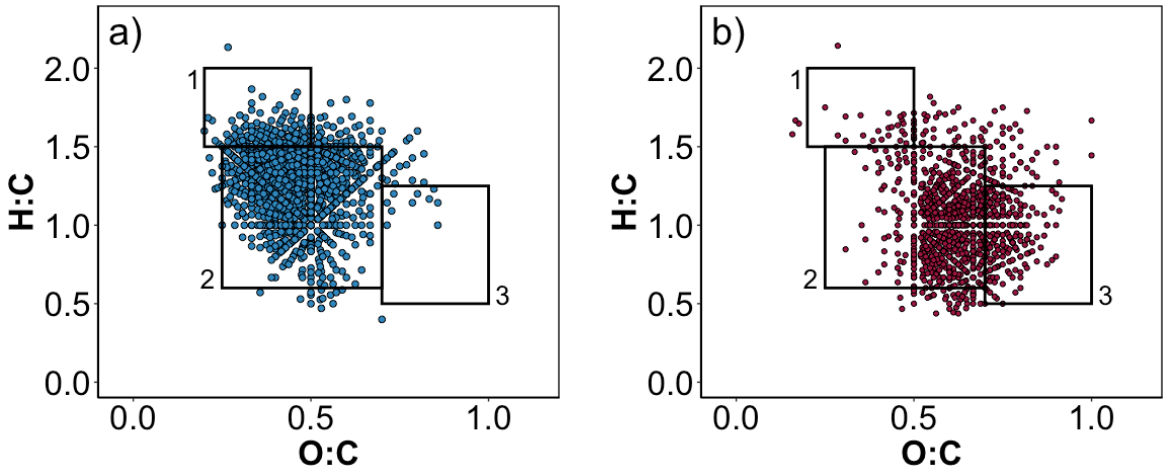

Figure 3.7. Identified formulas that a) decrease (rho < 0) or b) increase (rho > 0) with depth in the depth-discrete samples analyzed with FT-ICR MS. Only those formulas detected in at least 15 out of 20 samples are considered in this analysis. Boxes correspond to 1) protein-, 2) lignin- and 3) tannin-like formulas.[64]

$O:C_w$ ratios increase with depth while the lake is stratified, as well as temporally over our sampling period at all depths (**Figure 3.7b**). While increases in oxygenated formulas at the surface may be attributable to photochemical reactions (**Figure 3.4**), other processes must be at play in the

hypolimnion. Highly oxygenated formulas have been found enriched in the hypolimnion of other lakes including a mesotrophic pre-dam reservoir[11] and another stratified, humic lake in Sweden[83] and contain structures that are likely polyphenolic- and tannin-like. These types of formulas have been found in sediments and desorption may enrich them at the bottom of lakes.[11,80,82–88] In fact, highly oxygenated formulas are preferentially incorporated into redox active metal oxides, which then dissolve more readily under anoxic conditions.[11,77,84,85,89,90] This phenomenon may explain why O:C ratios increase at the bottom of the lake temporally as more minerals are able to dissolve in the anoxic conditions. Alternatively, heterotrophic metabolism may consume the smaller, simpler DOM leaving the larger, more oxidized left in solution. We are not able to distinguish between these two processes.

3.6 Conclusions

By focusing on a single location in a single lake, we are able to concurrently investigate how a combination of photochemical, biological, geochemical, and physical processing impacts DOM composition. At the surface of the lake, A_{254} decreases and E_2:E_3 increases indicating a shift to DOM that is smaller in molecular weight and a decrease in light absorbance by DOM which cannot be attributed to decreases in [DOC] alone. While these observations could be consistent with either microbial or photochemical processing, our molecular level analysis allows for the conclusion that much DOM transformation at the surface of Lake Mendota is driven by photochemical processes.

DOM composition also varies by depth within the water column with larger, more aromatic DOM enriched at the bottom of the lake during stratification. After lake mixing, [DOC] and optical properties could no longer be used to differentiate between DOM collected at different depths. However, differences in heteroatom content of the DOM are still observed via molecular level

analysis. Combined, these results show that single grab samples taken from a dynamic lake such as Lake Mendota should not be considered representative of all seasons nor all locations within the water column. This observation is in contrast to other studies which show [DOC] and DOM composition is more dependent on sample location rather than temporal variation (Chapter 2).

In particular, the effect of eutrophication on DOM composition is vital to understanding DOM in our changing climate. Eutrophication will affect an increasing number of water bodies as temperatures increase and more runoff makes its way into the surface water.[91] Understanding overall water quality including DOM composition is important to mitigate adverse effects of eutrophication including the production of cyanotoxins as well as hypoxia in water bodies.[92,93] Increases in [DOC], also referred to as browning waters, is commonly reported, particularly in European freshwaters, and while the exact mechanisms are still being debated, most link to a changing climate.[94–96] Interestingly, this phenomenon is not observed in all lakes including other NTL-LTER lakes in Wisconsin.[97] Both browning and eutrophication are expected to alter photochemistry in natural systems and may cause shifts in DOM composition that are difficult to predict.[98]

The distribution of DOM with varying composition throughout the water column is significant for many reasons. DOM composition is highly linked to bioactivity, and therefore any chemical or physical processes that affect DOM are also likely to affect microbial populations.[48,99–101] The relationship between photochemistry and microbial respiration is complicated, however, and both increases and decreases in bioavailability can be observed after irradiation.[99] While not explicitly tested here, the fact that the same types of formulas were classified as photodegraded and microbially degraded suggests that photochemistry may decrease bio-lability at our site. The effect that stratification has on DOM composition could also have important implications for fluxes of

greenhouse gases particularly after the lake mixes when DOM not yet exposed to sunlight reaches the surface. For example, fresher, less processed DOM from thawing arctic permafrost layers has been shown to be particularly photo- and bio-labile.[99] Thus, the effects of lake stratification on DOM composition may have important implications for climate change.

3.7 Acknowledgements

This work was funded by the National Science Foundation (CBET 1802388) and an Anna Grant Birge Memorial Scholarship from the Center for Limnology at University of Wisconsin-Madison. The authors acknowledge the North Temperature Lakes-Long Term Ecological Research (NTL-LTER) network supported by the National Science Foundation (DEB-1440297) for the historical data in Lake Mendota. We thank the Mendota Microbial Observatory field crews for the temperature and oxygen data collected by the buoy, Anna Schmidt and Diana Mendez for their help in sample collection, and Amber White for assistance with the SMARTS modelling. We acknowledge the UW-Madison Human Proteomics Program Mass Spectrometry Facility (initially funded by the Wisconsin partnership funds) for support in obtaining mass spectrometry data, NIH S10OD018475 for the acquisition of ultrahigh resolution mass spectrometer for biomedical research, and Ziqing Lin for assistance with the instrument.

3.8 References

(1) Buffam, I.; Turner, M. G.; Desai, A. R.; Hanson, P. C.; Rusak, J. A.; Lottig, N. R.; Stanley, E. H.; Carpenter, S. R. Integrating aquatic and terrestrial components to construct a complete carbon budget for a north temperate lake district. *Glob. Chang. Biol.* **2011**, *17* (2), 1193–1211.

(2) Boyle, E. S.; Guerriero, N.; Thiallet, A.; Del Vecchio, R.; Blough, N. V. Optical properties of humic substances and CDOM: Relation to structure. *Environ. Sci. Technol.* **2009**, *43* (7), 2262–2268.

(3) Remucal, C. K. The role of indirect photochemical degradation in the environmental fate of

pesticides: A review. *Environ. Sci.: Processes and Impacts*. **2014**, *16* (4), 628–653.

(4) Boreen, A. L.; Arnold, W. A.; McNeill, K. Photodegradation of pharmaceuticals in the aquatic environment: A review. *Aquat. Sci*. **2003**, *65* (4), 320–341.

(5) Berg, S. M.; Whiting, Q. T.; Herrli, J. A.; Winkels, R.; Wammer, K. H.; Remucal, C. K. The role of dissolved organic matter composition in determining photochemical reactivity at the molecular level. *Environ. Sci. Technol.* **2019**, 53 (20), 11725 - 11734.

(6) Silverman, A. I.; Peterson, B. M.; Boehm, A. B.; McNeill, K.; Nelson, K. L. Sunlight inactivation of human viruses and bacteriophages in coastal waters containing natural photosensitizers. *Environ. Sci. Technol.* **2013**, *47* (4), 1870–1878.

(7) Gonsior, M.; Peake, B. M.; Cooper, W. T.; Podgorski, D.; D'Andrilli, J.; Cooper, W. J. Photochemically induced changes in dissolved organic matter identified by ultrahigh resolution Fourier transform ion cyclotron resonance mass spectrometry. *Environ. Sci. Technol.* **2009**, *43* (3), 698–703.

(8) Zhou, Z.; Marie Muehe, E.; J. Tomaszewski, E.; Lezama-Pacheco, J.; Kappler, A.; M. Byrne, J. Effect of natural organic matter on the fate of cadmium during microbial ferrihydrite reduction. *Environ. Sci. Technol.* **2020**, *54* (15)*,* 9445-9453.

(9) M. Graham, A.; R. Aiken, G.; C. Gilmour, C. Effect of dissolved organic matter source and character on microbial Hg methylation in Hg–S–DOM solutions. *Environ. Sci. Technol.* **2013**, *47* (11), 5746–5754.

(10) Hertkorn, N.; Claus, H.; Schmitt-Kopplin, P.; Perdue, E. M.; Filip, Z. Utilization and transformation of aquatic humic substances by autochthonous microorganisms. *Environ. Sci. Technol.* **2002**, *36* (20), 4334–4345.

(11) Dadi, T.; Harir, M.; Hertkorn, N.; Koschorreck, M.; Schmitt-Kopplin, P.; Herzsprung, P. Redox conditions affect dissolved organic carbon quality in stratified freshwaters. *Environ. Sci. Technol.* **2017**, *51* (23), 13705–13713.

(12) Helms, J. R.; Stubbins, A.; Ritchie, J. D.; Minor, E. C.; Kieber, D. J.; Mopper, K. Absorption spectral slopes and slope ratios as indicators of molecular weight, source, and photobleaching of chromophoric dissolved organic Matter. *Limnol. Oceanogr.* **2008**, *53* (3), 955–968.

(13) Weishaar, J.; Aiken, G.; Bergamaschi, B.; Fram, M.; Fujii, R.; Mopper, K. Evaluation of specific ultra-violet absorbance as an indicator of the chemical content of dissolved organic carbon. *Environ. Sci. Technol.* **2003**, *37* (20), 4702–4708.

(14) Kim, S.; Kramer, R. W.; Hatcher, P. G. Graphical method for analysis of ultrahigh-resolution broadband mass spectra of natural organic matter, the van Krevelen diagram. *Anal. Chem.* **2003**, *75* (20), 5336–5344.

(15) Hertkorn, N.; Frommberger, M.; Witt, M.; Koch, B. P.; Schmitt-kopplin, P.; Perdue, E. M.; Natural Organic Matter and the Event Horizon of Mass Spectrometry. *Anal. Chem.* **2008**, *80*, 8908-8919.

(16) Lathrop, R. C.; Carpenter, S. R. Water quality implications from three decades of phosphorus loads and trophic dynamics in the Yahara chain of lakes. *Inl. Waters* **2014**, *4* (1), 1–14.

(17) Linz, A. M.; He, S.; Stevens, S. L. R.; Anantharaman, K.; Rohwer, R. R.; Malmstrom, R. R.; Bertilsson, S.; McMahon, K. D. Freshwater carbon and nutrient cycles revealed through reconstructed population genomes. *PeerJ* **2018**, *2018* (12), 1–24.

(18) Herzsprung, P.; Wentzky, V.; Kamjunke, N.; Von Tümpling, W.; Wilske, C.; Friese, K.; Boehrer, B.; Reemtsma, T.; Rinke, K.; Lechtenfeld, O. J. Improved understanding of

dissolved organic matter processing in freshwater using complementary experimental and machine learning approaches. *Environ. Sci. Technol.* **2020**, *54* (21), 13556–13565.

(19) Carpenter, S. R.; Benson, B. J.; Biggs, R.; Chipman, J. W.; Foley, J. A.; Golding, S. A.; Hammer, R. B.; Hanson, P. c.; Johnson, P. T. J.; Kamarainen, A. M.; Kratz, T. K.; Lathrop, R. C.; McMahon, K. D.; Provencher, B.; Rusak, J. A.; Solomon, C. T.; Stanley, E. H.; Turner, M. G.; Vander Zanden, J.; Wu, C. H.; Yuan, H. Understanding regional change: A comparison of two lake districts. *BioScience*, **2007**, *54* (4), 323-335.

(20) Hoffman, A. R.; Armstrong, D. E.; Lathrop, R. C. Influence of phosphorus scavenging by iron in contrasting dimictic lakes. *Can. J. Fish. Aquat. Sci.* **2013**, *70* (7), 941–952.

(21) Chen, X.; Motew, M. M.; Booth, E. G.; Zipper, S. C.; Loheide, S. P.; Kucharik, C. J. Management of minimum lake levels and impacts on flood mitigation: A case study of the Yahara watershed, Wisconsin, USA. *J. Hydrol.* **2019**, *577*, 123920.

(22) Joel D. Cline. Spectrophotometric determination of hydrogen sulfide in natural waters. *Limnol. Oceanogr.* **1969**, *14* (3), 454–458.

(23) Magnuson, J.; Carpenter, S.; Stanley, E. North temperate lakes LTER: High frequency data: meteorological, dissolved oxygen, chlorophyll, phycocyanin- Lake Mendota Buoy 2006 - Current Ver 31. Environmental Data Initiative, **2020**.

(24) Magnuson, J.; Carpenter, S.; Stanley, E. North temperate lakes LTER: Chemical limnology of primary study lakes: Nutrients, pH and carbon 1981-Current Ver 52. Environmental Data Initiative, **2020**.

(25) Maizel, A. C.; Li, J.; Remucal, C. K. Relationships between dissolved organic matter composition and photochemistry in lakes of diverse trophic status. *Environ. Sci. Technol.* **2017**, *51* (17), 9624–9632.

(26) Maizel, A. C.; Remucal, C. K. The effect of advanced secondary municipal wastewater treatment on the molecular composition of dissolved organic matter. *Water Res.* **2017**, *122*, 42–52.

(27) Maizel, A. C.; Remucal, C. K. Molecular composition and photochemical reactivity of size-fractionated dissolved organic matter. *Environ. Sci. Technol.* **2017**, *51* (4), 2113–2123.

(28) K. Remucal, C.; Salhi, E.; Walpen, N.; von Gunten, U. Molecular-level transformation of dissolved organic matter during oxidation by ozone and hydroxyl radical. *Environ. Sci. & Technol.* **2020**, *54* (16), 10351-10360.

(29) Dittmar, T.; Koch, B.; Hertkorn, N.; Kattner, A. G. Simple and efficient method for the solid-phase extraction of dissolved organic matter (SPE-DOM) from seawater. *Limnol. Oceanogr.: Methods* **2008**, *6*, 230–235.

(30) Koch, B. P.; Dittmar, T.; Witt, M.; Kattner, G. Fundamentals of molecular formula assignment to ultrahigh resolution mass data of natural organic matter. *Anal. Chem.* **2007**, *79* (4), 1758–1763.

(31) McConville, M. B.; Cohen, N. M.; Nowicki, S. M.; Lantz, S. R.; Hixson, J. L.; Ward, A. S.; Remucal, C. K. A field analysis of lampricide photodegradation in Great Lakes tributaries. *Environ. Sci. Process. Impacts* **2017**, *19* (7), 891–900.

(32) Remucal, C. K.; McNeill, K. Photosensitized amino acid degradation in the presence of riboflavin and its derivatives. *Environ. Sci. Technol.* **2011**, *45* (12), 5230–5237.

(33) Magnuson, J.; Carpenter, S.; Stanley, E. North temperate lakes LTER: Chemical limnology of primary study lakes: Nutrients, pH and carbon 1981 - Current Ver 52. Environmental Data Initiative, **2020**.

(34) Müller, R. A.; Kothawala, D. N.; Podgrajsek, E.; Sahlée, E.; Koehler, B.; Tranvik, L. J.;

Weyhenmeyer, G. A. Hourly, daily, and seasonal variability in the absorption spectra of chromophoric dissolved organic matter in a eutrophic, humic lake. *J. Geophys. Res. G Biogeosciences* **2014**, *119* (10), 1985–1998.

(35) Song, K. S.; Zang, S. Y.; Zhao, Y.; Li, L.; Du, J.; Zhang, N. N.; Wang, X. D.; Shao, T. T.; Guan, Y.; Liu, L. Spatiotemporal characterization of dissolved carbon for inland waters in semi-humid/semi-arid region, China. *Hydrol. Earth Syst. Sci.* **2013**, *17* (10), 4269–4281.

(36) Larson, J. H.; Frost, P. C.; Zheng, Z.; Johnston, C. A.; Bridgham, S. D.; Lodge, D. M.; Lamberti, G. A. Effects of upstream lakes on dissolved organic matter in streams. *Limnol. Oceanogr.* **2007**, *52* (1), 60–69.

(37) Sharpless, C. M.; Aeschbacher, M.; Page, S. E.; Wenk, J.; Sander, M.; McNeill, K. Photooxidation-induced changes in optical, electrochemical, and photochemical properties of humic substances. *Environ. Sci. Technol.* **2014**, *48* (5), 2688–2696.

(38) Kamjunke, N.; von Tümpling, W.; Hertkorn, N.; Harir, M.; Schmitt-Kopplin, P.; Norf, H.; Weitere, M.; Herzsprung, P. A new approach for evaluating transformations of dissolved organic matter (DOM) via high-resolution mass spectrometry and relating it to bacterial activity. *Water Res.* **2017**, *123*, 513–523.

(39) Valle, J.; Gonsior, M.; Harir, M.; Enrich-Prast, A.; Schmitt-Kopplin, P.; Bastviken, D.; Conrad, R.; Hertkorn, N. Extensive processing of sediment pore water dissolved organic matter during anoxic incubation as observed by high-field mass spectrometry (FTICR-MS). *Water Res.* **2018**, *129*, 252–263.

(40) Zhang, Y.; Liu, X.; Wang, M.; Qin, B. Compositional differences of chromophoric dissolved organic matter derived from phytoplankton and macrophytes. *Org. Geochem.* **2013**, *55*, 26–37.

(41) Bertilsson, S.; Jones, J. B. Supply of dissolved organic matter to aquatic ecosystems: autochthonous sources. *Aquat. Ecosyst. Interactivity Dissolved Org. Matter* **2003**, 3–19.

(42) Helms, J. R.; Stubbins, A.; Perdue, E. M.; Green, N. W.; Chen, H.; Mopper, K. Photochemical bleaching of oceanic dissolved organic matter and its effect on absorption spectral slope and fluorescence. *Mar. Chem.* **2013**, *155*, 81–91.

(43) Helms, J. R.; Mao, J.; Stubbins, A.; Schmidt-Rohr, K.; Spencer, R. G. M.; Hernes, P. J.; Mopper, K. Loss of optical and molecular indicators of terrigenous dissolved organic matter during long-term photobleaching. *Aquat. Sci.* **2014**, *76* (3), 353–373.

(44) Bittar, T. B.; Stubbins, A.; Vieira, A. A. H.; Mopper, K. Characterization and photodegradation of dissolved organic matter (DOM) from a tropical lake and its dominant primary producer, the cyanobacteria microcystis aeruginosa. *Mar. Chem.* **2015**, *177*, 205–217.

(45) Brinkmann, T.; Sartorius, D.; Frimmel, F. H. Photobleaching of humic rich dissolved organic matter. *Aquat. Sci.* **2003**, *65* (4), 415–424.

(46) Bade, D. L.; Carpenter, S. R.; Cole, J. J.; Pace, M. L.; Kritzberg, E.; Van De Bogert, M. C.; Cory, R. M.; McKnight, D. M. Sources and fates of dissolved organic carbon in lakes as determined by whole-lake carbon isotope additions. *Biogeochemistry* **2007**, *84* (2), 115–129.

(47) Kujawinski, E. B.; Del Vecchio, R.; Blough, N. V.; Klein, G. C.; Marshall, A. G. Probing molecular-level transformations of dissolved organic matter: Insights on photochemical degradation and protozoan modification of DOM from electrospray ionization Fourier ion cyclotron resonance mass spectrometry. *Mar. Chem.* **2004,** *92*, 23-37.

(48) Lønborg, C.; Nieto-Cid, M.; Hernando-Morales, V.; Hernández-Ruiz, M.; Teira, E.;

Álvarez-Salgado, X. A. Photochemical alteration of dissolved organic matter and the subsequent effects on bacterial carbon cycling and diversity. *FEMS Microbiol. Ecol.* **2016**, *92* (5), 1-14.

(49) Spencer, R. G. M.; Stubbins, A.; Hernes, P. J.; Baker, A.; Mopper, K.; Aufdenkampe, A. K.; Dyda, R. Y.; Mwamba, V. L.; Mangangu, A. M.; Wabakanghanzi, J. N.; Six, J. Photochemical degradation of dissolved organic matter and dissolved lignin phenols from the Congo river. *J. Geophys. Res. Biogeosciences* **2009**, *114* (3), 1-12.

(50) Hur, J.; Jung, K. Y.; Jung, Y. M. Characterization of spectral responses of humic substances upon UV irradiation using two-dimensional correlation spectroscopy. *Water Res.* **2011**, *45* (9), 2965–2974.

(51) Cory, R. M.; Kling, G. W.; Stanley, E.; Del Giorgio, P. Interactions between sunlight and microorganisms influence dissolved organic matter degradation along the aquatic continuum. *Limnol. Oceanogr. Lett.* **2018**, *3*, 102–116.

(52) Granéli, W.; Lindell, M.; Tranvik, L. Photo-oxidative production of dissolved inorganic carbon in lakes of different humic content. *Limnol. Oceanogr.* **1996**, *41* (4), 698–706.

(53) Chen, H.; Stubbins, A.; Perdue, E. M.; Green, N. W.; Helms, J. R.; Mopper, K.; Hatcher, P. G. Ultrahigh resolution mass spectrometric differentiation of dissolved organic matter isolated by coupled reverse osmosis-electrodialysis from various major oceanic water masses. *Mar. Chem.* **2014**, *164*, 48–59.

(54) Thorn, K. A.; Younger, S. J.; Cox, L. G. Order of functionality loss during photodegradation of aquatic humic substances. *J. Environ. Qual.* **2010**, *39* (4), 1416–1428.

(55) Hansen, A. M.; Kraus, T. E. C.; Pellerin, B. A.; Fleck, J. A.; Downing, B. D.; Bergamaschi, B. A. Optical properties of dissolved organic matter (DOM): Effects of biological and photolytic degradation. *Limnol. Oceanogr.* **2016**, *61* (3), 1015–1032.

(56) Lou, T.; Xie, H. Photochemical alteration of the molecular weight of dissolved organic Matter. *Chemosphere* **2006**, *65* (11), 2333–2342.

(57) Tranvik, L. J.; Bertilsson, S. Contrasting effects of solar UV radiation on dissolved organic sources for bacterial growth. *Ecol. Lett.* **2001**, *4* (5), 458–463.

(58) Cory, R. M.; Kling, G. W. Interactions between sunlight and microorganisms influence dissolved organic matter degradation along the aquatic continuum. *Limnol. Oceanogr. Lett.* **2018**, *3* (3), 102–116.

(59) Shade, A.; Kent, A. D.; Jones, S. E.; Newton, R. J.; Triplett, E. W.; McMahon, K. D. Interannual dynamics and phenology of bacterial communities in a eutrophic lake. *Limnol. Oceanogr.* **2007**, *52* (2), 487–494.

(60) Kara, E. L.; Hanson, P. C.; Hu, Y. H.; Winslow, L.; McMahon, K. D. A decade of seasonal dynamics and co-occurrences within freshwater bacterioplankton communities from eutrophic Lake Mendota, WI, USA. *ISME J.* **2013**, *7* (3), 680–684.

(61) Hawkes, J. A.; D'Andrilli, J.; Agar, J. N.; Barrow, M. P.; Berg, S. M.; Catalán, N.; Chen, H.; Chu, R. K.; Cole, R. B.; Dittmar, T.; Gavard, R.; Gleixner, G.; Hatcher, P. G.; He, C.; Hess, N. J.; Hutchins, R. H. S.; Ijaz, A.; Jones, H. E.; Kew, W.; Khaksari, M.; Palacio Lozano, D. C.; Lv, J.; Mazzoleni, L. R.; Noriega-Ortega, B. E.; Osterholz, H.; Radoman, N.; Remucal, C. K.; Schmitt, N. D.; Schum, S. K.; Shi, Q.; Simon, C.; Singer, G.; Sleighter, R. L.; Stubbins, A.; Thomas, M. J.; Tolic, N.; Zhang, S.; Zito, P.; Podgorski, D. C. An international laboratory comparison of dissolved organic matter composition by high resolution mass spectrometry: Are we getting the same answer? *Limnol. Oceanogr. Methods* **2020**, *18* (6), 235-258.

(62) Brown, A.; McKnight, D. M.; Chin, Y. P.; Roberts, E. C.; Uhle, M. Chemical characterization of dissolved organic material in Pony Lake, a saline coastal pond in Antarctica. *Mar. Chem*. **2004**, 89, 327–337.
(63) Berg, S. M.; T. Whiting, Q.; A. Herrli, J.; Winkels, R.; H. Wammer, K.; K. Remucal, C. The role of dissolved organic matter composition in determining photochemical reactivity at the molecular level. *Environ. Sci. Technol.* **2019**, *53* (20), 11725–11734.
(64) Minor, E. C.; Swenson, M. M.; Mattson, B. M.; Oyler, A. R. Structural characterization of dissolved organic matter: A review of current techniques for isolation and analysis. *Environ. Sci. Process. Impacts* **2014**, *16*, 2064–2079.
(65) Meon, B.; Kirchman, D. L. Dynamics and Molecular Composition of Dissolved Organic Material during Experimental Phytoplankton Blooms. *Mar. Chem*. **2001**, 75, 185-199.
(66) Mangal, V.; Stock, N. L.; Guéguen, C. Molecular characterization of phytoplankton dissolved organic matter (DOM) and sulfur components using high resolution orbitrap mass spectrometry. *Anal. Bioanal. Chem.* **2016**, *408* (7), 1891–1900.
(67) D'Andrilli, J.; Cooper, W. T.; Foreman, C. M.; Marshall, A. G. An ultrahigh-resolution mass spectrometry index to estimate natural organic matter lability. *Rapid Commun. Mass Spectrom.* **2015**, *29* (24), 2385–2401.
(68) Jiao, N.; Herndl, G. J.; Hansell, D. A.; Benner, R.; Kattner, G.; Wilhelm, S. W.; Kirchman, D. L.; Weinbauer, M. G.; Luo, T.; Chen, F.; Azam, F. Microbial production of recalcitrant dissolved organic matter: Long-term carbon storage in the global ocean. *Nat. Rev. Microbiol.* **2010**, *8*, 593–600.
(69) Zhang, C.; Dang, H.; Azam, F.; Benner, R.; Legendre, L.; Passow, U.; Polimene, L.; Robinson, C.; Suttle, C. A. .; Jiao, N. Evolving paradigms in biological carbon cycling in the ocean. *Natl. Sci. Rev.* **2018**, *5*, 481–499.
(70) Ward, C. P.; Cory, R. M. Complete and partial photo-oxidation of dissolved organic matter draining permafrost soils. *Environ. Sci. Technol.* **2016**, *50* (7), 3545–3553.
(71) Yang, W.; Ben Abdelmelek, S.; Zheng, Z.; An, T.; Zhang, D.; Song, W. Photochemical transformation of terbutaline (pharmaceutical) in simulated natural waters: Degradation kinetics and mechanisms. *Water Res.* **2013**, *47* (17), 6558–6565.
(72) Hessler, D. P.; Frimmel, F. H.; Oliveros, E.; Braun, M. Quenching of singlet oxygen by humic substances. *J. Photochem. Photobiol. Biol.* **1996**, *36*, 55–50.
(73) Bulman, D. M.; Remucal, C. K. Role of reactive halogen species in disinfection byproduct formation during chlorine photolysis. *Environ. Sci. Technol.* **2020**, *54* (15), 9629–9639.
(74) Krueger, K. M.; Vavrus, C. E.; Lofton, M. E.; McClure, R. P.; Gantzer, P.; Carey, C. C.; Schreiber, M. E. Iron and manganese fluxes across the sediment-water interface in a drinking water reservoir. *Water Res.* **2020**, *182*, 116003.
(75) Peterson, B. D.; Mcdaniel, E. A.; Schmidt, A. G.; Lepak, R. F.; Janssen, S. E.; Tran, P. Q.; Marick, R. A.; Ogorek, J. M.; Dewild, J. F.; Krabbenhoft, D. P.; Mcmahon, K. D. Mercury methylation genes identified across diverse anaerobic microbial guilds in a eutrophic sulfate-enriched lake. *Environ. Sci. Technol.* **2020**, *54* (24), 15840–15851.
(76) Seidel, M.; Beck, M.; Riedel, T.; Waska, H.; Suryaputra, I. G. N. A.; Schnetger, B.; Niggemann, J.; Simon, M.; Dittmar, T. Biogeochemistry of dissolved organic matter in an anoxic intertidal creek bank. *Geochim. Cosmochim. Acta* **2014**, *140*, 418–434.
(77) Barazesh, J. M.; Prasse, C.; Wenk, J.; Berg, S.; Remucal, C. K.; Sedlak, D. L. Trace element removal in distributed drinking water treatment systems by cathodic H_2O_2 production and UV photolysis. *Environ. Sci. Technol.* **2018**, *52* (1), 195–204.

(78) Bracchini, L.; Dattilo, A. M.; Hull, V.; Loiselle, S. A.; Martini, S.; Rossi, C.; Santinelli, C.; Seritti, A. The bio-optical properties of CDOM as descriptor of lake stratification. *J. Photochem. Photobiol. B Biol.* **2006**, *85* (2), 145–149.

(79) Vairavamurthy, A. Mopper, K. Geochemical formation of organosulphur compounds (thiols) by addition of H_2S to sedimentary organic matter. *Nature* **1987**, *329*, 623–625.

(80) L. Sleighter, R.; Chin, Y.-P.; A. Arnold, W.; G. Hatcher, P.; J. McCabe, A.; C. McAdams, B.; C. Wallace, G. Evidence of incorporation of abiotic S and N into prairie wetland dissolved organic matter. *Environ. Sci. Technol. Lett.* **2014**, *1* (9), 345–350.

(81) Poulin, B. A.; Ryan, J. N.; Nagy, K. L.; Stubbins, A.; Dittmar, T.; Orem, W.; Krabbenhoft, D. P.; Aiken, G. R. Spatial dependence of reduced sulfur in everglades dissolved organic matter controlled by sulfate enrichment. *Environ. Sci. Technol.* **2017**, *51* (7), 3630–3639.

(82) Schmidt, F.; Koch, B. P.; Goldhammer, T.; Elvert, M.; Witt, M.; Lin, Y. S.; Wendt, J.; Zabel, M.; Heuer, V. B.; Hinrichs, K. U. Unraveling signatures of biogeochemical processes and the depositional setting in the molecular composition of pore water DOM across different marine environments. *Geochim. Cosmochim. Acta* **2017**, *207*, 57–80.

(83) Gonsior, M.; Schmitt-Kopplin, P.; Bastviken, D. Depth-dependent molecular composition and photo-reactivity of dissolved organic matter in a boreal lake under winter and summer conditions. *Biogeosciences* **2013**, *10* (11), 6945–6956.

(84) Riedel, T.; Zak, D.; Biester, H.; Dittmar, T. Iron traps terrestrially derived dissolved organic matter at redox interfaces. *Proc. Natl. Acad. Sci.*. **2013**, *110* (25), 10101–10105.

(85) Yang, L.; Choi, J. H.; Hur, J. Benthic flux of dissolved organic matter from lake sediment at different redox conditions and the possible effects of biogeochemical processes. *Water Res.* **2014**, *61*, 97–107.

(86) Valle, J.; Harir, M.; Gonsior, M.; Enrich-Prast, A.; Schmitt-Kopplin, P.; Bastviken, D.; Hertkorn, N. Molecular differences between water column and sediment pore water SPE-DOM in ten Swedish boreal lakes. *Water Res.* **2020**, *170*, 115320.

(87) Schmidt, F.; P. Koch, B.; Elvert, M.; Schmidt, G.; Witt, M.; Hinrichs, K.-U. Diagenetic transformation of dissolved organic nitrogen compounds under contrasting sedimentary redox conditions in the black sea. *Environ. Sci. Technol.* **2011**, *45* (12), 5223–5229.

(88) Herzsprung, P.; von Tümpling, W.; Wendt-Potthoff, K.; Hertkorn, N.; Harir, M.; Schmitt-Kopplin, P.; Friese, K. High field FT-ICR mass spectrometry data sets enlighten qualitative DOM alteration in lake sediment porewater profiles. *Org. Geochem.* **2017**, *108*, 51–60.

(89) Linkhorst, A.; Dittmar, T.; Waska, H. Molecular fractionation of dissolved organic matter in a shallow subterranean estuary: The role of the iron curtain. *Environ. Sci. Technol.* **2017**, *51* (3), 1312–1320.

(90) Lv, J.; Zhang, S.; Wang, S.; Luo, L.; Cao, D.; Christie, P. Molecular-scale investigation with ESI-FT-ICR-MS on fractionation of dissolved organic matter induced by adsorption on iron oxyhydroxides. *Environ. Sci. Technol.* **2016**, *50* (5), 2328–2336.

(91) Sinha, E.; Michalak, A. M.; Balaji, V. Eutrophication will increase during the 21st century as a result of precipitation changes. *Science.* **2017,** 357, 405-408.

(92) Song, W.; Yan, S.; Cooper, W. J.; Dionysiou, D. D.; O'Shea, K. E. Hydroxyl radical oxidation of cylindrospermopsin (cyanobacterial toxin) and its role in the photochemical transformation. *Environ. Sci. Technol.* **2012**, *46* (22), 12608–12615.

(93) Hao, Z.; Ma, J.; Miao, C.; Song, Y.; Lian, L.; Yan, S.; Song, W. Carbonate radical oxidation of cylindrospermopsin (Cyanotoxin): Kinetic studies and mechanistic consideration. *Environ. Sci. Technol.* **2020**, *54* (16), 10118-10127.

(94) Freeman, C.; Fenner, N.; Ostle, N. J.; Kang, H.; Dowrick, D. J.; Reynolds, B.; Lock, M. A.; Sleep, D.; Hughes, S.; Hudson, J. Export of dissolved organic carbon from peatlands under elevated carbon dioxide levels. *Nature* **2004**, *430* (6996), 195–198.
(95) Worrall, F.; Harriman, R.; Evans, C.; Watts, D.; Adamson, J.; Neal, C.; Tipping, E. Trends in dissolved organic carbon in UK. *Biogeochem*. **2004**, 70, 369-402.
(96) Evans, C. D.; Chapman, P. J.; Clark, J. M.; Monteith, D. T.; Cresser, M. S. Alternative explanations for rising dissolved organic carbon export from organic soils. *Glob. Chang. Biol.* **2006**, *12* (11), 2044–2053.
(97) Jane, S. F.; Winslow, L. A.; Remucal, C. K.; Rose, K. C. Long-term trends and synchrony in dissolved organic matter characteristics in Wisconsin, USA, lakes: Quality, not quantity, is highly sensitive to climate. *J. Geophys. Res. Biogeosciences* **2017**, *122* (3), 546–561.
(98) Vione, D.; Scozzaro, A. Photochemistry of surface fresh waters in the framework of climate change. *Environ. Sci. Technol.* **2019**, *53* (14), 7945–7963.
(99) Ward, C. P.; Nalven, S. G.; Crump, B. C.; Kling, G. W.; Cory, R. M. Photochemical alteration of organic carbon draining permafrost soils shifts microbial metabolic pathways and stimulates respiration. *Nat. Commun.* **2017**, *8* (1). 1-8.
(100) Bowen, J. C.; Kaplan, L. A.; Cory, R. M. Photodegradation disproportionately impacts biodegradation of semi-labile DOM in streams. *Limnol. Oceanogr.* **2020**, *65* (1), 13–26.
(101) Guerrero-Feijóo, E.; Nieto-Cid, M.; Sintes, E.; Dobal-Amador, V.; Hernando-Morales, V.; Álvarez, M.; Balagué, V.; Varela, M. M. Optical properties of dissolved organic matter relate to different depth-specific patterns of archaeal and bacterial community structure in the North Atlantic Ocean. *FEMS Microbiol. Ecol.* **2017**, *93* (1), 1-14.

Chapter 4

The role of dissolved organic matter composition in photochemical reactivity in the St. Louis River

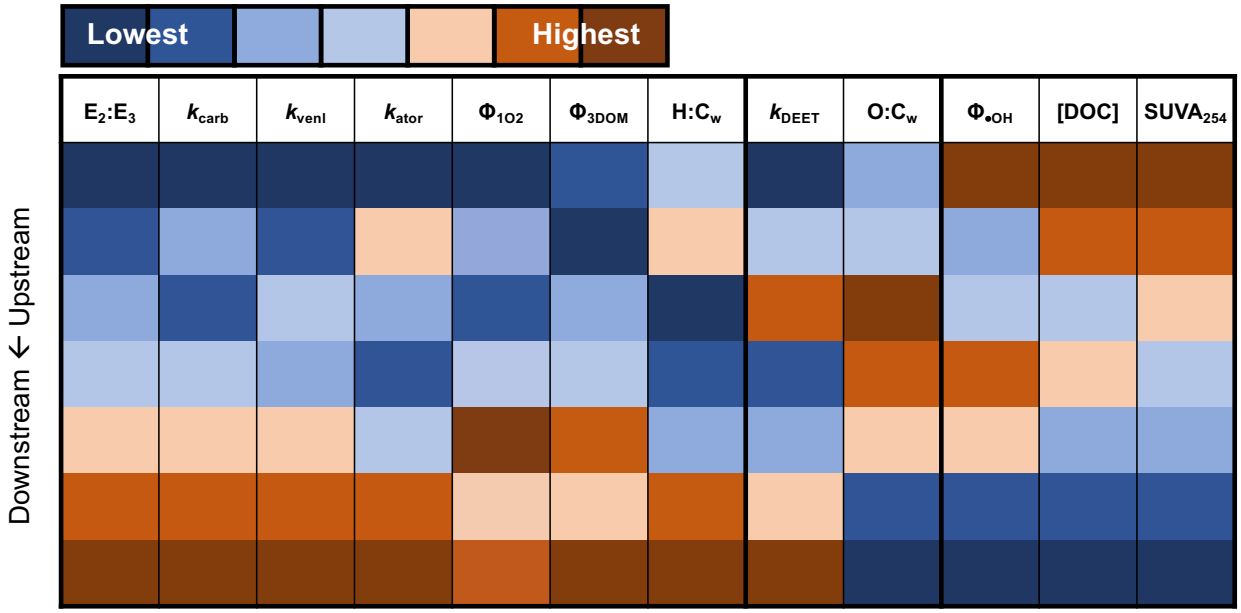

4.1 Details on Collaboration

Chapter 4 is a collaboration between Stephanie Berg, Christina Remucal, Kristine Wammer, Quinn Whiting, Joseph Herrli, and Ronan Winkels. All authors helped with sample collection. S.B. performed the DOM composition analyses and PPRI quantification. Q.W., J.H., and R.W. conducted the contaminant degradation experiments. S.B. wrote the manuscript with input from C.K. and K.W. This paper was published in *Environmental Science and Technology*, 2019, 53 (2), 11725 – 11734.

4.2 Abstract

Dissolved organic matter (DOM) composition influences its ability to form photochemically produced reactive intermediates (PPRI). While relationships have been established between bulk DOM properties and triplet DOM (^{3}DOM) and singlet oxygen ($^1O_2$) quantum yields, contradictory evidence exists for hydroxyl radical ($^\bullet$OH) and hydroxylating species. Furthermore, little is known about these relationships at the molecular level. We evaluated DOM composition and photochemical reactivity of water samples from a wastewater treatment plant and the St. Louis River in Minnesota and Wisconsin, USA. Bulk characterization using ultraviolet-visible spectroscopy demonstrates that color and apparent size of DOM decrease downstream, while molecular composition analysis using Fourier-transform ion cyclotron resonance mass spectrometry reveals that saturation and chemodiversity is highest near Lake Superior. ^{3}DOM quantum yield coefficients and $^1O_2$ quantum yields increase downstream and correlate strongly with saturated formulas. Similar results are observed for carbon-normalized photodegradation rate constants of atorvastatin, carbamazepine, and venlafaxine, which react primarily with ^{3}DOM and $^1O_2$. In contrast, $^\bullet$OH quantum yields are lowest downstream and correlate with less saturated, more oxygenated DOM, suggesting that ^{3}DOM is not its major precursor. Mixed relationships are observed for DEET, which reacts with multiple PPRI. Molecular-level compositional data reveal insights into the differing formation pathways of individual PPRI, but information about specific contaminants is needed to predict their photochemical fate.

4.3 Introduction

Dissolved organic matter (DOM) represents a significant pool of organic carbon in aquatic systems and participates in many reactions in the environment.[1,2] For example, DOM affects the transport of contaminants,[3] microbial metabolism,[4] formation of disinfection by-products during drinking water treatment,[5] and photochemical reactions that influence contaminant fate.[6] DOM reactivity in these processes depends on its composition,[7] which varies widely among natural waters and in engineered systems.

DOM forms highly reactive species called photochemically produced reactive intermediates (PPRI) in sunlit waters.[8–10] PPRI are strong oxidants and can degrade many organic contaminants via indirect photolysis.[6,11] Triplet DOM (^{3}DOM) is formed after ground state DOM absorbs a photon of light and undergoes intersystem crossing. ^{3}DOM can react with contaminants through energy or electron transfer. Furthermore, ^{3}DOM can transfer energy to molecular oxygen[12] or participate in electron-transfer reactions[13,14] to form singlet oxygen ($^1O_2$) and hydroxyl radical ($^\bullet$OH), respectively, which may also react with contaminants. Some PPRI, like $^\bullet$OH, are nonselective and react at diffusion-controlled rates with most contaminants.[15] However, the concentration of $^\bullet$OH is generally orders of magnitude lower than more selective PPRI, including ^{3}DOM and $^1O_2$.[16,17]

The ability of DOM to form PPRI depends on its composition and therefore varies among water samples.[7,18–20] Both microbially-derived and more processed DOM are considered to be more photochemically reactive based on higher quantum yields of ^{3}DOM and $^1O_2$ (Φ_{3DOM} and Φ_{1O2}).[18,20–22] Additionally, analysis of the molecular composition of DOM in lakes and stormwater reveals that more saturated formulas, which are more common in microbially-derived and processed DOM, are most strongly correlated with the formation of ^{3}DOM and $^1O_2$.[7,19]

There is conflicting evidence on the role of DOM composition in the quantum yields for $^{\bullet}OH$ ($\Phi_{\bullet OH}$), which may be formed through multiple pathways. The most commonly described mechanism involves reduction of O_2 to form superoxide radical anion ($O_2^{-\bullet}$), which undergoes dismutation to form hydrogen peroxide (H_2O_2)[23–25] and eventually $^{\bullet}OH$.[26] However, it is unclear whether ^{3}DOM is responsible for the initial reduction of O_2. Furthermore, some $^{\bullet}OH$ formation is observed even when H_2O_2 is quenched, suggesting that an additional H_2O_2-independent pathway is also possible.[26] This pathway could involve H-atom abstraction from water to produce free $^{\bullet}OH$ or other hydroxylating species.[26] In any of these pathways, the involvement of ^{3}DOM will dictate if $\Phi_{\bullet OH}$ follows the same trends as Φ_{3DOM} and Φ_{1O2}. In several studies, DOM that is highly efficient at producing ^{3}DOM and $^1O_2$ is inefficient at forming $^{\bullet}OH$, suggesting that ^{3}DOM is not a major $^{\bullet}OH$ precursor.[17,27–29] In contrast, other studies conclude that DOM samples with the highest Φ_{3DOM} and Φ_{1O2} also have the highest $\Phi_{\bullet OH}$, implying that ^{3}DOM is involved in either O_2 reduction or H-atom abstraction from water.[16,21,30] Relationships between composition and $\Phi_{\bullet OH}$ formation have yet to be shown at the molecular level.

Understanding the production of individual PPRI is important because these species react with contaminants of interest at different rates[31] and they are present at different concentrations in aquatic systems.[16] Therefore, when considering the role of photodegradation for contaminant fate, both the contaminant in question and the composition of DOM must be considered. In this study, we characterize DOM in water samples from the St. Louis River in terms of bulk properties, molecular composition, and photochemical reactivity towards formation of ^{3}DOM, $^1O_2$, and $^{\bullet}OH$. This watershed was selected because DOM in this system is highly diverse due to differing sources and extents of processing throughout the river.[32–34] Therefore, the insights about photochemical reactivity in the St. Louis River drawn from this data set can inform studies about DOM reactivity

from other freshwater and urban-impacted systems. Additionally, the rates of photodegradation of four target contaminants (i.e., atorvastatin, carbamazepine, *N*,*N*-diethyl-*m*-toluamide (DEET), and venlafaxine; **Figure C.1**) are quantified in each of the waters. These contaminants were selected because they degrade primarily by indirect photolysis and have been detected in the St. Louis River.[35–38] This unique combination of contaminant degradation studies with optical, molecular, and photochemical characterization of the DOM provides insights into the role of DOM composition in the production of PPRI and, ultimately, indirect photodegradation of contaminants.

4.4 Materials and Methods

4.4.1 Chemicals

All chemicals were used as received. Details are listed in **Appendix C.1**.

4.4.2 Sampling

Grab samples were collected from the surface of the river and from Lake Superior at least 1 m from the shore on August 16 – 17, 2016 (**Table C.1**; **Figure C.2**). Sand Creek (Site A), the furthest upstream sample, was collected from a tributary feeding the St. Louis River. Meadowlands (B) was collected directly from the St. Louis River near Sand Creek, and the River Inn (c) East Detroit (D) and Munger Landing (E) samples were taken from the river upstream of the effluent discharge. Final effluent was collected from the Western Lake Superior Sanitary District wastewater treatment plant (F), which treats a combination of municipal and industrial wastewater using advanced secondary treatment with pure oxygen, seasonal (April – October) disinfection with sodium hypochlorite and dechlorination with sodium bisulfite, and mixed media filtration.

The Blatnik Bridge sample (G) was collected downstream of the discharge within the river and the Wisconsin Point sample (H) was collected from the shore of Lake Superior.

4.4.3 Water Chemistry

pH, alkalinity, ions, cations, metals, and dissolved organic carbon concentrations ([DOC]) were quantified and absorbance spectra were collected from whole water samples (**Appendix C.3**; **Tables C.2 – C.5**).

4.4.4 Mass Spectrometry

Organic matter was extracted by solid phase extraction as described previously[39] and analyzed by Fourier-transform ion cyclotron resonance mass spectrometry (FT-ICR MS; SolariX XR 12T). Exported *m/z* peaks were converted to neutral masses and calibrated using common DOM formulas (**Appendix C.4**).[7,40] Assigned formulas were required to be within <0.5 ppm mass error and part of a homologous series (+CH_2 or CH_4 vs. O) with ≥3 members. Weighted averages of elemental ratios (H:C_w and O:C_w) and double bond equivalents (DBE_w) were calculated from identified formulas.[7,41] DOM isolated by the Agilent PPL cartridges used in this study is highly reflective of whole water DOM in terms of optical properties,[42] photochemical reactivity,[42] and FT-ICR MS analysis.[43]

4.4.5 Photochemistry

Quantum yield coefficients for ^{3}DOM (f_{TMP}), $\Phi_{^1O_2}$, and $\Phi_{\bullet OH}$ were quantified using whole water samples irradiated with 365 nm bulbs (full width half max = ± 10 nm)[44] in a Rayonet photoreactor. f_{TMP} is reported rather Φ_{3DOM} than to avoid the assumption of a constant ^{3}DOM

deactivation rate constant.[42] Experiments were performed in triplicate alongside a *p*-nitroanisole (PNA)/pyridine actinometer, which was used to quantify light intensity.[45,46] Probe compound stock solutions were prepared in Milli-Q water and spiked into water samples so that their initial concentration was 10 μM. 2,4,6-Trimethylphenol (TMP), furfuryl alcohol (FFA), and terephthalic acid (TPA) were used to measure ^{3}DOM, $^1O_2$, and $^\bullet$OH, respectively.[47] Note that TPA quantifies both free $^\bullet$OH and other low-energy hydroxylators;[26,48] the collection of these species are denoted as $^\bullet$OH for simplicity. Experiments were conducted at ambient pH (**Table C.2**) held constant with 10 mM phosphate. $^1O_2$ and $^\bullet$OH experiments were conducted at ambient [DOC], while TMP experiments were conducted with waters diluted to 2.5 mg-C L^{-1} because this probe is sensitive to [DOC].[19,42,49] FFA and TMP loss rates and hydroxyterephthalic acid formation rates were measured by high performance liquid chromatography (HPLC; **Appendix C.5**) and used to calculate PPRI steady-state concentrations and quantum yields in combination with UV-vis spectra as described in **Appendix C.6**.

Photodegradation rate constants of atorvastatin, carbamazepine, DEET, and venlafaxine degradation were quantified in the water samples. Solutions (10 μM) of each compound were prepared in each river water sample from 1 mM stock solutions. Samples were irradiated using an Atlas Suntest CPS+ solar simulator equipped with a xenon lamp (500 W/m^2) and an Atlas UV Suntest filter. DEET photodegradation was studied using the Rayonet photoreactor due to the relatively slow photodegradation rate of the compound. Contaminant concentrations were quantified by HPLC (**Appendix C.5**).

Quencher experiments were performed to investigate the role of PPRI in contaminant degradation. Contaminant degradation experiments were performed as described above with the addition of a quencher molecule (3 mM) to selected water samples. 1,4-Diazobicyclo[2.2.2]octane

(DABCO) and/or L-histidine were used to quench $^1O_2$, potassium sorbate was used to quench ^{3}DOM with energies >250 kJ mol^{-1}, and isopropanol was used to quench radicals, including $^{\bullet}$OH. Additional experiments were conducted under anoxic conditions (sparging with N_2 gas for 15 minutes) to measure impacts on photolysis rates when oxygen was not present.

4.5 Results and Discussion

4.5.1 Variability in Bulk DOM Composition

The St. Louis River and estuary is an ideal site to study the role of DOM composition in photochemistry because its composition varies widely throughout the system. Wetlands dominate the landcover surrounding the upstream sites, resulting in large inputs of terrestrial DOM into the river (**Appendix C.2**).[32–34,50–54] Sand Creek, a tributary that feeds the river, has the highest [DOC] of 69 mg-C L^{-1} (**Figure 4.1a**; **Table C.5**). Within the river, [DOC] ranges from 26.0 – 33.5 mg-C L^{-1}, which is similar to other measurements in the same system[32,33] and similar to [DOC] in the wastewater effluent. As urbanization surrounding the river increases,[34,53] [DOC] decreases.[55] The lowest [DOC] (i.e., 3.45 mg-C L^{-1}) is quantified in nearshore Lake Superior.

UV-vis spectroscopy shows that $SUVA_{254}$ decreases and E_2:E_3 increases moving downstream in the river (**Figure 4.1**; **Table C.5**). $SUVA_{254}$ is proportional to DOM aromaticity,[56] whereas E_2:E_3 is inversely proportional to molecular weight.[18,57] These parameters are typically inversely related[58] and processes such as photobleaching and microbial degradation, as well as increases in impervious land cover, can decrease $SUVA_{254}$ and increase E_2:E_3.[19,55,59–68] Therefore, the changes in bulk optical properties imply that DOM becomes less aromatic and smaller in molecular weight throughout the river and estuary. DOM in the headwaters is likely terrestrially-derived and has undergone limited environmental processing.[7,32,34,56,57,69] The optical properties of DOM in the

wastewater effluent and Lake Superior (sites F and H) are indicative of larger inputs of microbially-derived DOM or more extensive environmental processing of terrestrially-derived DOM.[19,55,59–68]

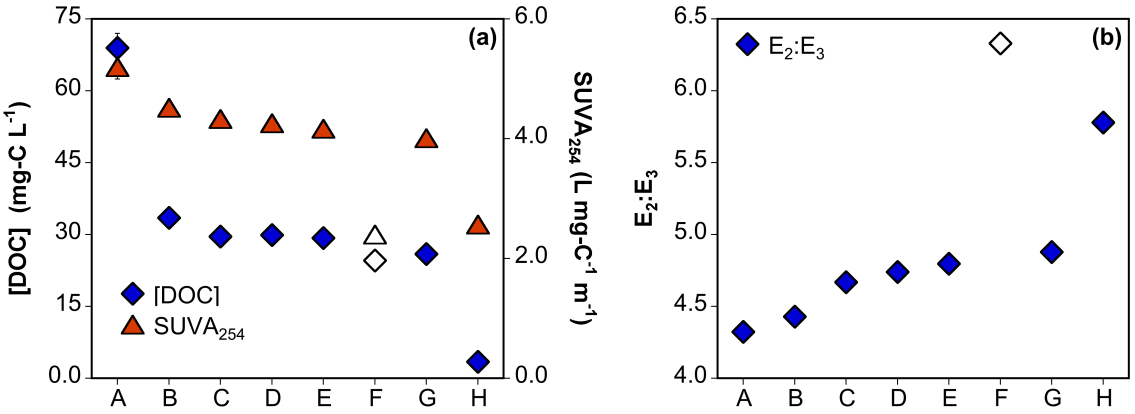

Figure 4.1. (a) [DOC], $SUVA_{254}$, and (b) E_2:E_3 for each sampling location. The wastewater sample (F) is denoted using hollow symbols. Site names are listed in **Table 4.1**. Error bars represent the standard deviation of triplicate measurements.

The bulk composition of DOM in the wastewater effluent is unique compared to the DOM in the natural waters. The wastewater effluent has the lowest $SUVA_{254}$ (2.40 L mg-C^{-1} m^{-1}) and highest E_2:E_3 (6.33; **Table C.5**), which is indicative of the microbially-derived DOM produced during secondary treatment. Similarly low $SUVA_{254}$ (range = 0.8 – 2.9 L mg-C^{-1} m^{-1}) and high E_2:E_3 values (range = 4.6 – 7.2) are reported in other wastewater effluents.[20,21,41,70] Although the Blatnik Bridge site shows elevated E_2:E_3 and lower $SUVA_{254}$ compared to upstream samples, <5% of the river downstream of the discharge location is comprised of wastewater (**Appendix C.2**) and it is not possible to distinguish between contributions of wastewater DOM and processing of terrestrial DOM using bulk measurements.

4.5.2 Molecular Composition of DOM

The molecular composition of DOM revealed by FT-ICR MS advances our knowledge of DOM sources and ultimately enables us to move beyond correlations with bulk properties to inform our understanding of photochemical reactivity. A total of 4,833 unique $C_{1-180}H_{1-140}O_{0-80}N_{0-1}S_{0-1}P_{0-1}Cl_{0-1}$ formulas are identified in the eight samples. An average of 1,779 formulas are identified in each sample, with the greatest number in the wastewater effluent (3,823 formulas; **Table C.6**; **Figures C.3 – C.7**). The percentage of formulas containing only CHO atoms decreases moving downstream in the river, while the percentages of CHON and CHOS formulas increases (**Table 4.1**). These changes may be attributable to increases in microbially-derived DOM inputs, which typically contain more nitrogen and sulfur.[7,41,71–73] Additionally, the high abundance of CHOS formulas in wastewater-derived samples is influenced by the presence of sulfur-containing surfactants, which ionize very well by electrospray.[41,74] Therefore, the high percentage of CHOS formulas in the Blatnik Bridge site (G) likely reflects the increased ionization ability of these wastewater-derived compounds even though the amount of wastewater in the river is low.

Weighted averages calculated from intensities of matched formulas provide additional insight into how DOM composition changes in the river. $H:C_w$ increases and DBE_w decreases moving downstream throughout the river (**Figure C.8**; **Table 4.1**). The wastewater effluent has the highest $H:C_w$ and lowest DBE_w values of 1.26 and 8.03, respectively, which agrees with past observations of wastewater effluent.[41,73] Sites downstream of the discharge also show higher $H:C_w$ and lower DBE_w values compared to upstream sites. The decrease in aromaticity agrees with the observed decrease in $SUVA_{254}$ (**Figure 4.1a**), while the decrease in $O:C_w$ demonstrates that the DOM becomes less oxidized.

Table 4.1. Total number of formulas, percent of heteroatom-containing formulas, and weighted averages of O:C, H:C, and DBE in each sample as detected by FT-ICR MS.

Sample	Total #	% CHO	% CHON	% CHOS	% CHOP	% CHOCl	$H:C_w$	$O:C_w$	DBE_w
A. Sand Creek	1179	84.1	2.2	6.4	1.6	5.7	1.096	0.540	9.942
B. Meadowlands	1309	80.4	4.4	10.9	0.7	3.5	1.098	0.540	10.054
C. River Inn	1437	78.4	4.1	11	1.3	5.2	1.089	0.546	10.158
D. East Detroit	1526	74.7	4.3	11.9	1.5	7.5	1.093	0.544	10.086
E. Munger Landing	1286	78.9	3.6	11.1	1.6	4.8	1.096	0.541	9.984
F. Wastewater	3823	43.1	5.2	34	4.2	13.6	1.263	0.481	8.029
G. Blatnik Bridge	2479	66.1	6.9	20.1	0.8	6.0	1.123	0.528	9.656
H. Wisconsin Point	1662	66.5	4.2	10.8	4.4	14.2	1.212	0.494	8.865

The mass spectrometry data confirms that DOM shifts from terrestrially-derived DOM to DOM that is more processed and/or more microbial in composition. This shift is evidenced by decreases in molecular weight and aromaticity, as well as increases in saturation and chemodiversity of DOM (**Figure C.8**; **Table 4.1**). Bray-Curtis dissimilarity analysis, based on the presence and absence of formulas, shows that samples generally cluster together based on geographical location within the river (**Figure C.9**). The composition of wastewater DOM is unique and clusters separately from the riverine samples, while the site located downstream of the discharge (i.e., Blatnik Bridge) falls between the wastewater effluent and the other natural samples. This analysis complements our observations of the elevated percentage of CHOS formulas and

lower DBE_w values at this site, which we attribute to influence of highly ionizable CHOS formulas from wastewater effluent. These analyses show that mass spectrometry data can be used to observe impacts of discharge on DOM composition in downstream sites which was inconclusive considering bulk properties alone.

The optical and molecular DOM characterization provides complementary insight into how the DOM changes in the St. Louis River. This is shown further by Spearman rank correlations between optical measurements with relative intensities of formulas commonly detected by FT-ICR MS. Formulas positively correlated with $SUVA_{254}$ are located in the more oxygenated and less saturated region of the plot, which is dominated by tannin- and lignin-like compounds that are typically highly aromatic (**Figure C.10**).[7,75–77] In contrast, formulas most positively correlated with E_2:E_3 are more saturated.

4.5.3 Formation of ^{3}DOM and $^1O_2$

Quantum yields are used to assess the photochemical reactivity of the samples because they are normalized to rate of light absorbance, which corrects for the variable [DOC] observed in the St. Louis River. Steady-state concentrations are reported in **Appendix C.6**. Measured Φ_{1O2} (range = (5.4 – 10.3) x 10^{-3}) follow the same trends as f_{TMP} (range = 35.2 – 69 M^{-1}; **Table C.9**) which is expected because ^{3}DOM is a precursor for $^1O_2$ and the yield for this process is quite high.[12] It is important to note that O_2 and TMP likely probe different pools of ^{3}DOM. All triplets that react by energy transfer are theorized to be able to be quenched by O_2. However, only triplets with reduction potentials sufficient to oxidize TMP are detected in ^{3}DOM quantification experiments.[12,78] Quantum yields for both PPRI fall within ranges reported for other waters.[7,16,17,19,79] Generally, f_{TMP} and Φ_{1O2} increase moving downstream in the river as the DOM becomes more efficient at

producing ^{3}DOM and $^{1}O_2$ per photon of light absorbed (**Figure 4.2a**). Wastewater effluent is highly efficient at forming ^{3}DOM and $^{1}O_2$, in agreement with previous observations.[20,21,80]

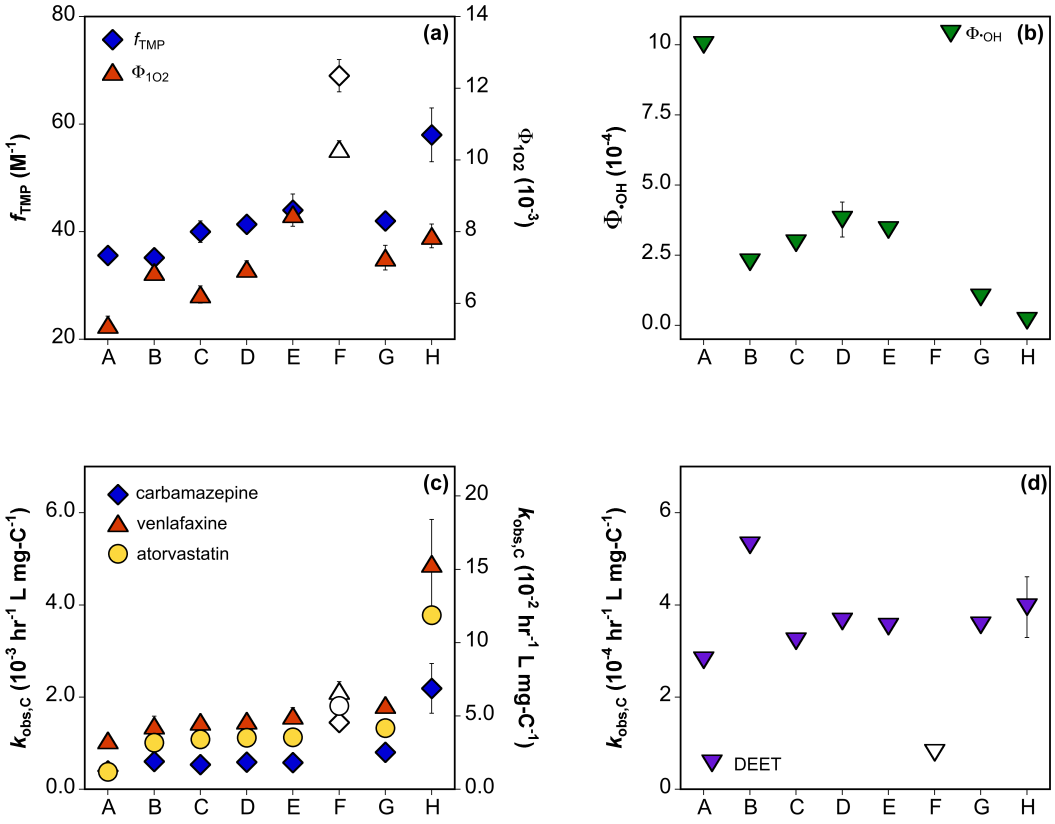

Figure 4.2. (a) f_{TMP} and Φ_{1O2} (right axis), (b) $\Phi_{\bullet OH}$ (c) $k_{obs,C}$ for carbamazepine, venlafaxine, atorvastatin (right axis), and (d) $k_{obs,C}$ for DEET for each sampling location. Site names are listed in **Table C.1**. The wastewater sample (F) is denoted by hollow points. Error bars represent the standard deviation of triplicate measurements except for $k_{obs,C}$ for DEET, which was measured in duplicate.

Linear regressions between optical properties and ^{3}DOM-related quantum yields suggest that predicting these parameters is possible based on simple bulk measurements. For example, E_2:E_3 is typically positively correlated with Φ_{1O2} and loss rates of 2,4,6-trimethylphenol.[7,19,20,22,80–82] This trend is also observed within our data, with positive correlations between E_2:E_3 and f_{TMP} (p

$<10^{-5}$) and Φ_{1O2} ($p = 0.008$; **Figure C.12**). Negative correlations between $SUVA_{254}$ and f_{TMP} ($p = 0.0002$) or Φ_{1O2} ($p = 0.01$) are weaker, but still significant (**Figure C.13**).

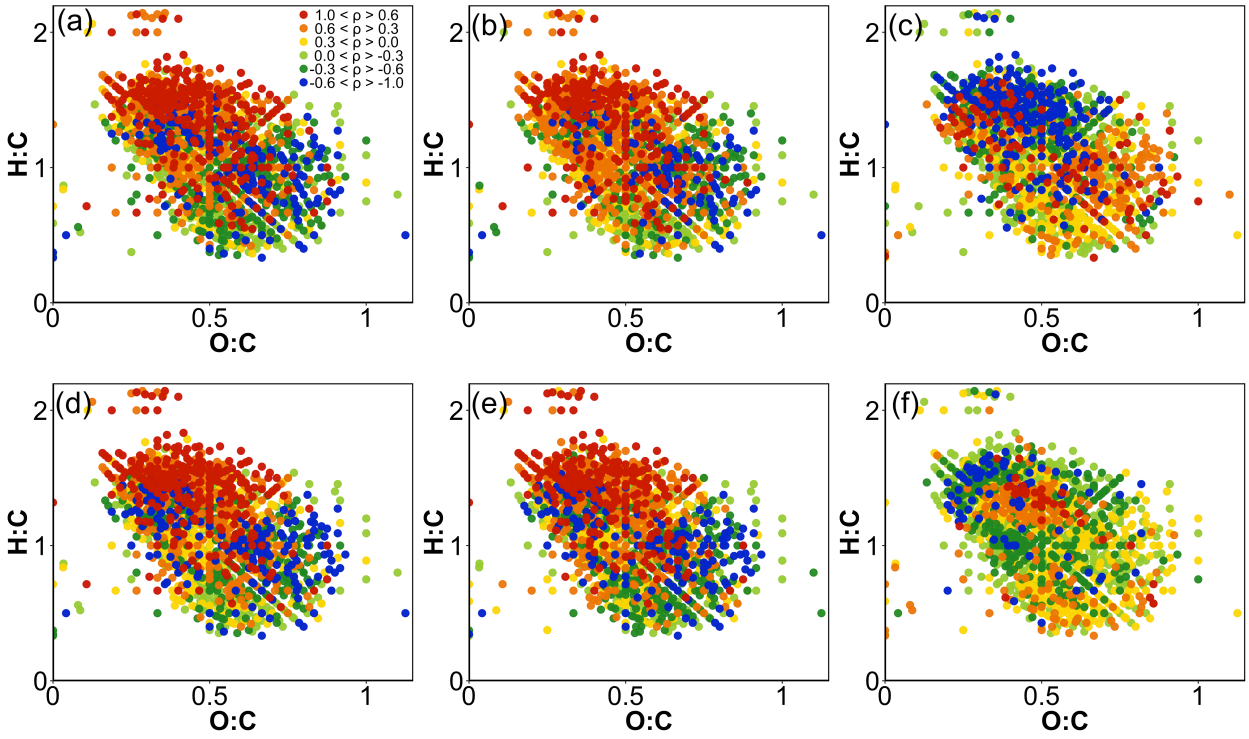

Figure 4.3. Spearman rank correlations between relative formula intensities as detected by FT-ICR MS in at least six samples and (a) f_{TMP}, (b) Φ_{1O2}, and (c) $\Phi_{\bullet OH}$. Spearman rank correlations between relative formula intensities as detected by FT-ICR MS and $k_{obs,C}$ for (d) carbamazepine, (e) atorvastatin, and (f) DEET. Warmer colors correspond to positive correlations; cooler colors correspond to negative correlations.

Comparisons between FT-ICR MS data and PPRI quantum yields demonstrate which specific pools of DOM within a single sample are most strongly associated with PPRI formation, rather than simply samples as a whole. The relationships between formula intensities determined by FT-ICR MS and quantum yields are investigated using Spearman rank correlations for common formulas found in ≥6 samples. Highly saturated formulas are most positively correlated with f_{TMP} and Φ_{1O2} (**Figure 4.3**). Similar trends are observed in rural lake samples using FFA and hexadienoic acid as energy transfer probes for $^1O_2$ and ^{3}DOM, respectively, and for stormwaters

using TMP as an electron-transfer ^{3}DOM probe.[7,19] Spearman rank rho values between formula intensity and f_{TMP} are strongly correlated with values for Φ_{1O2}, suggesting that a very similar pool of DOM is associated with the formation of these PPRI ($p < 10^{-5}$; **Figure C14a**; **Table C.10**) as expected because ^{3}DOM is a known precursor to $^1O_2$. Additionally, the DOM pool most correlated with f_{TMP} and Φ_{1O2} is similar to the pool positively correlated to E_2:E_3 ($p < 10^{-5}$ for both; **Figure C.15**) and negatively correlated to $SUVA_{254}$ ($p < 0^{-5}$ for both; **Figure C.16**).

The combination of characterization data and photochemical measurements inform observed differences in production of ^{3}DOM and $^1O_2$. Correlations between E_2:E_3 and quantum yields indicate that low molecular weight DOM molecules are most efficient at forming ^{3}DOM and $^1O_2$. These results are consistent with the observation that ^{3}DOM formation rates are similar across DOM types, but that the rate of light absorbance is higher for larger, more aromatic molecules.[18] Because not all chromophores participate in photochemical reactions to produce ^{3}DOM, a smaller quantum yield is observed. As a result, low molecular weight and aliphatic DOM have higher f_{TMP}. Because ^{3}DOM is a direct precursor to $^1O_2$,[7,18,20,83,84] this trend is also observed for $^1O_2$. This is the first study to show that these relationships hold across DOM samples with very different composition, implying that the trends observed here are potentially universal in freshwaters and wastewater-impacted sites.

4.5.4 Differing Formation Pathways of $^{\bullet}$OH

There are multiple mechanisms for generating $^{\bullet}$OH in sunlit waters. In the H_2O_2-dependent pathway, a species formed during irradiation (e.g., ^{3}DOM) reduces O_2 to $O_2^{-\bullet}$. $O_2^{-\bullet}$ undergoes dismutation to form H_2O_2, which forms $^{\bullet}$OH through homolytic cleavage. Quenching $O_2^{-\bullet}$ and H_2O_2 decreases $^{\bullet}$OH production, providing evidence that this pathway is important in natural

waters.[23,24,26] However, an H_2O_2-independent pathway which involves H-atom abstraction from water to generate $^{\bullet}OH$ has also been proposed because $^{\bullet}OH$ is still detected when H_2O_2 is quenched.[26] ^{3}DOM could be involved in either O_2 reduction or H-atom abstraction, but its role is unclear. While the aim of this study is not to distinguish between these possible pathways, the molecular-level analysis allows us to test the hypothesis that ^{3}DOM is a key precursor in $^{\bullet}OH$ formation. Note that photo-Fenton reactions and nitrate/nitrite photolysis as sources of $^{\bullet}OH$ can be neglected due to negligible concentrations of iron and nitrite (**Tables C.3** and **C.4**) and the minimal overlap between the 365-nm bulbs and the nitrate absorbance spectrum.[85]

If ^{3}DOM is a precursor to $^{\bullet}OH$ as it is for $^1O_2$, $\Phi_{\bullet OH}$ should follow similar trends as f_{TMP} and Φ_{1O2}. However, conflicting evidence exists about the relationship between $\Phi_{\bullet OH}$ and other PPRI. In some cases, positive correlations between $\Phi_{\bullet OH}$ and other PPRI or E_2:E_3 indicate that low molecular weight DOM is most efficient at producing $^{\bullet}OH$.[16,21,86] Conversely, other studies show $\Phi_{\bullet OH}$ correlates inversely with other PPRI or E_2:E_3.[28,29,82] Additionally, H_2O_2 quantum yields are inversely proportional to Φ_{1O2},[17] which is important because H_2O_2 can produce $^{\bullet}OH$.[87] Finally, $\Phi_{\bullet OH}$ correlates with f_{TMP} in one study, while Φ_{1O2} follows the opposite trend;[27] this observation is unusual because ^{3}DOM does not correlate with $^1O_2$.

In this study, $\Phi_{\bullet OH}$ follows opposite trends as f_{TMP} and Φ_{1O2}. $\Phi_{\bullet OH}$ ranges from (2.16 – 100) x 10^{-5} (**Table C.9**), which is similar to other water samples.[16,79,86,88] In contrast to f_{TMP} and Φ_{1O2}, $\Phi_{\bullet OH}$ does not consistently increase moving downstream in the river (**Figure 4.2b**) and the highest $\Phi_{\bullet OH}$ is measured in the sample collected farthest upstream. $\Phi_{\bullet OH}$ does not correlate significantly with E_2:E_3 or $SUVA_{254}$ ($p = 0.2$ and 0.1, respectively; **Figures C.12c** and **C.13c**), although interestingly the directions of the relationships are opposite those of f_{TMP} and Φ_{1O2}. At the molecular level, Spearman rank correlations with $\Phi_{\bullet OH}$ show nearly the opposite arrangement of

f_{TMP} and $\Phi_{^1O_2}$ on the van Krevelen diagram (**Figure 4.3c**). Formulas most positively correlated with $\Phi_{\bullet OH}$ are more oxygenated and less saturated than formulas positively correlated with f_{TMP} and $\Phi_{^1O_2}$. Plotting Spearman rank rho values for correlations between formula intensity and $\Phi_{\bullet OH}$ compared to the other two PPRI results in a negative relationship ($p < 10^{-5}$ for both; **Figure C.14**; **Table C.10**). At the molecular level, $\Phi_{\bullet OH}$ decreases with increasing E_2:E_3 and increases with $SUVA_{254}$ ($p < 10^{-5}$ for both; **Figures C.15c** and **C.16c**).

These results suggest that DOM formulas that are more aromatic and oxygenated are most efficient at forming $^{\bullet}OH$ per photon absorbed, which is opposite the trend observed for ^{3}DOM and $^1O_2$. This is the first time that this relationship has been shown for $\Phi_{\bullet OH}$ at the molecular level. The clear divergence between formulas associated with ^{3}DOM and $^{\bullet}OH$ provide evidence that the major $^{\bullet}OH$ formation pathway does not involve ^{3}DOM as a precursor. Other potential precursors include ^{1}DOM, charge-transfer states, or exciplexes involving photochemically excited DOM;[23,24] more research is needed differentiate between these possibilities. In the H_2O_2-dependent pathway, $\Phi_{\bullet OH}$ should increase with increasing electron donating capacity (EDC) of the DOM. For example, reducing DOM leads to enhanced $^{\bullet}OH$ formation in the dark.[89,90] EDC is attributed to phenolic molecules[91] which are located on the same region of the van Krevelen diagram as the formulas positively correlated with $\Phi_{\bullet OH}$ in this study. Thus, our results in the context of existing literature support an $^{\bullet}OH$ formation pathway where a non-^{3}DOM species formed during irradiation reduces O_2, ultimately forming $^{\bullet}OH$ with H_2O_2 as an intermediate.

4.5.5 Indirect Photodegradation of Pharmaceuticals

The four target contaminants primarily undergo indirect photolysis. Indirect photodegradation rate constants are up to 11x, 19x, 1200x, and 6.7x faster for atorvastatin, carbamazepine, DEET,

and venlafaxine, respectively, than direct photodegradation rate constants (**Table C.11**). Additionally, carbon-normalized indirect photodegradation rate constants ($k_{obs,C}$) vary among the water samples for all of the contaminants (**Figure 4.2**; **Table C.12**). For atorvastatin, carbamazepine, and venlafaxine, the largest $k_{obs,C}$ is measured in the furthest downstream site, with enhanced photodegradation also observed in wastewater effluent. Less variability exists in $k_{obs,C}$ for DEET, but it is noteworthy the lowest $k_{obs,C}$ is observed in wastewater effluent. The variability of these rate constants, even after normalized to [DOC], indicates DOM composition plays a key role in the indirect photodegradation of contaminants.

Because contaminants react with individual PPRI with different rate constants, changes in PPRI formation affect contaminant degradation. Bulk characteristics are largely unsuccessful at predicting $k_{obs,C}$. For carbamazepine and venlafaxine, $k_{obs,C}$ correlates positively with E_2:E_3 ($p = 0.008$ and 0.045, respectively; **Figure C.12**) and negatively with $SUVA_{254}$ ($p = 0.002$ and 0.011, respectively; **Figure C.13**). Insignificant relationships are observed for venlafaxine and DEET, but it should be noted that the direction of trends for $k_{obs,C}$ for venlafaxine match those of carbamazepine and atorvastatin but are opposite for DEET. At the molecular level, Spearman rank correlations between relative formula intensity and $k_{obs,C}$ vary amongst the contaminants (**Figures 4.3** and **C.17**). For atorvastatin, carbamazepine, and venlafaxine, more saturated formulas generally correlate positively with contaminant degradation. Spearman rank rho values for these three contaminants correlate positively with rho values for Φ_{3DOM} and Φ_{1O2} ($p < 10^{-5}$; **Figures C.18** and **C19**), but negatively with rho values for $\Phi_{\bullet OH}$ ($p < 10^{-5}$; **Figure C.20**; **Table C.10**). A less pronounced pattern of correlations is observed between $k_{obs,C}$ for DEET and relative formula intensity (**Figure 4.3f**). However, unlike the other contaminants, the strongest negative correlations are observed in highly saturated formulas (**Figure 4.3f**). Spearman rank rho values

between $k_{obs,C}$ for DEET correlate negatively with rho values for all of the PPRI quantum yields ($p < 10^{-5}$ for all; **Figures C.18 – C.20**), although the slope of this correlation for $^{\bullet}OH$ is much shallower. Together, these results suggest that atorvastatin, carbamazepine, and venlafaxine react with ^3DOM and/or $^1O_2$, while the PPRI involved in DEET photodegradation are less clear.

Contaminant photodegradation experiments with quenchers corroborate Spearman rank correlations and confirm which PPRI are most responsible for contaminant degradation. For carbamazepine, sorbate decreases the unquenched rate constant by 76% on average (**Figure C.21**; **Table C.13**), suggesting that carbamazepine reacts with ^3DOM and/or $^1O_2$ since $^1O_2$ precursors are also quenched by sorbate. The 2,500% increase in carbamazepine degradation under anoxic conditions confirms that ^3DOM is most important since the lifetime of triplets is much longer in the absence of O_2. Quencher experiments with venlafaxine are similar to those with carbamazepine, indicating that ^3DOM is also important for its degradation (**Figure C.22**). We conclude that other PPRI also contribute to the photodegradation of venlafaxine because the addition of DABCO and isopropyl alcohol also decrease its photodegradation rate constant (68% and 36%, respectively). Quenchers have a less pronounced effect on the degradation rate constant for atorvastatin (**Figure C.23**), although the 145% enhancement under anoxic condition suggest that low energy triplets not quenched by sorbate may contribute.[12] Lastly, the degradation rate constant for DEET decreases in the presence of sorbate (85%), histidine (36%), and isopropyl alcohol (88%; **Figure C.24**). Importantly, the rate constant for degradation of DEET decreases more significantly with the addition of isopropyl alcohol compared to any other contaminant tested and agrees with the observed $[^{\bullet}OH]_{ss}$ (**Appendix C.7**), indicating that $^{\bullet}OH$ plays the largest role in the degradation of this compound.

Our work corroborates previous studies concluding indirect photolysis is more important than direct photolysis for atorvastatin,[36,92] carbamazepine,[36,93,94] DEET,[38] and venlafaxine.[37] Most studies cite ^{3}DOM and $^1O_2$ as important for the contaminants,[36,38,92–94] which is also noted in this study. However, it is surprising that venlafaxine appears to degrade through reaction with $^1O_2$ due to a lack functional groups known to react with this PPRI.[95,96] What varies the most among studies is the relative importance of $^\bullet$OH towards the degradation of each contaminant, although this is likely dependent on the composition of DOM used in the study and the relative amounts of sensitizer and contaminant. We conclude that $^\bullet$OH plays an important role in the degradation of venlafaxine and DEET, with only minor roles in the degradation of atorvastatin and carbamazepine.

4.6 Environmental Implications

Indirect photodegradation plays an important role in the fate many organic contaminants in natural waters, particularly in high [DOC] waters like the St. Louis River where direct photodegradation is limited.[97] It is not yet possible to predict rates of contaminant photodegradation because the production of PPRI and the reaction of PPRI with individual compounds depends on the composition of DOM and the contaminant, respectively. For this reason, our study includes detailed characterization at both the bulk and molecular level along with full photochemical analysis including PPRI formation and contaminant degradation experiments. The comprehensive approach taken in this study using DOM that spans a wide range in composition makes conclusions drawn transferrable to other systems and contaminants.

Both bulk and molecular characterization techniques used in this study confirm that DOM composition varies within the St. Louis River and estuary. Combined, we observe that DOM

becomes less aromatic and smaller in molecular weight moving towards Lake Superior. This shift in DOM composition may make DOM more bioavailable to microorganisms,[4,61] which can alter metabolic pathways.[98] Additionally, the compositional data presented here demonstrate that bulk and molecular characterization techniques agree with one another, suggesting that simple UV-vis parameters can be applied to study overall changes in DOM composition. However, the addition of FT-ICR MS analysis allows us to evaluate chemodiversity and observe influences of wastewater effluent on DOM composition in downstream samples.

The photochemical reactivity of DOM with respect to formation of PPRI changes with DOM composition. f_{TMP} and Φ_{1O2} increase moving downstream, while patterns for $\Phi_{\bullet OH}$ are less pronounced. At the molecular level, we observe that the aromatic pool of DOM correlates positively with $\Phi_{\bullet OH}$ and negatively with f_{TMP} and Φ_{1O2}. Links between f_{TMP} and Φ_{1O2} and molecular characterization have been observed previously,[7,19] but this study is the first to show correlations with $\Phi_{\bullet OH}$. This is important given the lack of significant trends between $\Phi_{\bullet OH}$ and bulk DOM parameters in this study, as well as the disagreeing trends for $\Phi_{\bullet OH}$ and bulk DOM characteristics in the literature. Our approach reveals that molecular level detail can provide insight into DOM reactivity when such trends cannot be obtained using bulk measurements and provides evidence for a mechanism of $^{\bullet}$OH formation that does not involve ^{3}DOM as a precursor.

Results of this study have important implications for contaminant fate in the environment. Contaminant photodegradation experiments show that photodegradation rates will change as DOM composition changes. Furthermore, the ways in which degradation rates change are dependent upon the contaminant in question, complicating our ability to predict contaminant fate with respect to photodegradation. In fact, the individual formulas within DOM most correlated to contaminant degradation are compound-specific and depend on the PPRI most responsible for the degradation

of that contaminant. Therefore, data is needed both about the composition of DOM and the role of PPRI in target contaminant photodegradation to predict contaminant fate in the environment. This is complicated by the fact that simple measurements of DOM composition like UV-vis spectroscopy may not be enough to predict PPRI quantum yields, especially $\Phi_{\bullet OH}$. Future work should focus on properties of DOM that may control formation of PPRI and especially $^{\bullet}OH$, including the redox activity of DOM.

4.7 Acknowledgements

This work was supported by Wisconsin Sea Grant (R/HCE-31) and the University of St. Thomas Undergraduate Research Opportunities Program (UROP). We acknowledge Andrew Maizel for assistance with sampling, Joseph Mayasich at WLSSD for assistance with wastewater effluent sampling, and Jonathan Remucal for assistance with GIS. We also thank Michael Tate at USGS for acquisition of excitation emission matrices. The authors acknowledge the UW-Madison Human Proteomics Program Mass Spectrometry Facility (initially funded by the Wisconsin partnership funds) for support in obtaining mass spectrometry data, NIH S10OD018475 for the acquisition of ultrahigh resolution mass spectrometer for biomedical research, and Ziqing Lin for assistance with the instrument.

4.8 References

(1) Buffam, I.; Turner, M. G.; Desai, A. R.; Hanson, P. C.; Rusak, J. A.; Lottig, N. R.; Stanley, E. H.; Carpenter, S. R. Integrating aquatic and terrestrial components to construct a complete carbon budget for a north temperate lake district. *Glob. Chang. Biol.* **2011**, *17* (2), 1193–1211.

(2) Tranvik, L. J.; Downing, J. A.; Cotner, J. B.; Loiselle, S. A.; Striegl, R. G.; Ballatore, T. J.; Dillon, P.; Finlay, K.; Fortino, K.; Knoll, L. B.; Kortelainen, P. L.; Kutser, T.; Larsen, S.; Laurion, I.; Leech, D. M.; McCallister, S. L.; McKnight, D. M.; Melack, J. M.; Overholt, E.; Porter, J. A.; Prairie, Y.; Renwick, W. H.; Roland, R.; Sherman, B. S.; Schindler, D. W.;

Sobek, S.; Tremblay, A.; Vanni, M. J.; Verschoor, A. M.; von Wachenfeldt, E. Weyhenmeyer, G. A. Lakes and reservoirs as regulators of carbon cycling and climate. *Limnol. Oceanogr.* **2009**, *54* (6), 2298–2314.

(3) Aiken, G. R.; Hsu-Kim, H.; Ryan, J. N. Influence of dissolved organic matter on the environmental fate of metals, nanoparticles, and colloids. *Environ. Sci. Technol.* **2011**, *45* (8), 3196–3201.

(4) Bai, L.; Cao, C.; Wang, C.; Xu, H.; Zhang, H.; Slaveykova, V. I.; Jiang, H.-L. Towards quantitative understanding of the bioavailability of dissolved organic matter in freshwater lake during cyanobacteria blooming. *Environ. Sci. Technol.* **2017**, *51*, 6018–6026.

(5) Rook, J. J. Chlorination reactions of fulvic acids in natural waters. *Environ. Sci. Technol.* **1977**, *11* (5), 478–482.

(6) Remucal, C. K. The role of indirect photochemical degradation in the environmental fate of pesticides: A review. *Environ. Sci.: Processes and Impacts*. **2014,** *16* (4), 628–653.

(7) Maizel, A. C.; Li, J.; Remucal, C. K. Relationships between dissolved organic matter composition and photochemistry in lakes of diverse trophic status. *Environ. Sci. Technol.* **2017**, *51* (17), 9624–9632.

(8) Haag, W. R.; Hoigné, J.; Gassman, E.; Braun, A. M. Singlet oxygen in surface waters - Part II: Quantum yields of its production by some natural humic materials as a function of wavelength. *Chemosphere* **1984**, *13* (5–6), 641–650.

(9) Haag, W. R.; Hoigné, J. Photo-sensitized oxidation in natural water via $^{\bullet}$OH radicals. *Chemosphere* **1985**, *14* (11–12), 1659–1671.

(10) Zepp, Richard G.; Solfe, N. Lee; Baughman, G. L.; Hollis, R. C. Singlet oxygen in natural waters. *Nature* **1977**, *267*, 421–428.

(11) Boreen, A. L.; Arnold, W. A.; McNeill, K. Photodegradation of pharmaceuticals in the aquatic environment: A review. *Aquat. Sci***. 2003**, *65* (4), 320–341.

(12) McNeill, K.; Canonica, S. Triplet state dissolved organic matter in aquatic photochemistry: Reaction mechanisms, substrate scope, and photophysical properties. *Environ. Sci.: Process. Impacts* **2016**, *18* (11), 1381–1399.

(13) Zhang, Y.; Del Vecchio, R.; Blough, N. V. Investigating the mechanism of hydrogen peroxide photoproduction by humic substances. *Environ. Sci. Technol.* **2012**, *46* (21), 11836–11843.

(14) Canonica, S. Oxidation of aquatic organic contaminants induced by excited triplet states. *Chimia (Aarau).* **2007**, *61* (10), 641–644.

(15) Shemer, H.; Sharpless, C. M.; Elovitz, M. S.; Linden, K. G. Relative rate constants of contaminant candidate list pesticides with hydroxyl radicals. *Environ. Sci. Technol.* **2006**, *40* (14), 4460–4466.

(16) McCabe, A. J.; Arnold, W. A. Seasonal and spatial variabilities in the water chemistry of prairie pothole wetlands influence the photoproduction of reactive intermediates. *Chemosphere* **2016**, *155*, 640–647.

(17) Dalrymple, R. M.; Carfagno, A. K.; Sharpless, C. M. Correlations between dissolved organic matter optical properties and quantum yields of singlet oxygen and hydrogen peroxide. *Environ. Sci. Technol.* **2010**, *44* (15), 5824–5829.

(18) Maizel, A. C.; Remucal, C. K. Molecular composition and photochemical reactivity of size-fractionated dissolved organic matter. *Environ. Sci. Technol.* **2017**, *51*, 2113–2123.

(19) McCabe, A. J.; Arnold, W. A. Reactivity of triplet excited states of dissolved natural organic matter in stormflow from mixed-use watersheds. *Environ. Sci. Technol.* **2017**, *51*, 9718–

9728.
(20) Bodhipaksha, L. C.; Sharpless, C. M.; Chin, Y. P.; Sander, M.; Langston, W. K.; Mackay, A. A. Triplet photochemistry of effluent and natural organic matter in whole water and isolates from effluent-receiving rivers. *Environ. Sci. Technol.* **2015**, *49* (6), 3453–3463.
(21) Dong, M. M.; Rosario-Ortiz, F. L. Photochemical formation of hydroxyl radical from effluent organic matter: *Environ. Sci. Technol.* **2012**, *46* (7), 3788–3794.
(22) Peterson, B. M.; McNally, A. M.; Cory, R. M.; Thoemke, J. D.; Cotner, J. B.; McNeill, K. Spatial and temporal distribution of singlet oxygen in Lake Superior. *Environ. Sci. Technol.* **2012**, *46* (13), 7222–7229.
(23) Garg, S.; Rose, A. L.; Waite, T. D. Photochemical production of superoxide and hydrogen peroxide from natural organic matter. *Geochim. Cosmochim. Acta* **2011**, *75* (15), 4310–4320.
(24) Garg, S.; Rose, A. L.; Waite, T. D. Production of reactive oxygen species on photolysis of dilute aqueous quinone solutions. *Photochem. Photobiol.* **2007**, *83* (4), 904–913.
(25) Zhang, Y.; V. Blough, N. Photoproduction of one-electron reducing intermediates by chromophoric dissolved organic matter (CDOM): Relation to O_2^- and H_2O_2 photoproduction and CDOM photooxidation. *Environ. Sci. Technol.* **2016**, *50* (20), 11008–11015.
(26) Page, S. E.; Arnold, W. A.; McNeill, K. Assessing the contribution of free hydroxyl radical in organic matter- sensitized photo-hydroxylation reactions. *Environ. Sci. Technol.* **2011**, *45* (7), 1–11.
(27) Sharpless, C. M.; Aeschbacher, M.; Page, S. E.; Wenk, J.; Sander, M.; McNeill, K. Photooxidation-induced changes in optical, electrochemical, and photochemical properties of humic substances. *Environ. Sci. Technol.* **2014**, *48* (5), 2688–2696.
(28) Page, S. E.; Logan, J. R.; Cory, R. M.; McNeill, K. Evidence for dissolved organic matter as the primary source and sink of photochemically produced hydroxyl radical in arctic surface waters. *Environ. Sci. Process. Impacts* **2014**, *16* (4), 807–822.
(29) Glover, C. M.; Rosario-Ortiz, F. L. Impact of halides on the photoproduction of reactive intermediates from organic matter. *Environ. Sci. Technol.* **2013**, *47* (24), 13949–13956.
(30) McKay, G.; Couch, K. D.; Mezyk, S. P.; Rosario-Ortiz, F. L. Investigation of the coupled effects of molecular weight and charge-transfer interactions on the optical and photochemical properties of dissolved organic matter. *Environ. Sci. Technol.* **2016**, *50* (15), 8093–8102.
(31) McConville, M. B.; Mezyk, S. P.; Remucal, C. K. Indirect photodegradation of the lampricides TFM and niclosamide. *Environ. Sci. Process. Impacts* **2017**, *19* (8), 1028–1039.
(32) Minor, E.; Stephens, B. Dissolved organic matter characteristics within the Lake Superior watershed. *Org. Geochem.* **2008**, *39* (11), 1489–1501.
(33) Minor, E. C.; Steinbring, C. J.; Longnecker, K.; Kujawinski, E. B. Characterization of dissolved organic matter in Lake Superior and its watershed using ultrahigh resolution mass spectrometry. *Org. Geochem.* **2012**, *43*, 1–11.
(34) Stephens, B. M.; Minor, E. C. DOM Characteristics along the continuum from river to receiving basin: A comparison of freshwater and saline transects. *Aquat. Sci.* **2010**, *72* (4), 403–417.
(35) Christensen, V. G.; Lee, K. E.; Kieta, K. A.; Elliott, S. M. Presence of selected chemicals of emerging concern in water and bottom sediment from the St. Louis River, St. Louis Bay, and Superior Bay, Minnesota and Wisconsin, 2010. **2012**, U.S. Geological Survey Scientific

Investigations Report, 1-36.
(36) Lam, M. W.; Mabury, S. A. Photodegradation of the pharmaceuticals atorvastatin, carbamazepine, levofloxacin, and sulfamethoxazole in natural waters. *Aquat. Sci.* **2005**, *67* (2), 177–188.
(37) Rúa-Gómez, P. C.; Püttmann, W. Degradation of lidocaine, tramadol, venlafaxine and the metabolites *o*-desmethyltramadol and *o*-desmethylvenlafaxine in surface waters. *Chemosphere* **2013**, *90* (6), 1952–1959.
(38) Antonopoulou, M.; Skoutelis, C. G.; Daikopoulos, C.; Deligiannakis, Y.; Konstantinou, I. K. Probing the photolytic-photocatalytic degradation mechanism of DEET in the presence of natural or synthetic humic macromolecules using molecular-scavenging techniques and EPR spectroscopy. *J. Environ. Chem. Eng.* **2015**, *3* (4), 3005–3014.
(39) Thorsten D.; Boris K.; Norbert H.; Kattner, G. A. Simple and efficient method for the solid-phase extraction of dissolved organic matter (SPE-DOM) from seawater. *Limnol. Oceanogr.: Methods*. **2008**, *6*, 230–235.
(40) Koch, B. P.; Dittmar, T.; Witt, M.; Kattner, G. Fundamentals of molecular formula assignment to ultrahigh resolution mass data of natural organic matter. *Anal. Chem.* **2007**, *79* (4), 1758–1763.
(41) Maizel, A. C.; Remucal, C. K. The effect of advanced secondary municipal wastewater treatment on the molecular composition of dissolved organic matter. *Water Res.* **2017**, *122*, 42–52.
(42) Maizel, A. C.; Remucal, C. K. The effect of probe choice and solution conditions on the apparent photoreactivity of dissolved organic matter. *Environ. Sci. Process. Impacts* **2017**, *19*, 1040–1050.
(43) Raeke, J.; Lechtenfeld, O. J.; Wagner, M.; Herzsprung, P.; Reemtsma, T. Selectivity of solid phase extraction of freshwater dissolved organic matter and its effect on ultrahigh resolution mass spectra. *Environ. Sci. Process. Impacts* **2016**, *18* (7), 918–927.
(44) Bulman, D. M.; Mezyk, S. P.; Remucal, C. K. The impact of pH and irradiation wavelength on the production of reactive oxidants during chlorine photolysis. *Environ. Sci. Technol.* **2019**, *53* (8), 4450–4459.
(45) McConville, M. B.; Hubert, T. D.; Remucal, C. K. Direct photolysis rates and transformation pathways of the lampricides TFM and niclosamide in simulated sunlight. *Environ. Sci. Technol.* **2016**, *50* (18), 9998-10006.
(46) Laszakovits, J. R.; Berg, S. M.; Anderson, B. G.; O'Brien, J. E.; Wammer, K. H.; Sharpless, C. M. *p*-Nitroanisole/pyridine and *p*-nitroacetophenone/pyridine actinometers revisited: Quantum yield in comparison to ferrioxalate. *Environ. Sci. Technol. Lett.* **2017**, *4* (1), 11–14.
(47) Rosario-Ortiz, F. L.; Canonica, S. Probe compounds to assess the photochemical activity of dissolved organic matter. *Environ. Sci. Technol.* **2016**, *51*, 12532–12547.
(48) McKay, G.; Dong, M. M.; Kleinman, J.; Mezyk, S. P.; Rosario-Ortiz, F. L. Temperature dependence of the reaction between the hydroxyl radical and organic matter. *Environ. Sci. Technol.* **2011**, *45*, 329–333.
(49) Canonica, S.; Laubscher, H.-U. Inhibitory effect of dissolved organic matter on triplet-induced oxidation of aquatic contaminants. *Photochem. Photobiol. Sci.* **2008**, *7* (5), 547–551.
(50) Aitkenhead-Peterson, J. A.; Smart, R. P.; Aitkenhead, M. J.; Cresser, M. S.; McDowell, W. H. Spatial and temporal variation of dissolved organic carbon export from gauged and

ungauged watersheds of Dee Valley, Scotland: Effect of land cover and C:N. *Water Resour. Res.* **2007**, *43* (5) 1-11.

(51) Kellerman, A. M.; Dittmar, T.; Kothawala, D. N.; Tranvik, L. J. Chemodiversity of dissolved organic matter in lakes driven by climate and hydrology. *Nat. Commun.* **2014**, *5* (3804), 1-8.

(52) Bellinger, B. J.; Hoffman, J. C.; Angradi, T. R.; Bolgrien, D. W.; Starry, M.; Elonen, C.; Jicha, T. M.; Lehto, L. R. P.; Seifert-Monson, L. R.; Pearson, M. S.; Anderson, L.; Hill, B. H. Water quality in the St. Louis River area of concern, Lake Superior: Historical and current conditions and delisting implications. *J. Great Lakes Res.* **2016**, *42* (1), 28–38.

(53) Loken, L. C.; Small, G. E.; Finlay, J. C.; Sterner, R. W.; Stanley, E. H. Nitrogen cycling in a freshwater estuary. *Biogeochemistry* **2016**, *127* (2–3), 199–216.

(54) Bartsch, W. M.; Axler, R. P.; Host, G. E. Evaluating a Great Lakes scale landscape stressor index to assess water quality in the St. Louis River area of concern. *J. Great Lakes Res.* **2015**, *41* (1), 99–110.

(55) McElmurry, S. P.; Long, D. T.; Voice, T. C. Stormwater dissolved organic matter: Influence of land cover and environmental factors. *Environ. Sci. Technol.* **2014**, *48* (1), 45–53.

(56) Weishaar, J.; Aiken, G.; Bergamaschi, B.; Fram, M.; Fujii, R.; Mopper, K. Evaluation of specific ultra-violet absorbance as an indicator of the chemical content of dissolved organic carbon. *Environ. Sci. Technol.* **2003**, *37* (20), 4702–4708.

(57) Helms, J. R.; Stubbins, A.; Ritchie, J. D.; Minor, E. C.; Kieber, D. J.; Mopper, K. Absorption spectral slopes and slope ratios as indicators of molecular weight, source, and photobleaching of chromophoric dissolved organic matter. *Limnol. Oceanogr.* **2008**, *53* (3), 955–968.

(58) Fichot, C. G.; Benner, R. A novel method to estimate DOC concentrations from CDOM absorption coefficients in coastal waters. *Geophys. Res. Lett.* **2011**, *38* (3), 1–5.

(59) Qian, C.; Wang, L. F.; Chen, W.; Wang, Y. S.; Liu, X. Y.; Jiang, H.; Yu, H. Q. Fluorescence approach for the determination of fluorescent dissolved organic matter. *Anal. Chem.* **2017**, *89* (7), 4264–4271.

(60) Stubbins, A.; Spencer R. G. M.; Chen, H.; Hatcher, P. G.; Mopper, K.; Hernes, P. J.; Mwamba, V. L.; Mangangu, A. M.; Wabakanghanzi, J. N.; Siz, J. Illuminated darkness: molecular signatures of Congo River dissolved organic matter and its photochemical alteration as revealed by ultrahigh precision mass spectrometry. *Limnol. Oceanogr.* **2010**, *39*, 1416–1428.

(61) Hosen, J. D.; McDonough, O. T.; Febria, C. M.; Palmer, M. A. Dissolved organic matter quality and bioavailability changes across an urbanization gradient in headwater streams. *Environ. Sci. Technol.* **2014**, *48* (14), 7817–7824.

(62) Brinkmann, T.; Sartorius, D.; Frimmel, F. H. Photobleaching of humic rich dissolved organic matter. *Aquat. Sci.* **2003**, *65* (4), 415–424.

(63) Cory, R. M.; McKnight, D. M.; Chin, Y. P.; Miller, P.; Jaros, C. L. Chemical characteristics of fulvic acids from arctic surface waters: Microbial contributions and photochemical transformations. *J. Geophys. Res. Biogeosciences* **2007**, *112* (4), 1–14.

(64) Dalzell, B. J.; Minor, E. C.; Mopper, K. M. Photodegradation of estuarine dissolved organic matter: A multi-method assessment of DOM transformation. *Org. Geochem.* **2009**, *40* (2), 243–257.

(65) Gonsior, M.; Peake, B. M.; Cooper, W. T.; Podgorski, D.; D'Andrilli, J.; Cooper, W. J. Photochemically induced changes in dissolved organic matter identified by ultrahigh

resolution Fourier transform ion cyclotron resonance mass spectrometry. *Environ. Sci. Technol.* **2009**, *43*, 698–703.

(66) Helms, J. R.; Mao, J.; Stubbins, A.; Schmidt-Rohr, K.; Spencer, R. G. M.; Hernes, P. J.; Mopper, K. Loss of optical and molecular indicators of terrigenous dissolved organic matter during long-term photobleaching. *Aquat. Sci.* **2014**, *76* (3), 353–373.

(67) Helms, J. R.; Stubbins, A.; Perdue, E. M.; Green, N. W.; Chen, H.; Mopper, K. Photochemical bleaching of oceanic dissolved organic matter and its effect on absorption spectral slope and fluorescence. *Mar. Chem.* **2013**, *155*, 81–91.

(68) Kujawinski, E. B.; Del Vecchio, R.; Blough, N. V.; Klein, G. C.; Marshall, A. G. Probing molecular-level transformations of dissolved organic matter: Insights on photochemical degradation and protozoan modification of DOM from electrospray ionization Fourier transform ion cyclotron resonance mass spectrometry. *Mar. Chem.* **2004**, *92*, 23–37.

(69) Eimers, M. C.; Buttle, J.; Watmough, S. A. Influence of seasonal changes in runoff and extreme events on dissolved organic carbon trends in wetland- and upland-draining streams. *Can. J. Fish. Aquat. Sci.* **2008**, *65* (5), 796–808.

(70) Dong, M. M.; Mezyk, S. P.; Rosario-Ortiz, F. Reactivity of effluent organic matter (EfOM) with hydroxyl radical as a function of molecular weight. *Environ. Sci. Technol.* **2010**, *44* (15), 5714–5720.

(71) Fimmen, R. L.; Cory, R. M.; Chin, Y. P.; Trouts, T. D.; McKnight, D. M. Probing the oxidation-reduction properties of terrestrially and microbially derived dissolved organic matter. *Geochim. Cosmochim. Acta* **2007**, *71* (12), 3003–3015.

(72) Sleighter, R. L.; Hatcher, P. G. Molecular characterization of dissolved organic matter (DOM) along a river to ocean transect of the Lower Chesapeake Bay by ultrahigh resolution electrospray ionization Fourier transform ion cyclotron resonance mass spectrometry. *Mar. Chem.* **2008**, *110* (3–4), 140–152.

(73) Arnold, W. A.; Longnecker, K.; Kroeger, K. D.; Kujawinski, E. B. Molecular signature of organic nitrogen in septic-impacted groundwater. *Environ. Sci. Process. Impacts* **2014**, *16* (10), 2400–2407.

(74) Gonsior, M.; Zwartjes, M.; Cooper, W. J.; Song, W.; Ishida, K. P.; Tseng, L. Y.; Jeung, M. K.; Rosso, D.; Hertkorn, N.; Schmitt-Kopplin, P. Molecular characterization of effluent organic matter identified by ultrahigh resolution mass spectrometry. *Water Res.* **2011**, *45* (9), 2943–2953.

(75) Kellerman, A. M.; Kothawala, D. N.; Dittmar, T.; Tranvik, L. J. Persistence of dissolved organic matter in lakes related to its molecular characteristics. *Nat. Geosci.* **2015**, *8* (6), 454–457.

(76) Lavonen, E. E.; Kothawala, D. N.; Tranvik, L. J.; Gonsior, M.; Schmitt-Kopplin, P.; Köhler, S. J. Tracking changes in the optical properties and molecular composition of dissolved organic matter during drinking water production. *Water Res.* **2015**, *85*, 286–294.

(77) Kim, S.; Kramer, R. W.; Hatcher, P. G. Graphical method for analysis of ultrahigh-resolution broadband mass spectra of natural organic matter, the van Krevelen diagram. *Anal. Chem.* **2003**, *75* (20), 5336–5344.

(78) Zhou, H.; Yan, S.; Lian, L.; Song, W. Triplet-state photochemistry of dissolved organic matter: Triplet-state energy distribution and surface electric charge conditions. *Environ. Sci. Technol.* **2019**, *53* (5), 2482–2490.

(79) De Laurentiis, E.; Buoso, S.; Maurino, V.; Minero, C.; Vione, D. Optical and photochemical characterization of chromophoric dissolved organic matter from lakes in Terra Nova Bay,

Antarctica. Evidence of considerable photoreactivity in an extreme environment. *Environ. Sci. Technol.* **2013**, *47* (24), 14089–14098.
(80) Mostafa, S.; Rosario-Ortiz, F. L. Singlet oxygen formation from wastewater organic matter. *Environ. Sci. Technol.* **2013**, *47* (15), 8179–8186.
(81) Sharpless, C. M. Lifetimes of triplet dissolved natural organic matter (DOM) and the effect of $NaBH_4$ reduction on singlet oxygen quantum yields: Implications for DOM photophysics. *Environ. Sci. Technol.* **2012**, *46* (8), 4466–4473.
(82) Sharpless, C. M.; Blough, N. V. The importance of charge-transfer interactions in determining chromophoric dissolved organic matter (CDOM) optical and photochemical properties. *Environ. Sci. Process. Impacts* **2014**, *16* (4), 654–671.
(83) Canonica, S.; Hellrung, B.; Wirz, J. Oxidation of phenols by triplet aromatic ketones in aqueous solution. *J. Phys. Chem. A* **2000**, *104* (6), 1226–1232.
(84) Cavani, L.; Halladja, S.; Ter Halle, A.; Guyot, G.; Corrado, G.; Ciavatta, C.; Boulkamh, A.; Richard, C. Relationship between photosensitizing and emission properties of peat humic acid fractions obtained by tangential ultrafiltration. *Environ. Sci. Technol.* **2009**, *43* (12), 4348–4354.
(85) Benedict, K. B.; McFall, A. S.; Anastasio, C. Quantum yield of nitrite from the photolysis of aqueous nitrate above 300 nm. *Environ. Sci. Technol.* **2017**, *51* (8), 4387–4395.
(86) Mckay, G.; Huang, W.; Romera-Castillo, C.; Crouch, J. E.; Rosario-Ortiz, F. L.; Jaffe, R. Predicting reactive intermediate quantum yields from dissolved organic matter photolysis using optical properties and antioxidant capacity. *Environ. Sci. Technol.* **2017**, *51*, 5404–5413.
(87) McKay, G.; Rosario-Ortiz, F. L. Temperature dependence of the photochemical formation of hydroxyl radical from dissolved organic matter. *Environ. Sci. Technol.* **2015**, *49* (7), 4147–4154.
(88) Rosario-Ortiz, F. L.; Mezyk, S. P.; Doud, D. F. R.; Snyder, S. A. Quantitative correlation of absolute hydroxyl radical rate constants with non-isolated effluent organic matter bulk properties in water. *Environ. Sci. Technol.* **2008**, *42* (16), 5924–5930.
(89) Page, S. E.; Sander, M.; Arnold, W. A.; McNeill, K. Hydroxyl radical formation upon oxidation of reduced humic acids by oxygen in the dark. *Environ. Sci. Technol.* **2012**, *46* (3), 1590–1597.
(90) Page, S. E.; Kling, G. W.; Sander, M.; Harrold, K. H.; Robert, J.; Mcneill, K.; Cory, R. M. Dark production of hydroxyl radical in arctic soil and surface waters. *Environ. Sci. Technol.* **2013**, *47*, 12860–12867.
(91) Aeschbacher, M.; Graf, C.; Schwarzenbach, R. P.; Sander, M. Antioxidant properties of humic substances. *Environ. Sci. Technol.* **2012**, *46* (9), 4916–4925.
(92) Razavi, B.; Ben Abdelmelek, S.; Song, W.; O'Shea, K. E.; Cooper, W. J. Photochemical fate of atorvastatin (Lipitor) in simulated natural waters. *Water Res.* **2011**, *45* (2), 625–631.
(93) Dong, M. M.; Trenholm, R.; Rosario-Ortiz, F. L. Photochemical degradation of atenolol, carbamazepine, meprobamate, phenytoin and primidone in wastewater effluents. *J. Hazard. Mater.* **2015**, *282*, 216–223.
(94) Carlos, L.; Martire, D. O.; Gonzalez, M. C.; Gomis, J.; Bernabeu, A.; Amat, A. M.; Arques, A. Photochemical fate of a mixture of emerging pollutants in the presence of humic substances. *Water Res.* **2012**, *46* (15), 4732–4740.
(95) Boreen, A. L.; Arnold, W. A.; McNeill, K. Triplet-sensitized photodegradation of sulfa drugs containing six-membered heterocyclic groups: Identification of an SO_2 extrusion

photoproduct. *Environ. Sci. Technol.* **2005**, *39* (10), 3630–3638.

(96) Latch, D. E.; Stender, B. L.; Packer, J. L.; Arnold, W. A.; McNeill, K. Photochemical fate of pharmaceuticals in the environemnt: Cimetidine and ranitidine. *Environ. Sci. Technol.* **2003**, *37*, 3342–3350.

(97) Cory, R. M.; Harrold, K. H.; Neilson, B. T.; Kling, G. W. Controls on dissolved organic matter (DOM) degradation in a headwater stream: The influence of photochemical and hydrological conditions in determining light-limitation or substrate-limitation of photo-degradation. *Biogeosciences* **2015**, *12* (22), 6669–6685.

(98) Ward, C. P.; Nalven, S. G.; Crump, B. C.; Kling, G. W.; Cory, R. M. Photochemical alteration of organic carbon draining permafrost soils shifts microbial metabolic pathways and stimultes respiration. *Nat. Commun.* **2017**, 1–7.

Chapter 5

Molecular composition of dissolved organic matter and its relationships to optical, photochemical, and redox activity

5.1 Details on Collaboration

Chapter 5 is a collaboration between Stephanie Berg, Christina Remucal, and Kristine Wammer. S.B. performed the experiments and wrote the manuscript with input from C.R. and K.W.

5.2 Abstract

The composition of dissolved organic matter (DOM) affects its photochemical reactivity and thus contaminant fate in surface waters. This study relates quantum yields for singlet oxygen ($\Phi_{^1O_2}$) and hydroxyl radical and other hydroxylating species ($\Phi_{\bullet OH}$) to DOM composition in terms of its optical properties, molecular composition obtained via Fourier-transform ion cyclotron resonance mass spectrometry (FT-ICR MS), and its electron donating capacity (EDC). This diverse set of 48 samples includes bogs with terrestrially-derived DOM, oligotrophic lakes with microbially-derived DOM, and wastewater and wastewater-impacted samples. $\Phi_{^1O_2}$ increases from terrestrial < aquatic < wastewater samples. $\Phi_{\bullet OH}$ does not follow a clear order in terms of DOM source. Terrestrial samples have higher $\Phi_{\bullet OH}$ than aquatic samples, but the wastewater samples show a wide range. Bulk properties including E_2:E_3 and EDC correlate to $\Phi_{^1O_2}$, but no bulk property could be used to predict $\Phi_{\bullet OH}$ in the combined data set. Molecular composition related to EDC, $\Phi_{^1O_2}$, and $\Phi_{\bullet OH}$ and results show that a similar subset of DOM is positively

correlated to $\Phi_{\bullet OH}$ and EDC which is distinct from the formulas relating to $\Phi_{^1O_2}$. Furthermore, we show that even relationships to molecular composition are not universal and depend on the sample set. Finally, multiple linear regressions are presented to simultaneously consider parameters most strongly related to $\Phi_{^1O_2}$ and $\Phi_{\bullet OH}$.

5.3 Introduction

Dissolved organic matter exists in a complex mixture of organic molecules that originate from plant and microbial sources.[1,2] Additionally, it undergoes environmental processing which increases its molecular complexity.[3] DOM participates in many reactions in the environment affecting microbial metabolism,[4] transformation of contaminants,[5–7] and drinking water treatment processes.[8–10] In surface waters, DOM is the predominant light absorbing component and forms photochemically produced reactive intermediates (PPRI) as a result.[11,12]

Upon absorption of light, DOM enters its singlet excited state (^{1}DOM) and a fraction undergoes intersystem crossing to form the longer-lived species triplet excited state (^{3}DOM).[12] The predominant quencher of ^{3}DOM is O_2 which excites to singlet oxygen ($^1O_2$) via energy transfer from ^{3}DOM. Both ^{3}DOM and $^1O_2$ can react to transform some organic contaminants.[6,13,14] Autochthonous DOM or DOM originating from wastewater has been shown to be more photoreactive in terms of producing these PPRI.[13,15] Other PPRI including hydrogen peroxide (H_2O_2), superoxide, ($O_2^{\bullet-}$), and hydroxyl radical ($^\bullet$OH) form through electron transfer reactions but exact pathways are less well understood.[16] However, the two predominant mechanisms discussed in the literature include initial steps of reduction of O_2 or H-atom abstraction from water. DOM precursors may include ^{1}DOM, ^{3}DOM, charge transfer species, or other photochemically excited complexes associated with DOM.[17–19]

Conflicting evidence exists in the literature about relationships between quantum yields of ^{3}DOM and $^1O_2$ (Φ_{3DOM} and Φ_{1O2}, respectively) as compared to those for $\Phi_{\bullet OH}$, which is likely because the former two form via energy transfer and the latter results from electron transfer. Measures of redox activity have been used to attempt to explain photochemical reactivity in terms of formation of these PPRI. Measurements of antioxidant capacity, via reaction of DOM with 2,2-diphenyl-1-picrylhydrazyl, have been negatively correlated to Φ_{3DOM} and Φ_{1O2}.[20] Electron donating capacity (EDC) measured via cyclic voltammetry is unrelated to Φ_{1O2} but positively correlated to quantum yields for H_2O_2 formation (Φ_{H2O2}) in another study.[21] Absorbance and fluorescence data have been correlated with redox activities of DOM in photochemical studies, but have not been related to composition data at the molecular level such as that acquired via ultrahigh-resolution mass spectrometry.

Because predicting $^{\bullet}$OH formation has remained elusive in the literature,[20,22] we present a complete picture of DOM absorptive properties, DOM redox properties via measurements of EDC, DOM molecular composition via FT-ICR MS, and DOM photochemical properties including Φ_{1O2} and $\Phi_{\bullet OH}$ for a diverse sample set including terrestrially-derived bogs, microbially-derived and altered DOM from oligotrophic lakes, and wastewater and wastewater impacted samples. Multiple linear regression models are developed for Φ_{1O2} and $\Phi_{\bullet OH}$ to show how DOM properties collectively affect PPRI formation. In the St. Louis River, correlations to molecular composition show that a separate pools of DOM are mostly strongly related to Φ_{1O2} and $\Phi_{\bullet OH}$.[23] Here, we include a much more diverse sample set to investigate whether this observation is universally true.

5.4 Methods

5.4.1 Sample Collection

A total of 48 grab samples were taken from five different geographical locations between August 2018 and September 2020 are classified as rural, urban, agricultural depending on their surrounding landcover (**Table D.1**). These samples include lakes of diverse trophic status (n = 13), rivers and their tributaries (n = 20), and agricultural ditches (n = 2). Additionally, 13 wastewater effluent samples were collected from four different wastewater treatment plants. More information about sample sites and collection can be found **Appendix D.1** of Appendix D. Origins of all chemicals used in experiments and analyses can be found in **Appendix D.2**.

5.4.2 Water Chemistry Analysis

Water chemistry parameters including concentrations of chloride, nitrate, nitrite, and sulfate were measured using ion chromatography. Concentrations of metals including calcium, iron, potassium, magnesium, and sodium were measured using inductively coupled plasma-optical emission spectroscopy. Concentrations of dissolved organic carbon ([DOC]) and dissolved inorganic carbon ([DIC]) were measured using a Shimadzu Total Organic Carbon Analyzer. More information on analytical methods for these measurements can be found in **Appendix D.3**.

Bulk DOM composition was evaluated using absorbance measurements collected via a Horiba Aqualog Fluorimeter (**Appendix D.3**). Parameters including the specific absorbance at 254 nm ($SUVA_{254}$) and the ratio of absorbance at 250 nm to 365 nm (E_2:E_3) were calculated as described previously.[24,25] $SUVA_{254}$ and E_2:E_3 have been related to increasing aromaticity and decreases molecular weight, respectively.[24,25] Excitation emission matrices (EEMs) were also exported from the instrument. In this study, the humification index (HIX) is used due to its lack of dependence

on any inner filtering effects.[26] HIX is calculated as the sum of the emission from 435 – 480 nm divided by the sums of the emission from 300 – 345 nm and 435 – 480 nm all with excitation at 254 nm.[26]

Molecular composition of DOM was evaluated using Fourier transform-ion cyclotron resonance mass spectrometry (FT-ICR MS). Briefly, prior to analysis, DOM was extracted from whole water samples using solid phase extraction and re-diluted in methanol.[27] Aliquots were diluted in 50:50 acetonitrile:ultrapure water and directly injected into a Bruker FT-ICR MS instrument (Solarix XR 12T) via electrospray ionization operating in negative mode. Exported formulas were linearly calibrated and compared with a list of potential formulas containing combinations of $^{13}C_{0\text{-}1}{}^{12}C_{5\text{-}80}H_{0\text{-}120}O_{0\text{-}80}N_{0\text{-}3}S_{0\text{-}1}$ atoms. Matches were verified using a 0.2 ppm mass error cutoff and requirement of homologous series as described previously.[13,28] Further information can be found in **Appendix D.4**. Weighted averages of properties including hydrogen to carbon ratios ($H{:}C_w$), oxygen to carbon ratio ($O{:}C_w$), and double bond equivalents (DBE_w) were calculated for each sample.

Electron donating capacity (EDC) was measured using a spectrophotometric assay with the radical cation of 2,2'-azino-bis(3-ehtylbenzothiazoline-6-sulfonate) ($ABTS^{\bullet+}$) as described by Walpen *et al*.[29] Briefly, 125 μu $ABTS^{\bullet+}$ was added to at four concentrations of DOM from each site. Reactions proceeded for 15 minutes during which DOM reduced $ABTS^{\bullet+}$ back to ABTS which was quantified by loss of absorbance at 728 nm. EDC was then calculated from the difference in delta $ABTS^{\bullet+}$ between DOM samples and ultrapure water samples. Further details are included in **Appendix D.5**.

5.4.3 Photochemical Experiments

Steady-state concentrations and quantum yields for $^1O_2$ and $^{\bullet}OH$ were quantified during irradiation of whole water samples in a Rayonet photoreactor equipped with 365 nm bulbs (full width half max = ± 10 nm).[30] 10 μM of the probe compounds furfuryl alcohol (FFA) and terephthalic acid (TPA) were used in separate experiments to measure $^1O_2$ and $^{\bullet}OH$, respectively.[31,32] Triplicate measurements were taken alongside triplicates of actinometer solution containing *p*-nitroanisole and pyridine to quantify intensity of the light source.[33] Buffer was not added to any solutions due to precipitation during some irradiations, but the pH never varied by more than 0.3 units during experiments. Importantly, TPA captures both free $^{\bullet}OH$ as well as other hydroxylating species.[34] We will refer to the combination as $^{\bullet}OH$ for the remainder of this study. The degradation of FFA and the formation of the hydroxylation product of TPA, hydroxy-terephthalic acid (hTPA) were measured with high performance liquid chromatography (HPLC). Further experimental details and analytical methods are included in **Appendix D.6**.

5.4.4 Statistics Analyses

For all figures, error bars represent the one standard deviation of at least three replicates. In the box and whisker plots, the whiskers represent the first and fourth quartile, the height of the box represents the second and third quartile, and the line through the box represents the median of the data set. Statistical significance between categorical groups were calculated by ANOVA-Tukey tests. Any individual points shown on the plot are outliers in the data set. Spearman rank correlations are calculated by relating the relative formula intensity of individual formulas in individual samples to another measurement made for that samples (e.g., Φ_{1O2} and $\Phi_{\bullet OH}$). For all of these plots, only formulas identified in at least three samples are included.

Multiple linear regressions (MLR) models were constructed for $\Phi_{^1O_2}$ and $\Phi_{^{\bullet}OH}$ using pH, concentrations of anions, concentrations of cations, ionic strengths, [DOC], [DIC], $SUVA_{254}$, E_2:E_3, HIX, EDC, H:C_w, O:C_w, and DBE_w as potential predictor variables. All of parameters were considered because both DOM composition and water chemistry can affect photochemical reactivity.[35–37] Models were reduced using Bayesian information criterion (BIC) with backwards stepwise regression. Variation inflation (VIF) scores meet model assumption about collinearity (i.e., < 1.5). Details from model output are included in **Tables D.15** and **D.16**.

5.5 Results and Discussion

5.5.1 Water Chemistry

We collected 48 samples collected across Wisconsin and Minnesota, USA with the goal of comparing DOM that spans the range of DOM in freshwater systems. Water chemistry parameters vary substantially among the collected samples. Natural water samples were categorized into four groups (e.g., rural (n = 14), urban (n = 8), agriculture (n = 12), and wastewater (n = 14)) based on the predominate land cover type in the surrounding watersheds, and wastewater effluents were all grouped together in their own class.

Concentrations of dissolved organic carbon ([DOC]) range from 1.8 – 69 mg-C L^{-1}. Sites classified as urban and agricultural show little variability in [DOC] while rural and wastewater sites show large differences. Rural samples include both bogs and oligotrophic lakes so that range is unsurprising.[38] [DOC] in wastewater samples range widely, but WLSSD in particular has higher than usual [DOC] due to large amounts of industrial inputs (**Figure 5.1a**).[23,39] In general, the highest concentrations of [DOC] are observed in waters with large terrestrial inputs of carbon and the lowest are found in clear, oligotrophic lakes (**Table D.2**). Inorganic carbon concentrations

([DIC]) range from 1.42 – 92.7 mg-C L^{-1} with significantly lower concentrations observed in the rural sites than any other samples (**Figure 5.1b**; **Table D.2**). Sample pH (**Table D.2**), concentrations of anions (**Table D.3**), and concentrations of cations (**Table D.4**) are available in **Appendix D.3**.

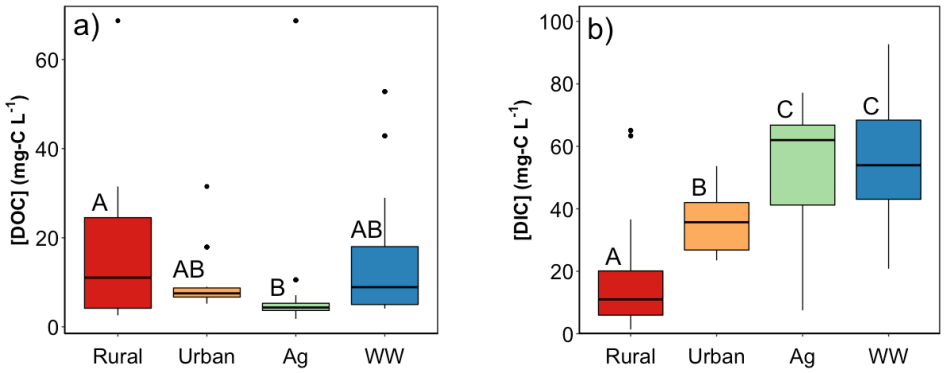

Figure 5.1. Box and whisker plots for a) [DOC] and b) [DIC] in rural (n = 14), urban (n = 8), agricultural (n = 12), and wastewater (n = 14) samples. Letters designate statistical significance between groups.

5.5.2 DOM Composition

Optical properties derived from UV-vis spectroscopy show that DOM composition also varies widely between the samples (**Figure 5.2**; **Table D.2**). High $SUVA_{254}$ and low E_2:E_3 values are indicative of large, aromatic DOM, while low $SUVA_{254}$ and high E_2:E_3 indicates smaller, simpler molecules.[24,25] Here, urban samples have especially low $SUVA_{254}$ values likely arising from minimal terrestrial inputs in and around Minneapolis and St. Paul, Minnesota. Urban and agricultural samples have low E_2:E_3 indicating important contributions from microbially produced DOM or large amounts of older, more processed DOM. Although low $SUVA_{254}$ and high E_2:E_3 are expected in wastewater effluent,[39,40] the wastewater-derived samples have optical properties near the middle of ranges observed in this study (**Figure 5.2**).

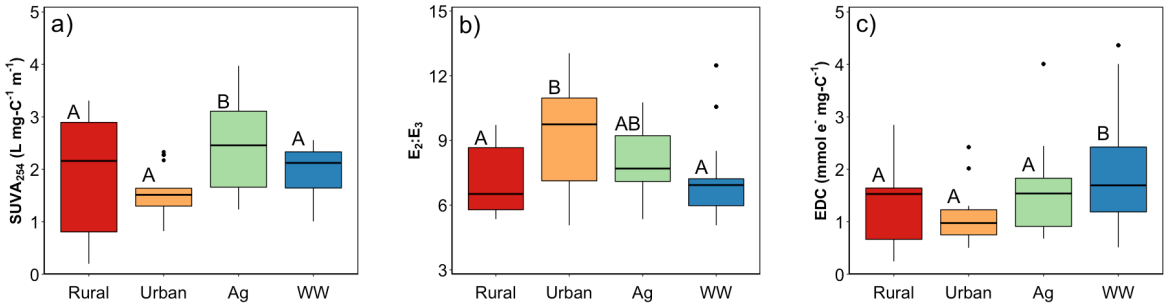

Figure 5.2. Box and whisker plots for a) $SUVA_{254}$, b) E_2:E_3, and c) EDC in rural (n = 14), urban (n = 8), agricultural (n = 12), and wastewater (n = 14) samples.

For all samples, DOM was also characterized at the molecular level via FT-ICR MS. A total of 14,318 unique formulas were identified in the samples with an average of 4,026 formulas in each sample (**Table D.6**). Weighted averages of H:C_w were higher in the wastewater and urban samples compared to the rural or agriculture samples (**Figure 5.3a**). O:Cw ratios were lower in the urban samples than in any other group (**Figure 5.3b**) The numbers of heteroatom containing formulas varied, with more N- and S- containing formulas identified in wastewater effluent than the natural water samples and more CHO-only formulas identified in the samples with mostly terrestrial DOM inputs (**Table D.6**).

To compare DOM molecular composition from different land cover types, formulas only identified in rural, urban, agricultural, or wastewater samples are plotted on van Krevelen diagrams (**Figure 5.4**). A large number of formulas are unique to samples categorized as rural (**Figure 5.4a**). This may be due to this DOM being relatively fresh and containing large amounts of labile DOM not found in other samples. Additionally, the rural samples in contain an especially high amount of variability due to the different trophic statuses of the lakes.[38] Formulas only found in samples collected from urban sites were mainly found at low O:C ratios (**Figure 5.4b**). Reports of urban runoff containing low amounts of oxygen have been made previously.[41] Agricultural samples show

a unique group of tannin- and lignin-like unsaturated formulas (**Figure 5.4c**). It is unclear just from this plot where these formulas originate but potentially they are coming directly from farmland. Like the rural sites, wastewater also shows large number of uniquely identified formulas. These formulas vary in their H:C and O:C ratios but are somewhat concentrated in lipid- and protein-regions as has been observed for other wastewater effluents.[13,39,40]

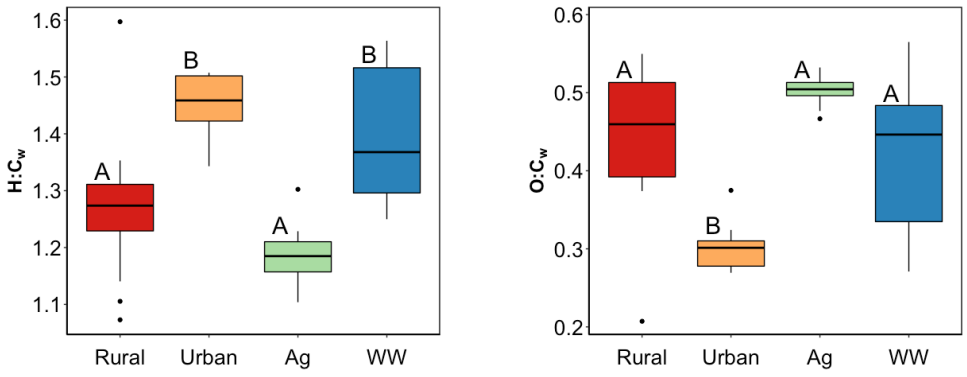

Figure 5.3. Box and whisker plots for a) $H:C_w$, and b) $O:C_w$ in rural (n = 14), urban (n = 8), agricultural (n = 12), and wastewater (n = 14) samples.

5.5.3 EDC

EDC is potentially linked to the photochemical reactivity of DOM, yet is infrequently reported in the literature and has not yet been compared with the molecular composition of DOM. EDC values for the diverse set of waters range from 0.26 – 5.38 mmol e^- g-C^{-1} which is within the range of other waters measured by the same spectrophotometric method (**Table D.5**).[10,29] Geographic location does not seem to play a huge role in controlling EDC, but overall terrestrial samples (e.g., bogs and upstream St. Louis River) have higher values than more microbial- or otherwise environmentally processed DOM (e.g., oligotrophic lakes). Interestingly, wastewaters show a large amount of variability in EDC, with values spanning the range of that observed in the natural

waters (0.51 – 5.38 mmol e^- mg-C^{-1}; **Figure 5.2c**; **Table D.5**). Largely, the two samples taken from each plant (i.e., before and after disinfection) were very close to one another and more variability was observed between the different WWTPs. However, EDC decreased after disinfection with either chlorine or UV which has been observed in other studies using both chlorine[43,44] and ozone[10,29,44] as disinfectants. This trend was not observed at WLSSD, which uses UV light for disinfection.

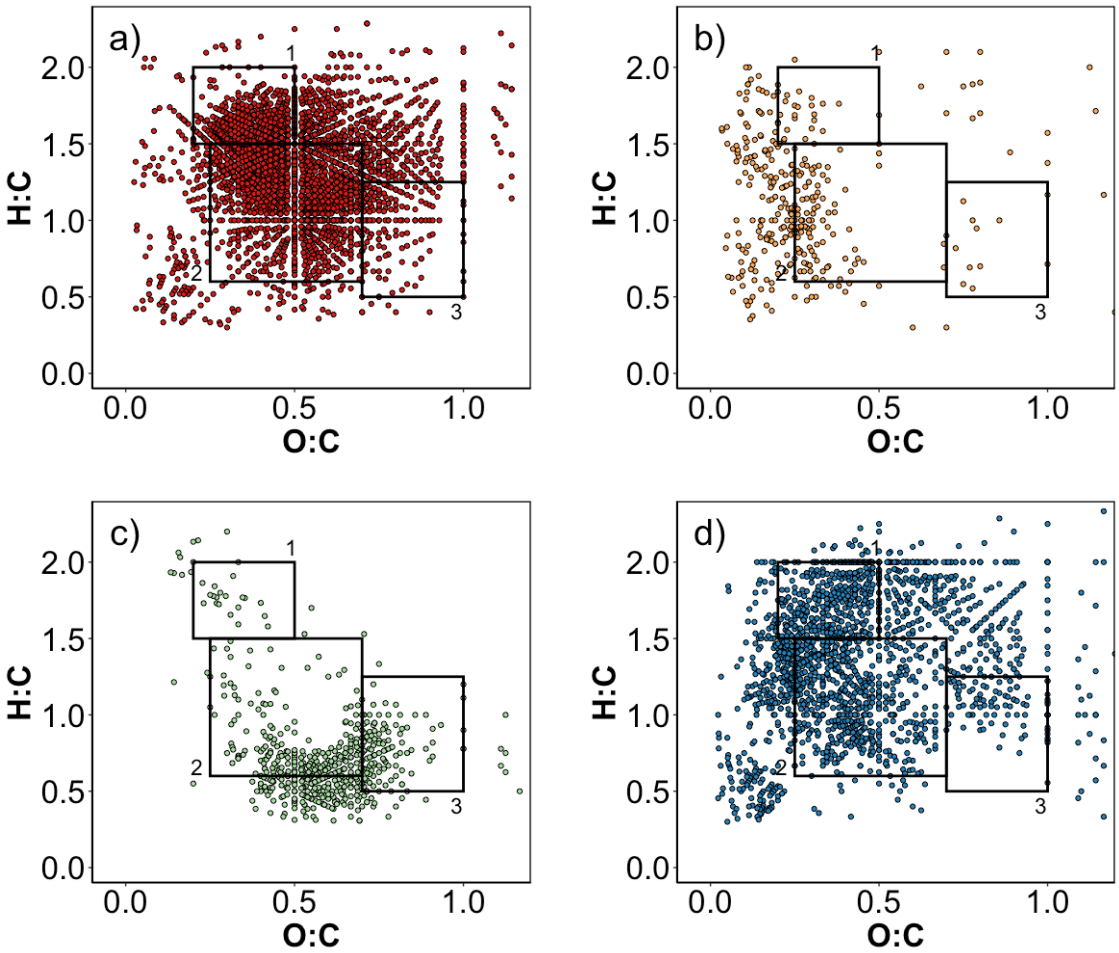

Figure 5.4. Identified formulas found in at least one sample that are exclusive in a) rural, b) urban, c) agriculture, and d) wastewater samples. Boxes on plot correspond to 1) protein-, 2) lignin-, and 3) tannin- like formulas.[42]

Relationships are observed between EDC and optical properties including positive relationships with $SUVA_{254}$ and negative relationships to E_2:E_3. The slope for EDC versus

$SUVA_{254}$ is similar for all natural water types regardless of land cover designation or composition of DOM ($p = 1.4 \times 10^{-8}$; **Figure 5.4a**). However, while the slope for the wastewater samples is still positive, it is much steeper than that of the natural water samples ($p = 4.7 \times 10^{-3}$; **Figure 5.4a**). Different slopes have been documented for EDC between terrestrial and aquatic samples,[45] but not specifically for wastewater samples. EDC is negatively related to E_2:E_3 for the entire data set with some wastewater samples having unexpectedly high EDC ($p = 3.5 \times 10^{-4}$; **Figure 5.4b**).

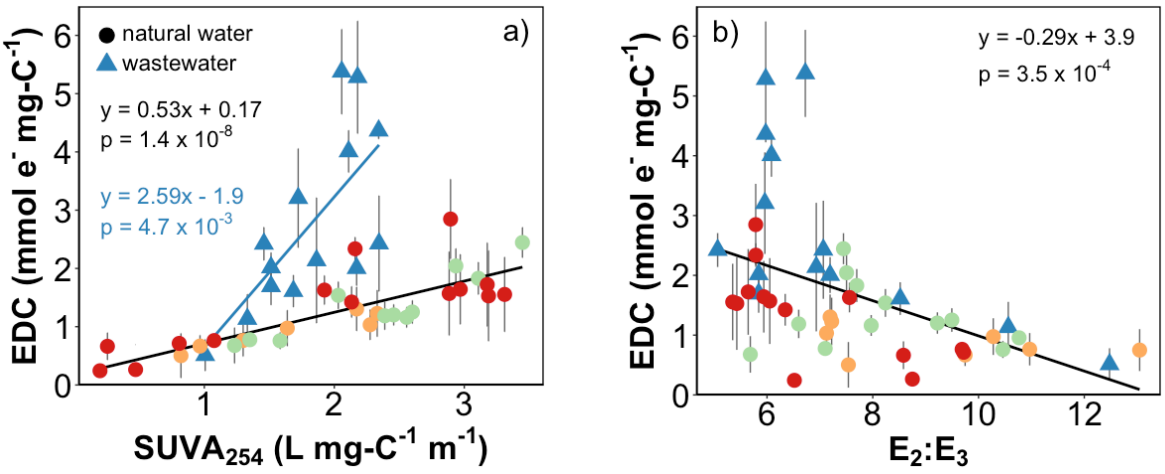

Figure 5.5. EDC versus a) $SUVA_{254}$ and b) E_2:E_3 for natural water samples and wastewater samples. Red, yellow, and green points represent rural, urban, and agriculture sites, respectively.

Positive relationships between EDC and measurements of aromaticity via UV-vis[46] and ^{13}C NMR[45] have been made previously and much evidence exists that EDC in DOM rises primarily from phenolic moieties.[19,45,47] Phenols have been implicated in other redox reactions including the quenching of triplet radical cations and photochemical reduction of O_2 to form superoxide ($O_2^{\bullet-}$).[19] Additionally, reactions such as those with ozone which are known to preferentially react with phenols, resulting in the reduction of EDC.[10]

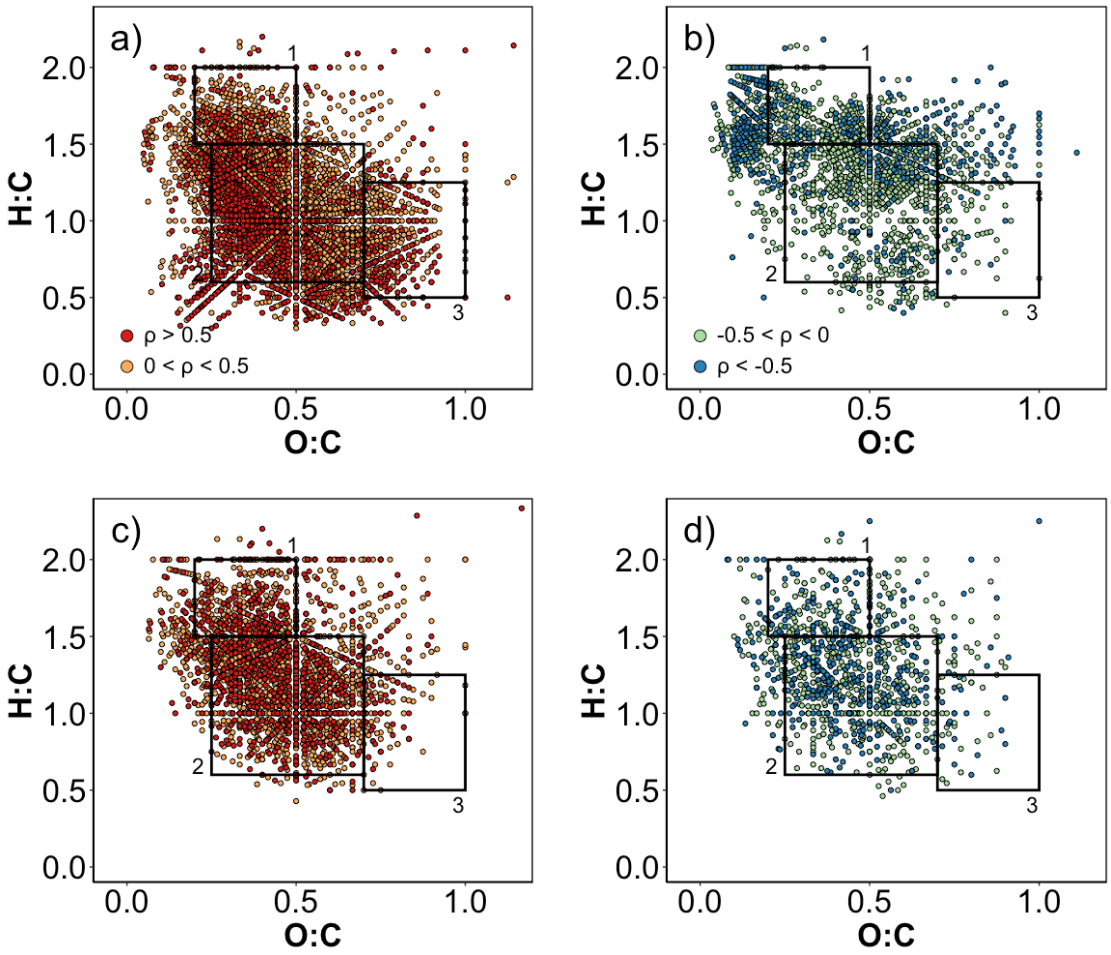

Figure 5.6. Positive (a and c) and negative (b and d) Spearman rank correlations between EDC and relative formula intensity for natural water samples (a and b) and wastewater samples (c and d). Formulas visualized are present in at least three samples.

EDC measurements are also related to DOM molecular composition. For natural waters, most lignin- and tannin- like formulas are positively related to EDC (**Figure 5.6a**), while negatively related formulas are mostly relatively saturated (**Figure 5.6b**). This is consistent the understanding that polyphenolic-like structures give rise to redox activity of DOM and agrees with similar analysis comparing $SUVA_{254}$ with molecular composition of DOM.[23,38] In contrast, the formulas positively and negatively related to EDC in the wastewaters are clustered together on van Krevelen diagrams (**Figure 5.6c and 5.6d**).

Combined, these observations of differences in relationships between EDC to DOM molecular combination potentially provide evidence that other structures or interferences within wastewater DOM give rise to EDC that are not present or are depleted in natural water samples. Given the relatively narrow range in $SUVA_{254}$, the large range in EDC in wastewater samples is unexpected (**Figure 5.5a**). Furthermore, the fact that large differences in EDC in the effluent DOM samples does not correspond to discernable classes of formulas on van Krevelen diagrams suggests there must be a yet unaccounted for factor.

Studies of DOM redox activity have concluded that phenol and quinone structures are the predominant but not only redox active groups within DOM.[19,45,47–49] In fact, observations from cyclic voltammetry experiments have shown that there is some redox activity that cannot be attributed to phenols and quinones due to its irreversibility.[49,50] Heteroatom-containing functional groups such as have been suggested as contributing to overall redox activity and are generally enriched in wastewater effluent in general as well as in the samples included in this study (**Table D.7**).[51] However, other interferences may be a confounding factor in our EDC measurements such as reduced forms of metals and ions although these have bene ruled negligible in another study considering EDC of wastewater.[29]

5.5.4 Photochemistry

Steady-steady concentrations and quantum yields for formation of $^1O_2$ and $^{\bullet}OH$ range widely within the 48 samples and are within ranges observed in other studies.[14,52,53] Steady-state concentrations vary from (0.43– 12.6) x 10^{-13} and (0.57 – 32.5) x 10^{-15} M for $[^1O_2]_{ss}$ and $[^{\bullet}OH]_{ss}$, respectively. Generally, steady-state concentrations of both PPRI increase with increasing [DOC]. Quantum yields range from (0.6 – 8.27) x 10^{-2} and (0.34 – 105) x 10^{-5} for $^1O_2$ and $^{\bullet}OH$, respectively.

The range in $\Phi_{\bullet OH}$ is nearly two orders of magnitude which is in line with other compilations of quantum yields from large data sets.[52] Overall, steady-state concentrations and quantum yields do not vary by land cover type with the exception of rural sites having lower $\Phi_{^1O_2}$ (**Figure 5.7**).

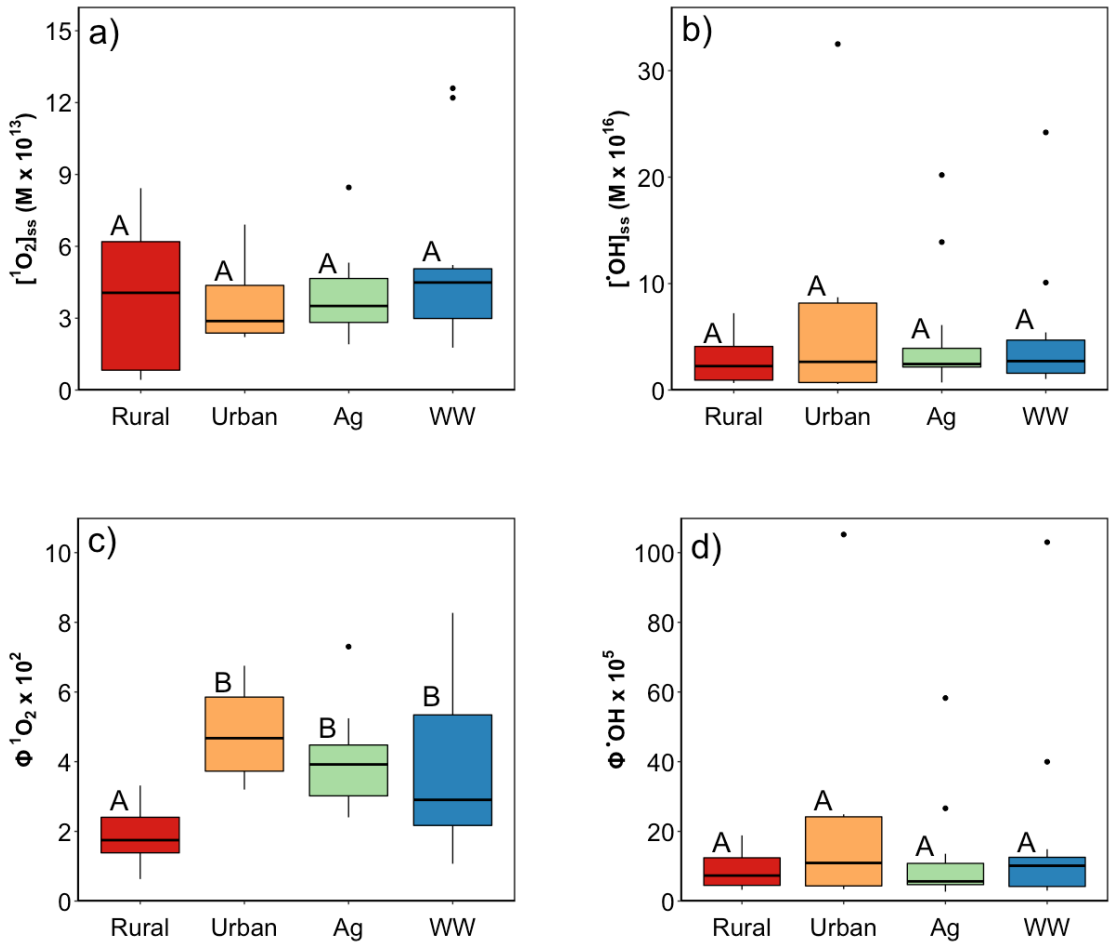

Figure 5.7. Box and whisker plots for a) $[^1O_2]_{ss}$, b) $[^{\bullet}OH]_{ss}$, c) $\Phi_{^1O_2}$ and d) $\Phi_{\bullet OH}$. Letters indicate statistical differences between sample groups.

Relationships between measurements of bulk composition and $\Phi_{^1O_2}$ and $\Phi_{\bullet OH}$ are observed for some DOM properties. Additionally, some are consistent across the entire data set while others are only observed in some types of waters. $SUVA_{254}$ shows no relationship to $\Phi_{^1O_2}$ or $\Phi_{\bullet OH}$ overall in the data set (**Figure 5.8**; **Table D.10**). However, significant negative correlations between

$SUVA_{254}$ and $\Phi_{^1O_2}$ are observed for the rural and wastewater samples ($p = 3.15 \times 10^{-5}$ and 1.80×10^{-3}, respectively; **Tables D.11** and **D.14**). $SUVA_{254}$ is not correlated to $\Phi_{\bullet OH}$ for any of the land cover types. E_2:E_3 is positively related to $\Phi_{^1O_2}$ in the entire data set which has been observed in many other studies ($p = 1.9 \times 10^{-3}$; **Figure 5.8b**; **Table D.10**).[53] Additionally, E_2:E_3 is negatively correlated to $\Phi_{\bullet OH}$ overall although this is largely driven by a few wastewater samples with exceptionally high $\Phi_{\bullet OH}$ ($p = 2.46 \times 10^{-2}$; **Figure 5.8e**; **Table D.10**). EDC is negatively correlated with E_2:E_3 ($p = 2.0 \times 10^{-2}$; **Figure 5.8c**; **Table D.10**) and not related to $\Phi_{\bullet OH}$ (**Figure 5.8f**; **Table D.10**) in the whole data set. In fact, EDC is not related to $\Phi_{\bullet OH}$ for any of the land cover types (**Table D.11-D.14**). The lack of universal relationship between EDC and $\Phi_{\bullet OH}$ refutes our hypothesis that EDC may be a better bulk DOM composition better than optical properties to predict $\Phi_{\bullet OH}$ in natural waters.

E_2:E_3 is the most successful bulk parameter at predicting $\Phi_{\bullet OH}$ and opposing relationships are observed as compared to $\Phi_{^1O_2}$ (**Figure 5.8**). This is similar to other observations of opposing trends between $\Phi_{^1O_2}$ and $\Phi_{\bullet OH}$ or other PPRI formed through redox reactions in other studies.[13,21,35,54] However, directly comparing $\Phi_{^1O_2}$ and $\Phi_{\bullet OH}$ to one another from this study yields a significantly positive relationship ($p = 2.0 \times 10^{-2}$; **Figure 5.9**), albeit this again is largely due to the incredibly photoreactive Metro WWTP effluent samples. Without those two samples, no relationship is observed across the entire data set. However, if considering the relationship in the different land cover types, a negative relationship is observed between the two quantum yields in the rural sites ($p = 1.8 \times 10^{-2}$; **Table D.11**). This is consistent with the relationship developed between the two PPRI in the St. Louis River (Chapter 4) and demonstrates that trends observed in specific types of samples or geographical regions are not likely universal across all DOM types and sources.

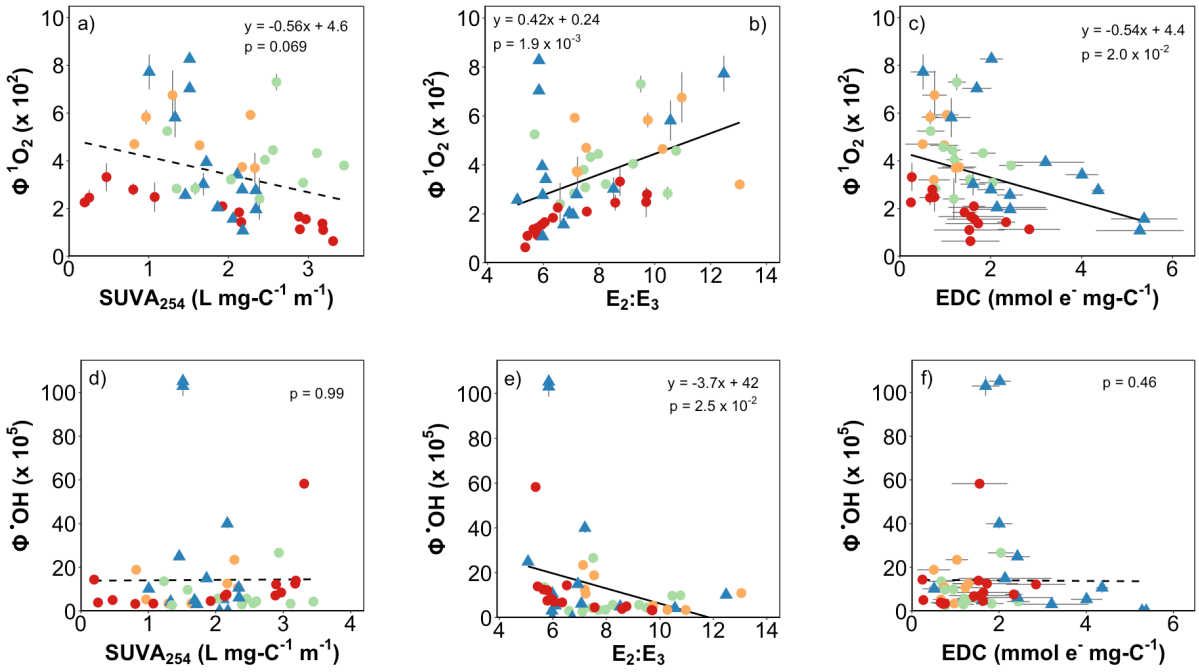

Figure 5.8. Relationships between Φ_{1O2} and a) $SUVA_{254}$, b) E_2:E_3, and c) EDC and $\Phi_{\bullet OH}$ to a) $SUVA_{254}$, b) E_2:E_3, and c) EDC. Red, yellow, and green points represent rural, urban, and agriculture sites, respectively. Solid regression lines indicate significant simple linear correlations across the entire data set ($p < 0.05$); dashed lines indicate correlations with $p > 0.05$.

Molecular composition is better suited to predict quantum yields than bulk parameters and correlations illustrate why many bulk properties could not be correlated to quantum yield across the entire data set. For Φ_{1O2}, rural and urban sites show similar correlations where relatively saturated formulas are most positively related and more oxygenated formulas are negatively related (**Figure 5.10a-d**). However, even between the two there are some differences which likely can be attributed to original composition of the DOM. For example, many formulas falling in the protein-like region of the plot (i.e., box 1 in **Figure 5.10**) are negatively related to Φ_{1O2} in the rural samples (**Figure 5.10b**) but positively correlated in the urban samples (**Figure 5.10c**). In the agricultural sites, an unusual relationship of more saturated formulas being negatively related to Φ_{1O2} is observed which has not been observed in other sample sets before (**Figure 5.10e-f**). While

Φ_{1O2} does vary in the wastewater samples, there appears to be no net correlations to DOM composition (**Figure 5.10g-h**). In other studies, Φ_{1O2} is positively related to more saturated formulas, although it should be noted that all of these studies included sampling locations surrounded by primarily wetland- and forested- land cover.[13,38]

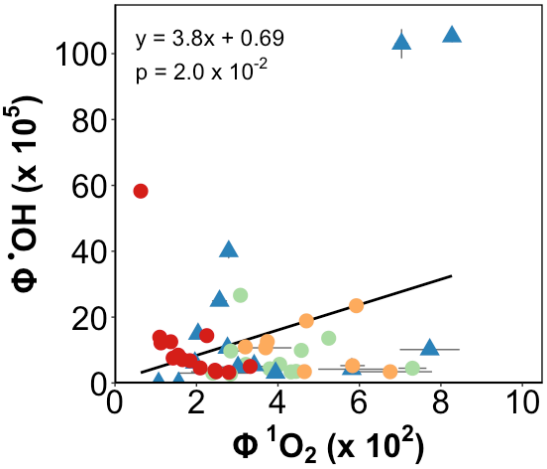

Figure 5.9. Linear correlation between Φ_{1O2} and $\Phi_{\bullet OH}$. Red, yellow, and green points represent rural, urban, and agriculture sites, respectively.

The difference in correlation patterns between Φ_{1O2} and the different land cover types likely arises from differences in original DOM composition. For example, the differences observed in correlations of protein-like formulas between rural and urban sites may arise from the fact that a group of relatively O-depleted formulas identified are uniquely identified in this samples (**Figure 5.4b**). Similarly, the surprising positive relationships between Φ_{1O2} and tannin- and lignin- like DOM in agriculture sites may be attributable to the unique pool of DOM only found in the agriculture sites (**Figure 5.4c**). The lack of clustered correlations in the wastewater is intriguing but not unsimilar to the lack of discernable correlations to EDC in this sample set (**Figure 5.6c-d**).

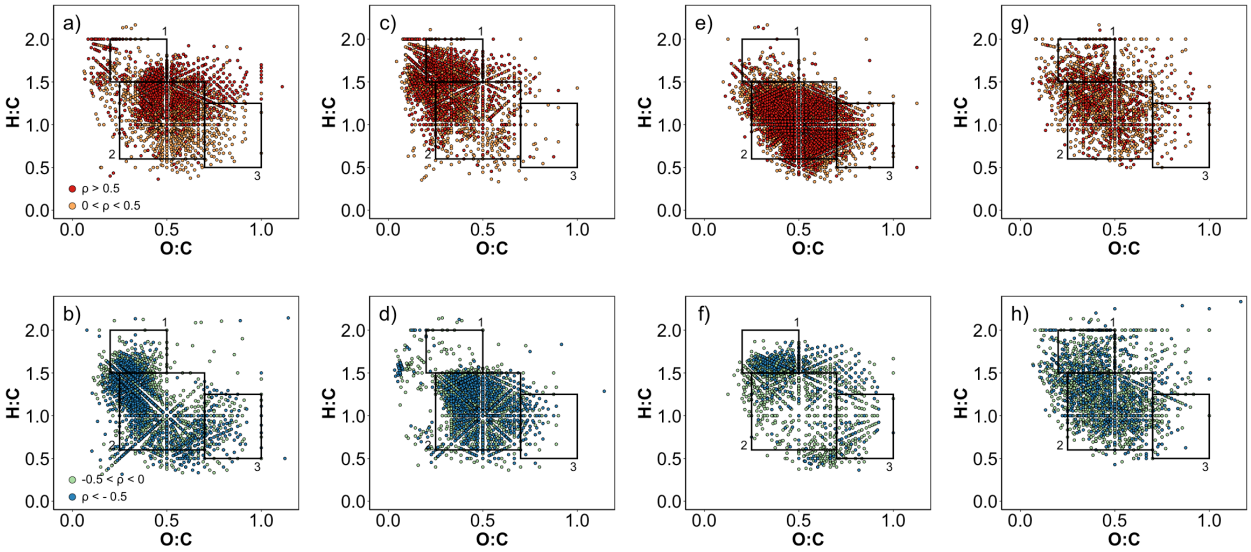

Figure 5.10. Positive (a, c, e, and g) and negative (b, d, f, and h) Spearman rank correlations to relative formula intensity and Φ_{1O2} in rural (a, b), urban (c, d), agriculture (e, f), and wastewater (g, h) samples. Only formulas identified in > 3 samples are plotted.

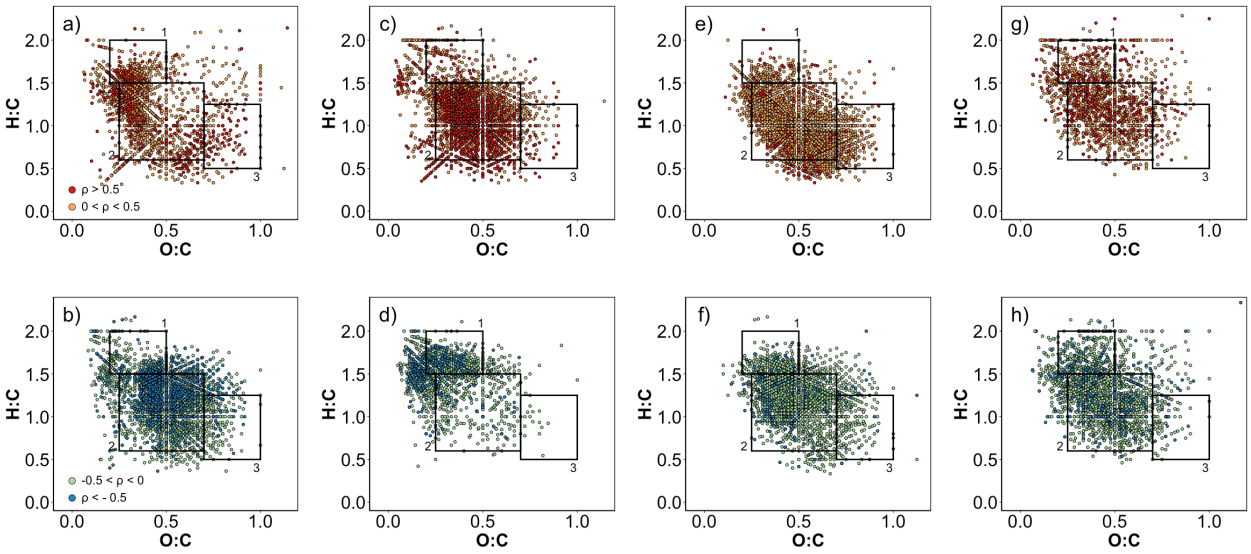

Figure 5.11. Positive (a, c, e, and g) and negative (b, d, f, and h) Spearman rank correlations to relative formula intensity and $\Phi_{\bullet OH}$ in rural (a, b), urban (c, d), agriculture (e, f), and wastewater (g, h) samples. Only formulas identified in > 3 samples are plotted.

For rural, urban, and agricultural sites, opposite relationships between molecular DOM composition and Φ_{1O2} and $\Phi_{\bullet OH}$ are observed at the molecular level. For rural sites, protein- like

and relatively unsaturated lignin- like formulas are positively related to $\Phi_{\bullet OH}$ (**Figure 5.11a**), while for urban sites, nearly all lignin-formulas show positive relationships (**Figure 5.11c**). Correlations in agriculture sites are overall weaker than those drawn in other sample types but overall, less saturated lignin-like formulas are positively related while more saturated are generally negatively related (**Figure 5.11e-f**). Like other correlations drawn in this study, relationships between $\Phi_{\bullet OH}$ and DOM molecular composition are unclear in the wastewater samples (**Figure 5.11g-h**).

Figure 5.12. Predicted values of Φ_{1O2} (a) and $\Phi_{\bullet OH}$ (b) plotted versus their experimentally measured values.

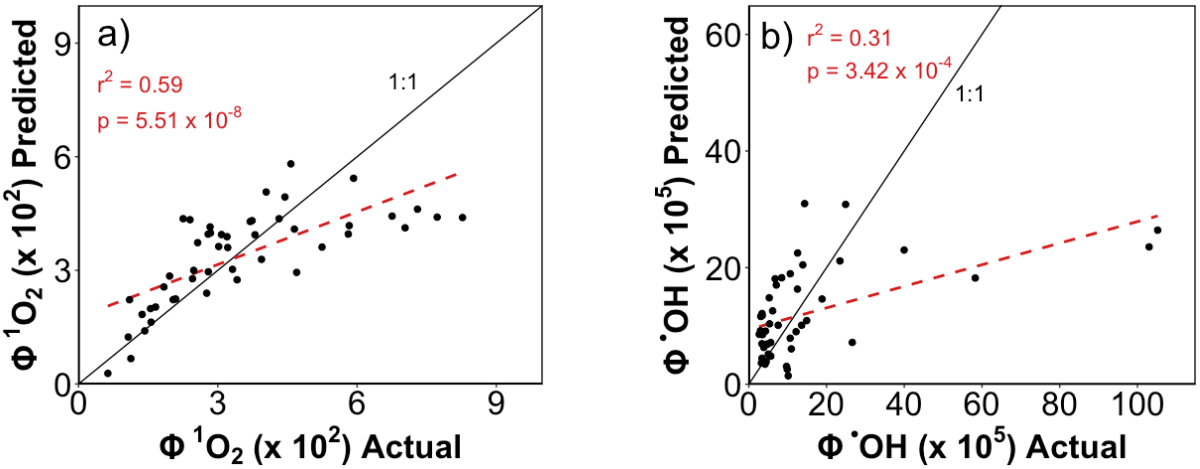

Because both bulk and molecular correlations between DOM composition and Φ_{1O2} and $\Phi_{\bullet OH}$ are complicated and no one parameter shows strong correlations to both PPRI, multiple linear regressions models were built for both quantum yields measured in this study using pH, concentrations of anions, concentrations of cations, ionic strengths, [DOC], [DIC], $SUVA_{254}$, E_2:E_3, HIX, EDC, H:C_w, O:C_w, and DBE_w as potential predictor variables. All of parameters were considered because both DOM composition and water chemistry can affect photochemical

reactivity. For example, ionic strength affects the lifetimes of ^{3}DOM,[35,36] and inorganic carbon species can quench $^{\bullet}$OH.[37]

The preferred model for $\Phi_{^1O_2}$ includes four terms including a negative terms for O:C_w, EDC, and [DOC] and a positive term for [DIC]. Overall, the model was able to describe $\Phi_{^1O_2}$ ($p = 5.51 \times 10^{-8}$; $r^2 = 0.59$; **Figure 5.12a**; **Table D.15**). However, it is clear that the model performs much better at low $\Phi_{^1O_2}$ than higher experimentally measured values (**Figure 5.12a**). For $\Phi_{\bullet OH}$, only two terms, a positive term for O:C_w and a negative term for E_2:E_3, are included in the preferred, reduced model (**Table D.16**). This model performs worse than that of $\Phi_{^1O_2}$ ($p = 3.42 \times 10^{-4}$; $r^2 = 0.31$, **Figure 5.12b**; **Table D.16**), and similarly also has a large amount of error in predicting especially high $\Phi_{\bullet OH}$.

5.6 Environmental Significance

EDC is an important water quality parameter that is essential to understanding processes involving DOM. For example, DOM can act as an electron acceptor in anoxic conditions and subsequent changes in EDC are observed.[55,56] EDC also has important implications in drinking water applications as it changes during disinfection and related to formation of chlorinated products and ozone reactivity.[10,29] Furthermore, the direct relationships drawn between EDC and DOM composition at the molecular level in this study are important because they show that EDC of natural water samples is predominantly determined by DOM composition and tannin- and lignin- like compounds give rise to this redox activity. In contrast, EDC in wastewater effluents is related to $SUVA_{254}$ but not obviously to DOM molecular composition. This could be evidence of a non-phenol donor group within DOM or potential interference from inorganic species.

Whether or not ^{3}DOM is a precursor for •OH remains up for debate. This PPRI is especially important because of the fast and non-selective way it reacts with organic contaminants.[57,58] Additionally, the widespread practice of using ^{3}DOM quenchers such as sorbic acid and subsequent comparison of results in anoxic versus oxic conditions to differentiate between ^{3}DOM and $^1O_2$ may be overlooking potential effects ^{3}DOM quenching as on •OH steady-state concentrations.[13,14,59] Thus, incomplete understanding of •OH formation pathways also results in incomplete understanding of contaminant transformation pathways.

Taken together, results of this study demonstrate that the ability to accurately predict $\Phi_{\bullet OH}$ is lacking compared to other PPRI like Φ_{1O2}. Compositional parameters including UV-vis and mass spectrometry data hold predictive power in some subsets of our data set but were largely incapable of describing $\Phi_{\bullet OH}$ across the entire data set. Surprisingly, EDC was not successful at predicting $\Phi_{\bullet OH}$ although it is negatively related to Φ_{1O2} likely because redox activities within DOM prevent the formation of ^{3}DOM.[60] The employment of an MLR model showed the closest correlation $\Phi_{\bullet OH}$ but was unable to account for samples with very high $\Phi_{\bullet OH}$. However, another finding of this study is that even $^1O_2$, which has well understood formation mechanisms, has differing relationships to DOM molecular composition in surface waters. Thus, even as the field learns more about PPRI formation, actual measurements of PPRI in whole water samples will likely remain necessary in order to ultimately predict photochemical transformation of organic contaminants.

5.7 Acknowledgements

This work was supported by the National Science Foundation (CBET 1802388). The authors acknowledge the North Temperate Lakes-Long Term Ecological Research (NTL-LTER) network

for their support and the UW-Madison Human Proteomics Program Mass Spectrometry Facility for the obtainment of all FT-ICR MS data and especially Yanlong Zhu for the assistance in instrument operation. Samples were collected with help from Noah Lottig, Amber White, Josh Gad, Ben Pedersen, Matt Seib, Joseph Herrli, Ronan Winkels, Kailey Beer, Alyssa Risch, and Bella Kelly. Sofia Staehly assisted with many photochemical experiments and James Lazarcik assisted with anion and cation quantification.

5.8 References

(1) Brown, A.; McKnight, D. M.; Chin, Y. P.; Roberts, E. C.; Uhle, M. Chemical characterization of dissolved organic material in Pony Lake, a saline coastal pond in Antarctica. *Mar. Chem.* **2004**, *89*, 327–337.

(2) Cole, J. J.; Prairie, Y. T.; Caraco, N. F.; McDowell, W. H.; Tranvik, L. J.; Striegl, R. G.; Duarte, C. M.; Kortelainen, P.; Downing, J. A.; Middelburg, J. J.; Melack, J. Plumbing the global carbon cycle: Integrating inland waters into the terrestrial carbon budget. *Ecosystems* **2007**, *10* (1), 171–184.

(3) Gonsior, M.; Peake, B. M.; Cooper, W. T.; Podgorski, D.; D'Andrilli, J.; Cooper, W. J. Photochemically induced changes in dissolved organic matter identified by ultrahigh resolution Fourier transform ion cyclotron resonance mass spectrometry. *Environ. Sci. Technol.* **2009**, *43* (3), 698–703.

(4) Ward, C. P.; Nalven, S. G.; Crump, B. C.; Kling, G. W.; Cory, R. M. Photochemical alteration of organic carbon draining permafrost soils shifts microbial metabolic pathways and stimultes respiration. *Nat. Commun.* **2017**, 1–7.

(5) Raeke, J.; Lechtenfeld, O. J.; Seiwert, B.; Meier, T.; Riemenschneider, C.; Reemtsma, T. Photochemically induced bound residue formation of carbamazepine with dissolved organic matter. *Environ. Sci. Technol.* **2017**, *51* (10), 5523–5530.

(6) Remucal, C. K. The role of indirect photochemical degradation in the environmental fate of pesticides: A review. *Environ. Sci/: Processes and Impacts*. **2014**, *16* (4), 628–653.

(7) Boreen, A. L.; Arnold, W. A.; McNeill, K. Photodegradation of pharmaceuticals in the aquatic environment: A review. *Aquat. Sci*. **2003**, *56* (4), pp 320–341.

(8) Barazesh, J. M.; Prasse, C.; Wenk, J.; Berg, S.; Remucal, C. K.; Sedlak, D. L. Trace element removal in distributed drinking water treatment systems by cathodic H_2O_2 production and UV photolysis. *Environ. Sci. Technol.* **2018**, *52* (1), 195–204.

(9) Bulman, D. M.; Remucal, C. K. Role of reactive halogen species in disinfection byproduct formation during chlorine photolysis. *Environ. Sci. Technol.* **2020**, *54* (15), 9629 - 9639.

(10) Remucal, C. K.; Salhi, E.; Walpen, N.; von Gunten, U. Molecular-level transformation of dissolved organic matter during oxidation by ozone and hydroxyl radical. *Environ. Sci. Technol.* **2020**, *54* (16), 10351-10360.

(11) Green, S. A.; Blough, N. V. Optical absorption and fluorescence properties of chromophoric

dissolved organic matter in natural waters. *Limnol. Oceanogr.* **1994**, *39* (8), 1903–1916.
(12) McNeill, K.; Canonica, S. Triplet state dissolved organic matter in aquatic photochemistry: Reaction mechanisms, substrate scope, and photophysical properties. *Environ. Sci. Process. Impacts* **2016**, *18* (11), 1381–1399.
(13) Berg, S. M.; Whiting, Q. T.; Herrli, J. A.; Winkels, R.; Wammer, K. H.; Remucal, C. K. The role of dissolved organic matter composition in determining photochemical reactivity at the molecular level. *Environ. Sci. Technol.* **2019**, *53* (20), 11725-11734.
(14) Zeng, T.; Arnold, W. A. Pesticide photolysis in prairie potholes: Probing photosensitized processes. *Environ. Sci. Technol.* **2013**, *47* (13), 6735–6745.
(15) Maizel, A. C.; Remucal, C. K. The effect of probe choice and solution conditions on the apparent photoreactivity of dissolved organic matter. *Environ. Sci. Process. Impacts* **2017**, *19* (8), 1040–1050.
(16) Garg, S.; Rose, A. L.; David Waite, T. Production of reactive oxygen species on photolysis of dilute aqueous quinone solutions. *Photochem. Photobiol.* **2007**, *83*, 904–913.
(17) Garg, S.; Rose, A. L.; Waite, T. D. Photochemical production of superoxide and hydrogen peroxide from natural organic matter. *Geochim. Cosmochim. Acta* **2011**, *75* (15), 4310–4320.
(18) McKay, G.; Couch, K. D.; Mezyk, S. P.; Rosario-Ortiz, F. L. Investigation of the coupled effects of molecular weight and charge-transfer interactions on the optical and photochemical properties of dissolved organic matter. *Environ. Sci. Technol.* **2016**, *50* (15), 8093–8102.
(19) Ma, J.; Nie, J.; Zhou, H.; Wang, H.; Lian, L.; Yan, S.; Song, W. Kinetic consideration of photochemical formation and decay of superoxide radical in dissolved organic matter solutions. *Environ. Sci. Technol.* **2020**, *54* (6), 3199–3208.
(20) McKay, G.; Huang, W.; Romera-Castillo, C.; Crouch, J. E.; Rosario-Ortiz, F. L.; Jaffé, R. Predicting reactive intermediate quantum yields from dissolved organic matter photolysis using optical properties and antioxidant capacity. *Environ. Sci. Technol.* **2017**, *51* (10), 5404–5413.
(21) Sharpless, C. M.; Aeschbacher, M.; Page, S. E.; Wenk, J.; Sander, M.; McNeill, K. Photooxidation-induced changes in optical, electrochemical, and photochemical properties of humic substances. *Environ. Sci. Technol.* **2014**, *48* (5), 2688–2696.
(22) Chen, Y.; Hozalski, R. M.; Olmanson, L. G.;Page, B. B.; Finlay, J. G.; Brezonik, P.; Arnold, W. A. Prediction of photochemically produced reactive intermediates in surface waters via satellite remote sensing. *Environ. Sci. Technol.* **2020**, *54* (11), 6671-6681.
(23) Berg, S. M.; T. Whiting, Q.; A. Herrli, J.; Winkels, R.; H. Wammer, K.; K. Remucal, C. The role of dissolved organic matter composition in determining photochemical reactivity at the molecular level. *Environ. Sci. Technol.* **2019**, *53* (20), 11725–11734.
(24) Weishaar, J.; Aiken, G.; Bergamaschi, B.; Fram, M.; Fujii, R.; Mopper, K. Evaluation of specific ultra-violet absorbance as an indicator of the chemical content of dissolved organic carbon. *Environ. Sci. Technol.* **2003**, *37* (20), 4702–4708.
(25) Helms, J. R.; Stubbins, A.; Ritchie, J. D.; Minor, E. C.; Kieber, D. J.; Mopper, K. Absorption spectral slopes and slope ratios as indicators of molecular weight, source, and photobleaching of chromophoric dissolved organic matter. *Limnol. Oceanogr.* **2008**, *53* (3), 955–968.
(26) Ohno, T. Fluorescence inner-filtering correction for determining the humification index of dissolved organic matter. *Environ. Sci. Technol.* **2002**, *36* (4), 742–746.

(27) Dittmar, T.; Koch, B.; Hertkorn, N.; Kattner. A. G. Simple and efficient method for the solid-phase extraction of dissolved organic matter (SPE-DOM) from seawater. *Limnol. Oceanogr.: Methods*. **2008**, *6*, 230–235.
(28) Koch, B. P.; Dittmar, T.; Witt, M.; Kattner, G. Fundamentals of molecular formula assignment to ultrahigh resolution mass data of natural organic matter. *Anal. Chem.* **2007**, *79* (4), 1758–1763.
(29) Walpen, N.; Houska, J.; Salhi, E.; Sander, M.; von Gunten, U. Quantification of the electron donating capacity and UV absorbance of dissolved organic matter during ozonation of secondary wastewater effluent by an assay and an automated analyzer. *Water Res.* **2020**, *185*, 116235.
(30) Bulman, D. M.; Mezyk, S. P.; Remucal, C. K. The impact of pH and irradiation wavelength on the production of reactive oxidants during chlorine photolysis. *Environ. Sci. Technol.* **2019**, *53* (8), 4450–4459.
(31) Page, S. E.; Arnold, W. A.; McNeill, K. Terephthalate as a probe for photochemically generated hydroxyl radical. *J. Environ. Monit.* **2010**, *12* (9), 1658–1665.
(32) Appiani, E.; Ossola, R.; Latch, D. E.; Erickson, P. R.; McNeill, K. Aqueous singlet oxygen reaction kinetics of furfuryl alcohol: Effect of temperature, pH, and salt content. *Environ. Sci. Process. Impacts* **2017**, *19* (4), 507–516.
(33) Laszakovits, J. R.; Berg, S. M.; Anderson, B. G.; O'Brien, J. E.; Wammer, K. H.; Sharpless, C. M. *p*-Nitroanisole/pyridine and *p*-nitroacetophenone/pyridine actinometers revisited: Quantum yield in comparison to ferrioxalate. *Environ. Sci. Technol. Lett.* **2017**, *4* (1), 11–14.
(34) Page, S. E.; Arnold, W. A.; McNeill, K. Assessing the contribution of free hydroxyl radical in organic matter-sensitized photohydroxylation reactions. *Environ. Sci. Technol.* **2011**, *45* (7), 2818–2825.
(35) Glover, C. M.; Rosario-Ortiz, F. L. Impact of halides on the photoproduction of reactive intermediates from organic matter. *Environ. Sci. Technol.* **2013**, *47* (24), 13949–13956.
(36) Parker, K. M.; Pignatello, J. J.; Mitch, W. A. Influence of ionic strength on triplet-state natural organic matter loss by energy transfer and electron transfer pathways. *Environ. Sci. Technol.* **2013**, *47* (19), 10987–10994.
(37) Jasper, J. T.; Sedlak, D. L. Phototransformation of wastewater-derived trace organic contaminants in open-water unit process treatment wetlands. *Environ. Sci. Technol.* **2013**, *47* (19), 10781–10790.
(38) Maizel, A. C.; Li, J.; Remucal, C. K. Relationships between dissolved organic matter composition and photochemistry in lakes of diverse trophic status. *Environ. Sci. Technol.* **2017**, *51* (17), 9624–9632.
(39) Maizel, A. C.; Remucal, C. K. The effect of advanced secondary municipal wastewater treatment on the molecular composition of dissolved organic matter. *Water Res.* **2017**, *122*, 42–52.
(40) Gonsior, M.; Zwartjes, M.; Cooper, W. J.; Song, W.; Ishida, K. P.; Tseng, L. Y.; Jeung, M. K.; Rosso, D.; Hertkorn, N.; Schmitt-Kopplin, P. Molecular characterization of effluent organic matter identified by ultrahigh resolution mass spectrometry. *Water Res.* **2011**, *45* (9), 2943–2953.
(41) Lusk, M. G.; Toor, G. S. Dissolved organic nitrogen in urban streams: Biodegradability and molecular composition studies. *Water Res.* **2016**, *96*, 225–235.
(42) Kim, S.; Kramer, R. W.; Hatcher, P. G. Graphical method for analysis of ultrahigh-

resolution broadband mass spectra of natural organic matter, the van Krevelen diagram. *Anal. Chem.* **2003**, *75* (20), 5336–5344.

(43) Zhou, Y.; Cheng, F.; He, D.; Zhang, Y.; Qu, J.; Yang, X.; Chen, J.; Peijnenburg, W. J. G. M. Effect of UV / chlorine treatment on photophysical and photochemical properties of dissolved organic matter. **2021**, *192*, 1–9.

(44) Önnby, L.; Walpen, N.; Salhi, E.; Sander, M.; von Gunten, U. Two analytical approaches quantifying the electron donating capacities of dissolved organic matter to monitor its oxidation during chlorination and ozonation. *Water Res.* **2018**, *144*, 677–689.

(45) Aeschbacher, M.; Graf, C.; Schwarzenbach, R. P.; Sander, M. Antioxidant properties of humic substances. *Environ. Sci. Technol.* **2012**, *46* (9), 4916–4925.

(46) Wu, Q. Y.; Zhou, T. H.; Du, Y.; Ye, B.; Wang, W. L.; Hu, H. Y. Characterizing the molecular weight distribution of dissolved organic matter by measuring the contents of electron-donating moieties, UV absorbance, and fluorescence intensity. *Environ. Int.* **2020**, *137*, 105570.

(47) Walpen, N.; Schroth, M. H.; Sander, M. Quantification of phenolic antioxidant moieties in dissolved organic matter by flow-injection analysis with electrochemical detection. *Environ. Sci. Technol.* **2016**, *50* (12), 6423–6432.

(48) Nurmi, J. T.; Tratnyek, P. G. Electrochemical properties of natural organic matter (NOM), fractions of NOM, and model biogeochemical electron shuttles. *Environ. Sci. Technol.* **2002**, *36* (4), 617–624.

(49) Ratasuk, N.; Nanny, M. A. Characterization and quantification of reversible redox sites in humic substances. *Environ. Sci. Technol.* **2007**, *41* (22), 7844–7850.

(50) Aeschbacher, M.; Sander, M.; Schwarzenbach, R. P. Novel electrochemical approach to assess the redox properties of humic substances. *Environ. Sci. Technol.* **2010**, *44* (1), 87–93.

(51) Fimmen, R. L.; Cory, R. M.; Chin, Y. P.; Trouts, T. D.; McKnight, D. M. Probing the oxidation-reduction properties of terrestrially and microbially derived dissolved organic Matter. *Geochim. Cosmochim. Acta* **2007**, *71* (12), 3003–3015.

(52) Wasswa, J.; Driscoll, C. T.; Zeng, T. Photochemical characterization of surface waters from lakes in the Adirondack region of New York. *Environ. Sci. Technol.* **2020**, *54* (17), 10654–10667.

(53) Ossola, R.; Martin Jönsson, O.; Moor, K.; McNeill, K. Singlet oxygen quantum yields in environmental waters. *Chem. Rev.* **2021**, *171* (7), 4100-4146.

(54) Dalrymple, R. M.; Carfagno, A. K.; Sharpless, C. M. Correlations between dissolved organic matter optical properties and quantum yields of singlet oxygen and hydrogen peroxide. *Environ. Sci. Technol.* **2010**, *44* (15), 5824–5829.

(55) Walpen, N.; Getzinger, G. J.; Schroth, M. H.; Sander, M. Electron-donating phenolic and electron-accepting quinone moieties in peat dissolved organic matter: Quantities and redox transformations in the context of peat biogeochemistry. *Environ. Sci. Technol.* **2018**, *52* (9), 5236–5245.

(56) Lovely, Derek R.; Coates, John D.; Blunt-Harris, Elizabeth L.; Phillips, Elizabeth J. P.; Woodward, J. C. Humic substances as electron acceptors for microbial respiration. *Lett. to Nat.* **1996**, *382*, 445–448.

(57) Lian, L.; Yao, B.; Hou, S.; Fang, J.; Yan, S.; Song, W. Kinetic study of hydroxyl and sulfate radical-mediated oxidation of pharmaceuticals in wastewater effluents. *Environ. Sci. Technol.* **2017**, *51* (5), 2954–2962.

(58) Buxton, G. V; Greenstock, C. L.; Helman, W. P.; Ross, A. B. Critical review of rate constants for reactions of hydrated electrons, hydrogen atoms, and hydroxyl radical (OH/O^-) in aqueous solutions. *J. Phys. Chem. Ref. Data* **1988**, *117*, 513–886.
(59) McConville, M. B.; Mezyk, S. P.; Remucal, C. K. Indirect photodegradation of the lampricides TFM and niclosamide. *Environ. Sci. Process. Impacts* **2017**, *19* (8), 1028–1039.
(60) McKay, G. Emerging investigator series: Critical review of photophysical models for the optical and photochemical properties of dissolved organic matter. *Environ. Sci. Process. Impacts* **2020**, *22* (5), 1139–1165.

Chapter 6

Conclusions

6.1 Summary

In the first half of this dissertation, a thorough picture of how dissolved organic matter (DOM) varies spatiotemporally in the environment is presented. In Lake Michigan tributaries (Chapter 2), dissolved organic carbon concentrations ([DOC]), dissolved inorganic carbon concentrations ([DIC]), and optical compositional parameters are affected more by spatial variability (e.g., land cover in the watershed) than by season of sample collection. The % wetland in the surrounding watershed had a large effect on DOM in the tributaries and was related to increases in [DOC] and the presence of more terrestrially-derived DOM (i.e., higher specific UV absorbance ($SUVA_{254}$) and lower E_2:E_3). A model including underlying bedrock geology of watersheds showed that watersheds with predominately carbonate lithology have higher [DIC] than those with geology of other types (i.e., sandstone, shale).

Seasonality was a determining factor for [DOC] and the optical properties but not for [DIC]. Additionally, seasonality was much more important for the compositional parameters than it was for [DOC]. Elevated [DOC] and DOM that was more terrestrially-derived was observed in the fall compared to all other seasons. The fact that [DIC] was not affected by season is further evidence that its concentrations are governed strongly by geology.

In Lake Mendota (Chapter 3), transformation of DOM composition occurred throughout the water column from May to November. Variation was depth was observed, but the magnitude of temporal variation was much greater. Throughout the water column, oxidation of DOM was

observed over the course of the sampling period. Variation by depth showed that DOM is larger, more aromatic, and more oxidized deeper in the water column when the lake is stratified. Both optical properties and Fourier transform-ion cyclotron resonance mass spectrometry (FT-ICR MS) data were able to discern lake stratification. Some variations by depth could be observed after mixing with FT-ICR MS.

At the surface of Lake Mendota, molecular weight of DOM decreases and O:C ratios increased throughout the summer and fall. These observations could be consistent with either predominantly photochemical or biological alteration of DOM.[1,2] Using a framework adopted from Herzsprung *et al*.,[3] net increases and decreases in individual formulas identified by FT-ICR MS were attributed to photochemical or biological formation or degradation via Spearman rank correlations to light intensity and chlorophyll concentrations, respectively. Based on these results, photochemical alteration likely explains much of the DOM transformation in the epilimnion of Lake Mendota in the summer and fall months.

Larger, more aromatic, and more oxidized DOM observed deeper in the lake could be a result of several processes. While larger, more complex DOM is generally not the most susceptible to microbial degradation,[4,5] our sampling methods could be detecting the recalcitrant DOM that was not degraded by heterotrophic bacteria. Alternatively, the larger, more oxidized DOM could be desorbing from the sediment under the anoxic conditions. In fact, preferential precipitation of large, aromatic DOM has been observed,[6,7] with subsequent dissolution in reducing conditions has been observed.[6,8]

In Chapters 4 and 5, the photochemical reactivity of diverse samples of DOM were evaluated. For Chapter 4, samples were collected from the St. Louis River and Estuary along with one taken from a tributary to the St. Louis River (e.g., Sand Creek) and the final effluent of a

wastewater treatment plant which flows into the St. Louis River. Optical properties show that the DOM becomes smaller and less aromatic moving downstream in the river. Consequently, the quantum yields of triplet DOM (^{3}DOM) and singlet oxygen ($^1O_2$) increase with the highest values observed in the wastewater effluent. In contrast, no clear trend to location in the river is observed for quantum yields of hydroxyl radical ($^{\bullet}$OH). Spearman rank correlations between quantum yield for each photochemically produced reactive intermediate (PPRI) and formula intensities measured by FT-ICR MS show that a separate pool of DOM is most correlated to $^{\bullet}$OH as compared to ^{3}DOM and $^1O_2$.

Chapter 5 extends the objectives of Chapter 4 to include a much more diverse set of 48 samples. These samples include oligotrophic, mesotrophic, and eutrophic lakes, dystrophic bogs, rivers, streams impacted by agricultural runoff and wastewater effluent, and waters in highly urbanized watersheds. Additionally, 13 effluent samples were collected from four different wastewater treatment plants.

Electron donating capacity (EDC) was quantified spectrophotometrically, and values were highest waters with large terrestrial inputs of DOM and in some of the wastewater samples. EDC was related to the composition of DOM and observations of a positive relationship to $SUVA_{254}$ and positive Spearman rank correlations to largely unsaturated identified formulas within DOM. Interestingly, the slope of the correlation with $SUVA_{254}$ was similar among all natural water samples but different from the wastewater samples. Furthermore, the wastewater samples contained a unique pool of DOM formulas positively correlated to EDC that were not found in the natural water samples that were highly saturated, depleted in oxygen, and similar to lipid- and protein-like formulas.[9]

Quantum yields of $^1O_2$ (Φ_{1O2}) increased with decreasing apparent molecular weight as observed in Chapter 4 and many other studies.[10–22] However, quantum yields of $^{\bullet}OH$ ($\Phi_{\bullet OH}$) did not show any trends with bulk composition parameters in the whole data set. At the molecular level, Φ_{1O2} was positively correlated with saturated formulas with the notable exception of in the agricultural sites where little correlation to composition was observed. $\Phi_{\bullet OH}$ was positively correlated to unsaturated and lignin- and tannin-like formulas.

No trend between $\Phi_{\bullet OH}$ and Φ_{1O2} were identified for the samples as a whole. Interestingly, the samples collected in the St. Louis River showed strong negative correlations between the two quantum yields, while strong positive correlations were observed in the Minnesota River. Because $\Phi_{\bullet OH}$ has remained difficult to predict using individual DOM compositional parameters, multiple linear regressions analysis was employed for both quantum yields. For Φ_{1O2}, the preferred model included positive terms for $O:C_w$ and [DIC] as well as negative terms for EDC and [DOC]. In contrast, the preferred model for $\Phi_{\bullet OH}$ includes negative terms for both $E_2:E_3$ and $O:C_w$. These relationships demonstrate that different precursors are involved in the formation of these two PPRI.

6.2 Future Research Directions

Based on the research presented within, several lines of additional study can be suggested. Several ideas are outlined briefly below.

6.2.1 Investigation of [DIC] Sources in Tributaries Using Stable Carbon Isotopes ($\delta^{13}C$)

In Chapter 2, predictor variables of [DIC] in Lake Michigan tributaries were associated with the presence of underlying carbonate bedrock and % urban land cover in the surrounding watershed. The underlying mechanisms for both of these observations are well documented and

include weathering of concrete to release carbonate species[23] and dissolution of carbonate species from the bedrock.[24] However, missing from this interpretation are relative amounts of carbonate material from minerals versus other potential sources not considered in our model including biological or photochemical oxidation of DOM. By comparison ratios of stable carbon isotopes ($\delta^{13}C$) of carbonate species in the tributaries samples in Chapter 2 to known ratios in carbonate minerals, or even potentially nearby groundwater, an estimation of the contribution of mineral-derived DIC to the tributaries could be made.[23,24]

6.2.2 Molecular Investigation into DOM Composition near Oxic/Anoxic Interfaces in Lakes

Depth-discrete Lake Mendota samples show the greatest range of [DOC] and optical properties is near the thermocline during lake stratification. Additionally, the single date that FT-ICR MS data is available shows molecular composition changes rapidly around the thermocline as well. It is unlikely that our single date FT-ICR MS data is an anomaly. First, optical properties also show substantial variability near the thermocline though the exact nature of the observations are not consistent on our sampling dates. Secondly, observations of high turbidity have been made at these same depths and sampling days potentially indicating the occurrence precipitation and/or increased bacterial mass at these depths.[24] Finally, the preferential sorption and precipitation with redox active metals has been shown for large, aromatic DOM.[7,26] However, because only one date has mass spectral data associated with it, it is difficult to draw conclusions beyond the simple fact that DOM composition changes rapidly near the thermocline. Additionally, finer scale sampling (e.g., more samples collected over a short depth interval) is needed to make definitive statements including observations both just above and just below the oxic/anoxic interface. Understanding these DOM dynamics is important for broader implications in aquatic chemistry. For example,

concentrations of methylmercury spike at the thermocline in Lake Mendota[25] and studies have shown that mercury methylation rates depend on DOM composition.[26]

Future sampling campaigns should focus sample collection near the thermocline. [DOC], UV-visible spectroscopy, and FT-ICR MS data should be collected for all samples. Additionally, quantification and characterization of the composition of particulate organic matter (POM) collected at the thermocline could test the hypothesis that the variability of DOM observed at the thermocline is due to precipitation/dissolution reactions of DOM with redox active metals. POM can be collected and separated from DOM using centrifugation and subsequent dissolving.[27]

6.2.3 Bidaily Sampling at the Surface of Lake Mendota

Beyond further sampling at the thermocline of Lake Mendota, higher frequency samples should be collected to determine the time scales at which degradation of DOM occurs. A sample collected shortly before sunrise would maximize the capture of biological degradation products since no photochemistry or photosynthesis occurs overnight. Another sample collected shortly before sunset on the same days should maximize the capture of photoproducts as well as carbon fixed by autotrophic organisms. In this way, the two transformation processes discussed in Chapter 3 could be further disentangled from one another.

6.2.4 Further Investigation into the DOM Precursors to ˙OH Formation

While numerous studies measuring $\Phi_{\bullet OH}$ exist and many relationships to DOM composition have been evaluated, the precursors within DOM that give rise to $\Phi_{\bullet OH}$ remain up for debate in the literature. While many studies conclude ^{3}DOM must not be a precursor based on divergent trends between $\Phi_{\bullet OH}$ both Φ_{3DOM} and $\Phi_{^1O_2}$,[14,19,28,29] this has not been directly tested using

quencher experiments commonly employed to assign contaminant degradation to individual PPRI. For example, if the addition of sorbic acid to a photochemical reaction slows the degradation rate of the substrate in question, then the degradation of that substrate is assigned to ^{3}DOM.[30] A similar approach could be taken to test the hypothesis that ^{3}DOM is a precursor to $^{\bullet}$OH.

Two conditions of DOM solutions would be prepared. A low concentration (i.e, 10 μM) of terephthalic acid to measure $^{\bullet}$OH production is added to both.[31] To one solution, a ^{3}DOM quencher such as sorbic acid, is also added in excess (i.e., mM concentrations). If a decrease in $[^{\bullet}OH]_{ss}$ is observed in the reaction with sorbic acid, ^{3}DOM must play some role in $^{\bullet}$OH formation. Notably, only relatively high energy ^{3}DOM are quenched by sorbic acid[32] which would need to be taken into consideration during these analyses. This type of experiment should be done with a wide variety of DOM types as the relative importance different $^{\bullet}$OH formation mechanisms may depend on DOM composition.

6.3 References

(1) Ward, C. P.; Cory, R. M. Complete and partial photo-oxidation of dissolved organic matter draining permafrost Soils. *Environ. Sci. Technol.* **2016**, *50* (7), 3545–3553.

(2) Judd, K. E.; Crump, B. C.; Kling, G. W. Bacterial responses in activity and community composition to photo-oxidation of dissolved organic matter from soil and surface waters. *Aquat. Sci.* **2007**, *69* (1), 96–107.

(3) Herzsprung, P.; Wentzky, V.; Kamjunke, N.; Von Tümpling, W.; Wilske, C.; Friese, K.; Boehrer, B.; Reemtsma, T.; Rinke, K.; Lechtenfeld, O. J. Improved understanding of dissolved organic matter processing in freshwater using complementary experimental and machine learning approaches. *Environ. Sci. Technol.* **2020**, *54* (21), 13556–13565.

(4) D'Andrilli, J.; Cooper, W. T.; Foreman, C. M.; Marshall, A. G. An ultrahigh-resolution mass spectrometry index to estimate natural organic matter lability. *Rapid Commun. Mass Spectrom.* **2015**, *29* (24), 2385–2401.

(5) Logue, J. B.; Stedmon, C. A.; Kellerman, A. M.; Nielsen, N. J.; Andersson, A. F.; Laudon, H.; Lindström, E. S.; Kritzberg, E. S. Experimental insights into the importance of aquatic bacterial community composition to the degradation of dissolved organic matter. *ISME J.* **2016**, *10* (3), 533–545.

(6) Dadi, T.; Harir, M.; Hertkorn, N.; Koschorreck, M.; Schmitt-Kopplin, P.; Herzsprung, P. Redox conditions affect dissolved organic carbon quality in stratified freshwaters. *Environ.*

Sci. Technol. **2017**, *51* (23), 13705–13713.
(7) Riedel, T.; Zak, D.; Biester, H.; Dittmar, T. Iron traps terrestrially derived dissolved organic matter at redox interfaces. *Proc. Natl. Acad. Sci.* **2013**, *110* (25), 10101–10105.
(8) Valle, J.; Gonsior, M.; Harir, M.; Enrich-Prast, A.; Schmitt-Kopplin, P.; Bastviken, D.; Conrad, R.; Hertkorn, N. Extensive processing of sediment pore water dissolved organic matter during anoxic incubation as observed by high-field mass spectrometry (FTICR-MS). *Water Res.* **2018**, *129*, 252–263.
(9) Kim, S.; Kramer, R. W.; Hatcher, P. G. Graphical method for analysis of ultrahigh-resolution broadband mass spectra of natural organic matter, the van Krevelen diagram. *Anal. Chem.* **2003**, *75* (20), 5336–5344.
(10) Berg, S. M.; T. Whiting, Q.; A. Herrli, J.; Winkels, R.; H. Wammer, K.; K. Remucal, C. The role of dissolved organic matter composition in determining photochemical reactivity at the molecular level. *Environ. Sci. Technol.* **2019**, *53* (20), 11725–11734.
(11) Bodhipaksha, L. C.; Sharpless, C. M.; Chin, Y.-P.; Sander, M.; K. Langston, W.; A. MacKay, A. Triplet photochemistry of effluent and natural organic matter in whole water and isolates from effluent-receiving rivers. *Environ. Sci. Technol.* **2015**, *49* (6), 3453–3463.
(12) Zhou, H.; Lian, L.; Yan, S.; Song, W. Insights into the photo-induced formation of reactive intermediates from effluent organic matter: The role of chemical constituents. *Water Res.* **2017**, *112*, 120–128.
(13) Zhou, Y.; Cheng, F.; He, D.; Zhang, Y.; Qu, J.; Yang, X.; Chen, J.; Peijnenburg, W. J. G. M. Effect of UV / chlorine treatment on photophysical and photochemical properties of dissolved organic matter. **2021**, *192*, 1–9.
(14) Wasswa, J.; Driscoll, C. T.; Zeng, T. Photochemical characterization of surface waters from lakes in the Adirondack region of New York. *Environ. Sci. Technol.* **2020**, *54* (17), 10654–10667.
(15) Dalrymple, R. M.; Carfagno, A. K.; Sharpless, C. M. Correlations between dissolved organic matter optical properties and quantum yields of singlet oxygen and hydrogen peroxide. *Environ. Sci. Technol.* **2010**, *44* (15), 5824–5829.
(16) Leresche, F.; McKay, G.; Kurtz, T.; Von Gunten, U.; Canonica, S.; Rosario-Ortiz, F. L. Effects of ozone on the photochemical and photophysical properties of dissolved organic matter. *Environ. Sci. Technol.* **2019**, *53* (10), 5622–5632.
(17) Maizel, A. C.; Remucal, C. K. Molecular composition and photochemical reactivity of size-fractionated dissolved organic matter. *Environ. Sci. Technol.* **2017**, *51* (4), 2113–2123.
(18) McCabe, A. J.; Arnold, W. A. Seasonal and spatial variabilities in the water chemistry of prairie pothole wetlands influence the photoproduction of reactive intermediates. *Chemosphere* **2016**, *155*, 640–647.
(19) McKay, G.; Huang, W.; Romera-Castillo, C.; Crouch, J. E.; Rosario-Ortiz, F. L.; Jaffé, R. Predicting reactive intermediate quantum yields from dissolved organic matter photolysis using optical properties and antioxidant capacity. *Environ. Sci. Technol.* **2017**, *51* (10), 5404–5413.
(20) Mostafa, S.; Rosario-Ortiz, F. L. Singlet oxygen formation from wastewater organic matter. *Environ. Sci. Technol.* **2013**, *47* (15), 8179–8186.
(21) Sharpless, C. M.; Aeschbacher, M.; Page, S. E.; Wenk, J.; Sander, M.; McNeill, K. Photooxidation-induced changes in optical, electrochemical, and photochemical properties of humic substances. *Environ. Sci. Technol.* **2014**, *48* (5), 2688–2696.
(22) Sharpless, C. M. Lifetimes of triplet dissolved natural organic matter (DOM) and the effect

of $NaBH_4$ reduction on singlet oxygen quantum yields: Implications for DOM photophysics. *Environ. Sci. Technol.* **2012**, *46* (8), 4466–4473.

(23) Schulte, P.; van Geldern, R.; Freitag, H.; Karim, A.; Négrel, P.; Petelet-Giraud, E.; Probst, A.; Probst, J. L.; Telmer, K.; Veizer, J.; Barth, J. A. C. Applications of stable water and carbon isotopes in watershed research: Weathering, carbon cycling, and water balances. *Earth-Science Rev.* **2011**, *109* (1–2), 20–31.

(24) Aucour, A. M.; Sheppard, S. M. F.; Guyomar, O.; Wattelet, J. Use of ^{13}C to trace origin and cycling of inorganic carbon in the Rhone River system. *Chem. Geol.* **1999**, *159* (1–4), 87–105.

(25) Peterson, B. D.; Mcdaniel, E. A.; Schmidt, A. G.; Lepak, R. F.; Janssen, S. E.; Tran, P. Q.; Marick, R. A.; Ogorek, J. M.; Dewild, J. F.; Krabbenhoft, D. P.; Mcmahon, K. D. Mercury methylation genes identified across diverse anaerobic microbial guilds in a eutrophic sulfate-enriched lake. *Environ. Sci. Technol.* **2020**, *54* (24), 15840–15851.

(26) Graham, A. M.; Cameron-Burr, K. T.; Hajic, H. A.; Lee, C.; Msekela, D.; Gilmour, C. C. Sulfurization of dissolved organic matter increases Hg-sulfide-dissolved organic matter bioavailability to a Hg-methylating bacterium. *Environ. Sci. Technol.* **2017**, *51* (16), 9080–9088.

(27) Cottrell, B. A.; Timko, S. A.; Devera, L.; Robinson, A. K.; Gonsior, M.; Vizenor, A. E.; Simpson, A. J.; Cooper, W. J. Photochemistry of excited-state species in natural waters: A role for particulate organic matter. *Water Res.* **2013**, *47* (14), 5189–5199.

(28) Berg, S. M.; Whiting, Q. T.; Herrli, J. A.; Winkels, R.; Wammer, K. H.; Remucal, C. K. The role of dissolved organic matter composition in determining photochemical reactivity at the molecular level. *Environ. Sci. Technol.* **2019**.

(29) Parker, K. M.; Pignatello, J. J.; Mitch, W. A. Influence of ionic strength on triplet-state natural organic matter loss by energy transfer and electron transfer pathways. *Environ. Sci. Technol.* **2013**, *47* (19), 10987–10994.

(30) McConville, M. B.; Mezyk, S. P.; Remucal, C. K. Indirect photodegradation of the lampricides TFM and niclosamide. *Environ. Sci. Process. Impacts* **2017**, *19* (8), 1028–1039.

(31) Page, S. E.; Arnold, W. A.; McNeill, K. Terephthalate as a probe for photochemically generated hydroxyl radical. *J. Environ. Monit.* **2010**, *12* (9), 1658–1665.

(32) McNeill, K.; Canonica, S. Triplet state dissolved organic matter in aquatic photochemistry: Reaction mechanisms, substrate scope, and photophysical properties. *Environ. Sci. Process. Impacts* **2016**, *18* (11), 1381–1399.

Appendix A

Supplementary Materials for Chapter 2

A.1 The Effect of Freezing and Thawing on DOM

The [DOC] 68 sites from the spring sampling trip were not measured due to instrument malfunction and too little volume was left to repeat the measurements. However, frozen archive samples were saved and these samples were thawed, re-filtered through 0.45 um (nylon, Agilent) filters and rerun on the instrument. To determine if the thawing and re-filtering would have an effect on [DOC], we also thawed and re-filtered 20 samples from the October sampling trip to compare to their original [DOC] (**Figure A.1**). About 23% of [DOC] was lost during this process.

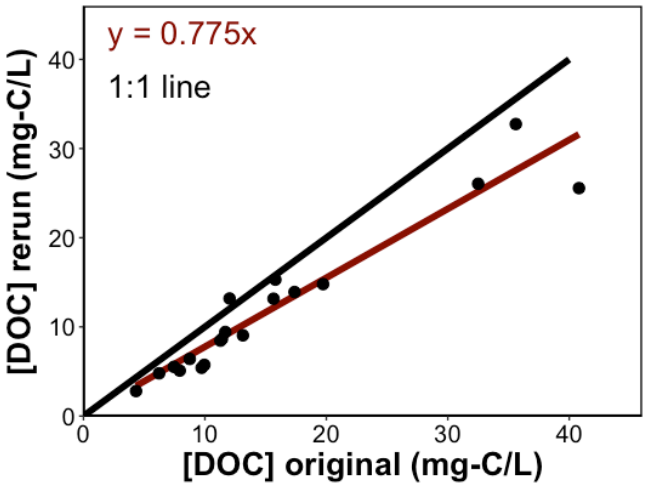

Figure A.1. Comparison between [DOC] measured in October 2016 samples originally and in aliquots of the samples that had been thawed and re-filtered.

To determine if there was any preferential removal of dissolved organic matter based on composition, we also compared E_2:E_3 values of 20 original October samples and from those that

had been thawed and re-filtered (**Figure A.2**). These results show that the composition of DOM was unaltered by sample storage.

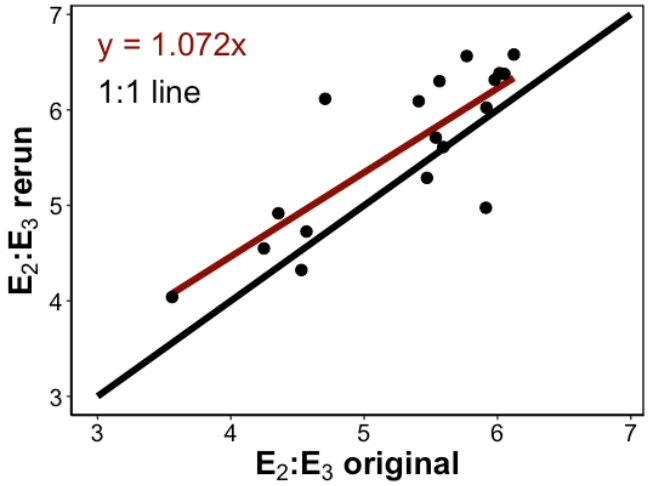

Figure A.2. Comparison between E_2:E_3 measured in October 2016 samples originally and in aliquots of the samples that had been thawed and re-filtered.

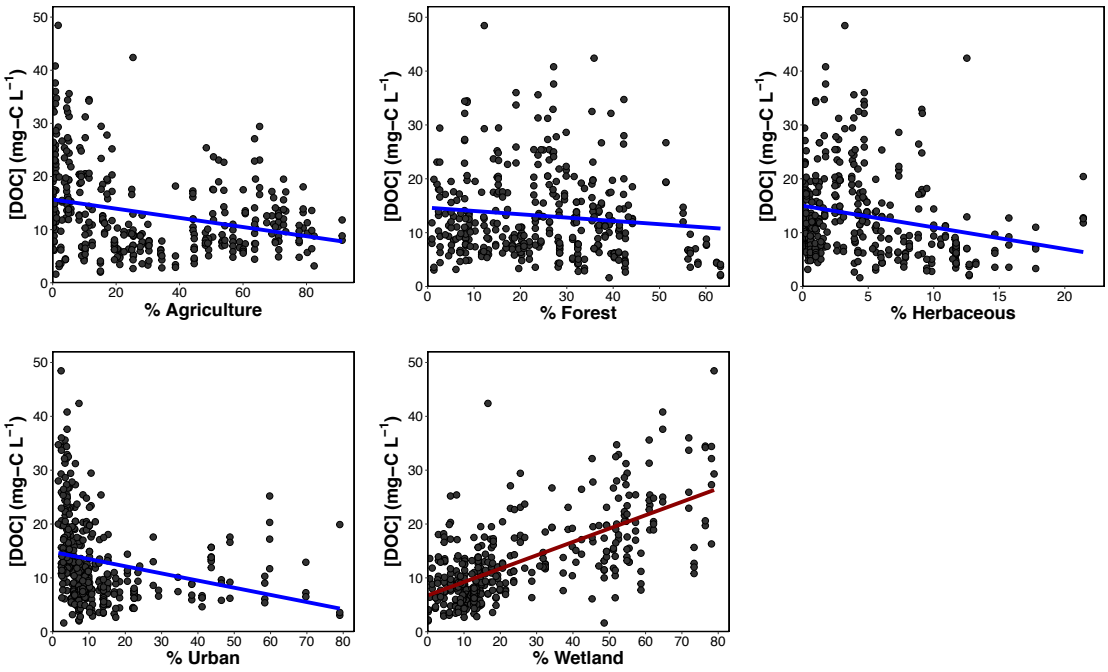

Figure A.3. Scatter plots of [DOC] and landcover types for all samples collected. Blue regression lines indicate a negative slope and red regression lines indicate a positive slope. Slopes, intercepts, and statistics for these plots are given in **Table A.13**.

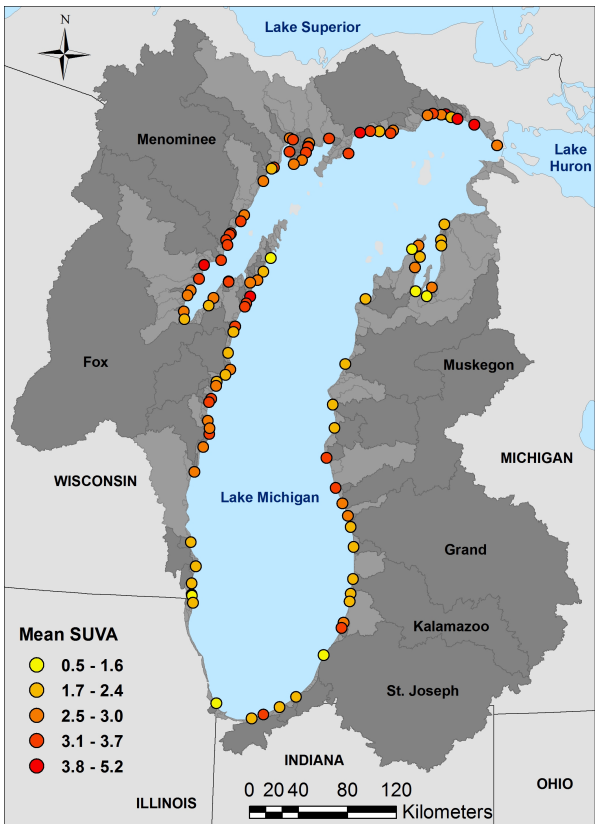

Figure A.4. Mean $SUVA_{254}$ values in Lake Michigan tributaries for all samples collected.

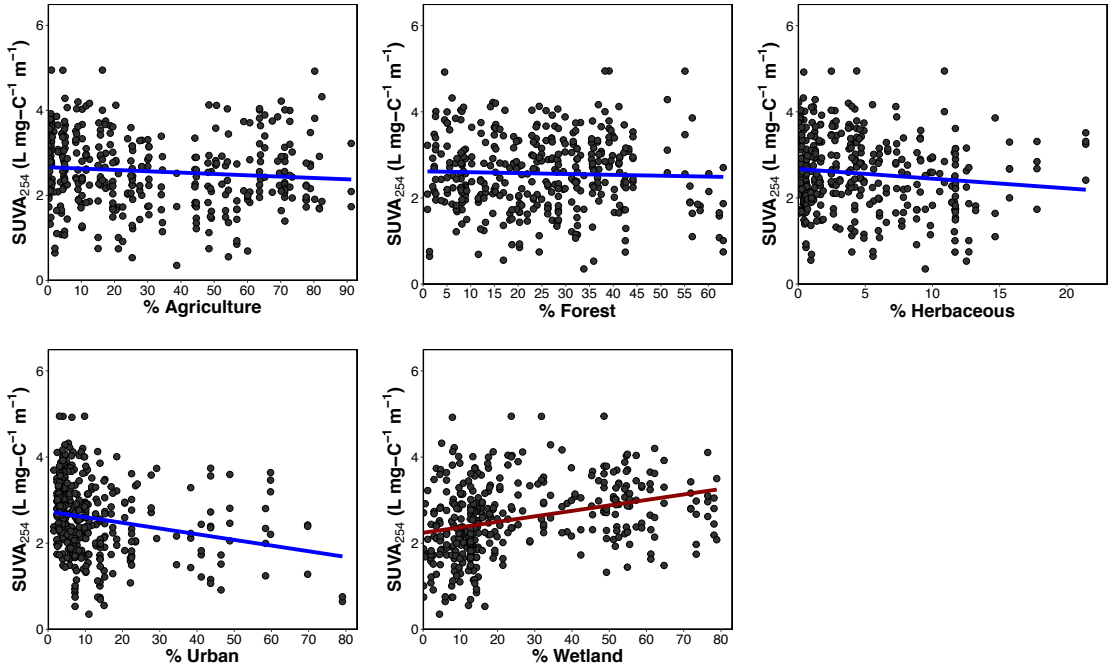

Figure A.5. Scatter plots of $SUVA_{254}$ and landcover types for all samples collected. Blue regression lines indicate a negative slope and red regression lines indicate a positive slope. Slopes, intercepts, and statistics for these plots are given in **Table A.13**.

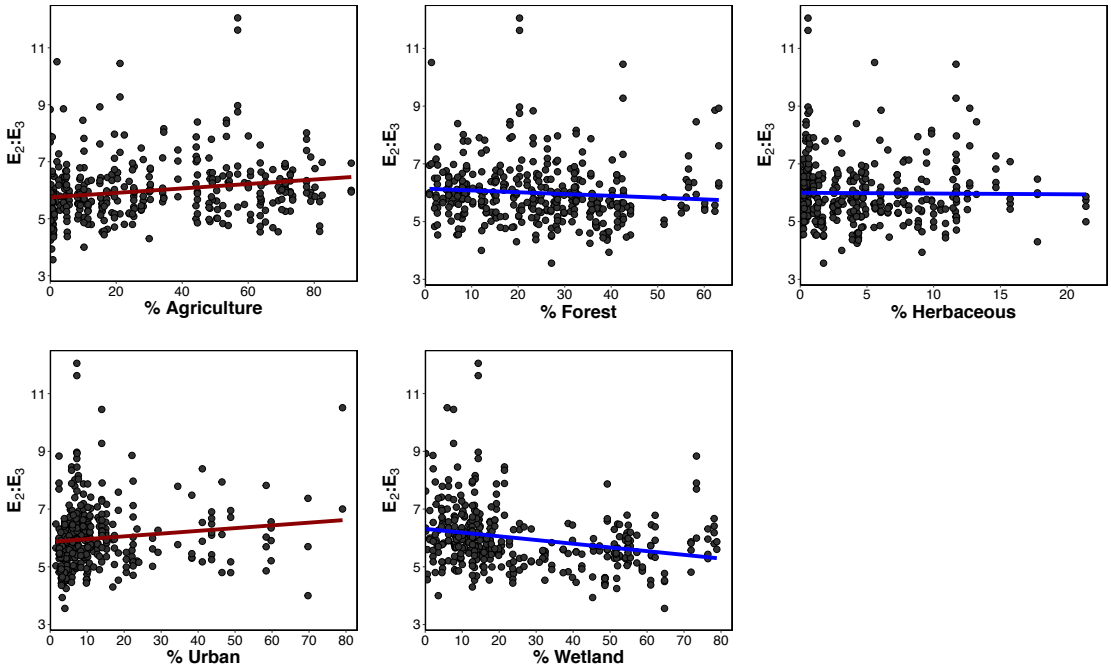

Figure A.6. Scatter plots of E_2:E_3 and landcover types for all samples collected. Blue regression lines indicate a negative slope and red regression lines indicate a positive slope. Slopes, intercepts, and statistics for these plots are given in **Table A.13**.

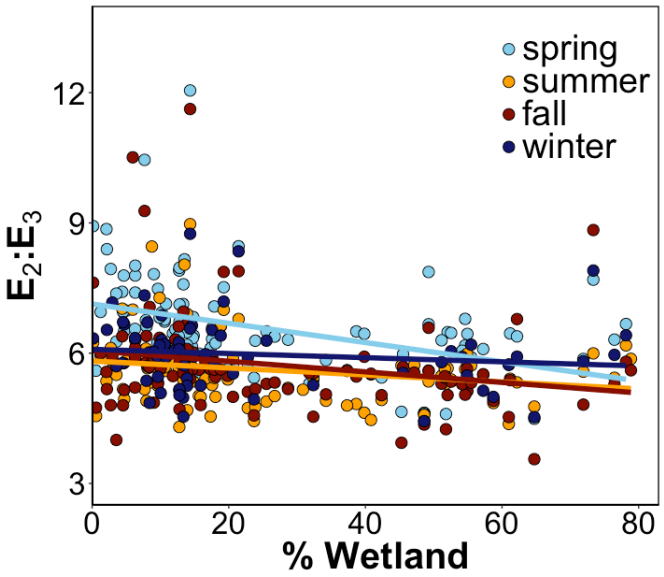

Figure A.7. E_2:E_3 versus % wetland in the watershed. Colors indicate season. Only tributaries that were measured in all four seasons are included. Slopes, intercepts, and statistics for this plot are given in **Table A.14**.

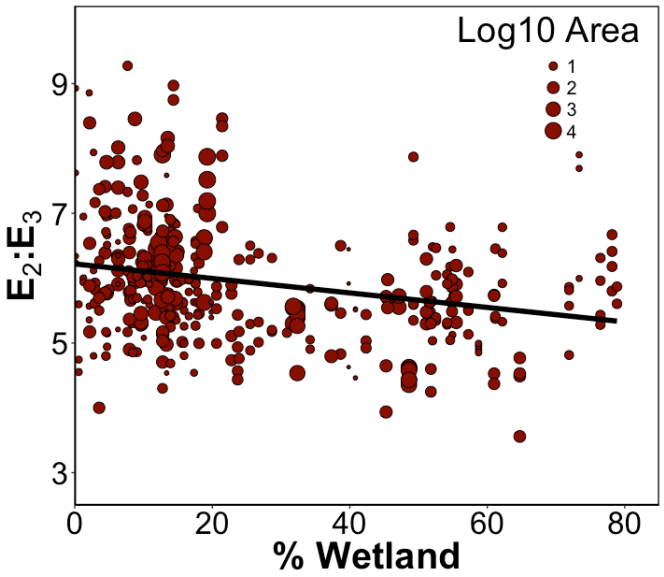

Figure A.8. E_2:E_3 versus % wetland for samples collected in all 4 seasons. The size of the point is proportional to the size of the watershed (km^2). Slopes, intercepts, and statistics for this plot are given in **Table A.13**.

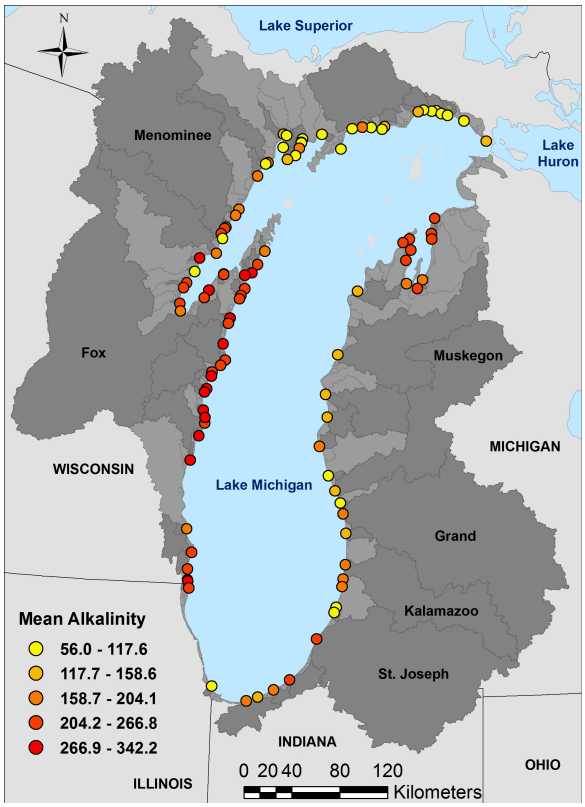

Figure A.9. Mean alkalinity values in Lake Michigan tributaries for all samples collected. Alkalinity is reported in units of mg L^{-1} as $CaCO_3$.

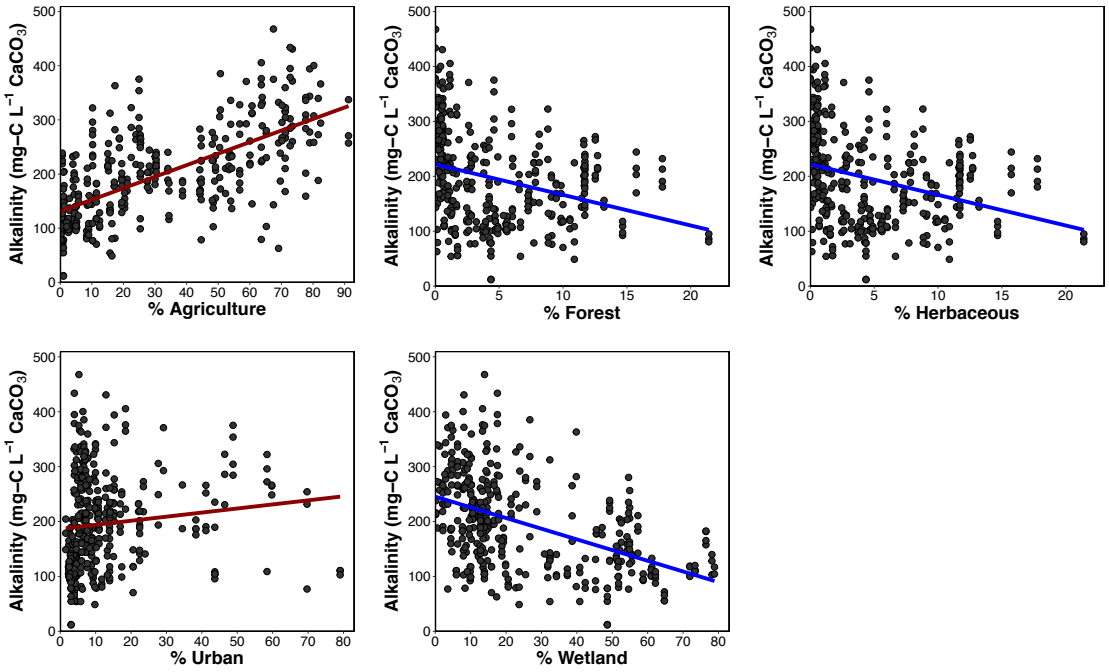

Figure A.10. Scatter plots of alkalinity and landcover types for all samples collected. Blue regression lines indicate a negative slope and red regression lines indicate a positive slope. Slopes, intercepts, and statistics for these plots are given in **Table A.13**.

Table A.1. Geographical location, sample information, frequency of sample collection, measurements made, and model types used in references compared in this study. Model type denoted as comparison refers to ANOVA, MANOVA, or other statistical analysis considering differences between two groups of samples.

Author and year	Location	Sample Info	Frequency	Measurement	Model
Aitkenhead-Peterson et al., 2009[1]	Texas	2 depths in 12 tributaries of different watersheds	1 sample / 2 weeks for 1 year	[DOC]	Simple Linear Regressions
Alvarez-Cobelas et al., 2012[2]	World-wide. Based on publicly available data sets	550 watersheds	data averaged over entire years	[DOC]	MLR
Cawley et al., 2014[3]	Experimental forest in New Hampshire	Streams in 9 watersheds	1 sample / month for 1 year	[DOC], composition via UV-vis and fluorescence	Comparison

Chen et al., 2017[4]	Residential and urban watersheds in China	231 samples collected after 16 rainfall events	15-minute intervals during overflow of stormwater	[DOC], composition via UV-vis and fluorescence	Simple Linear Regressions
Clark et al., 2004[5]	Northern Scotland	13 watersheds	1 sample / 14 days for 1 year	[DOC]	MLR
Dalmargo et al., 2017[6]	Central Western Brazil	40 sampling locations	2 samples / site. Once in wet season and once in dry season	[DOC], composition via UV-vis and fluorescence	Simple Linear Regressions
Dawson et al., 2011[7]	River Dee basin in Scotland	12 sites in a single watershed	1 sample / week for 2 years	[DOC]	MLR
Dillon and Molot, 1997[8]	Ontario	Tributaries in 20 watersheds draining into 7 different lakes	30-126 samples / site / year for 12 years	[DOC]	MLR
Eckhardt and Moore, 1990[9]	Appalachian Uplands and St. Lawrence Lowlands in Canada	Streams in 42 watersheds	1 sample / week for 8 months	[DOC]	MLR
Flint and McDowell, 2015[10]	New Hampshire	10 headwater wetlands in a single watershed	1 sample / month for 18 months	[DOC]	MLR
Frost et al., 2006[11]	Ontonagon River Watershed	60 streams from a single watershed	Single sample	[DOC], composition via UV-vis	MLR
Graeber et al., 2012[12]	Northern German Plains	53 streams ([DOC]), 42 streams (DOM composition), and 8 streams (seasonally)	Single sample with subset at 1 sample / 2 weeks for 1 year	[DOC], composition via fluorescence	MLR

Hanley et al., 2013[13]	Mouths of Large North American Rivers	17 rivers in different watersheds	Varies by river. Multiple samples/year in all cases.	[DOC], composition via UV-vis	MLR
Heinz et al., 2015[14]	Headwater streams in Germany dominated by either forest or agriculture	12 headwater streams	1 sample / month for 1 year	[DOC], composition via UV-vis and fluorescence	Comparison
Hosen et al., 2014[15]	Coastal Plain headwater streams in Maryland	8 headwater streams located in a single watershed	20 samples / site / 2 years	[DOC], composition via fluorescence	Simple Linear Regressions
Kortelainen et al., 1993[16]	Finland	streams in 42 watersheds	12 samples / year	[DOC]	MLR
Liu et al., 2014[17]	Ireland	55 streams which are outlets of watersheds	7 samples / 1 year.	[DOC]	MLR
Lu et al., 2014[18]	Chesapeake Bay region in Virginia	8 headwater streams in different watersheds	6 samples / 1 year	[DOC], [DIC], composition via fluorescence	Comparison
Macdonald and Minor, 2013[19]	Minnesota	5 streams that are tributaries to Lake Superior	3 samples / site for 1 year	[DOC], composition via UV-vis	Simple Linear Regressions
Mattsson et al., 2005[20]	Finland	Rivers in 86 watersheds	12-32 samples / year for 4 years	[DOC]	MLR
Mattsson et al., 2015[21]	Finland	30 rivers that flow into Baltic Sea	12 years	[DOC]	Comparison

McElmurry et al., 2014[22]	stormwater from urban and suburban sources	48 sites within a single watershed	Single sample	[DOC], composition via UV-vis	MLR
Mosher et al., 2010[23]	Bankhead National Forest in Alabama	6 streams flowing over different types of bedrock	Single sample	[DOC], [DIC], composition via HRMS	Comparison
Palviainen et al., 2016[24]	Finland	12 watersheds with lakes.	Single Sample	[DOC]	MLR
Schelker et al., 2012[25]	Sweden	4 boreal headwater streams impacted by clearcutting	At least 1 sample / month for 6 years	[DOC]	Comparison
Shang et al., 2018[26]	Alabama	6 streams in different watersheds	5 samples / 8 months	[DOC], composition via UV-vis and fluorescence	MLR
Singh et al., 2017[27]	Mississippi	5 lakes, an estuary, and coastal waters	Varies by site	[DOC], composition via UV-vis and fluorescence	MLR
Williams et al., 2010[28]	Canada	43 streams in different watersheds	Sample once	[DOC], composition via UV-vis and fluorescence	MLR
Xenopoulos et al., 2003[29]	Upper Great Lakes region	100 lakes	Sampled once	[DOC]	MLR

Table A.2. Results of [DOC] MLR. Multiple $R^2 = 0.5535$, Adjusted $R^2 = 0.5412$, $p < 2.2 \times 10^{-16}$. Estimates for seasons are compared to the fall values.

	Estimate	Std. Error	t value	p
Intercept	5.72×10^{-1}	5.77×10^{-2}	9.90	$< 2 \times 10^{-16}$
% agriculture	4.10×10^{-3}	7.54×10^{-4}	5.44	1.42×10^{-7}
spring	-1.49×10^{-2}	3.56×10^{-2}	-4.18×10^{-1}	6.76×10^{-1}
summer	-1.26×10^{-1}	3.56×10^{-2}	-3.55	4.75×10^{-4}
winter	-1.38×10^{-1}	3.56×10^{-2}	-3.89	1.33×10^{-4}
% urban	6.42×10^{-3}	$1.19x\ 10^{-3}$	5.39	1.85×10^{-7}
% wetland	1.22×10^{-2}	8.84×10^{-4}	13.8	$< 2 \times 10^{-16}$

Table A.3. Statistics for **Figure 2.2a** in the main text.

Season	Slope	Intercept	R^2	p
fall	0.317	7.154	0.528	2.30×10^{-10}
winter	0.238	4.397	0.697	1.29×10^{-15}
spring	0.169	9.031	0.317	6.28×10^{-6}
summer	0.262	5.024	0.487	2.32×10^{-9}

Table A.4. Statistics for **Figure 2.2b** in the main text.

Season	Slope	Intercept	R^2	p
fall	1.74×10^{-2}	1.959	0.258	7.51×10^{-5}
winter	1.23×10^{-2}	2.766	0.154	3.03×10^{-3}
spring	1.42×10^{-2}	1.514	0.294	2.02×10^{-5}
summer	5.86×10^{-3}	2.723	0.030	2.02×10^{-1}

Table A.5. Results of $SUVA_{254}$ MLR. Multiple $R^2 = 0.4464$, Adjusted $R^2 = 0.4227$, $p < 2.2 \times 10^{-16}$. Estimates for seasons are compared to the fall values.

	Estimate	Std. Error	t value	p
Intercept	9.54×10^{-2}	5.55×10^{-2}	1.72	8.74×10^{-2}
% agriculture	3.67×10^{-3}	9.92×10^{-4}	3.70	2.76×10^{-4}
$\log_{10}$ area	7.89×10^{-2}	2.09×10^{-2}	3.78	2.05×10^{-4}
spring	-1.06×10^{-1}	2.52×10^{-2}	-4.20	4.01×10^{-5}
summer	8.76×10^{-2}	2.52×10^{-2}	3.48	6.04×10^{-4}
winter	1.23×10^{-1}	2.51×10^{-2}	4.92	1.79×10^{-6}
% urban	5.20×10^{-3}	1.48×10^{-3}	3.52	5.29×10^{-4}
% wetland	3.51×10^{-3}	6.64×10^{-4}	5.30	2.99×10^{-7}
% agriculture: $\log_{10}$ area	-1.59×10^{-3}	4.46×10^{-4}	-3.58	4.29×10^{-4}
$\log_{10}$ area: % urban	-2.61×10^{-3}	9.36×10^{-4}	-2.79	5.72×10^{-3}

Table A.6. Results of E_2:E_3 MLR. Multiple $R^2 = 0.252$, adjusted $R^2 = 0.232$, $p = 1.70 \times 10^{-12}$. Estimates for seasons are compared to the fall values.

	Estimate	Std. Error	t value	p
Intercept	7.43×10^{-1}	1.50×10^{-2}	49.5	$< 2 \times 10^{-16}$
$\log_{10}$ area	2.75×10^{-2}	7.10×10^{-3}	3.88	1.39×10^{-4}
spring	5.69×10^{-2}	1.18×10^{-2}	4.80	2.85×10^{-6}
summer	-1.24×10^{-2}	1.19×10^{-2}	-1.04E	3.00×10^{-1}
winter	1.13×10^{-2}	1.19×10^{-2}	9.43×10^{-1}	3.47×10^{-1}
% wetland	1.05×10^{-3}	4.52×10^{-4}	2.33	2.08×10^{-2}
$\log_{10}$ area: % wetland	-1.29×10^{-3}	2.90×10^{-4}	-4.44	1.43×10^{-5}

Table A.7. Results of alkalinity MLR. Multiple $R^2 = 0.506$, adjusted $R^2 = 0.4965$, $p < 2.2 \times 10^{-16}$.

	Estimate	Std. Error	t value	p
Intercept	2.19	3.77×10^{-2}	58.1	$< 2 \times 10^{-16}$
% agriculture	3.57×10^{-3}	9.13×10^{-4}	3.91	1.27×10^{-4}
$\log_{10}$ area	-1.02×10^{-1}	2.12×10^{-2}	-4.82	2.72×10^{-6}
% urban	3.30×10^{-3}	8.39×10^{-4}	3.93	1.16×10^{-4}
% agriculture: $\log_{10}$ area	1.34×10^{-3}	4.87×10^{-4}	2.74	6.61×10^{-3}

Table A.8. Results of alkalinity MLR with lithology. Multiple R^2 = 0.04477, adjusted R^2 = 0.03099, p = 0.02281.

	Estimate	**Std. Error**	**t value**	**p**
Intercept	2.21	0.0432	51.2	$< 2 \times 10^{-16}$
$\log_{10}$ area	1.24×10^{-2}	1.77×10^{-2}	6.98×10^{-1}	4.86×10^{-1}
carbonate	1.63×10^{-1}	6.09×10^{-2}	2.67	8.12×10^{-3}
$\log_{10}$ area	-8.88×10^{-2}	3.15×10^{-2}	-2.82	5.27×10^{-3}

Table A.9. Results of ANOVA-Tukey tests to determine statistically significant differences in averages of [DOC] for each season.

Season	**p**
spring-fall	2.44×10^{-2}
summer-fall	3.90×10^{-6}
winter-fall	$< 1.00 \times 10^{-7}$
summer-spring	1.09×10^{-1}
winter-spring	4.34×10^{-4}
winter-summer	2.92×10^{-1}

Table A.10. Results of ANOVA-Tukey tests to determine statistically significant differences in averages of $SUVA_{254}$ for each season.

Season	**p**
spring-fall	2.00×10^{-7}
summer-fall	2.37×10^{-1}
winter-fall	4.62×10^{-4}
summer-spring	$< 1.00 \times 10^{-7}$
winter-spring	$< 1.00 \times 10^{-7}$
winter-summer	1.46×10^{-1}

Table A.11. Results of ANOVA-Tukey tests to determine statistically significant differences in averages of E_2:E_3 for each season.

Season	p
spring-fall	$< 1.00 \times 10^{-7}$
summer-fall	1.78×10^{-1}
winter-fall	7.93×10^{-1}
summer-spring	$< 1.00 \times 10^{-7}$
winter-spring	$< 1.00 \times 10^{-7}$
winter-summer	1.84×10^{-2}

Table A.12. Results of ANOVA-Tukey tests to determine statistically significant differences in averages of alkalinity for each season.

Season	p
spring-fall	9.98×10^{-1}
summer-fall	4.26×10^{-1}
winter-fall	9.99×10^{-1}
summer-spring	5.21×10^{-1}
winter-spring	9.90×10^{-1}
winter-summer	3.39×10^{-1}

Table A.13. Results of statistical analyses for simple linear regressions between the four parameters and each landcover type.

		[DOC]	$SUVA_{254}$	$E_2:E_3$	Alkalinity
% Agriculture	slope	-8.64×10^{-2}	-3.16×10^{-3}	7.82×10^{-3}	2.13
	intercept	15.67	2.66	5.75	131.24
	p	5.62×10^{-9}	5.69×10^{-2}	1.05×10^{-4}	$< 2.2 \times 10^{-16}$
% Forest	slope	-6.14×10^{-2}	-2.04×10^{-3}	-6.19×10^{-3}	-2.81
	intercept	14.64	2.62	6.14	265.94
	p	2.12×10^{-2}	0.491	8.52×10^{-2}	$< 2.2 \times 10^{-16}$
% Herbaceous	slope	-0.402	2.24×10^{-2}	-2.56×10^{-3}	-5.58
	intercept	15.00	2.67	6.00	221.93
	p	2×10^{-6}	1.68×10^{-2}	0.825	1.62×10^{-9}
% Urban	slope	-0.133	-1.32×10^{-2}	9.49×10^{-3}	0.743
	intercept	14.82	2.74	5.87	186.57
	p	1.40×10^{-6}	1.98×10^{-5}	1.47×10^{-2}	1.53×10^{-2}
% Wetland	slope	0.248	1.27×10^{-2}	-1.29×10^{-2}	-1.95
	intercept	6.75	2.24	6.31	245.36
	p	$< 2.2 \times 10^{-16}$	2.62×10^{-10}	3.39×10^{-7}	$< 2.2 \times 10^{-16}$

Table A.14. Statistics for **Figure A.7**.

Season	Slope	Intercept	R^2	p
fall	-0.122	6.23	0.0489	9.24×10^{-2}
winter	-5.29×10^{-3}	6.15	0.02013	2.88×10^{-1}
spring	-1.88×10^{-2}	7.20	0.1217	6.78×10^{-3}
summer	-7.75×10^{-3}	5.90	0.04452	1.09×10^{-1}

A.2 Coefficient of Variation Calculations

The following terms were used to calculate $CV_{spatial}$ and $CV_{seasonal.}$ The tributary means refers to the mean of the spring, summer, fall, and winter value in a single tributary (n = 4). The standard deviation of the tributary means is then the standard deviation of those means (n = 56, 59, 55, and 53 for [DOC], $E_2:E_3$, $SUVA_{254}$, and alkalinity, respectively). The seasonal mean refers to the mean of the value in each tributary for a given season (n = 56, 59, 55, and 53 for [DOC],

E_2:E_3, $SUVA_{254}$, and alkalinity respectively). The standard deviation of the seasonal means is then the standard deviation of each of those means (n = 4). The mean of the entire data set is the global mean overall (i.e., the mean of all tributaries in all four seasons). This calculation was performed for each parameter.

A.3 References

(1) Aitkenhead-Peterson, J. A.; Steele, M. K.; Nahar, N.; Santhy, K. Dissolved organic carbon and nitrogen in urban and rural watersheds of south-central Texas: Land use and land management influences. *Biogeochemistry* **2009**, *96* (1), 119–129.

(2) Alvarez-Cobelas, M.; Angeler, D. G.; Sánchez-Carrillo, S.; Almendros, G. A worldwide view of organic carbon export from catchments. *Biogeochemistry* **2012**, *107* (1–3), 275–293.

(3) Cawley, K. M.; Campbell, J.; Zwilling, M.; Jaffé, R. Evaluation of forest disturbance legacy effects on dissolved organic matter characteristics in streams at the Hubbard Brook Experimental Forest, New Hampshire. *Aquat. Sci.* **2014**, *76* (4), 611–622.

(4) Chen, H.; Liao, Z. L.; Gu, X. Y.; Xie, J. Q.; Li, H. Z.; Zhang, J. Anthropogenic influences of paved runoff and sanitary sewage on the dissolved organic matter quality of wet weather overflows: An excitation-emission matrix parallel factor analysis assessment. *Environ. Sci. Technol.* **2017**, *51* (3), 1157–1167.

(5) Clark, M. J.; Cresser, M. S.; Smart, R.; Chapman, P. J.; Edwards, A. C. The influence of catchment characteristics on the seasonality of carbon and nitrogen species concentraitons in upland rivers of northern Scotland. *Biogeochemistry.* **2004**, *68*, 1-19.

(6) Dalmagro, H. J.; Johnson, M. S.; de Musis, C. R.; Lathuillière, M. J.; Graesser, J.; Pinto-Júnior, O. B.; Couto, E. G. Spatial patterns of DOC concentration and DOM optical properties in a Brazilian tropical river-wetland system. *J. Geophys. Res. Biogeosciences* **2017**, *122* (8), 1883–1902.

(7) Dawson, J. J. C.; Tetzlaff, D.; Speed, M.; Hrachowitz, M.; Soulsby, C. Seasonal controls on DOC dynamics in nested upland catchments in NE Scotland. *Hydrol. Process.* **2011**, *25* (10), 1647–1658.

(8) Dillon, P. J.; Molot, L. A. Effect of landscape form on export of dissolved organic carbon, iron, and phosphorus from forested stream catchments. *Water Resour. Res.* **1997**, *33* (11), 2591–2600.

(9) Eckhardt, B. W.; Moore, T. R. Controls on dissolved organic carbon concentrations in streams, Southern Quebec. *Can. J. Fish. Aquat. Sci.* **1990**, *47* (8), 1537–1544.

(10) Flint, S. A.; McDowell, W. H. Effects of headwater wetlands on dissolved nitrogen and dissolved organic carbon concentrations in a suburban New Hampshire watershed. *Freshw. Sci.* **2015**, *34* (2), 456–471.

(11) Frost, P. C.; Larson, J. H.; Johnston, C. A.; Young, K. C.; Maurice, P. A.; Lamberti, G. A.; Bridgham, S. D. Landscape predictors of stream dissolved organic matter concentration and physicochemistry in a Lake Superior river watershed. *Aquat. Sci.* **2006**, *68* (1), 40–51.

(12) Graeber, D.; Gelbrecht, J.; Pusch, M. T.; Anlanger, C.; von Schiller, D. Agriculture has

changed the amount and composition of dissolved organic matter in central European headwater streams. *Sci. Total Environ.* **2012**, *438*, 435–446.

(13) Hanley, K. W.; Wollheim, W. M.; Salisbury, J.; Huntington, T.; Aiken, G. Controls on dissolved organic carbon quantity and chemical character in temperate rivers of North America. *Global Biogeochem. Cycles* **2013**, *27* (2), 492–504.

(14) Heinz, M.; Graeber, D.; Zak, D.; Zwirnmann, E.; Gelbrecht, J.; Pusch, M. T. Comparison of organic matter composition in agricultural versus forest affected headwaters with special emphasis on organic nitrogen. *Environ. Sci. Technol.* **2015**, *49* (4), 2081–2090.

(15) Hosen, J. D.; McDonough, O. T.; Febria, C. M.; Palmer, M. A. Dissolved organic matter quality and bioavailability changes across an urbanization gradient in headwater streams. *Environ. Sci. Technol.* **2014**, *48* (14), 7817–7824.

(16) Kortelainen, P.; Saukkonen, S. Organic vs. minerogenic acidity in headwater streams in Finland. *Water, Air, Soil Pollut.* **1995**, *85* (2), 559–564.

(17) Liu, W.; Xu, X.; McGoff, N. M.; Eaton, J. M.; Leahy, P.; Foley, N.; Kiely, G. Spatial and seasonal variation of dissolved organic carbon (DOC) concentrations in Irish streams: Importance of soil and topography characteristics. *Environ. Manage.* **2014**, *53* (5), 959–967.

(18) Lu, Y. H.; Bauer, J. E.; Canuel, E. A.; Chambers, R. M.; Yamashita, Y.; Jaffé, R.; Barrett, A. Effects of land use on sources and ages of inorganic and organic carbon in temperate headwater streams. *Biogeochemistry* **2014**, *119* (1–3), 275–292.

(19) Macdonald, M. J.; Minor, E. C. Photochemical degradation of dissolved organic matter from streams in the western Lake Superior watershed. *Aquat. Sci.* **2013**, *75* (4), 509–522.

(20) Mattsson, T.; Kortelainen, P.; Räike, A. Export of DOM from boreal catchments: Impacts of land use cover and climate. *Biogeochemistry* **2005**, *76* (2), 373–394.

(21) Mattsson, T.; Kortelainen, P.; Räike, A.; Lepistö, A.; Thomas, D. N. Spatial and temporal variability of organic C and N concentrations and export from 30 boreal rivers induced by land use and climate. *Sci. Total Environ.* **2015**, *508*, 145–154.

(22) McElmurry, S. P.; Long, D. T.; Voice, T. C. Stormwater dissolved organic matter: Influence of land cover and environmental factors. *Environ. Sci. Technol.* **2014**, *48* (1), 45–53.

(23) Mosher, J. J.; Klein, G. C.; Marshall, A. G.; Findlay, R. H. Influence of bedrock geology on dissolved organic matter quality in stream water. *Org. Geochem.* **2010**, *41* (11), 1177–1188.

(24) Palviainen, M.; Lauren, A.; Launiainen, S.; Piirainen, S. Predicting the export and concntrations of organic carbon, nitrogen and phosphorus in boreal lakes by catchment characterististics and land use: A practical approach. *AMBIO A J. Hum. Environ.* **2016**, *45* (8), 933-945.

(25) Schelker, J.; Eklöf, K.; Bishop, K.; Laudon, H. Effects of forestry operations on dissolved organic carbon concentrations and export in boreal first-order streams. *J. Geophys. Res. Biogeosciences* **2012**, *117* (1), 1-12.

(26) Shang, P.; Lu, Y. H.; Du, Y. X.; Jaffé, R.; Findlay, R. H.; Wynn, A. Climatic and watershed controls of dissolved organic matter variation in streams across a gradient of agricultural land use. *Sci. Total Environ.* **2018**, *612*, 1442–1453.

(27) Singh, S.; Dash, P.; Silwal, S.; Feng, G.; Adeli, A.; Moorhead, R. J. Influence of land use and land cover on the spatial variability of dissolved organic matter in multiple aquatic environments. *Environ. Sci. Pollut. Res.* **2017**, *24* (16), 14124–14141.

(28) Williams, C. J.; Yamashita, Y.; Wilson, H. F.; Jaffe, R.; Xenopoulos, M. A. Unraveling the

role of land use and microbial activity in shaping dissolved organic matter characteristics in stream ecosystems. *Limnol. Oceanogr.* **2010**, *55* (3), 1159–1171.

(29) Xenopoulos, M. A.; Lodge, D. M.; Frentress, J.; Kreps, T. A.; Bridgham, S. D.; Grossman, E.; Jackson, C. J. Regional comparisons of watershed determinants of dissolved organic carbon in temperate lakes from the Upper Great Lakes region and selected regions globally. *Limnol. Ocean.* **2003**, *48* (6), 2321–2334.

Appendix B

Supporting Information for Chapter 3

B.1 Lake Overview

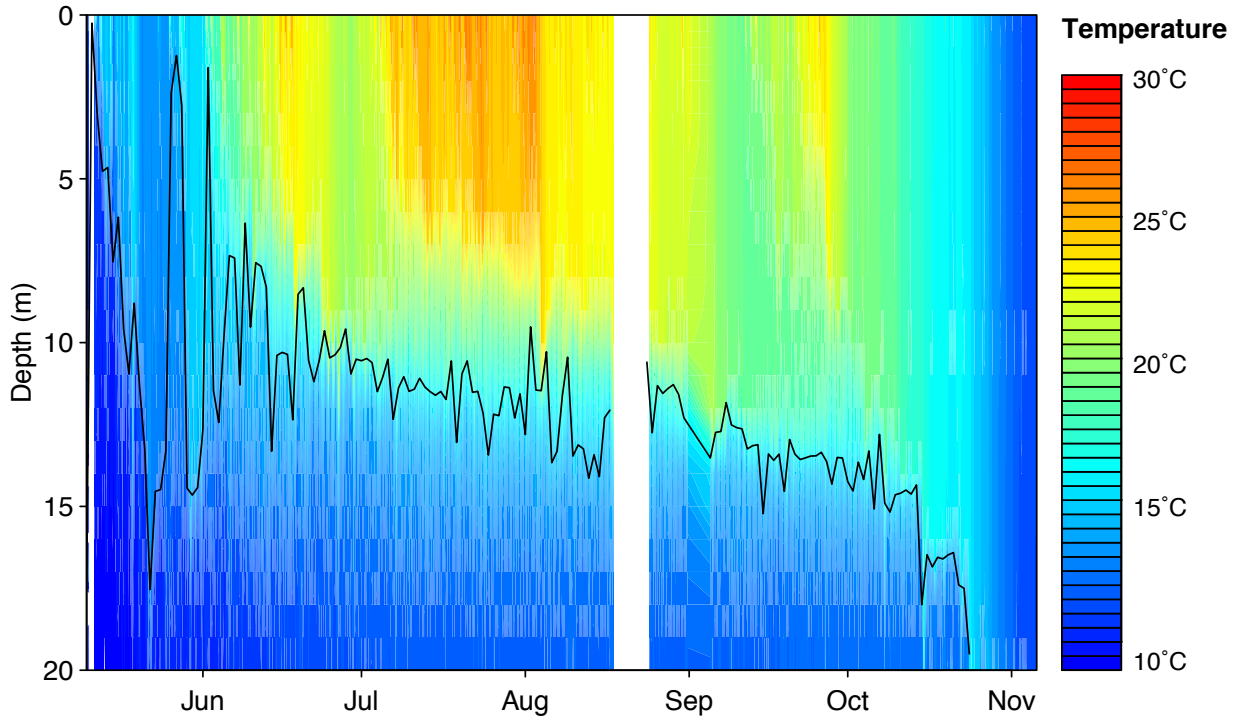

Figure B.1. Temperature profile heatmap collected by the NTL-LTER research buoy.[1] Missing data in August is due to the maintenance being done on the buoy. Black trace is thermocline calculated using the ts.thermo.depth function of RLakeAnalyzer program.

Table B.1. Inventory of samples collected form Lake Mendota in 2017. Surface samples (n = 28) were taken as a composite of the top 12 m of the lake. Depth-discrete samples were collected 1-2 times per month at the exact depth listed as measured by a YSI Exo2 multiparameter sonde.

Date	Type	Depth (m)	[DOC] and Optical Analysis	Molecular Analysis
June 2nd	Surface	NA	y	n
June 7th	Surface	NA	y	n
June 9th	Surface	NA	y	n
June 13th	Surface	NA	y	n
June 16th	Surface	NA	y	n
June 17th	Surface	NA	y	n
June 18th	Surface	NA	y	n
June 20th	Surface	NA	y	n
June 27th	Surface	NA	y	n
June 29th	Depth-Discrete	12.2	y	y
June 29th	Depth-Discrete	17.2	y	n
June 29th	Depth-Discrete	18	y	n
June 29th	Depth-Discrete	18.8	y	n
June 29th	Depth-Discrete	19.8	y	y
July 14th	Surface	NA	y	n
July 17th	Surface	NA	y	n
July 18th	Surface	NA	y	n
July 24th	Surface	NA	y	n
July 27th	Surface	NA	y	n
August 1st	Surface	NA	y	n
August 8th	Surface	NA	y	n
August 11th	Surface	NA	y	n
August 11th	Depth-Discrete	0.1	y	y
August 11th	Depth-Discrete	9.5	y	n
August 11th	Depth-Discrete	11.5	y	y
August 11th	Depth-Discrete	13.15	y	y
August 11th	Depth-Discrete	15.3	y	n
August 11th	Depth-Discrete	18.08	y	n
August 11th	Depth-Discrete	21.25	y	y
August 18th	Surface	NA	y	n
August 24th	Surface	NA	y	n
August 30th	Surface	NA	y	n

September 8th	Surface	NA	y	n
September 8th	Depth-Discrete	0.1	y	y
September 8th	Depth-Discrete	11.5	y	n
September 8th	Depth-Discrete	12.5	y	n
September 8th	Depth-Discrete	13.4	y	n
September 8th	Depth-Discrete	14.5	y	n
September 8th	Depth-Discrete	16.1	y	n
September 8th	Depth-Discrete	18	y	n
September 8th	Depth-Discrete	22.2	y	y
September 9th	Surface	NA	y	n
September 15th	Surface	NA	y	n
September 21st	Surface	NA	y	n
September 21st	Depth-Discrete	3	y	y
September 21st	Depth-Discrete	9.5	y	n
September 21st	Depth-Discrete	11.5	y	n
September 21st	Depth-Discrete	12.5	y	n
September 21st	Depth-Discrete	14	y	n
September 21st	Depth-Discrete	15	y	n
September 21st	Depth-Discrete	20.4	y	y
October 4th	Surface	NA	y	n
October 4th	Depth-Discrete	0.5	y	y
October 4th	Depth-Discrete	10.8	y	n
October 4th	Depth-Discrete	12.9	y	n
October 4th	Depth-Discrete	13	y	n
October 4th	Depth-Discrete	13.5	y	n
October 4th	Depth-Discrete	14.5	y	n
October 4th	Depth-Discrete	17.3	y	y
October 4th	Depth-Discrete	19.8	y	n
October 12th	Depth-Discrete	14.04	y	n
October 12th	Depth-Discrete	15.3	y	n
October 12th	Depth-Discrete	20.5	y	n
October 13th	Surface	NA	y	n
October 19th	Depth-Discrete	16.3	y	n
October 19th	Depth-Discrete	17.3	y	y
October 19th	Depth-Discrete	17.8	y	n
October 19th	Depth-Discrete	18.2	y	y
October 20th	Surface	NA	y	n
November 3rd	Surface	NA	y	n
November 3rd	Depth-Discrete	2.1	y	y

November 3rd	Depth-Discrete	11.9	y	n
November 3rd	Depth-Discrete	20	y	y

Table B.2. Geochemical measurements made for each of the depth-discrete samples. NA values indicate missing data due to instrument malfunction or not enough sample volume.

Date	Depth (m)	Iron ($\mu g\ L^{-1}$)	Manganese ($\mu g\ L^{-1}$)	Sulfide ($mg\ L^{-1}$)
June 29th	0.5	12.9	< 3	< 2
June 29th	12.2	108.6	< 3	< 2
June 29th	17.2	38.5	15.6	NA
June 29th	18	64.8	7.2	< 2
June 29th	18.8	245.39	21.8	< 2
June 29th	19.8	259.7	117.4	< 2
August 11th	9.5	22.3	< 3	< 2
August 11th	10.3	14.1	NA	< 2
August 11th	11.5	72.1	76.9	< 2
August 11th	15.3	15.9	143.9	< 2
August 11th	18.08	41.6	202.2	2.3
August 11th	21.25	58.6	249.5	< 2
September 8th	0.1	95.8	< 3	< 2
September 8th	11.5	113.8	< 3	< 2
September 8th	12.5	140.9	222.6	< 2
September 8th	13.4	85.3	174.5	< 2
September 8th	18	66.0	209.1	2.7
September 8th	22.2	58.3	262.8	4.1
September 21st	3	29.7	< 3	< 2
September 21st	9.5	46.6	< 3	< 2
September 21st	11.5	49.3	< 3	< 2
September 21st	12.5	13.0	< 3	< 2
September 21st	12.7	78.0	162.9	< 2
September 21st	13	74.7	270.4	< 2
September 21st	14	24.6	235.3	< 2
September 21st	15	27.6	195.4	2.1
September 21st	20.4	39.6	240.3	4.5
October 4th	0.5	39.1	< 3	< 2
October 4th	10.8	23.3	< 3	< 2
October 4th	12.9	31.7	70.7	< 2
October 4th	13	20.5	135.4	< 2
October 4th	13.5	99.2	188.0	< 2
October 4th	14.5	78.6	235.3	< 2
October 4th	17.3	49.0	222.6	4.1
October 4th	19.8	37.2	247.3	5.4
October 12th	14.04	< 3	27.1	< 2

October 12th	15.3	11.4	256.6	2.4
October 12th	20.5	21.1	240.7	5.0
October 19th	16.3	< 3	< 3	< 2
October 19th	17.3	8.0	348.4	< 2
October 19th	17.8	18.2	342.1	3.7
October 19th	18.2	21.6	292.8	4.4
November 3rd	2.1	< 3	< 3	< 2
November 3rd	11.9	< 3	< 3	< 2
November 3rd	20	< 3	< 3	< 2

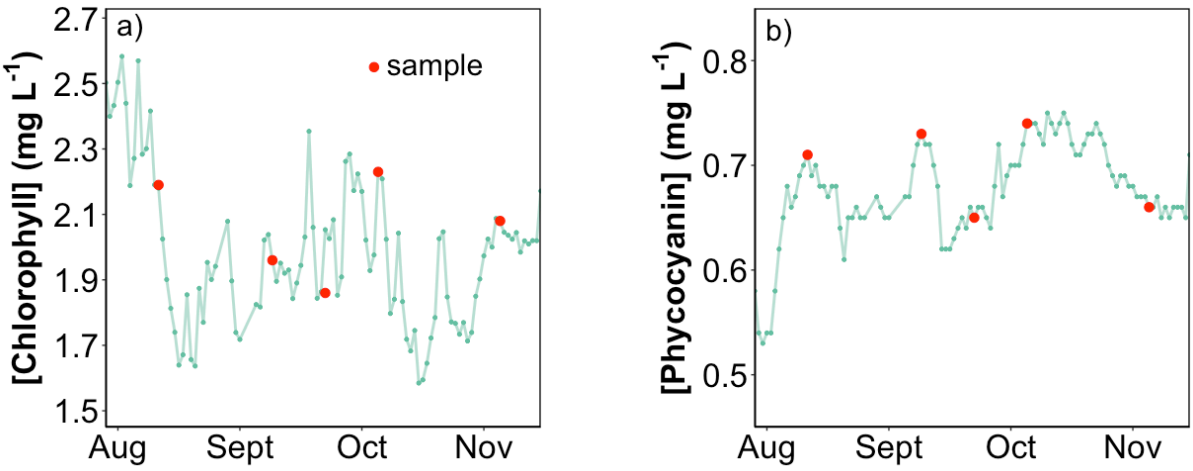

Figure B.2. Concentrations of a) chlorophyll and b) phycocyanin measured at the surface.[1]

Table B.3. Concentration of chlorophyll[1] and light intensity values for August 11th, September 8th, September 21st, October 4th, and November 3rd of 2017 used in Spearman rank calculations. Solar radiation values are modelled using SMARTS for Madison, WI at noon.

Date	[Chlorophyll] (mg L^{-1})	Intensity (mEi sec^{-1} cm^{-2})
August 11th	2.19	8.63×10^{-5}
September 8th	1.96	7.53×10^{-5}
September 21st	1.86	6.88×10^{-5}
October 4th	2.23	6.16×10^{-5}
November 3rd	2.08	4.47×10^{-5}

B.2 MS Formula Matching Results

Boxes on all van Krevelen diagrams refer to 1) protein-, 2) lignin- and 3) tannin-like formulas.[2]

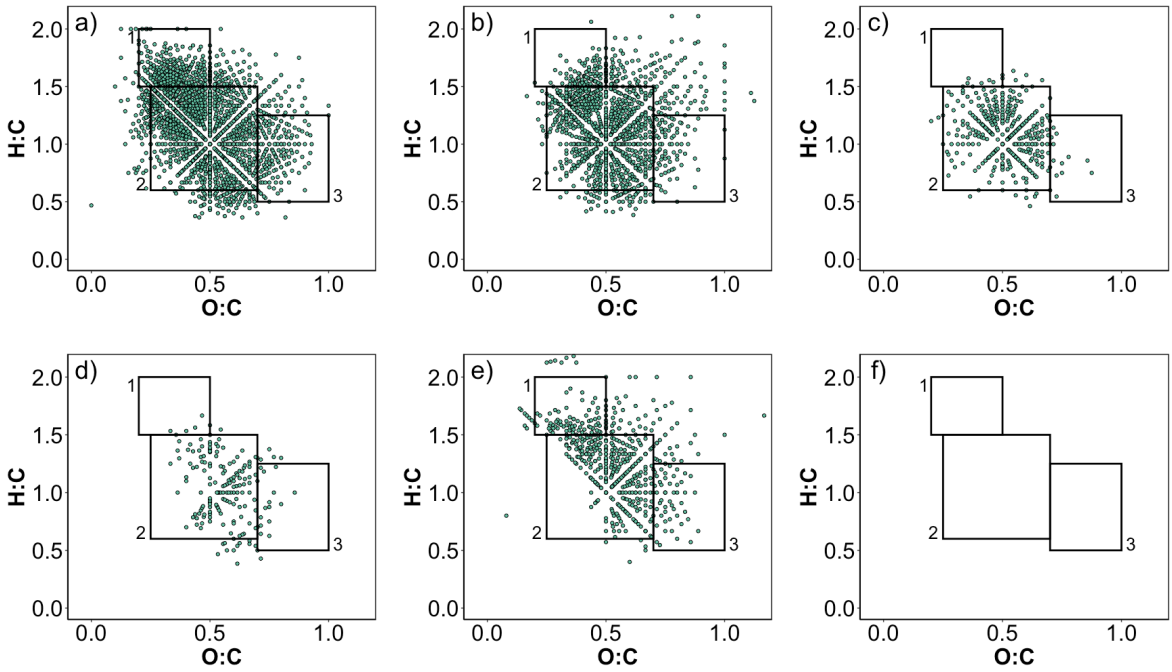

Figure B.3. van Krevelen diagrams for a) CHO, b) $CHON_1$, c) $CHON_2$, d) $CHON_1S_1$, e) $CHOS_1$, and f) $CHOP_1$ for the sample collected on June 29th at a depth of 12.2 m.

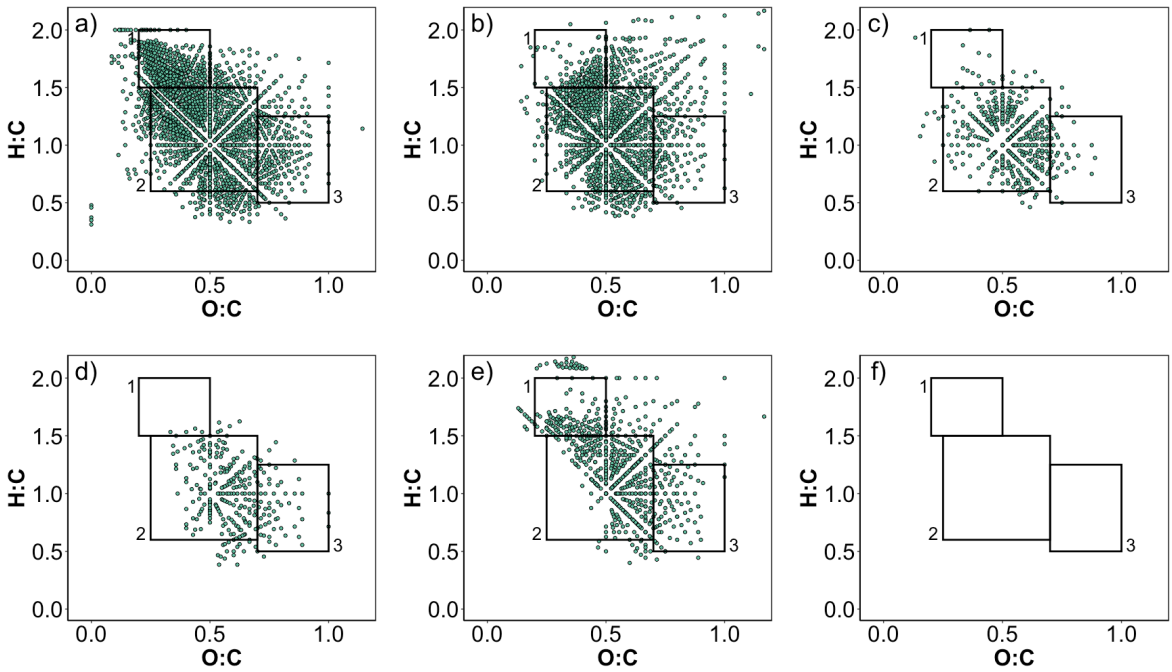

Figure B.4. van Krevelen diagrams for a) CHO, b) $CHON_1$, c) $CHON_2$, d) $CHON_1S_1$, e) $CHOS_1$, and f) $CHOP_1$ for the sample collected on June 29th at a depth of 19.8 m.

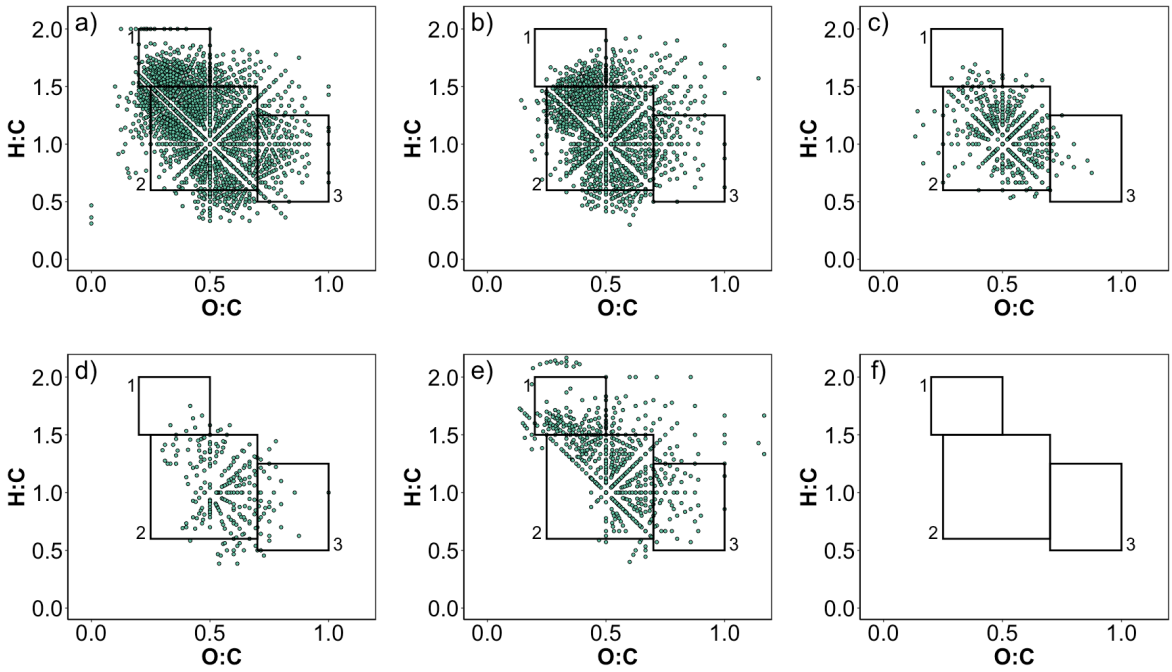

Figure B.5. van Krevelen diagrams for a) CHO, b) $CHON_1$, c) $CHON_2$, d) $CHON_1S_1$, e) $CHOS_1$, and f) $CHOP_1$ for the sample collected on August 11th at a depth of 0.1 m.

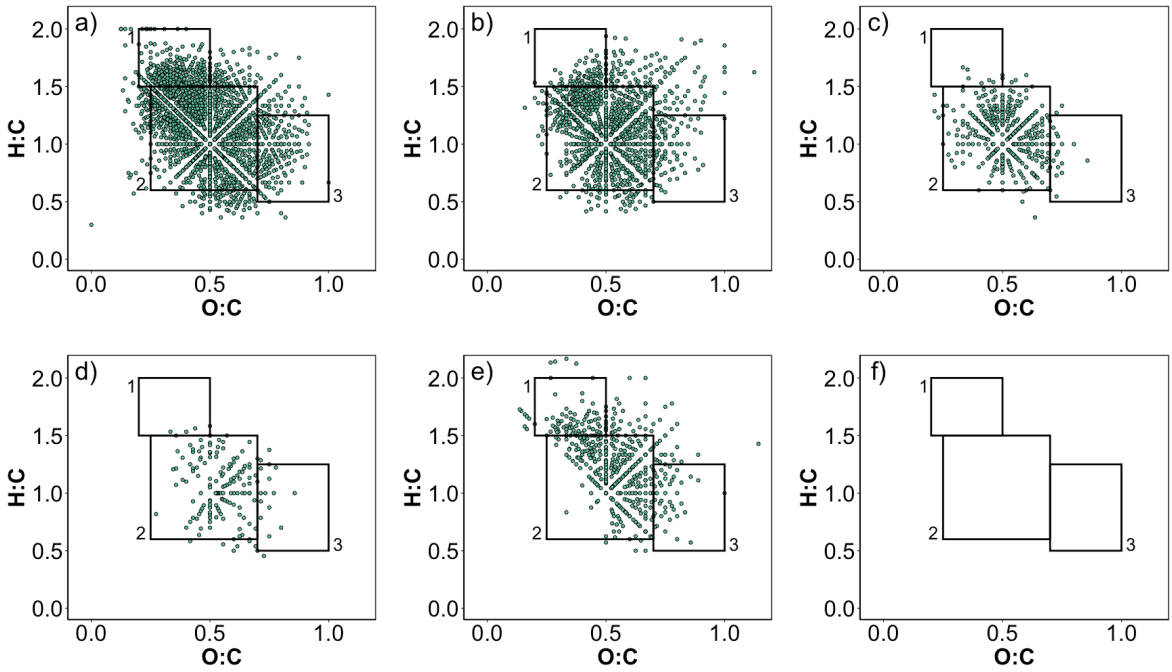

Figure B.6. van Krevelen diagrams for a) CHO, b) $CHON_1$, c) $CHON_2$, d) $CHON_1S_1$, e) $CHOS_1$, and f) $CHOP_1$ for the sample collected on August 11th at a depth of 11.5 m.

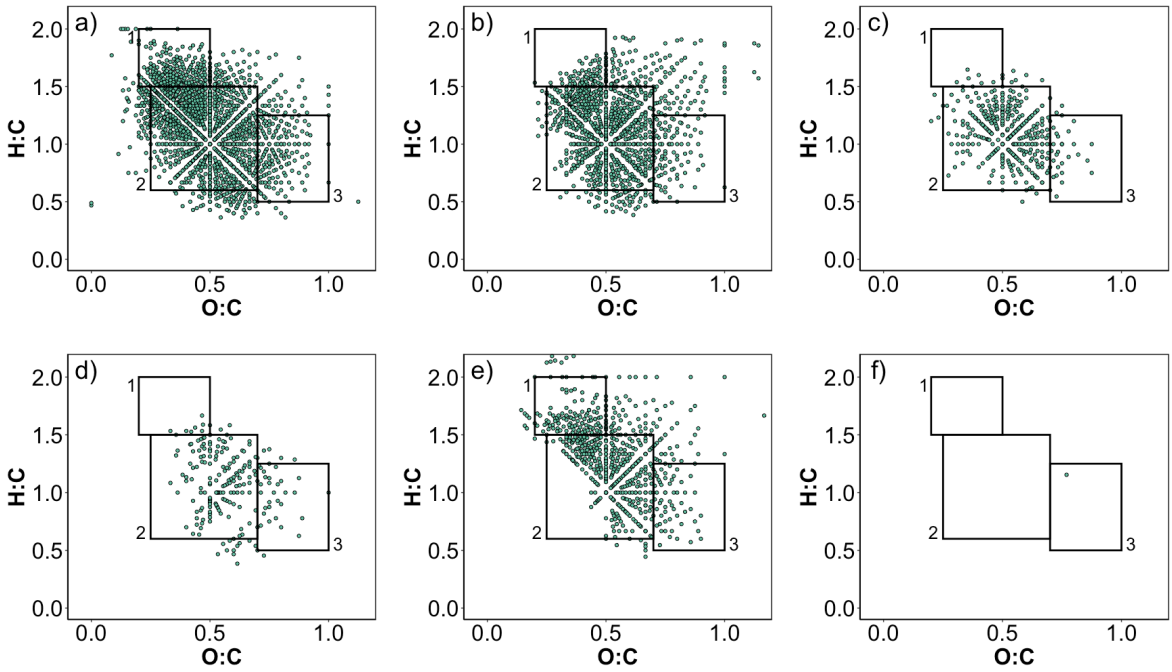

Figure B.7. van Krevelen diagrams for a) CHO, b) $CHON_1$, c) $CHON_2$, d) $CHON_1S_1$, e) $CHOS_1$, and f) $CHOP_1$ for the sample collected on August 11th at a depth of 21.25 m.

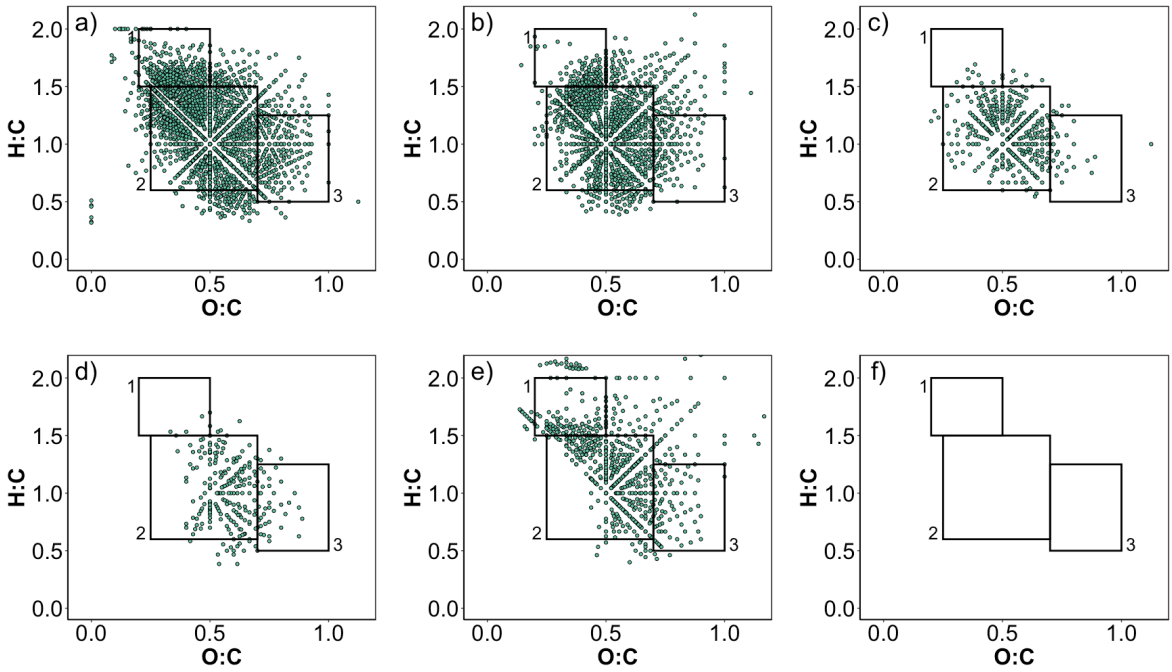

Figure B.8. van Krevelen diagrams for a) CHO, b) $CHON_1$, c) $CHON_2$, d) $CHON_1S_1$, e) $CHOS_1$, and f) $CHOP_1$ for the sample collected on September 8th at a depth of 0.1 m.

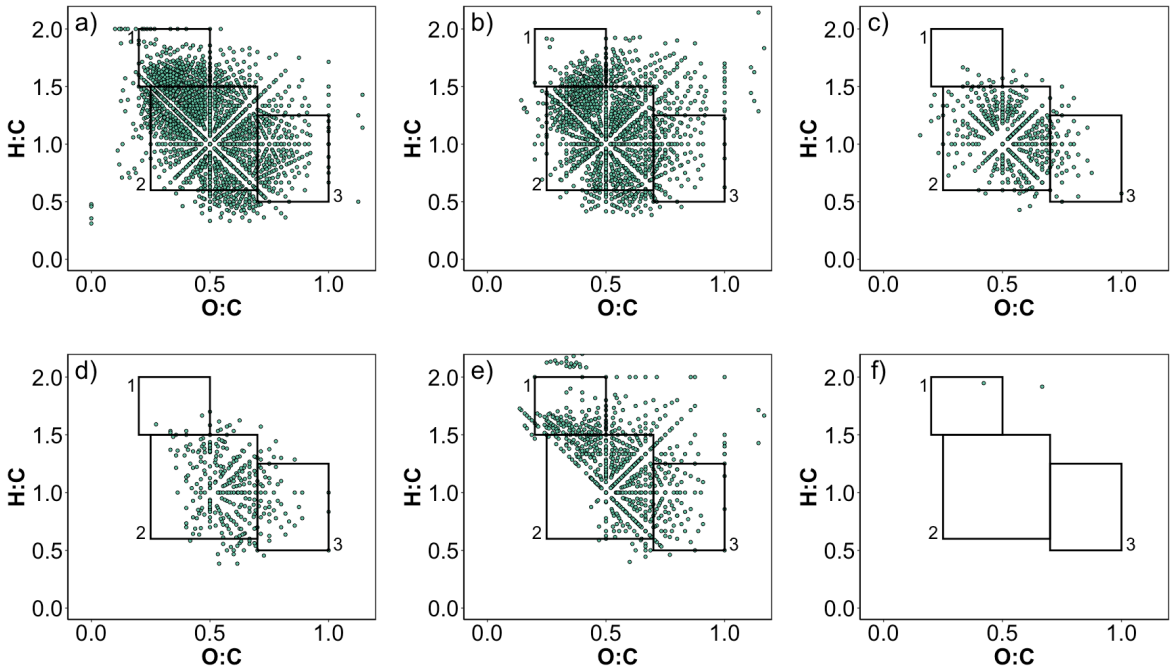

Figure B.9. van Krevelen diagrams for a) CHO, b) $CHON_1$, c) $CHON_2$, d) $CHON_1S_1$, e) $CHOS_1$, and f) $CHOP_1$ for the sample collected on September 8th at a depth of 22.2 m.

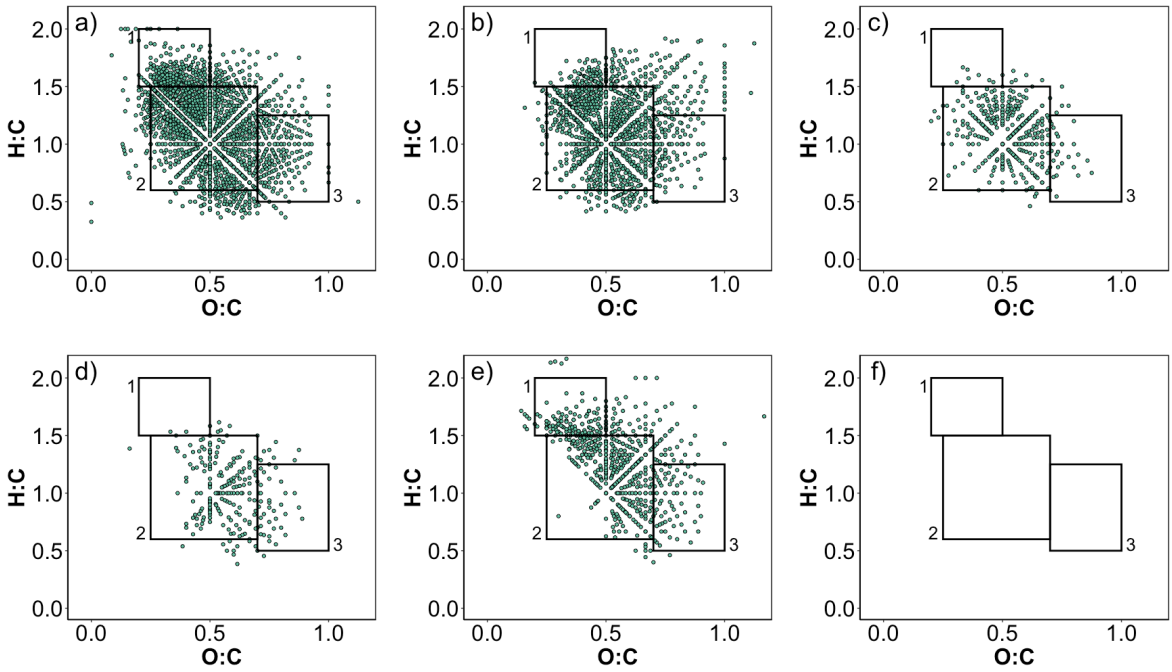

Figure B.10. van Krevelen diagrams for a) CHO, b) $CHON_1$, c) $CHON_2$, d) $CHON_1S_1$, e) $CHOS_1$, and f) $CHOP_1$ for the sample collected on September 21st at a depth of 3 m.

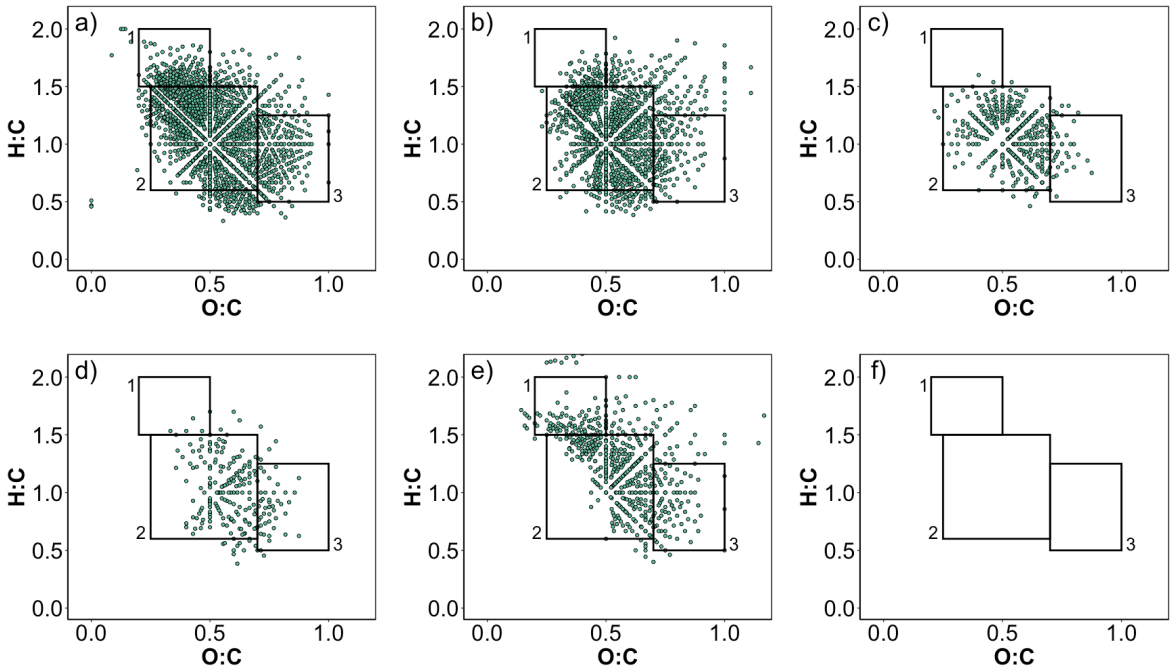

Figure B.11. van Krevelen diagrams for a) CHO, b) $CHON_1$, c) $CHON_2$, d) $CHON_1S_1$, e) $CHOS_1$, and f) $CHOP_1$ for the sample collected on September 21st at a depth of 20.4 m.

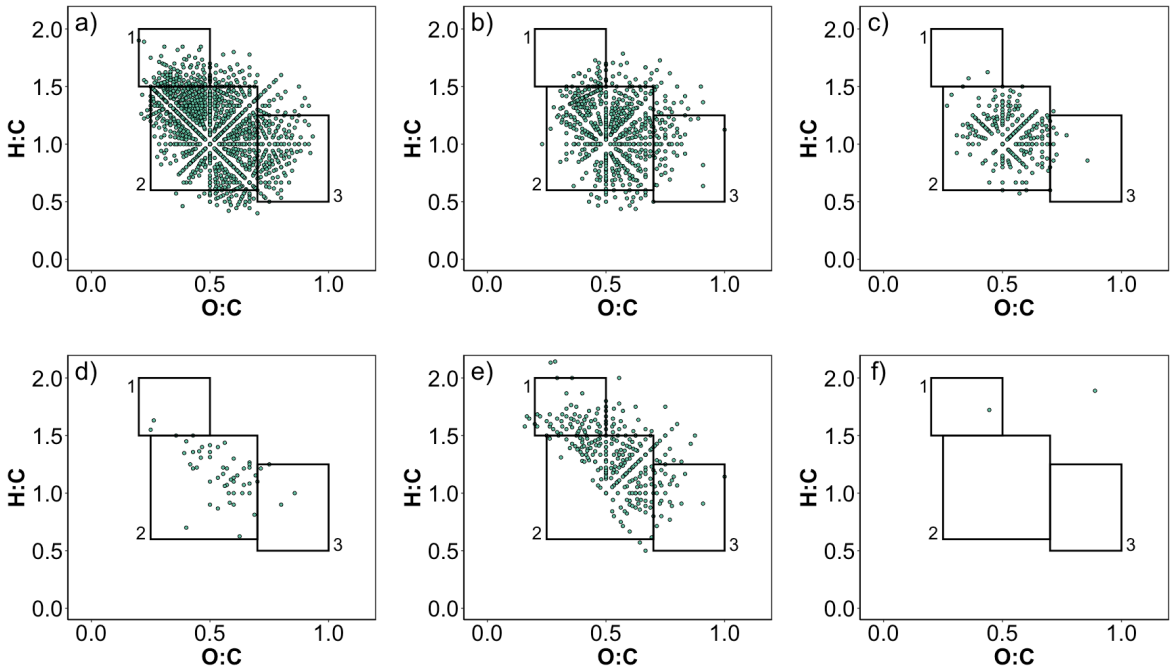

Figure B.12. van Krevelen diagrams for a) CHO, b) $CHON_1$, c) $CHON_2$, d) $CHON_1S_1$, e) $CHOS_1$, and f) $CHOP_1$ for the sample collected on October 4th at a depth of 0.5 m.

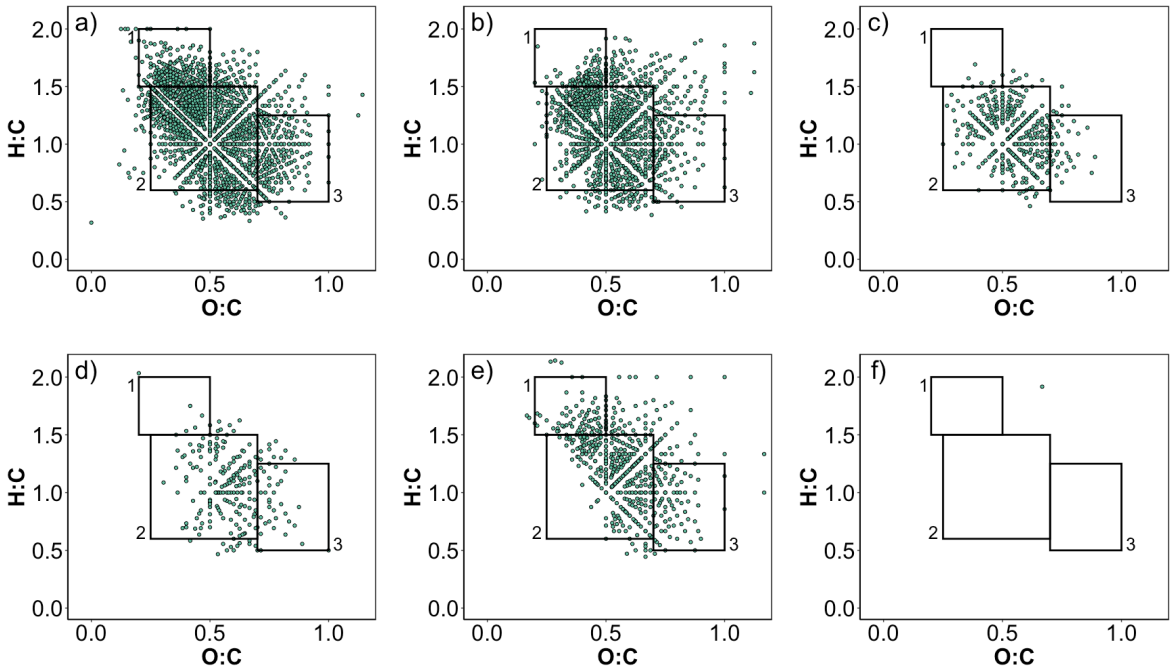

Figure B.13. van Krevelen diagrams for a) CHO, b) $CHON_1$, c) $CHON_2$, d) $CHON_1S_1$, e) $CHOS_1$, and f) $CHOP_1$ for the sample collected on October 4th at a depth of 17.3 m.

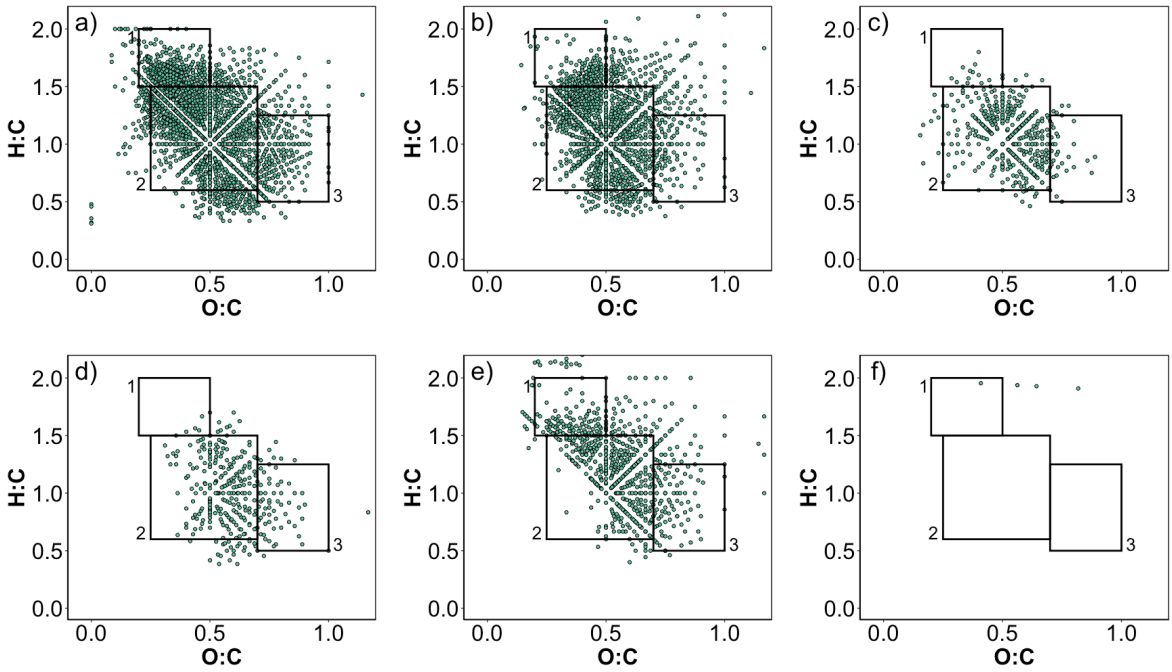

Figure B.14. van Krevelen diagrams for a) CHO, b) $CHON_1$, c) $CHON_2$, d) $CHON_1S_1$, e) $CHOS_1$, and f) $CHOP_1$ for the sample collected on October 19th at a depth of 17.3 m.

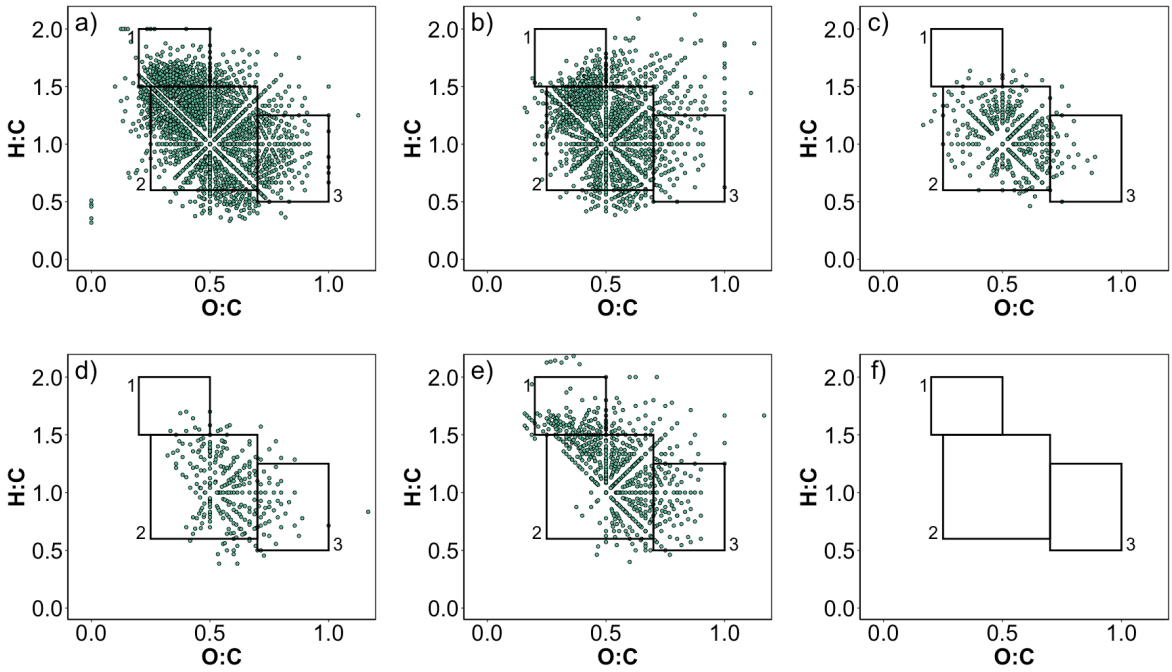

Figure B.15. van Krevelen diagrams for a) CHO, b) $CHON_1$, c) $CHON_2$, d) $CHON_1S_1$, e) $CHOS_1$, and f) $CHOP_1$ for the sample collected on October 19th at a depth of 18.2 m.

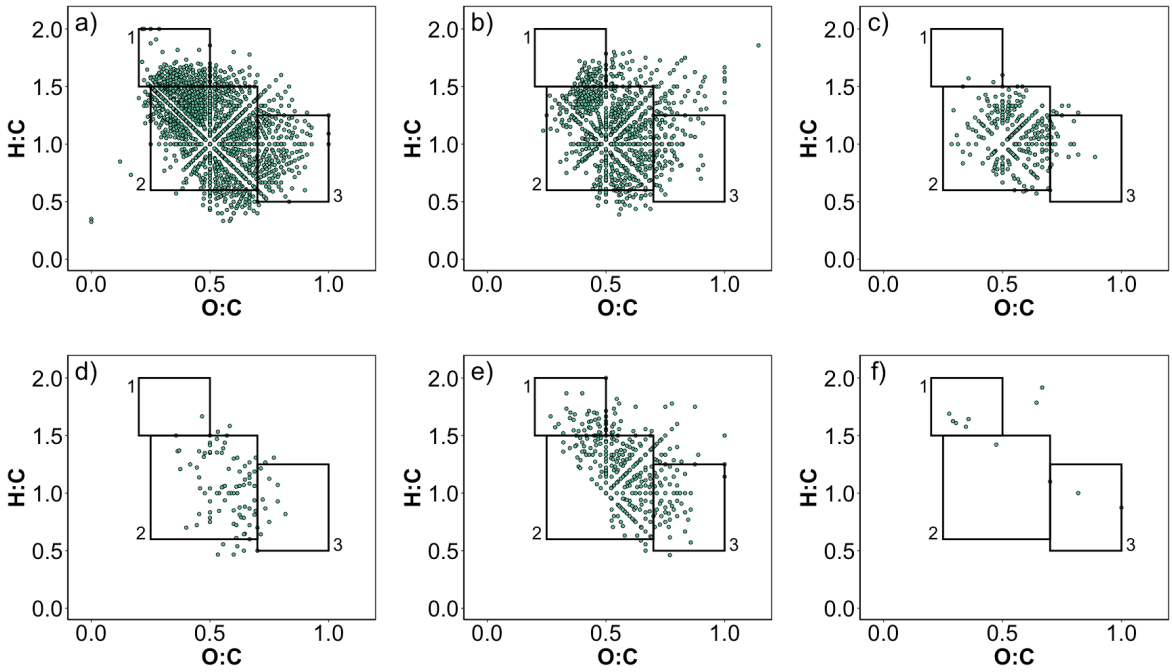

Figure B.16. van Krevelen diagrams for a) CHO, b) $CHON_1$, c) $CHON_2$, d) $CHON_1S_1$, e) $CHOS_1$, and f) $CHOP_1$ for the sample collected on November 3rd at a depth of 2.1 m.

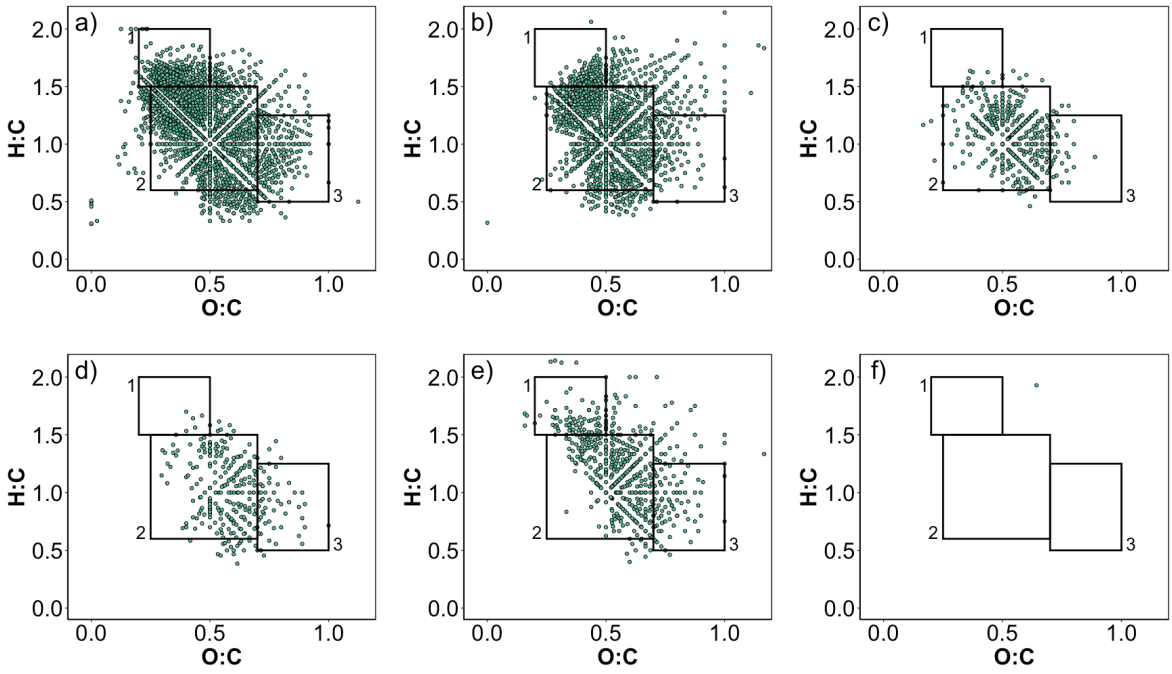

Figure B.17. van Krevelen diagrams for a) CHO, b) $CHON_1$, c) $CHON_2$, d) $CHON_1S_1$, e) $CHOS_1$, and f) $CHOP_1$ for the sample collected on November 3rd at a depth of 20 m.

Table B.4. Weighted-average properties for samples analyzed by FT-ICR MS.

Date	Depth (m)	$H:C_w$	$O:C_w$	DBE_w
June 29th	12.2	1.235	0.498	7.843
June 29th	19.8	1.249	0.501	7.691
August 11th	0.1	1.242	0.490	7.960
August 11th	11.5	1.248	0.493	7.623
August 11th	13.15	1.223	0.505	8.161
August 11th	21.25	1.239	0.505	7.580
September 9th	0.1	1.239	0.509	7.682
September 9th	22.2	1.232	0.509	7.888
September 21st	3	1.222	0.516	7.731
September 21st	20.4	1.205	0.525	7.862
October 4th	0.5	1.195	0.537	8.106
October 4th	17.3	1.183	0.543	8.170
October 19th	17.3	1.208	0.522	8.219
October 19th	18.2	1.215	0.514	8.018
November 3rd	2.1	1.174	0.549	8.697
November 3rd	20	1.184	0.533	8.708

Table B.5. Percentages of identified formulas with and without heteroatoms in samples analyzed by FT-ICR MS.

Date	Depth	% CHO	% N-containing	% S-containing
June 29th	12.2	43.71	42.28	17.92
June 29th	19.8	40.75	44.16	19.98
August 11th	0.1	41.73	43.64	19.12
August 11th	11.5	44.28	42.41	16.96
August 11th	13.15	41.74	43.74	19.55
August 11th	21.25	41.54	41.34	21.64
September 9th	0.1	41.42	43.34	20.29
September 9th	22.2	38.69	45.01	21.85
September 21st	3	42.2	42.50	20.31
September 21st	20.4	40.56	44.50	20.37
October 4th	0.5	49.85	37.07	15.16
October 4th	17.3	41.55	43.60	19.42
October 19th	17.3	39.72	44.11	21.65
October 19th	18.2	40.65	42.99	21.41
November 3rd	2.1	47.35	40.33	14.74
November 3rd	20	41.06	45.04	19.64

Table B.6. Numbers of identified formulas with and without heteroatoms in samples analyzed by FT-ICR MS.

Date	Depth	Total #	# CHO	# N-containing	# S-containing	# CHOP
June 29th	12.2	3962	1732	1675	710	0
June 29th	19.8	4726	1926	2087	944	0
August 11th	0.1	4294	1792	1874	821	0
August 11th	11.5	3697	1637	1568	627	0
August 11th	13.15	3097	1710	1792	801	0
August 11th	21.25	3965	1647	1639	858	1
September 9th	0.1	4239	1756	1837	860	0
September 9th	22.2	4590	1776	2066	1003	2
September 21st	3	3969	1675	1687	806	0
September 21st	20.4	3780	1533	1682	770	0
October 4th	0.5	2393	1193	887	363	2
October 4th	17.3	3872	1609	1688	752	1

October 19th	17.3	4577	1818	2019	991	4
October 19th	18.2	4236	1722	1821	907	0
November 3rd	2.1	2849	1349	1149	420	11
November 3rd	20	4043	1660	1821	794	1

B.3. Temporal Variation at the Surface

Table B.7. [DOC], $SUVA_{254}$, E_2:E_3, and A_{254} for each of the integrated surface samples. NA values are due to instrument malfunction or exclusion based on a Grubb's outlier test.

Date	[DOC] (mg-C L^{-1})	$SUVA_{254}$ (L mg-C^{-1} m^{-1})	E_2:E_2	A_{254} (cm^{-1})
June 2nd	6.12	1.64	8.73	0.100
June 7th	5.65	1.74	8.57	0.098
June 9th	5.69	1.74	8.42	0.099
June 13th	4.12	1.76	8.10	NA
June 16th	5.91	1.79	7.86	0.106
June 17th	5.78	1.69	8.27	0.098
June 18th	5.93	1.66	8.60	0.098
June 20th	6.08	1.64	8.34	0.100
June 27nd	6.04	1.65	8.82	0.100
July 14th	5.91	1.76	8.28	0.104
July 17th	6.21	1.61	8.53	0.100
July 18th	6.45	1.61	7.99	0.104
July 24th	5.95	1.74	7.97	0.104
July 27th	5.56	1.73	8.59	0.096
August 1st	NA	NA	8.63	NA
August 8th	5.80	1.63	8.71	0.095
August 11th	6.00	1.58	9.01	0.095
August 18th	6.10	1.54	9.21	0.094
August 24th	5.10	1.79	9.34	0.091
August 30th	7.07	1.33	9.71	0.094
September 8th	5.04	1.81	9.73	0.091
September 9th	6.26	1.48	9.52	0.093
September 15th	4.82	1.91	9.47	0.092
September 21st	5.98	1.99	9.64	0.119
October 4th	5.04	2.14	NA	0.108
October 13th	5.47	1.69	9.63	0.092
October 20th	5.47	1.69	9.63	0.092
November 3rd	5.10	1.77	10.18	0.090

Table B.8. Trends in [DOC] based on historical data collected in Lake Mendota.[3] Depth discrete samples from < 12 m were averaged for single days. Correlations are based on results of Mann-Kendall correlation test. p-values are calculated with a 95% confidence interval.

Year	Correlation	p-value	n
1996	-0.067	1.00	6
1997	-0.600	0.23	5
1998	-0.333	0.75	4
1999	0.316	0.45	5
2000	-0.600	0.14	6
2001	0.200	0.82	5
2002	0.200	0.82	5
2003	-0.200	0.72	6
2004	-0.667	0.33	4
2005	NA	NA	2
2006	-0.600	0.23	5
2007	-0.316	0.45	5
2008	-0.333	0.75	4
2009	0.400	0.48	5
2010	0.333	1.00	3
2011	NA	NA	1
2012	0.69	0.056	6
2013	-0.200	0.82	5
2014	-0.667	0.33	4
2015	-0.600	0.23	5
2016	-0.400	0.48	5
2017	-0.600	0.14	6

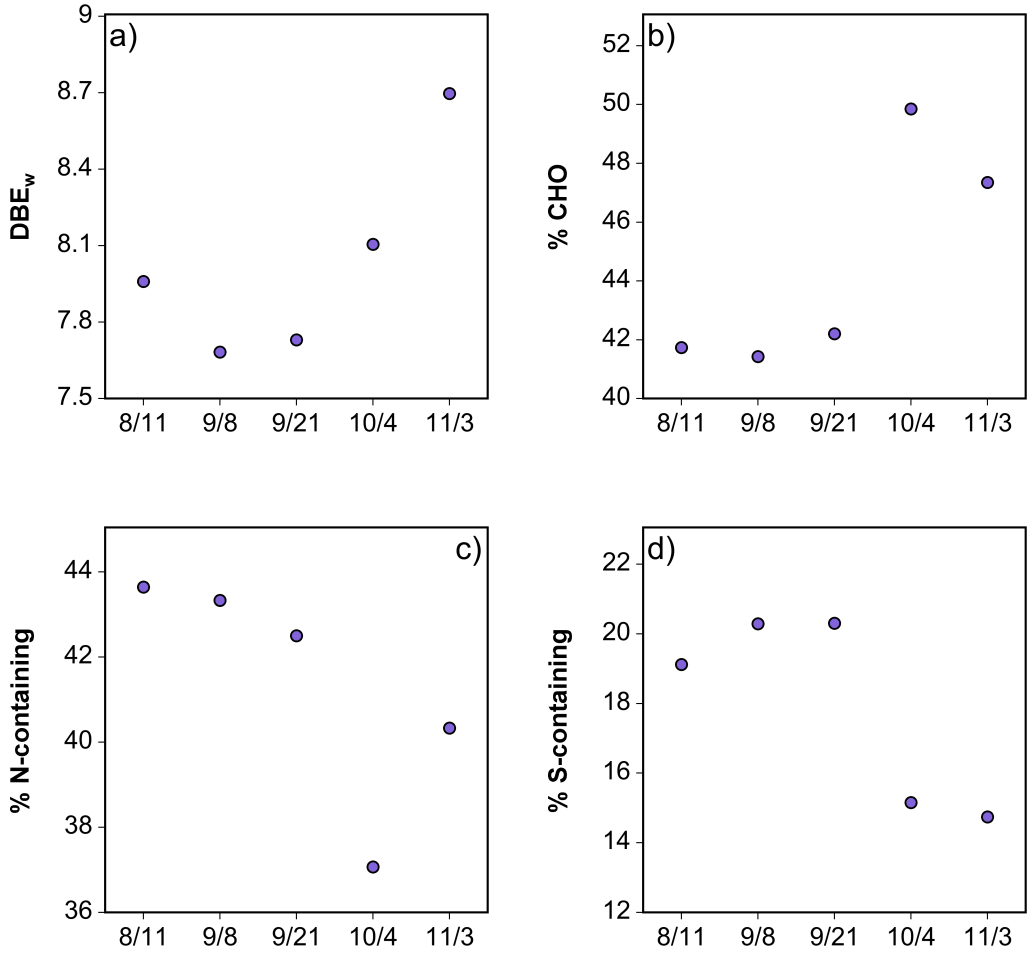

Figure B.18. a) DBE$_w$, b) % CHO, c) % N-containing, and d) % S-containing formulas identified in the surface samples analyzed by FT-ICR MS.

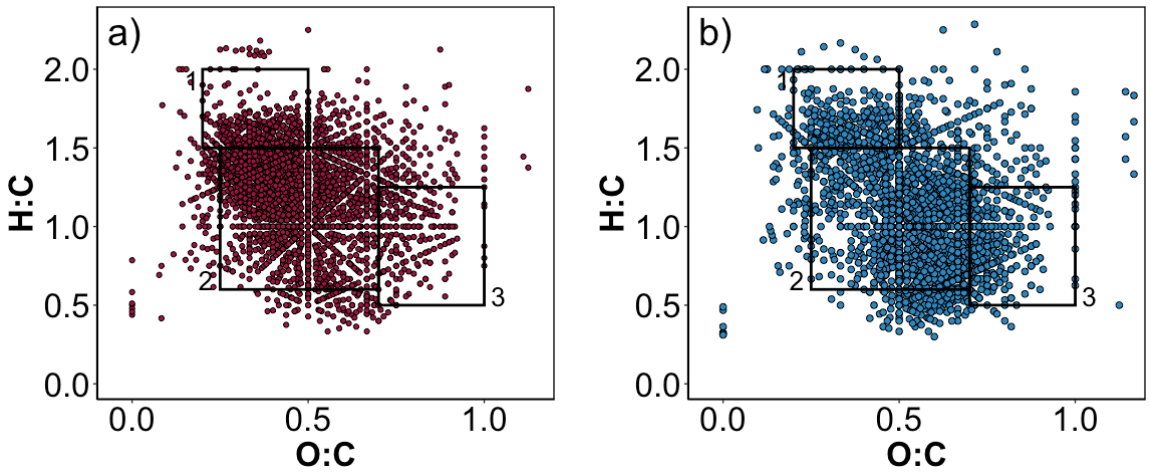

Figure B.19. Identified formulas that are a) positively or b) negatively correlated with [DO] in depth-discrete samples analyzed by FT-ICR MS. Only those formulas detected in at least 15 of the 20 samples are considered in this analysis.

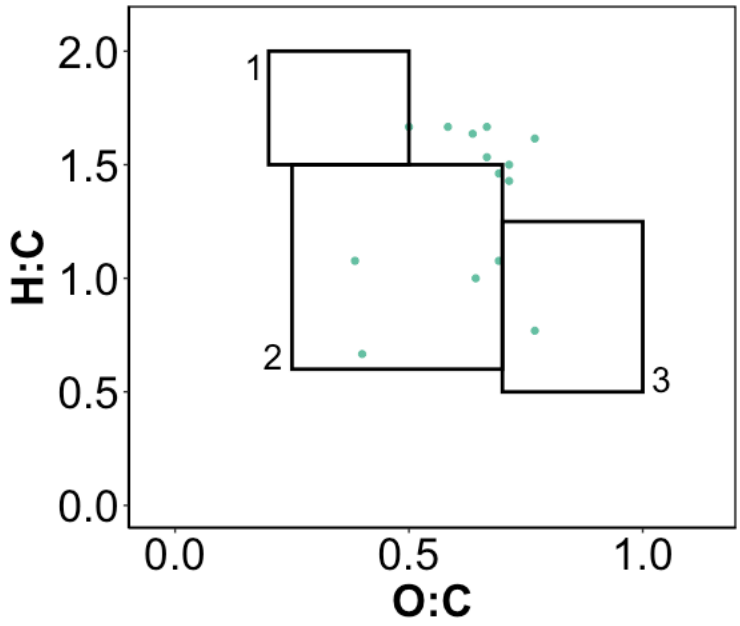

Figure B.20. Identified formulas classified as microbially derived products based on correlations to chlorophyll concentrations and light intensity.[4] Only formulas identified in all five surface samples are considered.

B.4. Variation with Depth

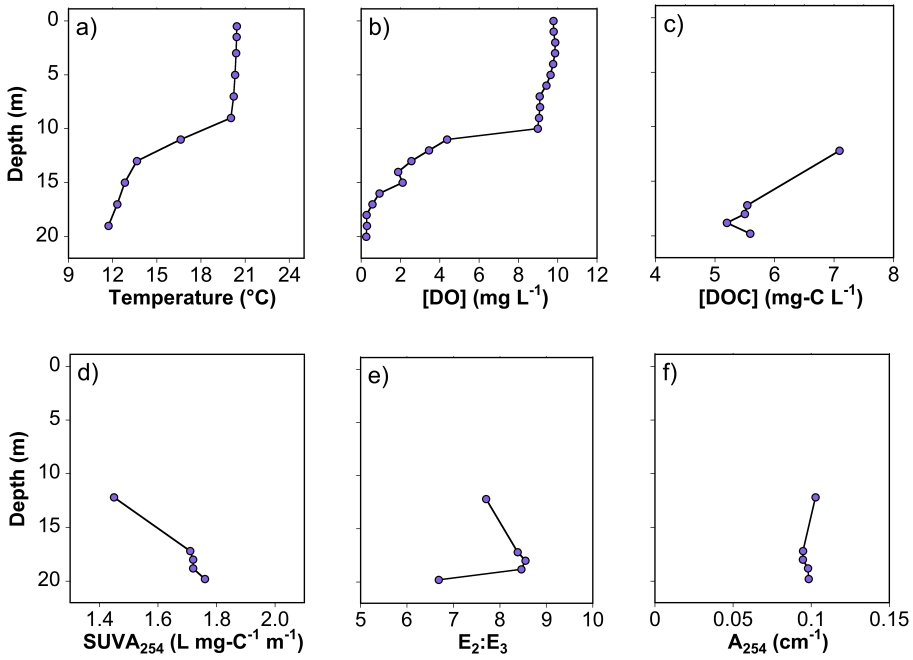

Figure B.21. a) Temperature, b) [DO], c) [DOC], d) $SUVA_{254}$, e) E_2:E_3, and f) A_{254} measured on June 29th at depth-discrete intervals.

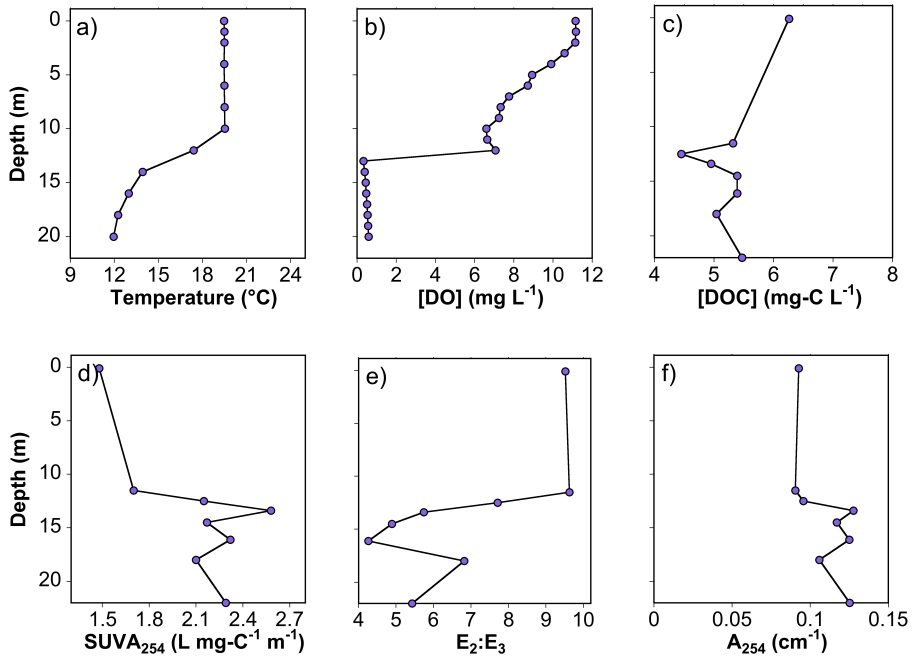

Figure B.22. a) Temperature, b) [DO], c) [DOC], d) $SUVA_{254}$, e) E_2:E_3, and f) A_{254} measured on September 8th at depth-discrete intervals.

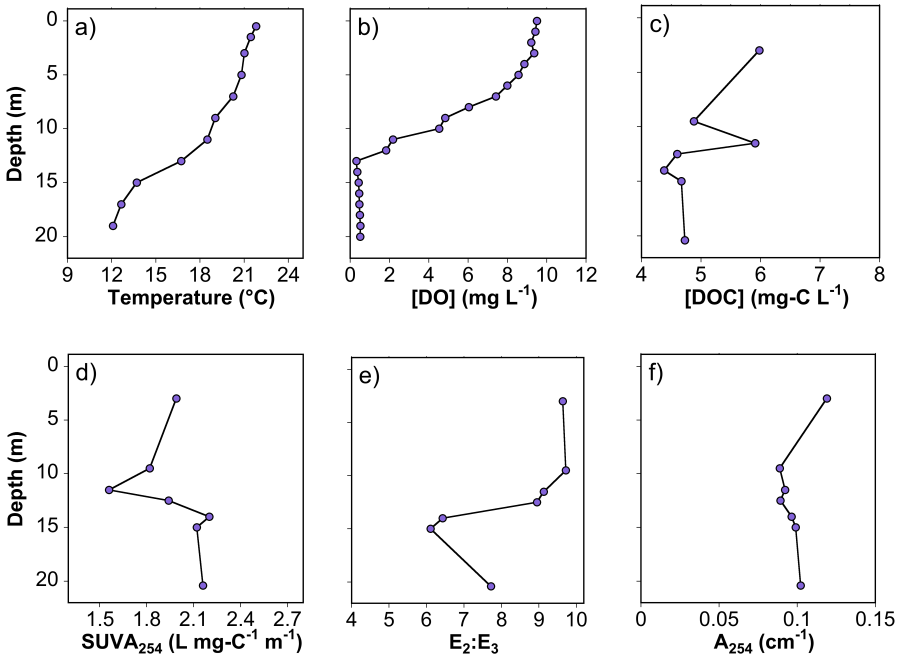

Figure B.23. a) Temperature, b) [DO], c) [DOC], d) $SUVA_{254}$, e) E_2:E_3, and f) A_{254} measured on September 21st at depth-discrete intervals.

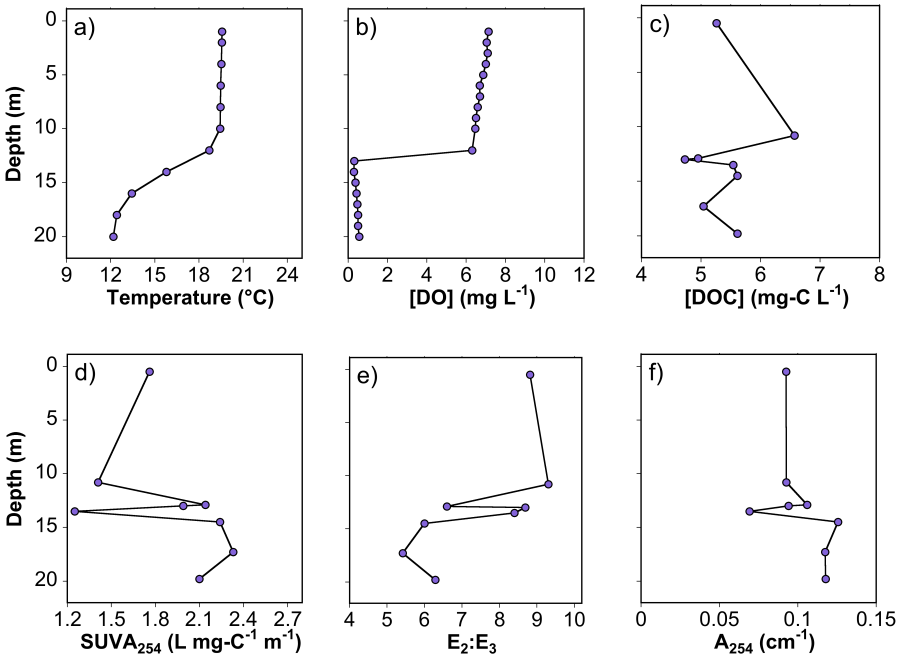

Figure B.24. a) Temperature, b) [DO], c) [DOC], d) $SUVA_{254}$, e) E_2:E_3, and f) A_{254} measured on October 4th at depth-discrete intervals

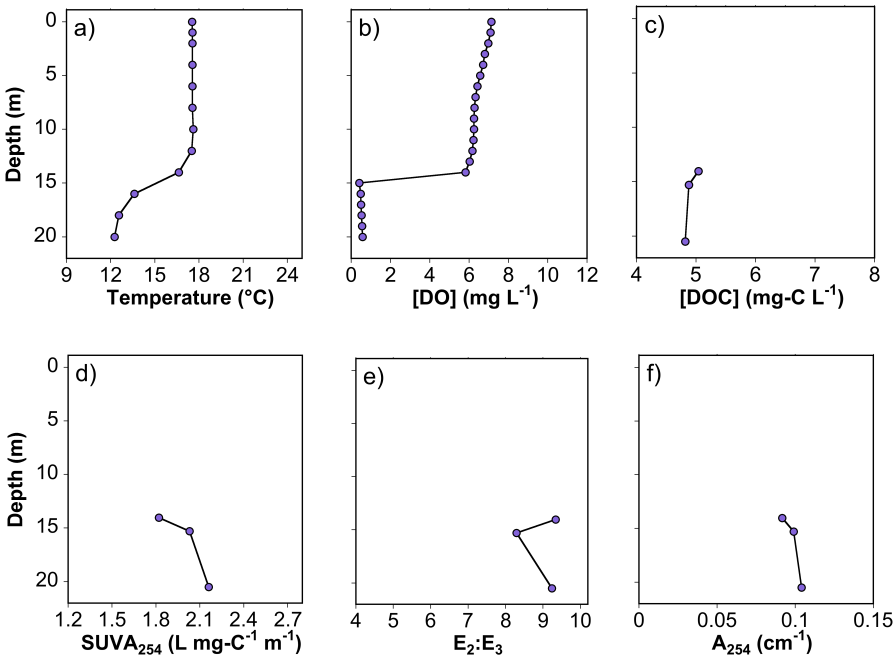

Figure B.25. a) Temperature, b) [DO], c) [DOC], d) $SUVA_{254}$, e) E_2:E_3, and f) A_{254} measured on October 12th at depth-discrete intervals.

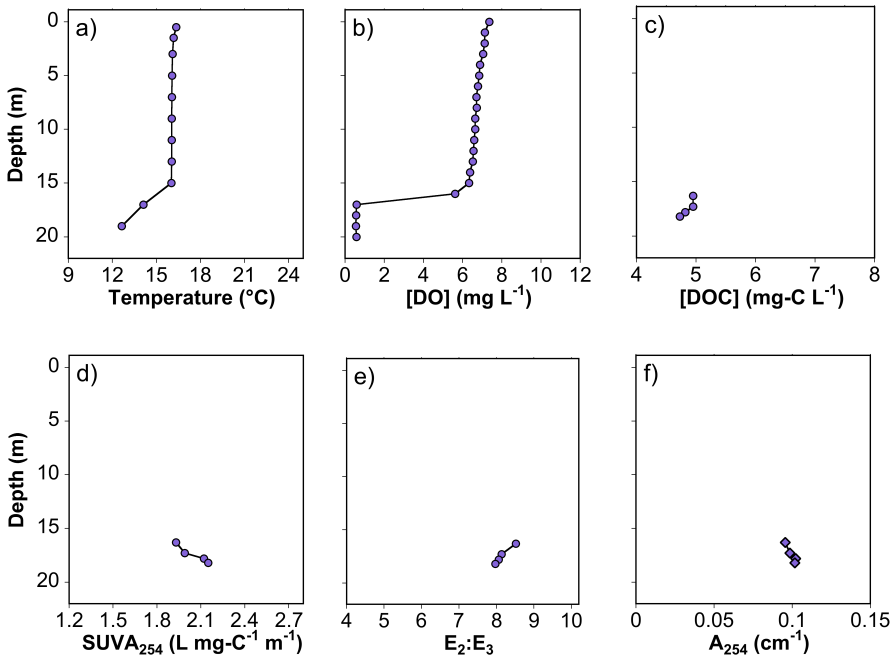

Figure B.26. a) Temperature, b) [DO], c) [DOC], d) $SUVA_{254}$, e) E_2:E_3, and f) A_{254} measured on October 19th at depth-discrete intervals.

Table B.9. [DOC], $SUVA_{254}$, E_2:E_3, and A_{254} for depth discrete samples.

Date	Depth (m)	DOC (mg-C L^{-1})	$SUVA_{254}$ (L mg-C^{-1} m^{-1})	E_2:E_3	A_{254} (cm^{-1})
June 29th	12.2	7.09	1.45	7.7	0.103
June 29th	17.2	5.54	1.71	8.38	0.095
June 29th	18	5.5	1.72	8.55	0.095
June 29th	18.8	5.52	1.72	8.46	0.095
June 29th	19.8	5.59	1.76	6.68	0.098
August 11th	0.1	6	1.58	9.01	0.095
August 11th	9.5	6.94	1.44	7.96	0.100
August 11th	10.3	5.82	1.8	6.9	0.105
August 11th	13.15	5.15	1.86	8.24	0.096
August 11th	15.3	5.33	1.88	7.51	0.100
August 11th	18.08	5.87	2.01	5.6	0.118
August 11th	21.25	6.69	1.94	5.76	0.130
September 8th	0.1	6.26	1.48	9.52	0.093
September 8th	11.5	5.32	1.7	9.63	0.090
September 8th	12.5	4.45	2.15	7.71	0.096
September 8th	13.4	4.95	2.58	5.74	0.128
September 8th	14.5	5.39	2.17	4.89	0.117
September 8th	16.1	5.39	2.32	4.26	0.125
September 8th	18	5.04	2.1	6.82	0.106
September 8th	22.2	5.47	2.29	5.43	0.125
September 21st	3	5.98	1.99	9.64	0.119
September 21st	9.5	4.88	1.82	9.72	0.089
September 21st	11.5	5.91	1.56	9.13	0.092
September 21st	12.5	4.6	1.94	8.95	0.089
September 21st	14	4.38	2.2	6.43	0.096
September 21st	15	4.67	2.12	6.11	0.099
September 21st	20.4	4.73	2.16	7.72	0.102
October 4th	0.5	5.26	1.76	8.82	0.093
October 4th	10.8	6.57	1.41	9.31	0.093
October 4th	12.9	4.95	2.14	6.6	0.106
October 4th	13	4.73	1.99	8.69	0.094
October 4th	13.5	5.54	1.25	8.4	0.069
October 4th	14.5	5.61	2.24	6	0.126
October 4th	17.3	5.04	2.33	5.42	0.117
October 4th	19.8	5.61	2.1	6.29	0.118

October 4th	14.04	5.04	1.82	9.34	0.092
October 12th	15.3	4.88	2.03	8.29	0.099
October 12th	20.5	4.82	2.16	9.24	0.104
October 19th	16.3	4.95	1.93	8.52	0.096
October 19th	17.3	4.95	1.99	8.14	0.099
October 19th	17.8	4.82	2.12	8.06	0.102
October 19th	18.2	4.73	2.15	7.97	0.102
November 3rd	2.1	5	1.83	9.61	0.092
November 3rd	11.9	5.1	1.8	9.65	0.092
November 3rd	20	0.3	1.73	9.84	0.005

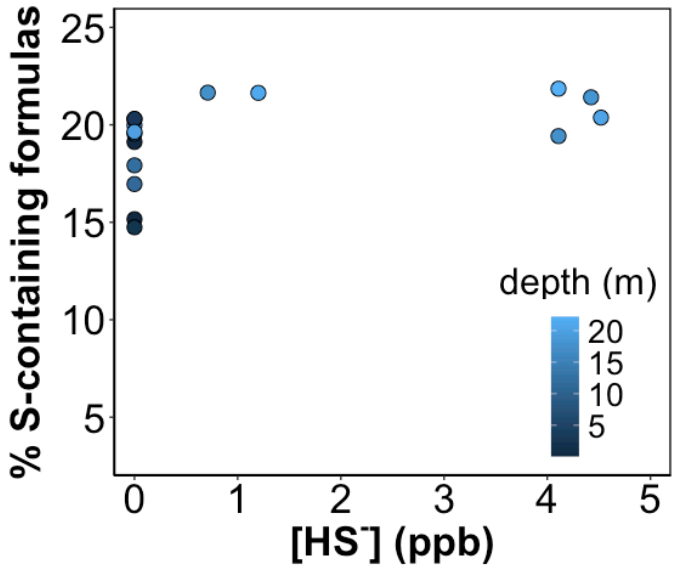

Figure B.27. % of S-containing formulas as a function of sulfide concentration. Color of the point indicates the depth the sample was taken from.

B.5. References

(1) Magnuson, J.; Carpenter, S.; Stanley, E. North Temperate Lakes LTER: High frequency data: Meteorological, dissolved oxygen, chlorophyll, phycocyanin- Lake Mendota buoy **2006** - Current Ver 31. Environmental. Data Initiative. **2020**.

(2) Minor, Elizabeth C.; Swenson, Michael M.; Mattson, Bruce M.; Oyler, A. R. Structural characterization of dissolved organic matter: A review of current techniques for isolation and analysis. *Environ. Sci. Process. Impacts* **2014**, *16*, 2064–2079.

(3) Magnuson, J.; Carpenter, S.; Stanley, E. . North Temperate Lakes LTER: Chemical limnology of primary study lakes: Nutrients, pH and carbon 1981-Current Ver 52. Environmental Data Initiative. **2020**.

(4) Herzsprung, P.; Wentzky, V.; Kamjunke, N.; Von Tümpling, W.; Wilske, C.; Friese, K.;

Boehrer, B.; Reemtsma, T.; Rinke, K.; Lechtenfeld, O. J. Improved understanding of dissolved organic matter processing in freshwater using complementary experimental and machine learning approaches. *Environ. Sci. Technol.* **2020**, *54* (21), 13556–13565.

Appendix C

Supplementary Materials for Chapter 4

C.1 Chemicals

Acetonitrile (HPLC grade), methanol (HPLC grade), hydrochloric acid (concentrated, ACS grade), *o*-phosphoric acid (concentration, ACS grade), glacial acetic acid (concentrated, ACS grade), sodium acetate trihydrate (ACS grade), and potassium hydrogen phthalate (ACS grade) were purchased from Fisher Scientific. Carbamazepine (>98%), N,N-diethyl-m-toluamide (DEET; 98.1%), sodium hydroxide (reagent grade), monobasic potassium phosphate (reagent grade), dibasic potassium phosphate (ACS grade), terephthalic acid (>98%), 1,4-diazobycyclo[2.2.2]octane (>99%), L-histidine (>99%), potassium sorbate (>99%), and sorbic acid (>99%) were purchased from Sigma Aldrich. Isopropyl alcohol (spectrophotometric grade) and *para*-nitroanisole (>99%) were purchased from Acros Organics. Formic acid (88% v/v, ACS grade) was purchased from Aqua Solution, furfuryl alcohol (>98%) and venlafaxine (>98%) were purchased from Tokyo Chemical Industry, and 2,4,6-trimethylphenol (>98%) and pyridine (>99%) were purchased from Alfa Aesar. Atorvastatin (>95%) was purchased from Matrix Scientific. Ultrapure water (18.2 MΩ cm) was used for all analyses and experiments and was obtained from a Milli-Q or Barnstead Nanopure water purification system.

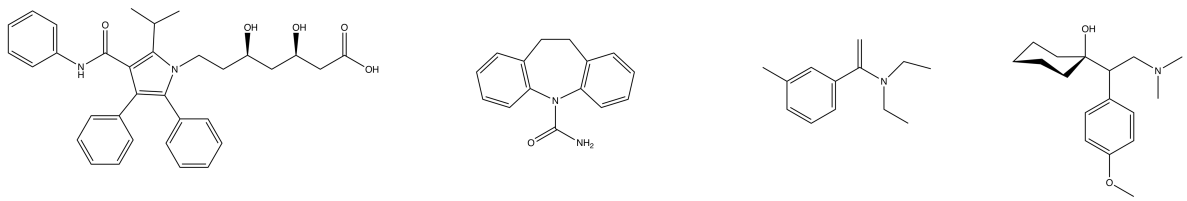

Figure C.1. Structures of contaminants selected for this study.

C.2 Sampling Locations

Samples were collected in acid washed amber glass bottles and filtered through 0.7 μm filters (Whatman GF/F, borosilicate glass) followed by 0.45 μm filters (MDI, nylon) within 24 hours of collection and stored in the dark at 4°C prior to analyses.

Table C.1. Sample names, abbreviations, and coordinates for each of the sampling locations.

Sample	Sample Label	Coordinates
Sand Creek	A	47.185510, -92.853331
Meadowlands	B	47.068966, -92.775002
River Inn	C	46.702892, -92.418854
East Detroit	D	46.651824, -92.203205
Munger Landing	E	46.700820, -92.207148
WLSSD	F	46.761325, -92.124443
Blatnik Bridge	B	46.751031, -92.102092
Wisconsin Point	H	46.688643, -91.972299

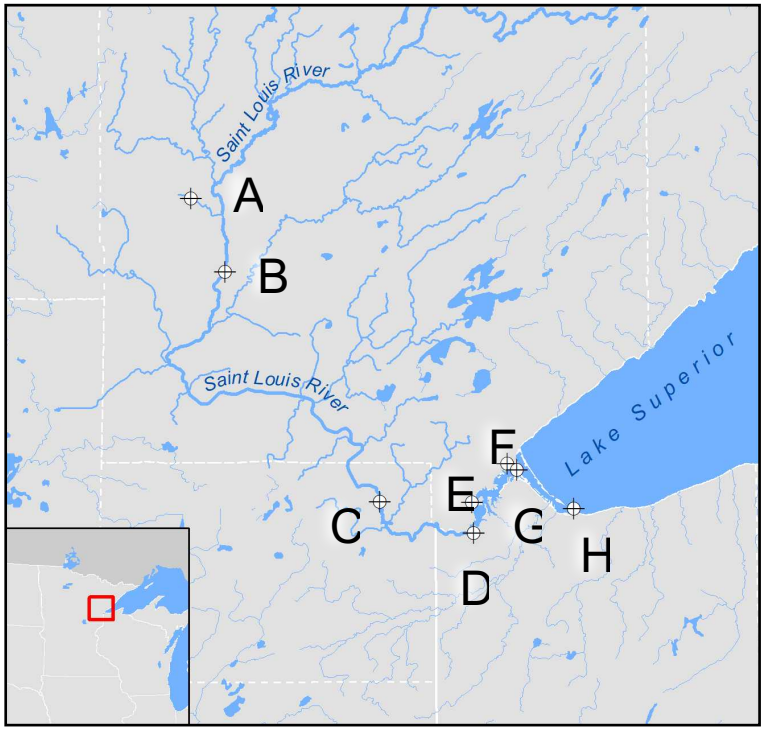

Figure C.2. Map of sampling locations in the St. Louis River and estuary created using ArcGIS software (10.6.1) by Esri. Data provided by the National Atlas of the United States, USGS.

The headwaters of the St. Louis river begin in northern Minnesota and the river flows into Lake Superior on its western side. The St. Louis River is the second largest tributary to Lake Superior and has a watershed of 9412 km^2. The landcover of the upper watershed is predominately characterized as forest or wetland.[1,2] Relatively high amounts of DOC are found in the river, but decrease moving towards Lake Superior.[3,4] The estuary, which connects the river to the lake, itself is 50 km^2.[5] Generally, inputs from the river dominate the water chemistry in the estuary. However, urban and Lake Superior inputs become relatively more important during baseflow conditions, which is when our samples were collected.[6] During this time, the water residence time within the estuary is estimated to be between 40 – 80 days.[6]

The Western Lake Superior Sanitary District (WLSSD) discharges its effluent into the St. Louis River estuary. This plant treats both municipal and industrial wastewater. Processes include advanced secondary treatment with pure oxygen and disinfection with sodium hypochlorite and dechlorinated with sodium bisulfite and mixed media filtration from April – October. WLSSD averages an outflow of 43 million gallons day^{-1} (mgd). The USGS Scanlon gauge (located near our River Inn site) measured a flow rate of 2070 ft^3 sec^{-1} on the day samples were collected. This means that, using a conservative mixing model, <5% of the water collected at our nearest downstream site (Blatnik Bridge) was effluent.

C.3 Water Chemistry

pH was measured with a Mettler Toledo EL20 meter within one week of sampling. The pH meter was calibrated using standards obtained from Aqua Solutions. The pH of the waters ranged from 6.4 (in the Sand Creek tributary flowing into the St. Louis River) to 7.9 in the Wisconsin Point sample collected on the shore of Lake Superior (**Table C.2**). Alkalinity was measured using a Mettler Toledo G20 autotitrator that was calibrated with standards obtained from Aqua Solutions. Alkalinity was determined by measuring the amount of strong acid needed to titrate samples to an endpoint of pH 4.5 and ranged from 25.3 to 252 mg L^{-1} as $CaCO_3$ (**Table C.2**).

Table C.2. pH, [DIC], and alkalinity for all samples. Error represents the standard deviation of triplicate measurements.

Sample	pH	[DIC] (mg-C L^{-1})	Alkalinity (mg L^{-1} as $CaCO_3$)
A. Sand Creek	6.4 ± 0.2	5.7 ± 0.1	25.3 ± 0.4
B. Meadowlands	7.7 ± 0.1	21.9 ± 0.1	101 ± 1
C. River Inn	6.55 ± 0.01	13.8 ± 0.1	64 ± 1
D. East Detroit	7.4 ± 0.2	14.8 ± 0.1	70 ± 1

E. Munger Landing	7.7 ± 0.2	15.4 ± 0.1	72 ± 1
F. Wastewater	7.7 ± 0.2	58.5 ± 0.1	252 ± 4
G. Blatnik Bridge	7.7 ± 0.2	19.3 ± 0.1	87 ± 2
H. Wisconsin Point	7.9 ± 0.2	11.1 ± 0.1	48.9 ± .9

Anions (i.e., chloride, nitrate, nitrite, and sulfate) were measured using anion exchange chromatography (IC) with conductivity detection on a Dionex ICS-2100 instrument. Certified standards purchased from Sigma Aldrich were used for calibration. A Dionex IonPac AS11-HC RFIC^{TM} 4 x 250 mm column was connected to a 4 x 50 mm guard column packed with the same material. An isocratic method with 30 mM sodium hydroxide as the mobile phase was used with a run time of 20 minutes at a flow rate of 1.0 mL per minute. Concentrations are listed in **Table C.3**.

Table C.3. Concentrations of anions in the sampled waters.

Sample	**[Cl^-] (ppm)**	**[NO_3^-] (ppm)**	**[NO_2^-] (ppm)**	**[SO_4^{3-}] (ppm)**
A. Sand Creek	2.09 ± 0.03	< 0.3	< 1.7	< 0.7
B. Meadowlands	8.5 ± 0.1	0.334 ± 0.001	< 1.7	36 ± 7
C. River Inn	4.42 ± 0.6	< 0.3	< 1.7	10 ± 2
D. East Detroit	4.99 ± 0.07	< 0.3	< 1.7	10 ± 2
E. Munger Landing	6.33 ± 0.09	< 0.3	< 1.7	10 ± 2
F. Wastewater	90 ± 1	0.928 ± 0.003	< 1.7	217 ± 40
G. Blatnik Bridge	16.2 ± 0.2	0.369 ± 0.001	< 1.7	30 ± 6
H. Wisconsin Point	2.26 ± 0.03	0.327 ± 0.001	< 1.7	4.9 ± 0.9

Cations and metals (i.e., calcium, iron, magnesium, potassium, and sodium) were measured using inductively coupled plasma-optical emission spectroscopy (ICP-OES) with a Perkin Elmer

4300 DV instrument. Calibration curves were made from standards obtained from Sigma Aldrich. Concentrations are listed in **Table C.4**.

Table C.4. Concentrations of cations and metals in the sampled waters.

Sample	$[Ca^{2+}]$ (ppm)	$[Fe]_{total}$ (ppm)	$[K^{+}]$ (ppm)	$[Mg^{2+}]$ (ppm)	$[Na^{+}]$ (ppm)
A. Sand Creek	14.8 ± 0.2	< 0.5	12.7 ± 0.7	4.0 ± 01	1.9 ± 0.1
B. Meadowlands	21.9 ± 0.2	< 0.5	9.5 ± 0.8	21.6 ± 0.2	10.1 ± 0.1
C. River Inn	17.0 ± 0.3	< 0.5	10.5 ± 0.4	9.9 ± 0.1	4.8 ± 0.1
D. East Detroit	18.4 ± 0.2	< 0.5	8.2 ± 0.7	10.1 ± 0.1	5.1 ± 0.1
E. Munger Landing	19.3 ± 0.2	< 0.5	8.9 ± 0.8	10.4 ± 0.1	5.8 ± 0.1
F. Wastewater	58 ± 1	< 0.5	4.3 ± 0.6	10.2 ± 0.2	202 ± 3
G. Blatnik Bridge	23.3 ± 0.3	< 0.5	8 ± 1	9.7 ± 0.2	23 ± 0.3
H. Wisconsin Point	15.2 ± 0.2	< 0.5	6.0 ± 0.2	3.5 ± 0.1	2.2 ± 0.1

A Shimadzu total organic carbon analyzer was used to measure concentrations of dissolved organic carbon (DOC) and dissolved inorganic carbon (DIC). The instrument was calibrated for DOC using known concentrations of potassium hydrogen phthalate as a standard (**Table C.5**). [DIC] ranged from 5.7 mg-C L^{-1} in a tributary flowing into the SLR to 58.5 mg-C L^{-1} in the wastewater effluent (**Table C.2**) and generally scaled with alkalinity.

Ultraviolet-visible (UV-vis) spectroscopy was used to measure absorbance of whole water samples (**Table C.5**). A Shimadzu 2401PC Recording Spectrophotometer was used and spectra were collected in 1 nm intervals from 200 – 800 nm. Spectra were blank subtracted referenced to Milli-Q water. The average absorbance from 700 – 800 nm was also subtracted to correct for any light scattering. $SUVA_{254}$ was calculated by dividing the absorbance at 254 nm by [DOC] and E_2:E_3 is calculated as the ratio of the absorbance at 250 nm to the absorbance at 365 nm.

Table C.5. [DOC], $SUVA_{254}$, and E_2:E_3 for each sample location.

Sample	[DOC] (mg-C L^{-1})	$SUVA_{254}$ (L mg-C^{-1} m^{-1})	E_2:E_3
A. Sand Creek	69 ± 3	5.20 ± 0.20	4.32 ± 0.01
B. Meadowlands	33.5 ± 0.4	4.52 ± 0.09	4.43 ± 0.01
C. River Inn	29.6 ± 0.3	4.33 ± 0.09	4.67 ± 0.01
D. East Detroit	29.9 ± 0.2	4.26 ± 0.06	4.74 ± 0.01
E. Munger Landing	29.3 ± 0.3	4.17 ± 0.07	4.80 ± 0.01
F. Wastewater	24.6 ± 0.2	2.40 ± 0.04	6.33 ± 0.03
G. Blatnik Bridge	25.97 ± 0.04	4.01 ± 0.06	4.88 ± 0.01
H. Wisconsin Point	3.45 ± 0.05	2.57 ± 0.08	5.78 ± 0.04

C.4 Mass Spectrometry

Organic matter was extracted from the whole water samples using solid phase extraction with 500 mg Agilent PPL cartridges as described previously.[7] Cartridges were rinsed with 5 mL of methanol prior to extraction. Samples (500 mL) were acidified to pH 2 ± 0.1 with hydrochloric acid and passed through the SPE cartridges. Afterwards, 1 mL of 0.01 M hydrochloric acid was passed through to remove salts retained on the material. Cartridges were dried for 5 minutes using HEPA filtered air and DOM was eluted with 5 mL of methanol. Extracts were stored in the dark at 4°C until analysis.

SPE extracts were diluted 100x in 60:40 acetonitrile:Milli-Q water and were directly injected into a SolariX XR 12T Fourier-transform ion cyclotron resonance mass spectrometer (FT-ICR MS; Bruker) equipped with a Triversa NanoMate sample delivery system (Advion). Electrospray ionization in negative mode was used and -1.4 kV was applied with a gas pressure of 0.3 psi. Accumulation time was varied to record approximately 10^8 counts per reading and 1000

readings were collected per sample. The *m/z* peaks with signal to noise > 3 were exported for data processing in *R*. Additionally, an absolute intensity threshold of 1,000,000 was required.

During data processing, exported *m/z* peaks were converted to neutral masses by adding the mass of a proton and were linearly calibrated using known formulas commonly found in DOM samples as described previously.[8–10] Potential masses considered for matching include $C_{1\text{-}180}{}^{13}C_{0\text{-}1}H_{1\text{-}140}O_{0\text{-}80}N_{0\text{-}1}S_{0\text{-}1}P_{0\text{-}1}Cl_{0\text{-}1}$. Potential masses were required to be less than 0.5 ppm mass error away from calibrated *m/z* and to be part of a homologous series ($+CH_2$ or CH_4 vs. O) with at least three members. **Table C.6** shows the number of formulas identified in each water sample. **Figures C.3 – C.7** show van Krevelen diagrams for CHO, CHON, CHOS, CHOP, and CHOCl identified in each formula.

FT-ICR MS results are visualized on van Krevelen diagrams to show formulas that are present in different compound classes (**Figures C.3 – C.7)**. While the location of a formula on the van Krevelen diagram does not demonstrate the formula fits that class, it is likely that it is structurally similar to compounds within that class.[11] Most formulas are classified as tannin- or lignin-like as expected for natural water samples that receive terrestrial DOM.[3,4,12,13] More saturated formulas (e.g., protein- and lipid-like formulas) are found downstream in the river, particularly in the wastewater effluent.

Table C.6. Numbers of types of formulas detected in each water sample.

Sample	# Total	# CHO	# CHON	# CHOS	# CHOP	# CHOCl
A. Sand Creek	1179	991	26	76	19	67
B. Meadowlands	1309	1053	58	143	9	46
C. River Inn	1437	1127	59	158	18	75
D. East Detroit	1526	1140	66	182	23	115
E. Munger Landing	1286	1015	46	143	20	62
F. Wastewater	3823	1646	199	1299	159	520
G. Blatnik Bridge	2479	1639	172	498	21	149
H. Wisconsin Point	1662	1105	69	179	73	236

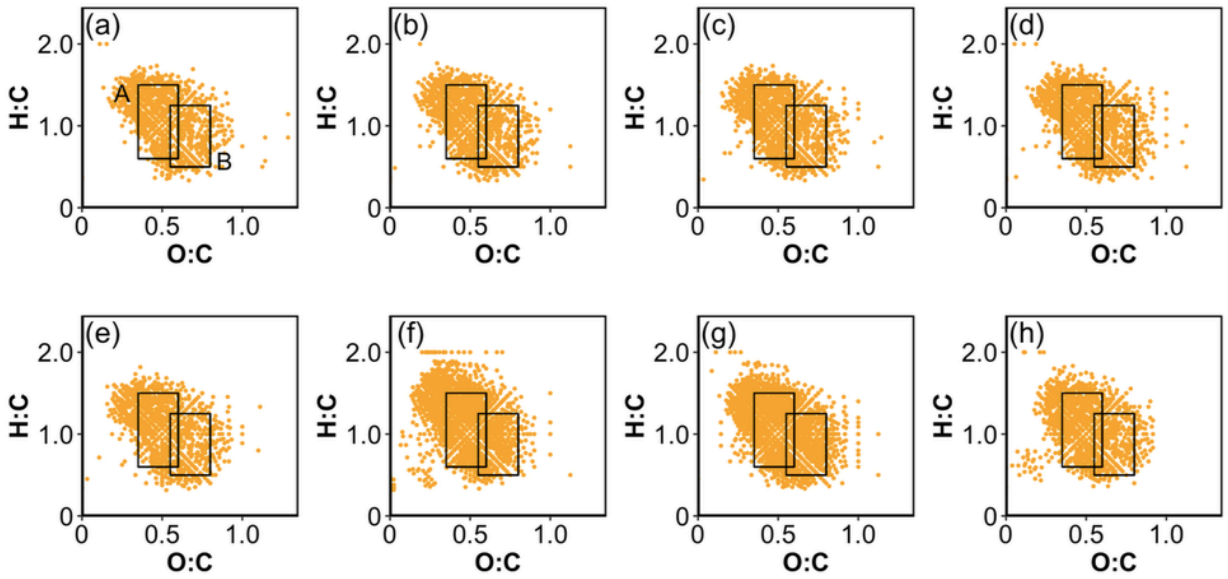

Figure C.3. van Krevelen diagrams showing identified CHO formulas in (a) Sand Creek, (b) Meadowlands, (c) River Inn, (d) East Detroit, (e) Munger Landing, (f) Wastewater, (g) Blatnik Bridge, and (h) Wisconsin Point. Box A and Box B denote approximate locations of tannin- and lignin-like formulas respectively.[11]

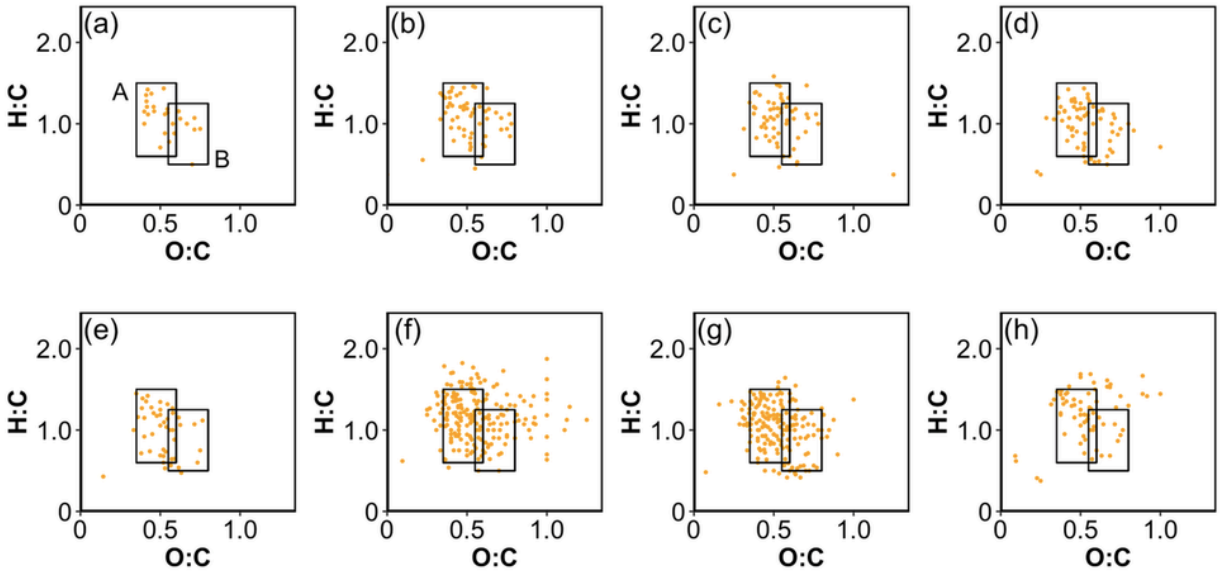

Figure C.4. van Krevelen diagrams showing identified CHON formulas in (a) Sand Creek, (b) Meadowlands, (c) River Inn, (d) East Detroit, (e) Munger Landing, (f) Wastewater, (g) Blatnik Bridge, and (h) Wisconsin Point. Box A and Box B denote approximate locations of tannin- and lignin-like formulas respectively.[11]

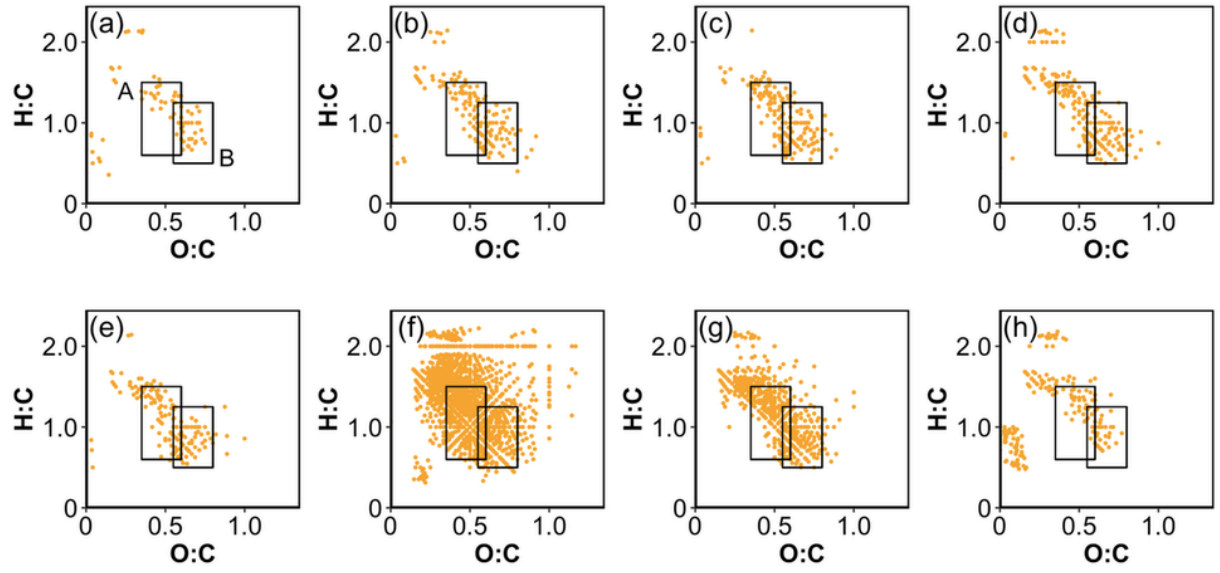

Figure C.5. van Krevelen diagrams showing identified CHOS formulas in (a) Sand Creek, (b) Meadowlands, (c) River Inn, (d) East Detroit, (e) Munger Landing, (f) Wastewater, (g) Blatnik Bridge, and (h) Wisconsin Point. Box A and Box B denote approximate locations of tannin- and lignin-like formulas respectively.[11]

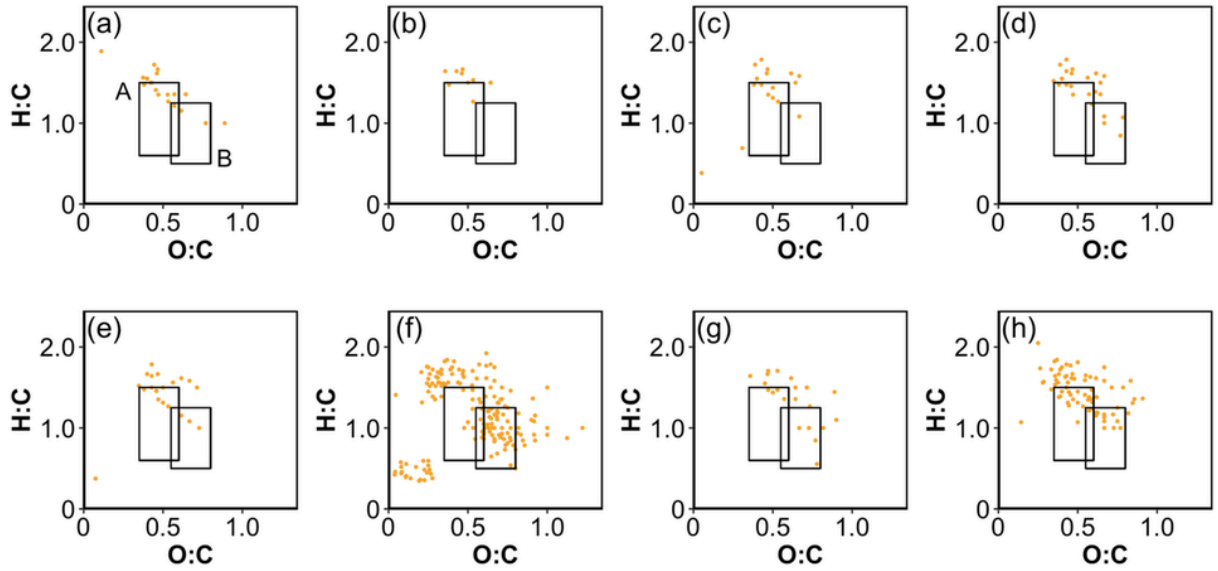

Figure C.6. van Krevelen diagrams showing identified CHOP formulas in (a) Sand Creek, (b) Meadowlands, (c) River Inn, (d) East Detroit, (e) Munger Landing, (f) Wastewater, (g) Blatnik Bridge, and (h) Wisconsin Point. Box A and Box B denote approximate locations of tannin- and lignin-like formulas respectively. [11]

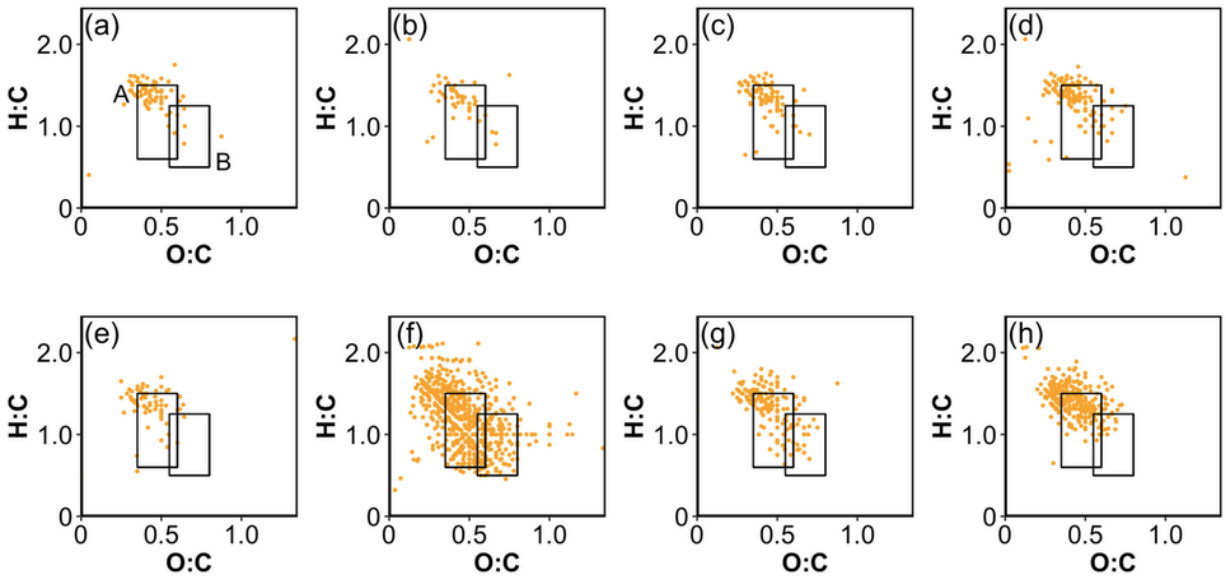

Figure C.7. van Krevelen diagrams showing identified CHOCl formulas in in (a) Sand Creek, (b) Meadowlands, (c) River Inn, (d) East Detroit, (e) Munger Landing, (f) Wastewater, (g) Blatnik Bridge, and (h) Wisconsin Point. Box A and Box B denote approximate locations of tannin- and lignin-like formulas respectively.[11]

Weighted averages calculated from the identified formulas show downstream samples are more saturated, less oxygenated, and are depleted in double bond equivalents as compared to upstream samples (**Figure C.8**).

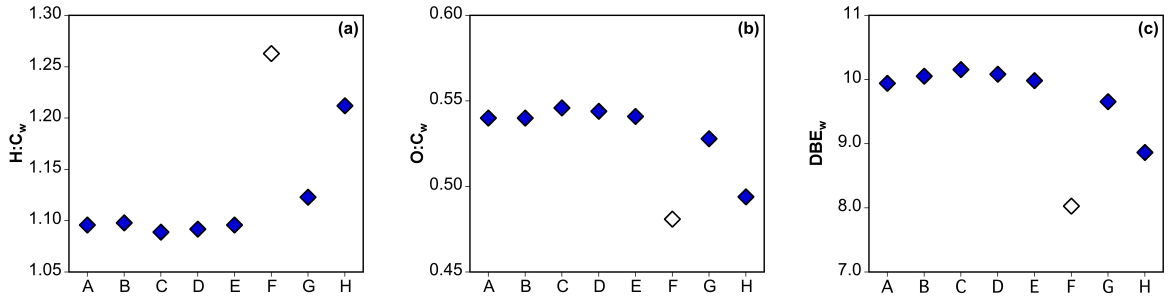

Figure C.8. Weighted averages of (a) H:C, (b) O:C, and (c) DBE for each sample as detected by FT-ICR MS.

Bray-Curtis dissimilarity was calculated based on the presence and absence of individual formulas identified by FT-ICR MS (**Figure C.9**). Samples with more formulas in common are listed on branches closer to each other in the dendrogram.

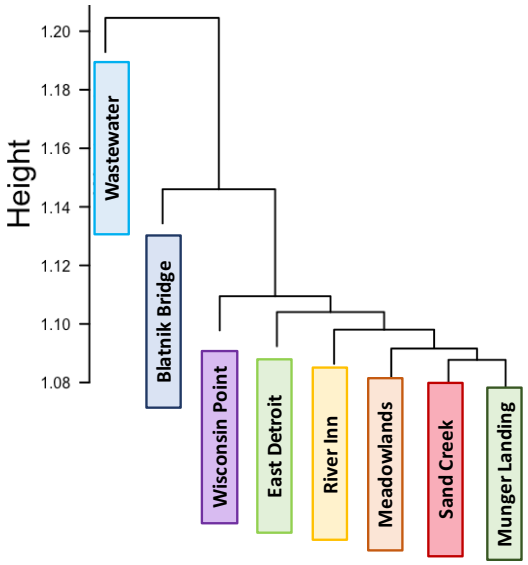

Figure C.9. Dendrogram showing results of Bray-Curtis dissimilarity analysis considering presence and absence of individual formulas matching in FT-ICR MS analysis.

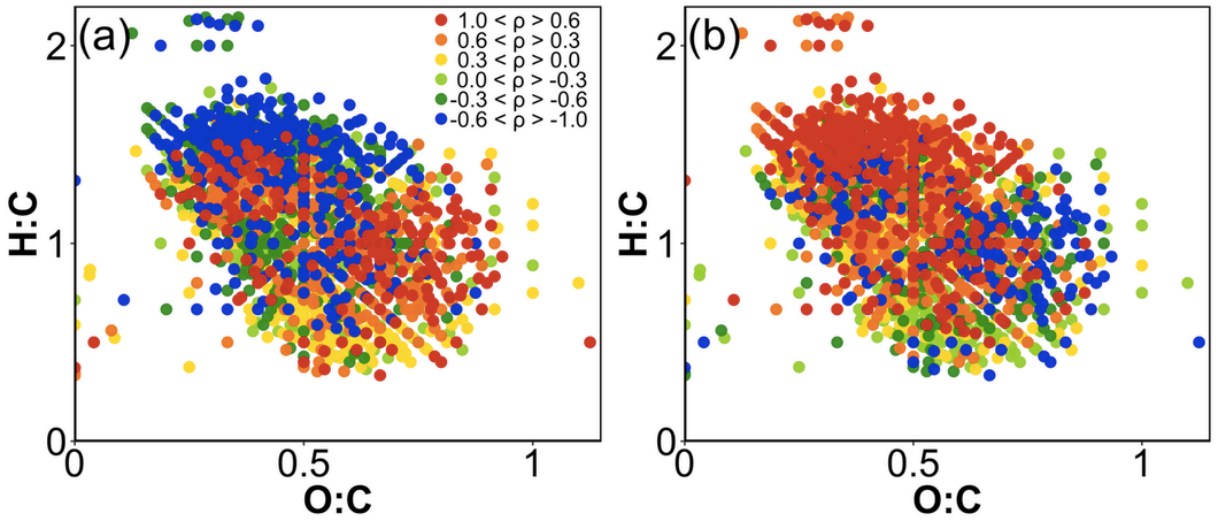

Figure C.10. Spearman rank correlations between relative formula intensity as detected by FT-ICR MS and the optical properties (a) $SUVA_{254}$ and (b) E_2:E_3. Only formulas identified in at least 6 samples are included in the plots.

C.5 HPLC Analysis

Either an Agilent 1260 instrument equipped with a diode array detector (Model 1260 DAD) and a fluorescence detector (Model 1260 FLD) or an Agilent 1100 series with DAD (Model 1100

DAD) was used. For each column used, a guard column (3.0 mm) was attached. Details about the HPLC methods of each analyte are listed in **Table C.7**.

Table C.7. Details of HPLC methods for probe quantification.

Analyte	Column	Eluent	Detection
Furfuryl Alcohol (FFA)	Agilent Poroshell 120 EC-C18 (3.0 x 50 mm)	100% 30 mM Acetate, 10% acetonitrile pH = 6	Diode array detection (DAD) at 217 nm
2,4,6-Trimethylphenol (TMP)	Agilent Poroshell 120 EC-C18 (3.0 x 50 mm)	50:50 0.1% formic acid with 10% acetonitrile: acetonitrile pH = 2.5	λ_{ex} = 230 nm; λ_{em} = 325 nm
Terephthalic Acid (TPA)	Agilent Poroshell 120 Bonus RP (3.0 x 100 mm)	50:50 0.1% formic acid with 10% acetonitrile:acetonitrile pH = 2.5	DAD at 245 nm
Hydroxy-terephthalic Acid (hTPA)			λ_{ex} = 250 nm; λ_{em} = 410 nm
p-Nitroanisole (PNA)	Agilent Poroshell 120 EC-C18 (3.0 x 50 mm)	55:45 10 mm Acetate, 10% acetonitrile, acetonitrile, pH = 6	DAD at 314 nm
Atorvastatin	Agilent Eclipse-XDB C18 (5µm, 4.6 x 150 mm)	28:72 acetonitrile:water, pH = 3	DAD at 244 nm
Carbamazepine	Agilent Eclipse-XDB C18 (5µm, 4.6 x 150 mm)	46:54 acetonitrile:water	DAD at 282 nm
DEET	Agilent Eclipse-XDB C18 (5µm, 4.6 x 150 mm)	50:50 acetonitrile:water	DAD at 220 nm
Venlafaxine	Agilent Eclipse-XDB C18 (5µm, 4.6 x 150 mm)	25:75 acetonitrile:water, pH = 3	DAD at 230

Due to background fluorescence, hTPA could not be detected quantitatively detected in the wastewater effluent. To show this, we collected excitation-emission matrices for both hTPA (10uM) and the wastewater using a Horiba Aqualog instrument (**Figure C.11)**. hTPA was run at a concentration of 12.5 ppb and the wastewater was run with a 5x dilution.

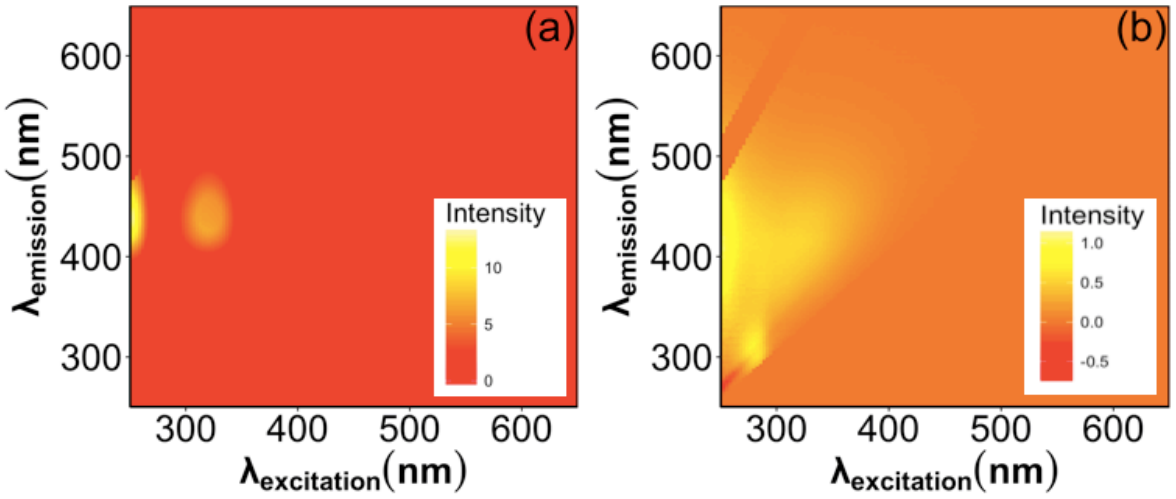

Figure C.11. Excitation-emission matrices for (a) hTPA and (b) wastewater effluent.

C.6 Photochemistry

$[^3DOM]_{ss}$ and f_{TMP} were calculated using the rate constant for reaction of ^3DOM with TMP (2.9×10^9 M^{-1} s^{-1}) and the rate of light absorbance.[12,14] $[^1O_2]_{ss}$ and Φ_{1O2} were calculated as described previously[9] with the updated rate constant of 1.00×10^8 M^{-1} s^{-1} for the reaction between $^1O_2$ and FFA.[15] $[^{\bullet}OH]_{ss}$ was calculated using rate constants for reactions between $^{\bullet}OH$ and both TPA and hTPA, as well as the direct degradation rate constant for hTPA measured in control experiments (4.4×10^9 M^{-1} s^{-1}, 6.3×10^9 M^{-1} s^{-1}, and 6.5×10^{-5} s^{-1}, respectively). $\Phi_{\bullet OH}$ were calculated using the rate of light absorbance concentrations of organic and inorganic carbon forms in the water samples.[16] The rate constants used were 1.7×10^4 L mg-C^{-1} s^{-1}, 8.5×10^6 M^{-1} s^{-1}, and 1.7×10^8 M^{-1} s^{-1} for reactions of $^{\bullet}OH$ with DOC, bicarbonate, and carbonate, respectively.[16]

The photochemical reactivity of waters throughout the St. Louis River is first assessed by quantifying PPRI steady-state concentrations, which are important for predicting contaminant fate. $[^3DOM]_{ss}$ (range = $(0.72 – 1.21) \times 10^{-13}$ M) and $[^1O_2]_{ss}$ (range = $(1.6 – 20.4) \times 10^{-13}$ M) are similar,

while $[^{\bullet}OH]_{ss}$ is orders of magnitude lower (range (2.9 – 20.5) x 10^{-16} M; **Table C.8**). $[^{\bullet}OH]_{ss}$ could not be quantified in the wastewater effluent because the fluorescence signal of the probe could not be separated from background fluorescence of the sample (**Figure C.11**), which has been noted previously.[17] Similar steady-state concentrations have been observed in other natural water samples.[12,16,18,19] $[^1O_2]_{ss}$ and $[^{\bullet}OH]_{ss}$ decrease moving downstream in the river. No trend is observed for $[^3DOM]_{ss}$ but the wastewater and Wisconsin Point samples show especially low concentrations. The decrease in $[^1O_2]_{ss}$ and $[^{\bullet}OH]_{ss}$ may be partially attributable to the decrease in [DOC] observed throughout the St. Louis River (**Figure 4.1a** in the manuscript). However, the $[^3DOM]_{ss}$ results demonstrate that DOM quality is also important since these measurements were made in [DOC]-normalized samples. Therefore, quantum yields for PPRI formation, which are normalized to light absorbance, are more appropriate for evaluating the role of DOM composition in its photochemical reactivity.

Table C.8. Steady-state concentrations of PPRI in each sampled location. Errors represent the standard deviation of triplicate measurements.

Sample	$[^3DOM]_{ss}$ (M)	$[^1O_2]_{ss}$ (M)	$[^{\bullet}OH]_{ss}$ (M)
A. Sand Creek	(1.13 ± 0.02) x 10^{-13}	(2.04 ± 0.08) x 10^{-12}	(2.05 ± 0.04) x 10^{-15}
B. Meadowlands	(1.08 ± 0.02) x 10^{-13}	(1.66 ± 0.06) x 10^{-12}	(7.32 ± 0.08) x 10^{-16}
C. River Inn	(1.13 ± 0.05) x 10^{-13}	(1.22 ± 0.01) x 10^{-12}	(1.00 ± 0.02) x 10^{-15}
D. East Detroit	(1.15 ± 0.03) x 10^{-13}	(1.29 ± 0.03) x 10^{-12}	(9 ± 1) x 10^{-16}
E. Munger Landing	(1.21 ± 0.08) x 10^{-13}	(1.75 ± 0.04) x 10^{-12}	(5.58 ± 0.04) x 10^{-16}
F. Wastewater	(7.9 ± 0.4) x 10^{-14}	(8.73 ± 0.05) x 10^{-13}	N/A
G. Blatnik Bridge	(1.12 ± 0.03) x 10^{-13}	(1.19 ± 0.02) x 10^{-12}	(2.9 ± 0.1) x 10^{-16}
H. Wisconsin Point	(7.2 ± 0.6) x 10^{-14}	(1.60 ± 0.05) x 10^{-13}	(4.0 ± 0.1) x 10^{-16}

Table C.9. Quantum yields and quantum yield coefficients for formation of PPRI in each sampled location.

Sample	f_{TMP} (M^{-1})	Φ_{1O2}	$\Phi_{\bullet OH}$
A. Sand Creek	35.6 ± 0.7	(5.4 ± 0.2) x 10^{-3}	(1.00 ± 0.02) x 10^{-3}
B. Meadowlands	35.2 ± 0.8	(6.9 ± 0.2) x 10^{-3}	(2.25 ± 0.02) x 10^{-4}
C. River Inn	40 ± 2	(6.3 ± 0.2) x 10^{-3}	(2.93 ± 0.06) x 10^{-4}
D. East Detroit	41.4 ± 0.9	(7.0 ± 0.2) x 10^{-3}	(3.8 ± 0.6) x 10^{-4}
E. Munger Landing	44 ± 3	(8.5 ± 0.2) x 10^{-3}	(3.40 ± 0.03) x 10^{-4}
F. Wastewater	69 ± 3	(1.03 ± 0.02) x 10^{-2}	N/A
G. Blatnik Bridge	42 ± 1	(7.3 ± 0.3) x 10^{-3}	(1.40 ± 0.06) x 10^{-4}
H. Wisconsin Point	58 ± 5	(7.9 ± 0.3) x 10^{-3}	(2.16 ± 0.04) x 10^{-5}

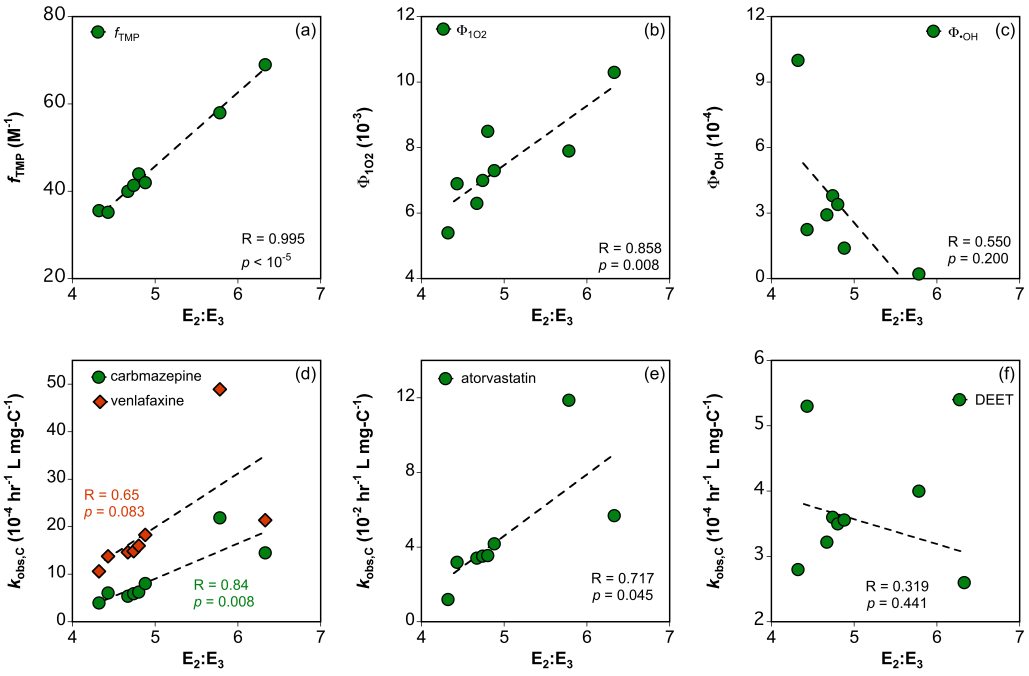

Figure C.12. Linear regressions between E_2:E_3 and (a) f_{TMP}, (b) Φ_{1O2}, (c) $\Phi_{\bullet OH}$, (d) $k_{obs,C}$ for carbamazepine and $k_{obs,C}$ for venlafaxine, (e) $k_{obs,C}$ for atorvastatin, and (f) $k_{obs,C}$ for DEET. Trend lines are based on a 95% confidence interval.

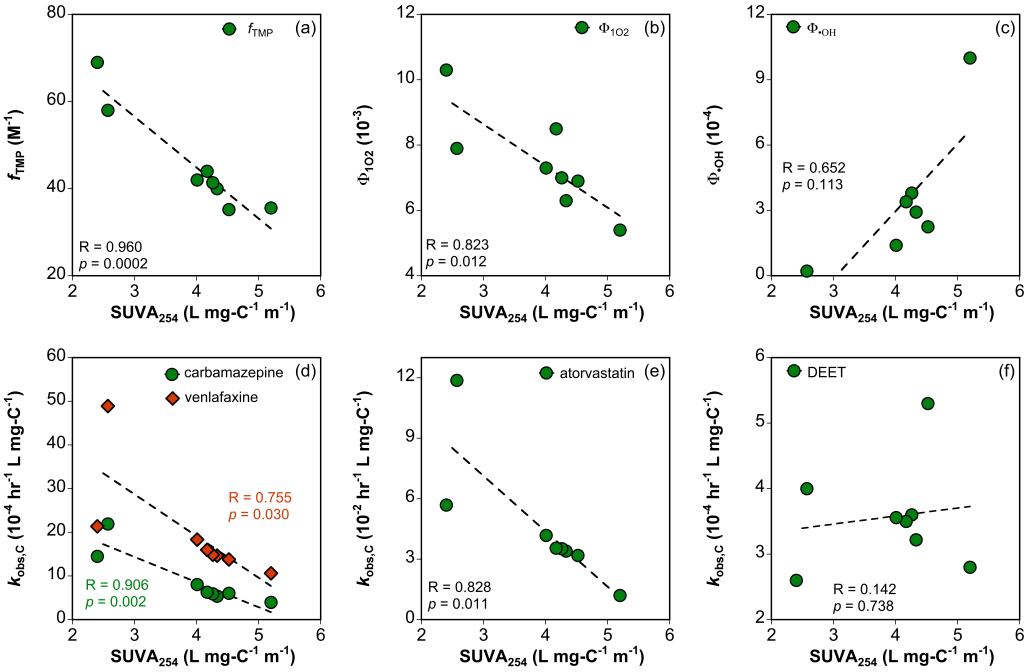

Figure C.13. Linear regressions between SUVA$_{254}$ and (a) f_{TMP}, (b) Φ_{1O2}, (c) $\Phi_{\bullet OH}$, (d) $k_{obs,C}$ for carbamazepine and $k_{obs,C}$ for venlafaxine, (e) $k_{obs,C}$ for atorvastatin, and (f) $k_{obs,C}$ for DEET. Trend lines are based on a 95% confidence interval.

Table C.10. Directions of correlations between Spearman rank rho values for formula intensity versus each parameter. All correlations were significant at a 95% confidence interval with $p < 10^{-5}$.

	SUVA$_{254}$	**E$_2$:E$_3$**	**f_{TMP}**	**Φ_{1O2}**	**$\Phi_{\bullet OH}$**	**$k_{obs,C}$** carbamazepine	**$k_{obs,C}$** atorvastatin	**$k_{obs,C}$** venlafaxine	**$k_{obs,C}$** DEET
SUVA$_{254}$		-	-	-	+	-	-	-	+
E$_2$:E$_3$			+	+	-	+	+	+	-
f_{TMP}				+	-	+	+	+	-
Φ_{1O2}					-	+	+	+	-
$\Phi_{\bullet OH}$						-	-	-	-

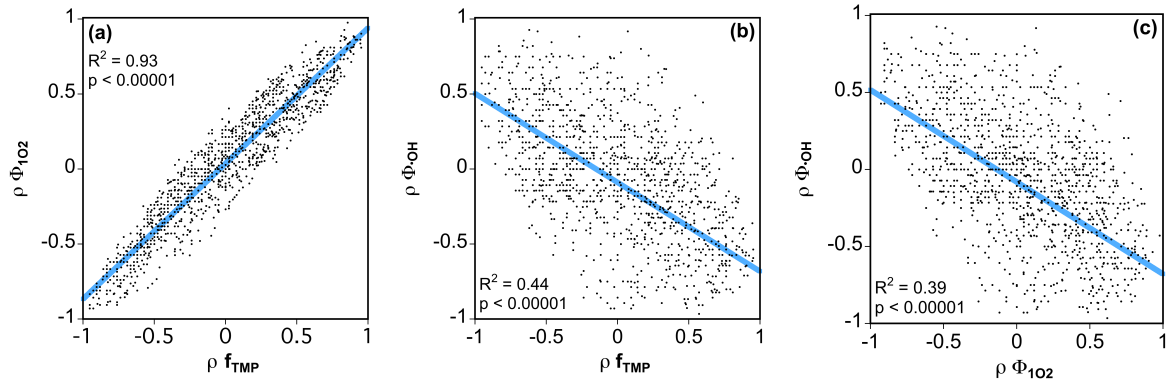

Figure C.14. Scatter plots showing the relationship between Spearman rank rho values for (a) formula intensity with Φ_{1O2} and formula intensity with f_{TMP}, (b) formula intensity with $\Phi_{\bullet OH}$ and formula intensity with f_{TMP}, and (c) formula intensity with $\Phi_{\bullet OH}$ and formula intensity with Φ_{1O2}.

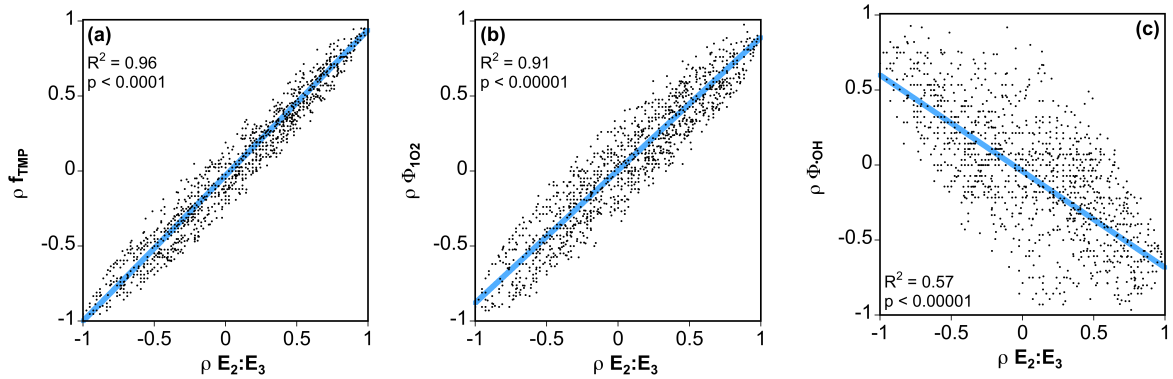

Figure C.15. Scatter plots showing the relationship between Spearman rank rho values for formula intensity with E_2:E_3 and (a) formula intensity with f_{TMP}, (b) formula intensity with Φ_{1O2}, and (c) formula intensity with $\Phi_{\bullet OH}$.

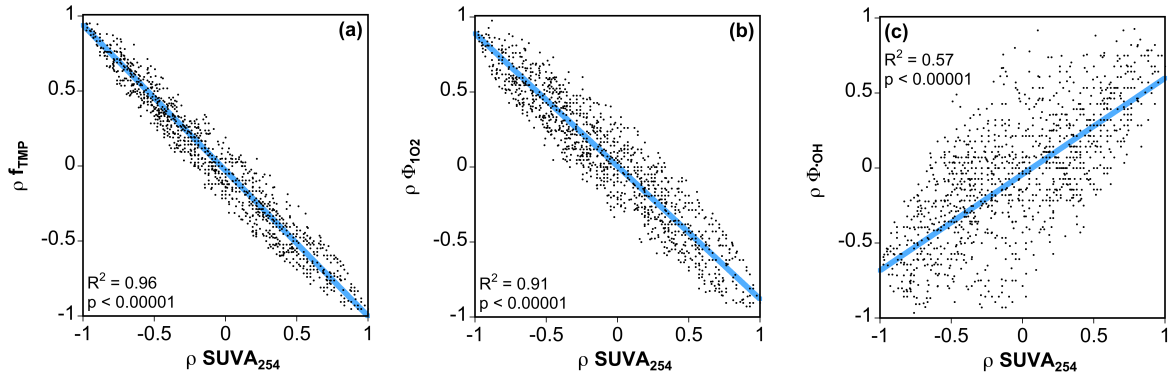

Figure C.16. Scatter plots showing the relationship between Spearman rank rho values for formula intensity with $SUVA_{254}$ and (a) formula intensity with f_{TMP}, (b) formula intensity with Φ_{1O2}, and (c) formula intensity with $\Phi_{\bullet OH}$.

C.7 Contaminant Degradation

The pseudo-first-order photodegradation rate constant was measured for each of the contaminants in the study (**Table C.11**). To consider how DOM composition, rather than concentration, affects contaminant degradation, carbon-normalized rate constants for each contaminant were also calculated by normalizing to [DOC] in each sample (**Table C.12**).

Spearman rank correlations were also calculated between formula intensity detected by FT-ICR MS and carbon-normalized photodegradation rank constant for venlafaxine degradation (**Figure C.17**). This nearly identical to the correlation pattern observed for carbamazepine and atorvastatin (**Figures 4.3d** and **4.3e** in the manuscript).

Table C.11. Pseudo-first-order photodegradation rate constants for each contaminant. The rate constant for degradation of atorvastatin, carbamazepine, and venlafaxine were measured in a Suntest Solar Simulator, while the degradation of DEET was measured in the Rayonet.

Sample	Atorvastatin (hr^{-1})	Carbamazepine (hr^{-1})	DEET (hr^{-1})	Venlafaxine (hr^{-1})
Direct Control	$(1.3 \pm 0.2) \times 10^{-1}$	$(2 \pm 3) \times 10^{-3}$	$(1.6 \pm 0.2) \times 10^{-5}$	$(1.1 \pm 0.4) \times 10^{-2}$
A: Sand Creek	$(8.4 \pm 0.2) \times 10^{-1}$	$(2.8 \pm 0.9) \times 10^{-2}$	$(1.9 \pm 0.2) \times 10^{-2}$	$(7.4 \pm 0.5) \times 10^{-2}$
B: Meadowlands	1.10 ± 0.02	$(2.1 \pm 0.2) \times 10^{-2}$	$(1.77 \pm 0.02) \times 10^{-2}$	$(4.7 \pm 0.7) \times 10^{-2}$
C: River Inn	1.04 ± 0.03	$(1.6 \pm 0.2) \times 10^{-2}$	$(9.5 \pm 0.2) \times 10^{-3}$	$(4.5 \pm 0.2) \times 10^{-2}$
D: East Detroit	1.06 ± 0.07	$(1.8 \pm 0.1) \times 10^{-2}$	$(1.1 \pm 0.1) \times 10^{-2}$	$(4.9 \pm 0.5) \times 10^{-2}$
E: Munger Landing	1.09 ± 0.03	$(1.9 \pm 0.4) \times 10^{-2}$	$(1.04 \pm 0.05) \times 10^{-2}$	$(4.5 \pm 0.2) \times 10^{-2}$
F: Wastewater	1.44 ± 0.06	$(3.7 \pm 0.5) \times 10^{-2}$	$(6.3 \pm 0.9) \times 10^{-3}$	$(5.4 \pm 0.5) \times 10^{-2}$
G: Blatnik Bridge	1.12 ± 0.02	$(2.2 \pm 0.3) \times 10^{-2}$	$(9.24 \pm 0.08) \times 10^{-3}$	$(4.9 \pm 0.3) \times 10^{-2}$
H: Wisconsin Point	$(4.4 \pm 0.2) \times 10^{-1}$	$(8 \pm 2) \times 10^{-3}$	$(1.4 \pm 0.8) \times 10^{-3}$	$(1.8 \pm 0.4) \times 10^{-2}$

Table C.12. $k_{obs,C}$ for each contaminant. $k_{obs,C}$ for atorvastatin, carbamazepine, and venlafaxine were measured in a Suntest Solar Simulator, while $k_{obs,C}$ for of DEET was measured in a Rayonet.

Sample	Atorvastatin (L mg-C^{-1} hr^{-1})	Carbamazepine (L mg-C^{-1} hr^{-1})	DEET (L mg-C^{-1} hr^{-1})	Venlafaxine (L mg-C^{-1} hr^{-1})
A: Sand Creek	(1.20 ± 0.03) x 10^{-2}	(3.9 ± 1) x 10^{-4}	(2.8 ± 0.3) x 10^{-4}	(1.06 ± 0.07) x 10^{-3}
B: Meadowlands	(3.19 ± 0.07) x 10^{-2}	(6.07 ± 0.6) x 10^{-4}	(5.30 ± 0.09) x 10^{-4}	(1.4 ± 0.2) x 10^{-3}
C: River Inn	(3.41 ± 0.09) x 10^{-2}	(5.4 ± 0.6) x 10^{-4}	(3.22 ± 0.07) x 10^{-4}	(1.47 ± 0.06) x 10^{-3}
D: East Detroit	(3.5 ± 0.2) x 10^{-2}	(5.9 ± 3) x 10^{-4}	(3.6 ± 0.4) x 10^{-4}	(1.6 ± 0.2) x 10^{-3}
E: Munger Landing	(3.6 ± 0.1) x 10^{-2}	(6 ± 1) x 10^{-4}	(3.5 ± 0.2) x 10^{-4}	(1.49 ± 0.08) x 10^{-3}
F: Wastewater	(5.7 ± 0.3) x 10^{-2}	(1.5 ± 0.2) x 10^{-3}	(2.6 ± 0.3) x 10^{-4}	(2.1 ± 0.2) x 10^{-3}
G: Blatnik Bridge	(4.18 ± 0.7) x 10^{-2}	(8.1 ± 1) x 10^{-4}	(3.56 ± 0.03) x 10^{-4}	(1.8 ± 0.1) x 10^{-3}
H: Wisconsin Point	(1.19 ± 0.06) x 10^{-1}	(2.2 ± 0.5) x 10^{-3}	(4 ± 2) x 10^{-4}	(5 ± 1) x 10^{-3}

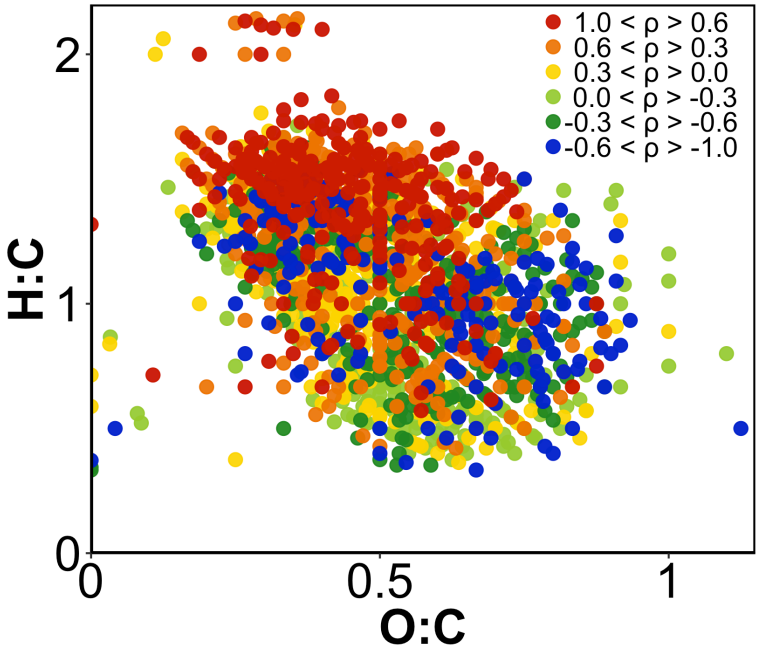

Figure C.17. Spearman rank correlations between formula intensity as detected by FT-ICR MS and $k_{obs,C}$ for venlafaxine photodegradation. Only formulas detected in ≥6 samples are included on the plot.

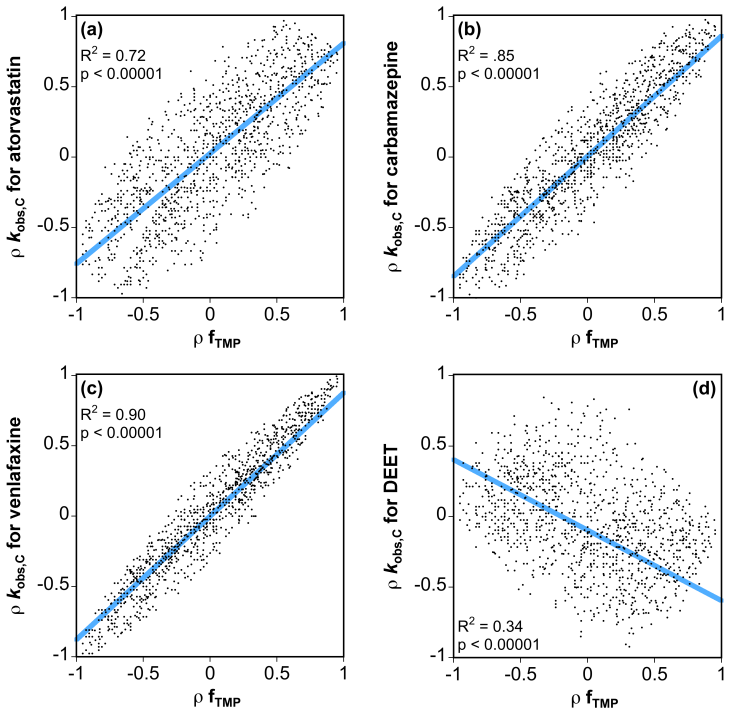

Figure C.18. Scatter plots showing the relationship between Spearman rank rho values for formula intensity with f_{TMP} and $k_{obs,C}$ (a) atorvastatin, (b) carbamazepine, (c) venlafaxine, and (d) DEET

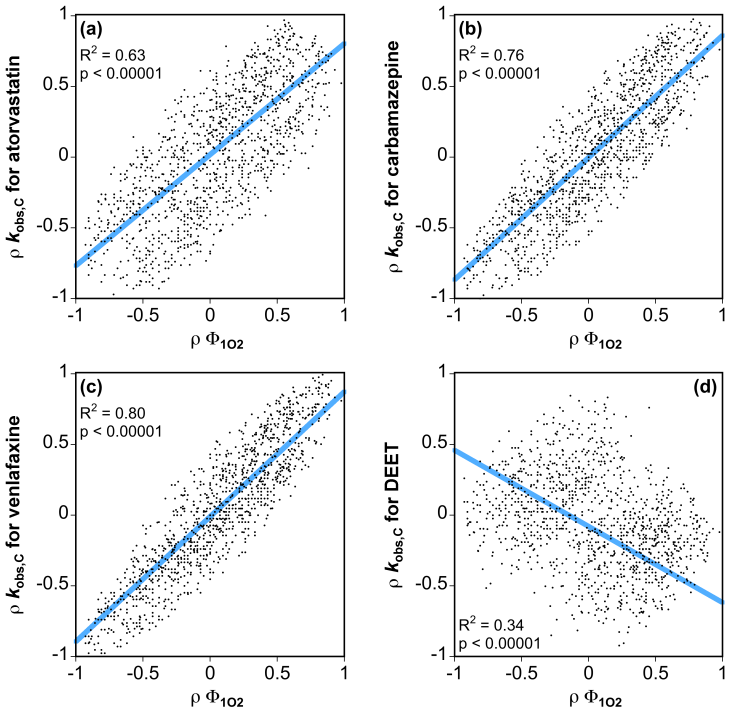

Figure C.19. Scatter plots showing the relationship between Spearman rank rho values for formula intensity with Φ_{1O2} and $k_{obs,C}$ (a) atorvastatin, (b) carbamazepine, (c) venlafaxine, and (d) DEET

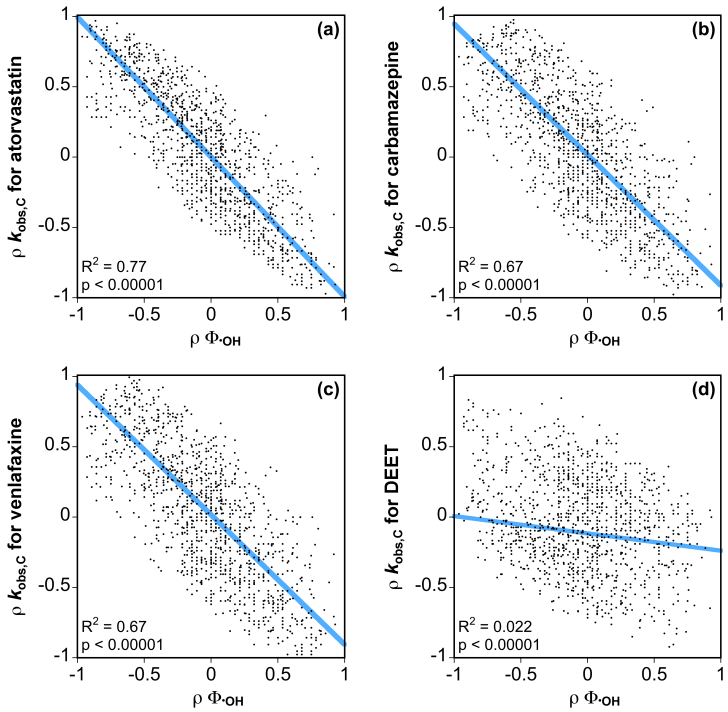

Figure C.20. Scatter plots showing the relationship between Spearman rank rho values for formula intensity with $\Phi_{\bullet OH}$ and $k_{obs,C}$ (a) atorvastatin, (b) carbamazepine, (c) venlafaxine, and (d) DEET

Quencher experiments were performed to further show that each PPRI has differing importance towards the fate of the contaminants. Direct controls were performed in Milli-Q water. Indirect controls were performed in the denoted water sample. Sorbate was added to quench high energy ^{3}DOM, histidine or DABCO to quench $^1O_2$, IPA to quench radicals including $^\bullet$OH, and anoxic experiments were performed by purging sample with N_2 prior to irradiation to increase the lifetimes of triplets.

Table C.13. Photodegradation rate constants for atorvastatin, carbamazepine, and venlafaxine in the presence of 3 mM quencher. Direct controls were performed in Nanopure water. Indirect controls were performed in the denoted water sample with no quencher present. DABCO was used as the $^1O_2$ quencher for carbamazepine and histidine was used for atorvastatin and venlafaxine. Error represents the standard deviation of triplicate measurements.

	Atorvastatin (hr^{-1})		**Carbamazepine (hr^{-1})**		**Venlafaxine (hr^{-1})**	
	Blatnik Bridge	Wastewater	Blatnik Bridge	Wastewater	Munger Landing	Wastewater
Direct	$(1 \pm 2) \times 10^{-2}$	$(1 \pm 2) \times 10^{-2}$	$(2 \pm 3) \times 10^{-3}$	$(2 \pm 3) \times 10^{-3}$	$(1.1 \pm 0.4) \times 10^{-2}$	$(1.1 \pm 0.4) \times 10^{-2}$
Indirect	1.12 ± 0.02	1.14 ± 0.06	$(2.2 \pm 0.3) \times 10^{-2}$	$(3.7 \pm 0.5) \times 10^{-2}$	$(4.5 \pm 0.2) \times 10^{-2}$	$(5.4 \pm 0.5) \times 10^{-2}$
Sorbate	$(9.1 \pm 0.3) \times 10^{-1}$	1.08 ± 0.06	$(7 \pm 2) \times 10^{-3}$	$(5 \pm 2) \times 10^{-3}$	$(9 \pm 4) \times 10^{-3}$	$(8 \pm 6) \times 10^{-3}$
DABCO/ Histidine	1.06 ± 0.04	1.39 ± 0.05	$(1.8 \pm 0.5) \times 10^{-2}$	$(1.4 \pm 0.1) \times 10^{-2}$	$(1.1 \pm 0.2) \times 10^{-2}$	$(1.9 \pm 0.3) \times 10^{-2}$
IPA	1.08 ± 0.02	1.53 ± 0.05	$(1.8 \pm 0.1) \times 10^{-2}$	$(3.8 \pm 0.2) \times 10^{-2}$	$(3.0 \pm 0.2) \times 10^{-2}$	$(3.2 \pm 0.7) \times 10^{-2}$
Anoxic	1.6 ± -0.3	1.8 ± 0.3	$(5 \pm 0.5) \times 10^{-1}$	$(5.1 \pm 0.3) \times 10^{-1}$	$(1.7 \pm 0.3) \times 10^{-1}$	$(2.1 \pm 0.2) \times 10^{-1}$

Table C.14. Photodegradation rate constants for DEET venlafaxine in the presence of 3 mM quencher. Direct controls were performed in Milli-Q water. Indirect controls were performed in the denoted water sample with no quencher present. Error represents the standard deviation of duplicate measurements.

	DEET (hr^{-1})			
	Sand Creek	East Detroit	Wastewater	Blatnik Bridge
Direct	$(1.6 \pm 0.2) \times 10^{-5}$	$(1.6 \pm 0.2) \times 10^{-5}$	$(1.6 \pm 0.2) \times 10^{-5}$	$(1.6 \pm 0.2) \times 10^{-5}$
Indirect	$(1.9 \pm 0.2) \times 10^{-2}$	$(1.1 \pm 0.1) \times 10^{-2}$	$(6.3 \pm 0.8) \times 10^{-3}$	$(9.24 \pm 0.08) \times 10^{-3}$
Sorbate	$(7 \pm 1) \times 10^{-4}$	$(2.63 \pm 0.08) \times 10^{-3}$	$(5 \pm 3) \times 10^{-4}$	$(2.4 \pm 0.8) \times 10^{-3}$
Histidine	$(1.72 \pm 0.03) \times 10^{-2}$	$(6.9 \pm 0.2) \times 10^{-3}$	$(2.5 \pm 0.2) \times 10^{-3}$	$(5.9 \pm 0.4) \times 10^{-3}$
IPA	$(2.52 \pm 0.08) \times 10^{-3}$	$(5.7 \pm 0.5) \times 10^{-4}$	$(1.1 \pm 0.2) \times 10^{-3}$	$(9 \pm 3) \times 10^{-4}$

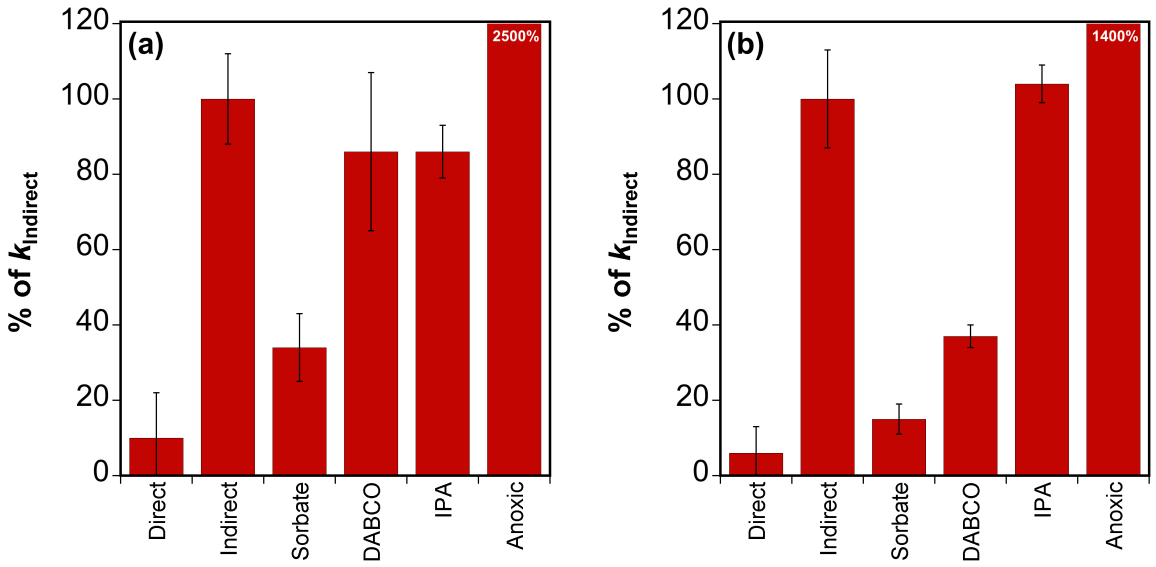

Figure C.21. Quencher experiments performed with carbamazepine in (a) Blatnik Bridge water and (b) wastewater effluent. Note that the photolysis rate increased by 2500 and 1400%, respectively, under anoxic conditions. Error bars represent the standard deviation of triplicate measurements.

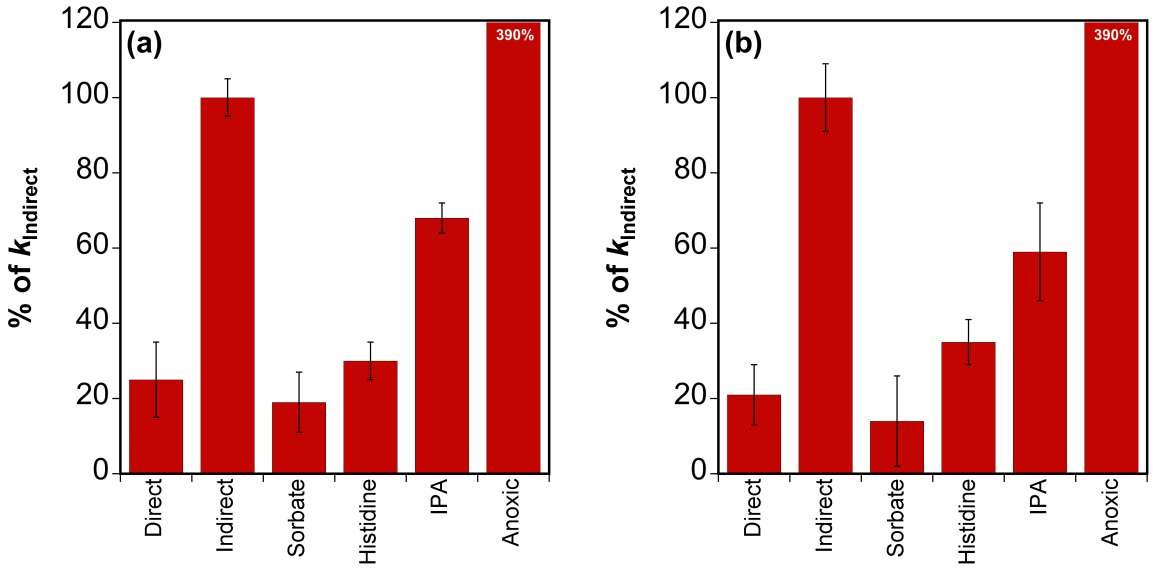

Figure C.22. Quencher experiments performed with venlafaxine in (a) Munger Landing water and (b) wastewater effluent. Note that the photolysis rate increased by 390% in both waters under anoxic conditions. Error bars represent the standard deviation in triplicate measurements.

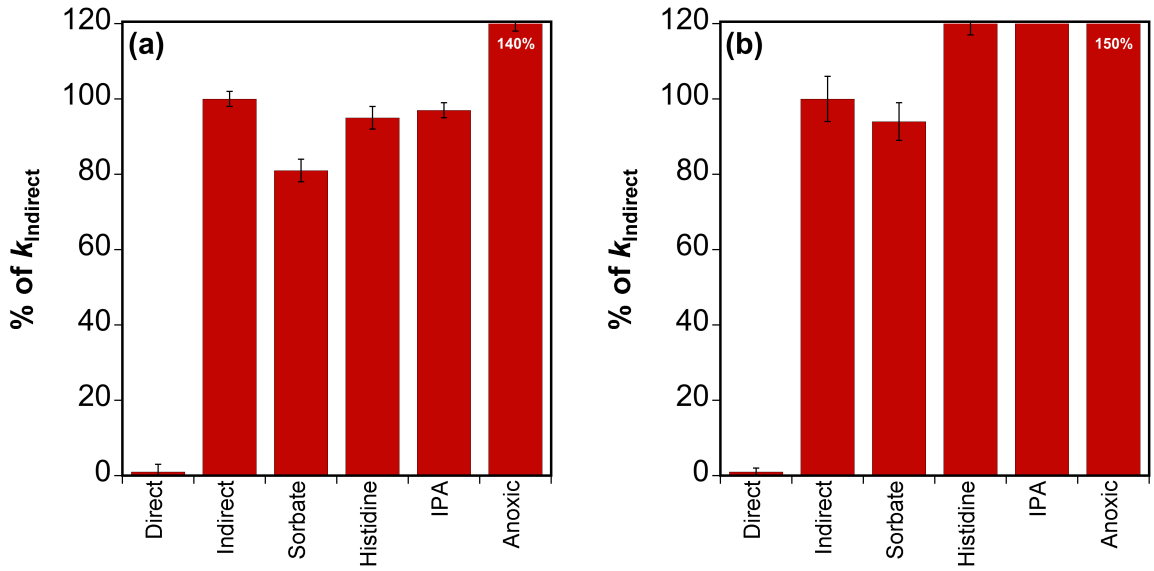

Figure C.23. Quencher experiments performed with atorvastatin in (a) Blatnik Bridge water and (b) wastewater effluent. Note that the photolysis rate increased by 140 and 150%, respectively, under anoxic conditions. Error bars represent the standard deviation in triplicate measurements.

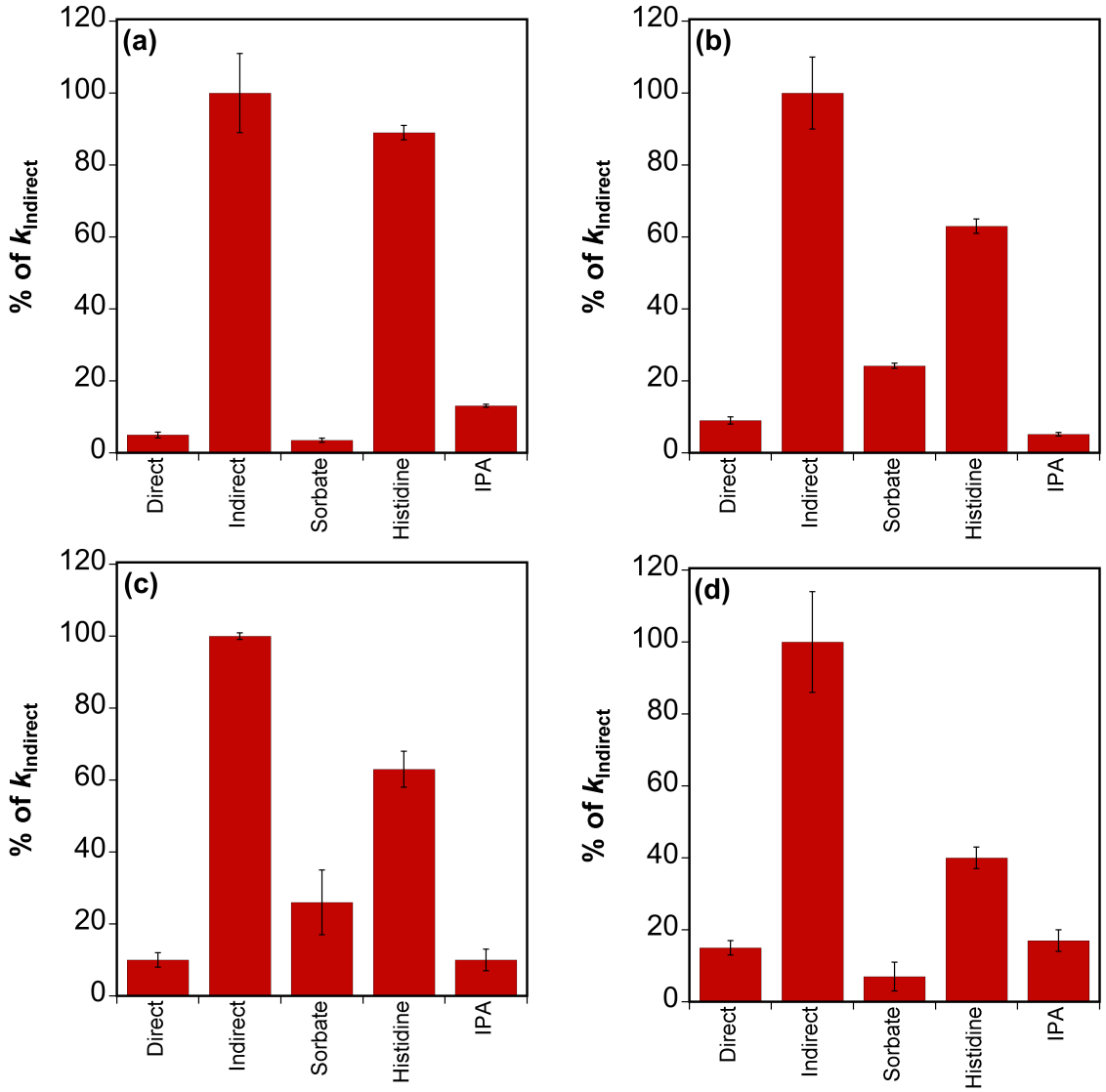

Figure C.24. Quencher experiments performed with DEET in (a) Sand Creek, (b) East Detroit, (c) Wastewater, and (d) Blatnik Bridge samples. Error bars represent the standard deviation of duplicate measurements.

The reactivity of DEET with •OH was further assessed by comparing measured $[•OH]_{ss}$ with the observed indirect photodegradation rate constant of DEET. First, the predicted pseudo-first order rate constant ($k'_{OH,pred}$) assuming DEET only reacts with •OH was calculated by multiplying $[•OH]_{ss}$ (**Table C.8**) by 4.95 x 10^9 M^{-1} sec^{-1} (i.e., the measured rate constant for the reaction with hydroxyl radical and DEET).[19] Second, the observed indirect photodegradation rate

constant of DEET attributable to •OH ($k'_{OH,obs}$) was calculated by subtracting the rate constant observed in the presence of IPA from the indirect photolysis rate constant observed in the absence of the quencher. These values are similar within a factor of 2 (**Table C.15**).

Table C.15. Comparison of DEET indirect photodegradation rate constants calculated based on observed $[^{\bullet}OH]_{ss}$ and quenching by IPA.

Sample	$k'_{OH,pred}$ (s^{-1})	$k'_{OH,obs}$ (s^{-1})	$k'_{OH,pred}$ / $k'_{OH,obs}$
Sand Creek	1.01×10^{-5}	4.57×10^{-6}	2.22
East Detroit	4.46×10^{-6}	2.89×10^{-6}	1.54
Blatnik Bridge	1.44×10^{-6}	2.31×10^{-6}	0.62

C.8 References

(1) Christensen, V. G.; Lee, K. E.; Kieta, K. A.; Elliott, S. M. Presence of selected chemicals of emerging concern in water and bottom sediment from the St. Louis River, St. Louis Bay, and Superior Bay, Minnesota and Wisconsin, 2010. **2012**, U.S. Geological Survey Scientific Investigations Report, 1-36.

(2) Angradi, T. R.; Pearson, M. S.; Bolgrien, D. W.; Bellinger, B. J.; Starry, M. A.; Reschke, C. Predicting submerged aquatic vegetation cover and occurrence in a Lake Superior Estuary. *J. Great Lakes Res.* **2013**, *39* (4), 536–546.

(3) Minor, E. C.; Steinbring, C. J.; Longnecker, K.; Kujawinski, E. B. Characterization of dissolved organic matter in Lake Superior and its watershed using ultrahigh resolution mass spectrometry. *Org. Geochem.* **2012**, *43*, 1–11.

(4) Stephens, B. M.; Minor, E. C. DOM Characteristics along the continuum from river to receiving basin: A comparison of freshwater and saline transects. *Aquat. Sci.* **2010**, *72* (4), 403–417.

(5) Bellinger, B. J.; Hoffman, J. C.; Angradi, T. R.; Bolgrien, D. W.; Starry, M.; Elonen, C.; Jicha, T. M.; Lehto, L. R. P.; Seifert-Monson, L. R.; Pearson, M. S.; Anderson, L.; Hill, B. H. Water quality in the St. Louis River area of concern, Lake Superior: Historical and current conditions and delisting implications. *J. Great Lakes Res.* **2016**, *42* (1), 28–38.

(6) Loken, L. C.; Small, G. E.; Finlay, J. C.; Sterner, R. W.; Stanley, E. H. Nitrogen cycling in a freshwater estuary. *Biogeochemistry* **2016**, *127* (2–3), 199–216.

(7) Dittmar, T.; Koch, B.; Hertkorn, N.; Kattner, G. A. A simple and efficient method for the solid-phase extraction of dissolved organic matter (SPE-DOM) from seawater. *Limnol. Oceanogr.: Methods.* **2008**, *6,* 230–235.

(8) Koch, B. P.; Dittmar, T.; Witt, M.; Kattner, G. Fundamentals of molecular formula

assignment to ultrahigh resolution mass data of natural organic matter. *Anal. Chem.* **2007**, *79* (4), 1758–1763.

(9) Maizel, A. C.; Remucal, C. K. Molecular composition and photochemical reactivity of size-fractionated dissolved organic matter. *Environ. Sci. Technol.* **2017**, *51*, 2113–2123.

(10) Maizel, A. C.; Remucal, C. K. The effect of advanced secondary municipal wastewater treatment on the molecular composition of dissolved organic matter. *Water Res.* **2017**, *122*, 42–52.

(11) Kim, S.; Kramer, R. W.; Hatcher, P. G. Graphical method for analysis of ultrahigh-resolution broadband mass spectra of natural organic matter, the van Krevelen diagram. *Anal. Chem.* **2003**, *75* (20), 5336–5344.

(12) Maizel, A. C.; Li, J.; Remucal, C. K. Relationships between dissolved organic matter composition and photochemistry in lakes of diverse trophic status. *Environ. Sci. Technol.* **2017**, *51* (17), 9624–9632.

(13) Minor, E.; Stephens, B. Dissolved organic matter characteristics within the Lake Superior watershed. *Org. Geochem.* **2008**, *39* (11), 1489–1501.

(14) Canonica, S.; Freiburghaus, M. Electron-rich phenols for probing the photochemical reactivity of freshwaters. *Environ. Sci. Technol.* **2001**, *35* (4), 690–695.

(15) Appiani, E.; Ossola, R.; Latch, D. E.; Erickson, P. R.; McNeill, K. Aqueous singlet oxygen reaction kinetics of furfuryl alcohol: Effect of temperature, pH, and salt content. *Environ. Sci. Process. Impacts* **2017**, *19* (4), 507–516.

(16) McCabe, A. J.; Arnold, W. A. Seasonal and spatial variabilities in the water chemistry of prairie pothole wetlands influence the photoproduction of reactive intermediates. *Chemosphere* **2016**, *155*, 640–647.

(17) Page, S. E.; Arnold, W. A; McNeill, K. Terephthalate as a probe for photochemically generated hydroxyl radical. *J. Environ. Monit.* **2010**, *12* (9), 1658–1665.

(18) De Laurentiis, E.; Buoso, S.; Maurino, V.; Minero, C.; Vione, D. Optical and photochemical characterization of chromophoric dissolved organic matter from lakes in Terra Nova Bay, Antarctica. Evidence of considerable photoreactivity in an extreme environment. *Environ. Sci. Technol.* **2013**, *47* (24), 14089–14098.

(19) Mostafa, S.; Rosario-Ortiz, F. L. Singlet oxygen formation from wastewater organic matter. *Environ. Sci. Technol.* **2013**, *47* (15), 8179–8186.

Appendix D

Supporting Information for Chapter 5

D.1 Sample Sites

Seven samples were collected from the North Temperate Lakes-Long Term Ecological Research (NTL-LTER) sites in northern Wisconsin (**Table D.1**), including two from dystrophic bogs (Crystal Bog and Trout Bog), one from a mesotrophic lake (Allequash Lake), and four from oligotrophic lakes (Big Muskellunge Lake, Crystal Lake, Sparkling Lake, and Trout Lake). Surrounding land cover from these sites includes primarily forests and wetlands.

Eight samples were collected in and around Mankato, Minnesota where waters are largely impacted by surrounding agricultural fields. Two samples were collected from the Minnesota River including from up- and downstream of the Mankato Water Resource Recovery Facility (WRRF) discharge (Memories and Kiwannis, respectively). Three effluent samples were taken directly from WRRF following secondary treatment. The WRRF pre-Cl sample was collected prior to disinfection and the WRRF post-Cl sample was taken following chlorination and subsequent dechlorination with sodium bisulfite. An additional sample, WRRF Reuse, is an effluent sample used to cool the Mankato Energy Center; it was chlorinated but not dechlorinated and therefore had a higher chlorine residual than the final effluent (i.e., >5.0 mg L^{-1}). Another sample was collected from a tributary to the Minnesota River (Seven-mile Creek). Finally, two samples were collected from agricultural ditches (Wammer Ditch and Olsen Ditch), which were both surrounding by cornfields.

Ten samples were collected from the Yahara watershed in and around Madison, Wisconsin. Three samples were taken from the Yahara River, including a sample collected upstream of the chain of lakes, downstream of the chain of lakes, and downstream of the confluence with Badfish Creek (North Yahara, South Yahara, and Confluence, respectively). Samples were also collected from Lake Mendota, Lake Wingra, and Lake Kegonsa, which are core NTL-LTER lakes. An additional two samples were collected from up- and downstream of discharge from the Madison Metropolitan Sewerage District (MMDS; Badfish Upstream and Badfish Downstream, respectively). Samples of the effluent from MMSD include one taken after secondary treatment (pre-UV) and after disinfection with ultraviolet light (post-UV).

Eleven samples were taken from the St. Louis River and Estuary and the Western Lake Superior Sanitary District (WLSSD) treatment plant. A tributary of the St. Louis River (Sand Creek) was sampled along with four samples collected from various locations within the river (Meadowlands, River Inn, Munger Landing, and East Detroit). Additional samples were collected downstream of the discharge from the WLSSD treatment plant (Blatnik Bridge) and at the end of the estuary to Lake Superior collected from the southern side of the peninsula (Wisconsin Point). In total, four effluent samples were collected from WLSSD treatment plant including two after secondary treatment (pre-Cl) and two following disinfection by chlorine and dichlorination with sodium bisulfite (post-Cl). One of each of these was collected in May of 2020 when local paper mills were shut off (no mill samples) and in September of 2020 while the plant was receiving its usual influent.

Twelve samples were collected in the Twin Cities in Minnesota including three in the Minnesota River (River Front Park, East River Parkway, and Minnesota River), another in the Minnesota River downstream of the Metropolitan Wastewater Treatment Plant (Metro WWTP)

effluent discharge (Metro Downstream), and another in the Minnesota River further downstream of the Eagles Point WWTP effluent discharge (Eagles Downstream). Three samples were taken from oligotrophic lakes within the city limits including Lake of the Isles, Vadnais Lake, and Lake Phalen. Effluent was from the Metro WWTP after secondary treatment (pre-Cl) and after chlorination and dechlorination with sodium bisulfite (post-Cl), and from Eagles WWTP after secondary treatment (pre-UV) and after following disinfection with UV light (post-UV).

All natural water samples were collected from the top 1 m of the water. Lake and bog samples were collected from near the middle of the water body via boat. Moving water samples were collected by wading into the water. After collection, all samples were filtered through 0.45 micron nylon filters within 36 hours and stored in the dark at 4ºC until analysis.

Table D.1. Names, data of collection, coordinates, designated sample type for analysis and a brief description for all samples analyzed in this study.

Sample	Date	Coordinates	Type	Description
Northern NTL-LTER Lakes				
Crystal Bog	August 29, 2018	46.00800, -89.60570	Rural	Dystrophic bog
Trout Bog	August 29, 2018	46.04170, -89.68540	Rural	Dystrophic bog
Allequash Lake	August 30, 2018	46.04810, -89.61240	Rural	Mesotrophic lake
Big Muskellunge Lake	August 30, 2018	46.02730, -89.59350	Rural	Oligotrophic lake
Crystal Lake	August 30, 2018	45.9989, -89.60820	Rural	Oligotrophic lake
Sparkling Lake	August 28, 2018	46.01580, -89.69450	Rural	Oligotrophic lake
Trout Lake	August 30, 2018	46.07900, -89.64640	Rural	Oligotrophic lake
Mankato, Minnesota				
Memories	June 24, 2019	44.15543, -94.04223	Agricultural	Minnesota River; upstream of WRRF discharge
Olsen Ditch	June 25, 2019	44.11394,	Agricultural	Agricultural ditch

		-94.26897		
Wammer Ditch	June 25, 2019	44.13387, -94.30944	Agricultural	Agricultural ditch
Seven-mile Creek	June 24, 2019	44.26217, -94.02657	Agricultural	Tributary to Minnesota River
WRRF pre-Cl	June 24, 2019	44.18249, -94.00132	Wastewater	Final effluent before chlorination
WRRF Reuse	June 24, 2019	44.18249, -94.00132	Wastewater	Post chlorination/ dechlorination, used to cool plant
WRRF post-Cl	June 24, 2019	44.18249, -94.00132	Wastewater	Final effluent chlorination/post chlorination
Kiwannis	June 24, 2019	44.200262, -94.01779	Agricultural	Minnesota River, downstream of WRRF discharge
Yahara Watershed				
North Yahara	July 26, 2019	43.156742 -89.343755	Agricultural	River that flows in Lake Mendota
Lake Mendota	July 25, 2019	43.11294, -89.42145	Agricultural	Eutrophic Lake
Lake Wingra	October 9, 2019	43.053768, -89.419910	Agricultural	Eutrophic Lake
Lake Kegonsa	October 9, 2019	42.963891, -89.254772	Agricultural	Eutrophic Lake
South Yahara	July 26, 2019	42.94137, -89.20235	Agricultural	Yahara River; downstream of Lake Kegonsa
Badfish Upstream	September 18, 2019	42.849748, -89.255665	Agricultural	Badfish Creek; upstream of MMSD discharge
Ninesprings Pre-UV	July 30, 2019	43.03967, -89.35752	Wastewater	Effluent collected before UV disinfection
Ninesprings Post-UV	July 30, 2019	43.03967, -89.35752	Wastewater	Effluent collected before UV disinfection
Badfish Downstream	September 18, 2019	42.849213, -89.255536	Wastewater	Badfish Creek; downstream of MMSD discharge
Confluence	July 26, 2019	42.82017, -89.16300	Agricultural	Yahara River; downstream of confluence with Badfish Creek
St. Louis River and Estuary				
Sand Creek	September 3, 2020	47.185510, -92.853331	Rural	Tributary to St. Louis River

Meadowlands	September 3, 2020	47.068966, -92.775002	Rural	St. Louis River
River Inn	September 3, 2020	46.702892, -92.418854	Rural	St. Louis River
Munger Landing	September 3, 2020	46.700820, -92.207148	Rural	St. Louis River
East Detroit	September 3, 2020	46.651824, -92.203205	Rural	St. Louis River
WLSSD Pre-Cl; Mill Shutdown	May 6, 2020	46.761325, -92.124443	Wastewater	WLSSD effluent collected during local paper mill shutdown, pre-chlorination
WLSSD PostCl: Mill Shutdown	May 6, 2020	46.761325, -92.124443	Wastewater	WLSSD effluent collected during local paper mill shutdown, post- chlorination/ dechlorination
WLSSD Pre-Cl	September 3, 2020	46.761325, -92.124443	Wastewater	WLSSD effluent pre-chlorination
WLSSD Post-Cl	September 3, 2020	46.761325, -92.124443	Wastewater	WLSSD effluent, post-chlorination/ dechlorination
Blatnik Bridge	September 2, 2020	46.751031, -92.102092	Rural	St. Louis River Estuary
Wisconsin Point	September 2, 2020	46.688643, -91.972299	Rural	Shore of Lake Superior
Twin Cities in Minnesota				
River Front Park	August 27, 2020	45.06769, -93.28108	Urban	Minnesota River
East River Parkway	August 27, 2020	44.9579, -93.21307	Urban	Minnesota River
Minnesota River	August 27, 2020	44.88484, -93.17476	Urban	Minnesota River
Metro WWTP Pre-Cl	August 31, 2020	44.92612, -93.04823	Wastewater	Effluent collected pre-chlorination
Metro WWTP Post-Cl	August 31, 2020	44.92569, -93.04829	Wastewater	Effluent collect post chlorination/dechlorination
Metro Downstream	August 31, 2020	44.88195, -93.01738	Urban	Minnesota River; downstream of Metro WWTP discharge
Eagles Point Pre-UV	August 31, 2020	44.78602, -92.91925	Wastewater	Effluent collected pre-UV disinfection
Eagles Point Post-UV	August 31, 2020	44.78602, -92.91925	Wastewater	Effluent collected post UV chlorination

Eagles Point Downstream	August 31, 2020	44.74611, -92.85624	Urban	Minnesota River; downstream of Eagles Point WWTP discharge
Lake of the Isles	August 27, 2020	44.95174, -93.30727	Urban	Oligotrophic Lake
Vadnais Lake	August 27, 2020	45.05128, -93.09446	Urban	Oligotrophic Lake
Lake Phalen	August 27, 2020	44.98705, -93.05589	Urban	Oligotrophic Lake

D.2 Chemicals

All chemicals were used as received. Ultrapure water (18.2 MΩ cm) was obtained from a Milli-Q water purification system. Acetonitrile (HPLC grade), methanol (HPLC grade), hydrochloric acid (concentrated, ACS grade), and potassium hydrogen phthalate (ACS grade) were purchased from Fisher Scientific. Sodium hydroxide (reagent grade), monobasic potassium phosphate (reagent grade), dibasic potassium phosphate (reagent grade), and sodium terephthalate (>98%) were purchased from Signa Aldrich. *para*-Nitroanisole (>99%) was purchased from Acros Organics, formic acid (88% v/v, ACS grade) was purchased from Aqua Solution, furfuryl alcohol (>98%) was purchased from Tokyo Chemical Industry, and pyridine (>99%) was purchased from Alfa Aesar.

D.3 Water Chemistry

A Mettler Toledo EL20 meter was used to measure pH. Values included in **Table D.2** are pH values taken within 2 weeks of photochemical experiments.

Concentrations of dissolved organic carbon ([DOC]) and dissolved inorganic carbon ([DIC]) were measured using a Shimadzu Total Organic Carbon Analyzer. The instrument is externally calibrated but was also verified during each sequence with standards of organic and inorganic carbon made with potassium hydrogen phthalate and sodium bicarbonate, respectively.

Anions including chloride, nitrate, nitrite, and sulfate were measured during anion exchange chromatography (IC) with detection via conductivity measurements on a Dionex ICS-2100 instrument. A Dionex IonPac AS11-HC RFIC^{TM} column was used for analysis (4 x 250 mm) with an attached guard column (4 x 50 mm) packed with the same material. The elution method was isocratic with 7.5 mM sodium hydroxide. Nitrite is not included in **Table D.3** because no detectable amounts (>1.5 ppm) were detected prior to photochemical experiments.

Cations and metals including calcium, iron, potassium, magnesium, and sodium were measured using inductively coupled plasma-optical emission spectroscopy (ICP-OES) on and Agilent 5110 VDV instrument. Concentrations are listed in **Table D.4**.

Absorbance and excitation emission matrices (EEMs) were recorded using a Horiba Aqualog instrument (**Table D.5**). For absorbance, scans were taken from 200-800 nm with 3 nm intervals and 0.1 second accumulation time. EEMs were collected with excitation ranging from 245 – 828 nm in 8 pixel or 4.66 nm intervals. Data processing including corrections for inner filter effects and Rayleigh masking was completed before exporting data.

Table D.2. pH, [DOC], and [DIC] measured in all samples.

Sample	pH	[DOC] (mg-C L^{-1})	[DIC] (mg-C L^{-1})
Crystal Bog	7.5 ± 0.1	11.04 ± 0.06	4.0 ± 0.4
Trout Bog	7.5 ± 0.1	23.7 ± 0.4	1.42 ± 0.02
Allequash Lake	8.4 ± 0.1	4.95 ± 0.09	10.20 ± 0.02
Big Muskellunge Lake	7.9 ± 0.1	4.17 ± 0.06	5.95 ± 0.5
Crystal Lake	7.0 ± 0.1	2.57 ± 0.02	1.38 ± 0.01
Sparkling Lake	8.1 ± 0.1	3.4 ± 0.1	10.70 ± 0.03
Trout Lake	7.9 ± 0.1	3.0 ± 0.2	10.70 ± 0.03
Memories	8.5 ± 0.1	4.60 ± 0.03	63.4 ± 0.1
Olsen Ditch	8.3 ± 0.1	1.8 ± 0.1	77.2 ± 0.2
Wammer Ditch	8.4 ± 0.1	3.3 ± 0.1	68.4 ± 0.1

Seven-mile Creek	8.5 ± 0.1	3.9 ± 0.1	66.8 ± 0.1
WRRF Pre-Cl	8.2 ± 0.1	4.8 ± 0.5	43.2 ± 0.3
WRRF Reuse	8.3 ± 0.1	6.4 ± 1	44.4 ± 0.2
WRRF Post-Cl	8.3 ± 0.1	5.0 ± 0.3	43.5 ± 0.2
Kiwannis	8.4 ± 0.1	4.3 ± 0.1	62.8 ± 0.2
North Yahara	8.4 ± 0.1	4.7 ± 0.1	62.60 ± 0.03
Lake Mendota	8.7 ± 0.1	3.80 ± 0.03	37.40 ± 0.03
Lake Wingra	8.5 ± 0.1	4.3 ± 0.1	41.2 ± 0.1
Lake Kegonsa	8.4 ± 0.1	10.5 ± 0.1	41.0 ± 0.1
South Yahara	8.4 ± 0.1	7.1 ± 0.1	46.8 ± 0.2
Badfish Upstream	8.5 ± 0.1	2.4 ± 0.1	62.0 ± 0.2
Ninesprings PreUV	8.4 ± 0.1	5.3 ± 0.1	67.8 ± 0.3
Ninesprings PostUV	8.6 ± 0.1	5.9 ± 0.3	66.9 ± 0.4
Badfish Downstream	8.4 ± 0.1	4.4 ± 0.6	68.4 ± 0.3
Confluence	8.4 ± 0.1	4.1 ± 0.1	54.8 ± 0.3
Sand Creek	7.7 ± 0.1	69 ± 6	7.5 ± 0.1
Meadowlands	8.1 ± 0.1	28.4 ± 0.8	30 ± 1
River Inn	8.2 ± 0.1	24.8 ± 0.8	20.10 ± 0.04
Munger Landing	8.2 ± 0.1	23.1 ± 0.5	18.24 ± 0.04
East Detroit	8.2 ± 0.1	24.20 ± 0.01	18.39 ± 0.03
WLSSD Pre-Cl; Mill Shutdown	7.3 ± 0.1	29 ± 2	65 ± 1
WLSSD Post-Cl; Mill Shutdown	8.1 ± 0.1	24 ± 2	72.0 ± 0.3
WLSSD Pre-Cl	8.2 ± 0.1	53 ± 5	88.8 ± 0.6
WLSSD Post-Cl	8.3 ± 0.1	43 ± 6	92.7 ± 0.4
Blatnik Bridge	8.4 ± 0.1	18 ± 5	20.8 ± 0.1
Wisconsin Point	8.3 ± 0.1	8 ± 1	11.00 ± 0.03
River Front Park	8.3 ± 0.1	31 ± 4	36.6 ± 0.2
East River Parkway	8.4 ± 0.1	18 ± 9	35.7 ± 0.2
Minnesota River	8.4 ± 0.1	5.2 ± 0.5	53.7 ± 0.2
Metro WWTP Pre-Cl	8.3 ± 0.1	8.2 ± 0.8	53.1 ± 0.4
Metro WWTP Post-Cl	8.3 ± 0.1	9 ± 1	46.8 ± 0.4
Metro Downstream	8.4 ± 0.1	9.03 ± 0.04	41.7 ± 0.2
Eagles Point Pre-UV	8.2 ± 0.1	7.5 ± 0.7	42.0 ± 0.3
Eagles Point Post-UV	8.2 ± 0.1	9 ± 2	42.60 ± 0.03
Eagles Point Downstream	8.4 ± 0.1	8.9 ± 0.4	38.4 ± 0.3

Lake of the Isles	8.5 ± 0.1	8.7 ± 0.3	23.50 ± 0.07
Vadnais Lake	8.5 ± 0.1	7.5 ± 0.4	28.1 ± 0.1
Lake Phalen	8.5 ± 0.1	6.7 ± 0.2	26.80 ± 0.05

Table D.3. Anions measured in all samples.

Sample	$[Cl^-]$ (ppm)	$[SO_4^{3-}]$ (ppm)	$[NO_3^-]$ (ppm)
Crystal Bog	1.1 ± 0.2	< 0.6	< 0.5
Trout Bog	< 0.8	< 0.6	< 0.5
Allequash Lake	< 0.8	2.9 ± 0.2	< 0.5
Big Muskellunge Lake	< 0.8	2.4 ± 0.2	< 0.5
Crystal Lake	0.8 ± 0.2	2.0 ± 0.2	< 0.5
Sparkling Lake	29.6 ± 0.2	3.5 ± 0.2	< 0.5
Trout Lake	2.3 ± 0.2	2.7 ± 0.2	< 0.5
Memories	16.5 ± 0.2	179.4 ± 0.5	18.0 ± 0.1
Olsen Ditch	19.4 ± 0.2	30.2 ± 0.2	44.4 ± 0.2
Wammer Ditch	12.7 ± 0.2	15.5 ± 0.2	32.3 ± 0.1
Seven-mile Creek	14.3 ± 0.2	21.1 ± 0.2	42.2 ± 0.1
WRRF Pre-Cl	317 ± 1	212.6 ± 0.8	70.9 ± 0.5
WRRF Reuse	375 ± 1	224.7 ± 0.8	90.2 ± 0.5
WRRF Post-Cl	371 ± 1	267.4 ± 0.9	86.2 ± 0.5
Kiwannis	16.2 ± 0.2	149.3 ± 0.5	21.4 ± 0.1
North Yahara	45.9 ± 0.2	15.0 ± 0.2	11.3 ± 0.1
Lake Mendota	52.3 ± 0.2	14.5 ± 0.2	< 0.5
Lake Wingra	81.2 ± 0.3	11.8 ± 0.2	< 0.5
Lake Kegonsa	63.9 ± 0.3	11.5 ± 0.2	< 0.5
South Yahara	66.5 ± 0.3	13.0 ± 0.2	0.8 ± 0.1
Badfish Upstream	71.9 ± 0.3	15.6 ± 0.2	14.1 ± 0.1
Ninesprings Pre-UV	357 ± 1	46.4 ± 0.6	76.4 ± 0.5
Ninesprings Post-UV	366 ± 1	47.5 ± 0.6	77.9 ± 0.5
Badfish Downstream	343 ± 1	40.4 ± 0.6	72.5 ± 0.5
Confluence	72.3 ± 0.3	18.1 ± 0.2	10.2 ± 0.1
Sand Creek	1.6 ± 0.5	< 0.6	< 0.5
Meadowlands	10.2 ± 0.4	42.3 ± 0.7	< 0.5
River Inn	6.6 ± 0.4	14.6 ± 0.7	< 0.5
Munger Landing	7.0 ± 0.4	11.0 ± 0.7	< 0.5
East Detroit	6.6 ± 0.4	12.2 ± 0.7	< 0.5

WLSSD Pre-Cl; Mill Shutdown	174 ± 4	93 ± 7	< 0.5
WLSSD Post-Cl; Mill Shutdown	172 ± 4	95 ± 7	< 0.5
WLSSD Pre-Cl	177 ± 4	292 ± 7	0.5 ± 0.3
WLSSD Post-Cl	199 ± 4	319 ± 7	< 0.5
Blatnik Bridge	20 ± 0.4	25.1 ± 0.7	1.1 ± 0.1
Wisconsin Point	1.8 ± 0.5	3.5 ± 0.7	1.2 ± 0.1
River Front Park	17.9 ± 0.4	9.8 ± 0.7	0.8 ± 0.1
East River Parkway	13.5 ± 0.4	8.5 ± 0.7	0.5 ± 0.1
Minnesota River	21.5 ± 0.4	61.3 ± 0.7	16.7 ± 0.1
Metro WWTP Pre-Cl	44.5 ± 0.9	12 ± 1	6.8 ± 0.3
Metro WWTP Post-Cl	227 ± 4	59 ± 7	63 ± 1
Metro Downstream	19.8 ± 0.4	25.5 ± 0.7	4.4 ± 0.1
Eagles Point Pre-UV	335 ± 5	45 ± 7	109 ± 1
Eagles Point Post-UV	341 ± 5	46 ± 7	111 ± 1
Eagles Point Downstream	22.2 ± 0.4	23.6 ± 0.7	5.4 ± 0.1
Lake of the Isles	115 ± 1	7.0 ± 0.7	< 0.5
Vadnais Lake	26.7 ± 0.5	9.0 ± 0.7	< 0.5
Lake Phalen	125 ± 1	7.4 ± 0.7	< 0.5

Table D.4. Concentrations of cations and metals measured in all samples.

Sample	**[Ca^{2+}] (ppm)**	**[Fe] (ppm)**	**[K^{+}] (ppm)**	**[Mg^{2+}] (ppm)**	**[Na^{+}] (ppm)**
Crystal Bog	< 0.8	< 0.1	< 1	< 0.3	1.83 ± 0.3
Trout Bog	1.14 ± 0.04	0.3 ± 0.1	< 1	0.33 ± 0.01	0.8 ± 0.1
Allequash Lake	< 0.8	0.7 ± 0.2	< 1	3.12 ± 0.09	2.0 ± 0.8
Big Muskellunge Lake	6.7 ± 0.3	< 0.1	2.7 ± 0.2	2.0 ± 0.1	1.3 ± 0.2
Crystal Lake	1.04 ± 0.05	< 0.1	< 1	< 0.3	0.7 ± 0.1
Sparkling Lake	15.6 ± 0.1	< 0.1	< 1	4.4 ± 0.1	15.3 ± 0.4
Trout Lake	12.7 ± 0.3	< 0.1	< 1	3.26 ± 0.09	2.7 ± 0.2
Memories	98 ± 12	< 0.1	4.18 ± 0.06	50 ± 3	21 ±1
Olsen Ditch	102 ± 15	< 0.1	2.1 ± 0.3	35 ± 2	8.2 ± 0.2
Wammer Ditch	78 ± 10	< 0.1	1.8 ± 0.3	33 ± 2	7.04 ± 0.02
Seven-mile Creek	89 ± 10	< 0.1	2.6 ± 0.4	31 ± 1	8.0 ± 0.2

WRRF Pre-Cl	96 ± 3	< 0.1	16.58 ± 0.03	36.3 ± 0.1	223 ± 4
WRRF Reuse	30 ± 2	< 0.1	5.6 ± 0.6	10.4 ± 0.7	68 ± 5
WRRF Post-Cl	113 ± 3	< 0.1	20.7 ± 0.8	42.5 ± 0.3	276 ± 6
Kiwannis	94 ± 12	< 0.1	3.7 ± 0.2	45 ± 3	18 ± 1
North Yahara	61 ± 5	< 0.1	2.0 ± 0.2	36 ± 2	22.8 ± 0.9
Lake Mendota	29.1 ± 0.1	< 0.1	3.3 ± 0.2	29 ± 1	27.6 ± 0.8
Lake Wingra	43 ± 1	< 0.1	1.97 ± 0.07	26.0 ± 0.5	40 ± 2
Lake Kegonsa	33.1 ± 0.3	< 0.1	2.86 ± 0.09	23.1 ± 0.8	34 ± 1
South Yahara	37.4 ± 0.6	< 0.1	2.78 ± 0.07	30.5 ± 1.3	35.5 ± 1.2
Badfish Upstream	59.7 ± 9	< 0.1	5.2 ± 0.5	30 ± 5	39 ± 1
Ninesprings Pre-UV	90 ± 4	< 0.1	12.5 ± 0.1	48.0 ± 0.8	230 ± 8
Ninesprings Post-UV	80 ± 7	< 0.1	12 ± 1	45 ± 6	215 ± 12
Badfish Downstream	43.30 ± 0.9	< 0.1	6.1 ± 0.7	22.4 ± 0.5	108 ± 4
Confluence	52 ± 2	< 0.1	33.82 ± .04	34 ± 1	41 ± 2
Sand Creek	12.7 ± 0.6	5.88 ± 0.01	< 0.1	3.62 ± 0.08	3.72 ± 0.49
Meadowlands	24.1 ± 0.3	1.93 ± 0.03	2.51 ± 0.49	25 ± 1	13.08 ± 0.08
River Inn	19.8 ± 0.3	1 ± 0.1	1.5 ± 0.4	13.6 ± 0.3	7.5 ± 0.1
Munger Landing	19.0 ± 0.4	0.66 ± 0.01	1.3 ± 0.3	13.3 ± 0.3	7.0 ± 0.2
East Detroit	19.4 ± 0.8	0.70 ± 0.02	1.4 ± 0.4	11.9 ± 0.8	7.4 ± 0.4
WLSSD Pre-Cl; Mill Shutdown	75 ± 2	0.50 ± 0.03	12.8 ± 0.9	19.220 ± 0.007	142 ± 1
WLSSD Post-Cl; Mill Shutdown	84 ± 2	0.44 ± 0.01	13.3 ± 0.9	19.5 ± 0.1	153 ± 1
WLSSD Pre-Cl	90 ± 4	0.88 ± 0.01	29.9 ± 1.0	14.22 ± 0.08	293 ± 4
WLSSD Post-Cl	90 ± 4	1.02 ± 0.03	34 ± 2	14.3 ± 0.1	299 ± 9
Blatnik Bridge	22.7 ± 0.1	0.33 ± 0.01	2.8 ± 0.3	9.1 ± 0.2	24.6 ± 0.3
Wisconsin Point	14.5 ± 0.5	< 0.1	< 1	3.22 ± 0.08	2.4 ± 0.2
River Front Park	40 ± 3	< 0.1	2.0 ± 0.4	13.2 ± 0.5	11.9 ± 0.1
East River Parkway	38.6 ± 0.3	< 0.1	2.0 ± 0.4	13.4 ± 0.2	8.93 ± 0.08
Minnesota River	68 ± 7	< 0.1	3.9 ± 0.4	30 ± 2	19.6 ± 0.6

Metro WWTP Pre-Cl	79 ± 2	< 0.1	12 ± 1	22.08 ± .06	153 ± 1
Metro WWTP Post-Cl	80 ± 2	< 0.1	13 ± 1	22.18 ± 0.08	159 ± 2
Metro Downstream	50 ± 3	< 0.1	2.7 ± 0.3	19.4 ± 0.5	14.8 ± 0.3
Eagles Point Pre-UV	74 ± 4	< 0.1	14.6 ± 0.1	26.2 ± 0.1	236 ± 4
Eagles Point Post-UV	74 ± 4	< 0.1	14.8 ± 0.2	26.42 ± 0.08	232 ± 33
Eagles Point Downstream	47 ± 3	< 0.1	2.7 ± 0.4	18.1 ± 0.8	16.1 ± 0.1
Lake of the Isles	30.9 ± 0.6	< 0.1	3.75± 0.04	12.1 ± 0.2	73 ± 1
Vadnais Lake	30.6 ± 0.8	< 0.1	2.0 ± 0.3	14.7 ± 0.2	16.5 ± 0.2
Lake Phalen	36.2 ± 0.1	< 0.1	2.46 ± 0.04	14.74 ± 0.05	72 ± 2

Table D.5. Absorbance, the fluorescence index HIX, and EDC measured in all samples.

Sample	**$SUVA_{254}$ (L mg-C^{-1} m^{-1})**	**E_2:E_3**	**HIX**	**EDC (mmol e^- g-C^{-1})**
Crystal Bog	2.16	5.79	1.17	2.34 ± 0.2
Trout Bog	2.89	5.79	0.53	2.85 ± 0.7
Allequash Lake	1.92	7.56	0.51	1.63 ± 0.2
Big Muskellunge Lake	0.47	8.75	0.31	0.26 ± 0.4
Crystal Lake	0.25	8.58	0.73	0.66 ± 0.2
Sparkling Lake	1.08	9.69	0.35	0.76 ± 0.06
Trout Lake	0.81	9.72	0.47	0.71 ± 0.09
Memories	2.6	9.5	0.39	1.25 ± 0.2
Olsen Ditch	4.0	10.77	0.49	0.96 ± 0.03
Wammer Ditch	2.46	9.22	0.29	1.20 ± 0.2
Seven-mile Creek	3.11	7.7	0.33	1.83 ± 0.3
WRRF Pre-Cl	1.68	8.52	0.59	1.61 ± 0.3
WRRF Reuse	1.01	12.48	0.55	0.51 ± 0.3
WRRF Post-Cl	1.33	10.56	0.52	1.13 ± 0.4
Kiwannis	2.56	7.97	0.52	1.16 ± 0.2
North Yahara	2.94	7.5	0.45	2.04 ± 0.3
Lake Mendota	1.58	10.46	0.40	0.76 ± 0.1
Lake Wingra	2.03	8.24	0.74	1.54 ± 0.2
Lake Kegonsa	1.23	5.68	3.18	0.68 ± 0.3
South Yahara	1.35	7.1	0.21	0.78 ±0.09
Badfish Upstream	3.45	7.44	0.38	2.44 ± 0.2
Ninesprings Pre-UV	2.11	6.08	0.34	4.01 ± 0.4
Ninesprings Post-UV	1.72	5.96	0.57	3.21 ± 0.8

Badfish Downstream	2.34	5.98	0.54	4.36 ± 0.1
Confluence	2.39	6.6	0.29	1.19 ± 0.2
Sand Creek	3.31	5.35	1.98	1.55 ± 0.6
Meadowlands	3.18	5.43	0.94	1.53 ± 0.8
River Inn	3.18	6.54	0.89	1.72 ± 0.7
Munger Landing	2.88	6.05	0.41	1.57 ± 0.7
East Detroit	2.97	5.94	0.55	1.64 ± 0.6
WLSSD Pre-Cl; Mill Shutdown	2.18	5.98	0.62	5.3 ± 1
WLSSD Post-Cl; Mill Shutdown	2.06	6.72	0.40	5.38 ± 0.7
WLSSD Pre-Cl	1.86	6.93	0.22	2.1 ± 1
WLSSD Post-Cl	2.34	7.06	0.52	2.43 ± 0.8
Blatnik Bridge	2.13	6.34	0.00	1.42 ± 0.3
Wisconsin Point	0.2	6.52	0.48	0.24 ± 0.02
River Front Park	0.82	7.54	0.41	0.50 ± 0.4
East River Parkway	4.72	13.05	0.52	0.45 ± 0.3
Minnesota River	2.28	7.12	0.41	1.03 ± 0.2
Metro WWTP Pre-Cl	1.51	5.84	0.41	2.01 ± 0.2
Metro WWTP Post-Cl	1.51	5.84	0.27	1.69 ± 0.2
Metro Downstream	2.33	7.22	0.37	1.23 ± 0.4
Eagles Point Pre-UV	1.46	5.07	0.37	2.42 ± 0.3
Eagles Point Post-UV	2.17	7.19	0.48	2.0 ± 0.3
Eagles Point Downstream	2.17	7.19	0.34	1.30 ± 0.4
Lake of the Isles	0.97	9.75	0.28	0.67 ± 0.2
Vadnais Lake	1.64	10.28	0.42	0.98 ± 0.3
Lake Phalen	1.3	10.97	0.32	0.76 ± 0.3

D.4 Mass Spectrometry

Samples were acidified to pH 2.01 ± 0.05 with hydrochloric acid (HCl) prior to solid phase extraction (SPE). Agilent PPL cartridges were used for the SPE as has been recommended elsewhere with recoveries typically between 50-70%.[1,2] Cartridges were activated with 5 mL of methanol and then 500 mL of acidified sample was drawn through the cartridges using vacuum filtration. Note that only about 300 mL of the Sand Creek sample was drawn through the cartridge because at this point the stationary phase was visibly saturated in this high [DOC] sample. Next, 1 mL of 0.01 M HCl was pulled through the cartridge to remove any salts, and the cartridge was

dried with air for 5 minutes. The extracted organic matter was then diluted in 5 mL of methanol. Recoveries with this method range generally range from 50 – 70%.[1]

Methanol extracts were diluted 100x in 50:50 acetonitrile:ultrapure water and directly injected into a SolariX XR 12T FT-ICR MS (Bruker) via a Hamilton syringe at a flow rate of 3.0 μL min^{-1} and electrospray ionization operating in negative mode. 350 scans were collected from 200 – 800 Da. Accumulation time was adjusted so total ion counts were approximately 10^8 prior to data collection and were generally 0.8 – 1 seconds. Masses with signal to noise > 3 were exported for processing.

Exported masses were linearly calibrated using known formulas in DOM.[3] Signatures were then compared to a list of $^{13}C_{0-1}{}^{12}C_{5-80}H_{0-120}O_{0-80}N_{0-3}S_{0-1}$ containing formulas. Matched formulas were required to have < 0.2 ppm error and be part of a homologous series (+ CH_2 or CH_4 versus O) to be considered an identified formula. Numbers (**Table D.6**), percentages (**Table D.7**), and weighted averages of hydrogen to carbon ($H:C_w$), oxygen to carbon ($O:C_w$) and double bond equivalents (DBE_w; **Table D.8**) were calculated for each sample.

Table D.6. Total number of identified formulas and numbers of CHO-only, $CHON_1$, $CHON_2$, $CHON_3$, $CHOS_1$, and $CHON_1S_1$ identified formulas in all samples.

Sample	# Total	# CHO	# $CHON_1$	# $CHON_2$	# $CHON_3$	# $CHOS_1$	# $CHON_1S_1$
Crystal Bog	2691	1519	888	70	56	157	1
Trout Bog	2172	1419	600	37	28	87	1
Allequash Lake	3300	1577	1123	146	102	283	69
Big Muskellunge Lake	3716	1435	1275	192	289	372	153
Crystal Lake	3231	1229	1223	126	231	329	93
Sparkling Lake	3960	1563	1303	192	268	472	162
Trout Lake	3555	1532	1238	154	197	337	97
Memories	4267	1502	1157	518	429	435	226

Olsen Ditch	3300	1236	995	447	346	185	91
Wammer Ditch	4290	1508	1179	567	468	369	199
Seven-mile Creek	4176	1525	1140	529	431	363	188
WRRF Pre-Cl	4772	1491	1133	379	461	854	454
WRRF Reuse	4336	1377	1145	279	377	808	350
WRRF Post-Cl	4689	1495	1105	364	420	856	449
Kiwannis	4217	1517	1152	510	428	403	207
North Yahara	4608	1711	1257	567	417	450	206
Lake Mendota	4970	1700	1312	619	522	536	281
Lake Wingra	4988	1841	1272	492	393	727	263
Lake Kegonsa	5045	1754	1305	616	513	576	281
South Yahara	5169	1773	1339	615	517	614	311
Badfish Upstream	4852	1770	1292	552	471	558	209
Ninesprings Pre-UV	5155	1713	1121	476	430	930	485
Ninesprings Post-UV	5047	1672	1072	432	496	895	480
Badfish Downstream	5322	1757	1189	527	480	899	470
Confluence	4955	1702	1269	574	516	591	303
Sand Creek	3057	1938	800	169	42	94	14
Meadowlands	3047	1948	813	151	37	85	13
River Inn	3266	1951	983	206	36	81	9
Munger Landing	3124	1858	868	171	69	149	9
East Detroit	3029	1768	824	183	74	162	18
WLSSD Pre-Cl; Mill Shutdown	3245	1563	561	24	88	975	34
WLSSD Post-Cl; Mill Shutdown	4272	1894	952	122	141	851	312
WLSSD Pre-Cl	3998	1932	1079	45	54	823	65
WLSSD Post-Cl	3878	1917	996	48	90	801	26
Blatnik Bridge	3338	1940	799	136	104	354	5
Wisconsin Point	2150	1606	285	65	22	169	3
River Front Park	3601	1851	946	324	231	244	5
East River Parkway	3822	2074	966	300	228	246	8
Minnesota River	3477	1557	881	381	308	321	29
Metro WWTP Pre-Cl	4842	1896	1136	483	429	658	240

Metro WWTP Post-Cl	4466	1615	1037	461	403	680	270
Metro Downstream	4028	2175	1054	336	236	219	8
Eagles Point Pre-UV	4451	1716	944	451	390	700	250
Eagles Point Post-UV	4417	1742	903	458	371	720	223
Eagles Point Downstream	4055	2204	1007	318	230	288	8
Lake of the Isles	4422	1960	988	317	268	771	118
Vadnais Lake	4038	2081	997	386	258	301	15
Lake Phalen	4419	2026	1007	306	282	745	53

Table D.7. Percentages of CHO-only, N-containing, and S-containing formulas identified in each sample.

Sample	% CHO-only	% N-containing	% S-containing
Crystal Bog	56.4	37.7	5.9
Trout Bog	65.3	30.7	4.1
Allequash Lake	47.8	43.6	10.7
Big Muskellunge Lake	38.6	51.4	14.1
Crystal Lake	38.0	51.8	13.1
Sparkling Lake	39.5	48.6	16.0
Trout Lake	43.1	47.4	12.2
Memories	35.2	54.6	15.5
Olsen Ditch	37.5	56.9	8.4
Wammer Ditch	35.2	56.2	13.2
Seven-mile Creek	36.5	54.8	13.2
WRRF Pre-Cl	31.2	50.9	27.4
WRRF Reuse	31.8	49.6	26.7
WRRF Post-Cl	31.9	49.9	27.8
Kiwannis	36.0	54.5	14.5
North Yahara	37.1	53.1	14.2
Lake Mendota	34.2	55.0	16.4
Lake Wingra	36.9	48.5	19.8
Lake Kegonsa	34.8	53.8	17.0
South Yahara	34.3	53.8	17.9
Badfish Upstream	36.5	52.0	15.8
Ninesprings Pre-UV	33.2	48.7	27.4

Ninesprings Post-UV	33.1	49.1	27.2
Badfish Downstream	33.0	50.1	25.7
Confluence	34.3	53.7	18.0
Sand Creek	63.4	33.5	3.5
Meadowlands	63.9	33.3	3.2
River Inn	59.7	37.8	2.8
Munger Landing	59.5	35.8	5.1
East Detroit	58.4	36.3	5.9
WLSSD Pre-Cl; Mill Shutdown	48.2	21.8	31.1
WLSSD Post-Cl; Mill Shutdown	44.3	35.7	27.2
WLSSD Pre-Cl	48.3	31.1	22.2
WLSSD Post-Cl	49.4	29.9	21.3
Blatnik Bridge	58.1	31.3	10.8
Wisconsin Point	74.7	17.4	8.0
River Front Park	51.4	41.8	6.9
East River Parkway	54.3	39.3	6.6
Minnesota River	44.8	46.0	10.1
Metro WWTP Pre-Cl	39.2	47.3	18.5
Metro WWTP Post-Cl	36.2	48.6	21.3
Metro Downstream	54.0	40.6	5.6
Eagles Point Pre-UV	38.6	45.7	21.3
Eagles Point Post-UV	39.4	44.3	21.3
Eagles Point Downstream	54.4	38.5	7.3
Lake of the Isles	44.3	38.2	20.1
Vadnais Lake	51.5	41.0	7.8
Lake Phalen	45.8	37.3	18.1

Table D.8. Weighted averages of H:C, O:C, DBE for identified formulas in all samples.

Sample	**$H:C_w$**	**$O:C_w$**	**DBE_w**
Crystal Bog	1.11	0.53	9.67
Trout Bog	1.09	0.55	9.93
Allequash Lake	1.15	0.52	9.19
Big Muskellunge Lake	1.28	0.51	7.78
Crystal Lake	1.36	0.49	6.65
Sparkling Lake	1.23	0.49	8.41

Trout Lake	1.23	0.51	8.42
Memories	1.16	0.52	9.49
Olsen Ditch	1.15	0.51	9.79
Wammer Ditch	1.17	0.50	9.30
Seven-mile Creek	1.15	0.51	9.63
WRRF Pre-Cl	1.27	0.48	8.10
WRRF Reuse	1.29	0.48	7.75
WRRF Post-Cl	1.28	0.49	7.97
Kiwannis	1.17	0.51	9.42
North Yahara	1.12	0.51	9.55
Lake Mendota	1.22	0.50	8.66
Lake Wingra	1.20	0.49	8.76
Lake Kegonsa	1.20	0.50	8.92
South Yahara	1.20	0.50	8.84
Badfish Upstream	1.20	0.48	9.02
Ninesprings Pre-UV	1.34	0.51	7.26
Ninesprings Post-UV	1.35	0.49	7.15
Badfish Downstream	1.26	0.47	8.22
Confluence	1.18	0.51	9.03
Sand Creek	1.28	0.41	7.81
Meadowlands	1.33	0.38	7.19
River Inn	1.26	0.43	8.05
Munger Landing	1.29	0.40	7.68
East Detroit	1.32	0.39	7.39
WLSSD Pre-Cl; Mill Shutdown	1.40	0.40	6.66
WLSSD Post-Cl; Mill Shutdown	1.43	0.39	6.25
WLSSD Pre-Cl	1.27	0.46	7.60
WLSSD Post-Cl	1.33	0.43	7.09
Blatnik Bridge	1.35	0.37	6.96
Wisconsin Point	1.60	0.20	4.52
River Front Park	1.34	0.38	7.09
East River Parkway	1.43	0.30	6.22
Minnesota River	1.49	0.30	5.55
Metro WWTP Pre-Cl	1.51	0.29	5.32
Metro WWTP Post-Cl	1.48	0.33	5.52
Metro Downstream	1.41	0.33	6.48
Eagles Point Pre-UV	1.55	0.28	4.93

Eagles Point Post-UV	1.54	0.28	4.96
Eagles Point Downstream	1.47	0.28	5.83
Lake of the Isles	1.51	0.28	5.47
Vadnais Lake	1.45	0.31	6.07
Lake Phalen	1.46	0.30	5.89

D.5 EDC

A 1 mM stock solution of 2,2'-azino-bis(3-ethyl-6-benzothiaolinesulfonate) (ABTS) solution was prepared in Milli-Q water and dilute sulfuric acid to prevent oxidation (pH = 2.08). The ABTS solution was subsequently oxidized by adding a 1 mM hypochlorous acid (HOCl) solution in a 0.35:1 HOCl to ABTS ratio. Measurement of absorbance of oxidized $ABTS^{\bullet+}$ indicated that > 65% of the ABTS was oxidized as expected.[4] Fresh $ABTS^{\bullet+}$ and HOCl solutions were prepared each day of analysis.

Four dilutions of each DOM solution in Milli-Q water were made such that each sample had 100%, 75%, 50%, and 25% of its original [DOC]. At least one replicate was measured for each concentration (i.e., 5 data points per sample). For each measurement, 125 μM $ABTS^{\bullet+}$, 25 mM of phosphate buffer (pH = 7), and 78% v/v of DOM solution were pipetted rapidly into a cuvette. Milli-Q water was added instead of a DOM solution every 30 samples as a control. The solutions were allowed to react for exactly 15 minutes and then their absorbance was measured at 728 nm. For each data point collected, the difference in $ABTS^{\bullet+}$ absorbance at 728 nm was calculated and plotted versus [DOC]. The slope of the linear regression is the EDC in units of mmol e^- mg-C^{-1}. Further details and verification of this method are described in Walpen *et al*.[4] Measured EDC values are listed in **Table D.5**.

D.6 Photochemistry

The degradation of furfuryl alcohol (FFA) and *p*-nitroanisole (PNA) and formation of hydroxy-terephthalic acid (hTPA) were quantified using high performance liquid chromatography (HPLC; Agilent 1260 instrument with a 1260 diode array detector and a 1260 fluorescence detector). For FFA, an Agilent Poroshell 120 EC-C18 (3.0 x 50 mm) with a guard column (3.0 mm) was used with a mobile phase of 90% 0.1% v/v/ formic acid and 10% acetonitrile and flow rate of 0.6 mL min^{-1}. The method was isocratic and FFA eluted at approximately 1.7 minutes. It was detected via absorption at 217 nm. The degradation PNA was accomplished with the same column. 50:50 0.1% v/v formic acid and acetonitrile was used for the mobile phase at a flow rate of 0.6 mL min^{-1}. PNA eluted at approximately 1.5 minutes and was detected via absorption at 314 nm. To detect hTPA, an Agilent Poroshell 120 Bonus RP (3.0 x 100 nm) column with a 3.0 mm guard column was used. Mobile phase was 60:40 of 0.1% phosphoric acid to acetonitrile. Phosphoric acid was required to keep hTPA in its protonated form.[5] The flow rate was 1.5 mL min^{-1} and hTPA was detected via fluorescence measurements with excitation at 250 nm and emission at 410 nm. Steady-state concentrations and quantum yields are listed in **Table D.9** and calculations are detailed previously.[6] Triplicate measurements were made for all samples.

Table D.9. Steady-state concentrations and quantum yields of $^1O_2$ and $^{\bullet}OH$ in all samples. NA values indicate measurement not made for the sample due to insufficient sample volume.

Sample	$[^1O_2]_{ss}$ (M)	$[^{\bullet}OH]_{ss}$ (M)	Φ_{1O2}	$\Phi_{\bullet OH}$
Crystal Bog	$(4.1 \pm 0.5) \times 10^{-13}$	$(3.8 \pm 0.5) \times 10^{-16}$	$(1.4 \pm 0.2) \times 10^{-2}$	$(8 \pm 1) \times 10^{-5}$
Trout Bog	$(8.4 \pm 0.9) \times 10^{-13}$	$(6.3 \pm 0.6) \times 10^{-16}$	$(1.1 \pm 0.1) \times 10^{-2}$	$(1.2 \pm 0.1) \times 10^{-4}$
Allequash Lake	$(2.00 \pm 0.04) \times 10^{-13}$	$(1.9 \pm 0.4) \times 10^{-16}$	$(2.1 \pm 0.1) \times 10^{-2}$	$(4.6 \pm 0.8) \times 10^{-5}$

Big Muskellunge Lake	$(9 \pm 2) \times 10^{-14}$	$(8 \pm 1) \times 10^{-17}$	$(3.3 \pm 0.6) \times 10^{-2}$	$(5.0 \pm 0.8) \times 10^{-5}$
Crystal Lake	$(4.3 \pm 0.7) \times 10^{-14}$	$(7 \pm 2) \times 10^{-17}$	$(2.5 \pm 0.3) \times 10^{-2}$	$(4 \pm 1) \times 10^{-5}$
Sparkling Lake	$(7.8 \pm 0.9) \times 10^{-14}$	$(8.8 \pm 0.5) \times 10^{-17}$	$(2.5 \pm 0.6) \times 10^{-2}$	$(3.4 \pm 0.2) \times 10^{-5}$
Trout Lake	$(7.4 \pm 0.6) \times 10^{-14}$	$(7 \pm 2) \times 10^{-17}$	$(2.8 \pm 0.2) \times 10^{-2}$	$(3.2 \pm 0.96) \times 10^{-5}$
Memories	$(4.22 \pm 0.05) \times 10^{-13}$	$(1.9 \pm 0.2) \times 10^{-16}$	$(7.3 \pm 0.3) \times 10^{-2}$	$(4.5 \pm 0.3) \times 10^{-5}$
Olsen Ditch	$(4.7 \pm 0.6) \times 10^{-13}$	$(6.1 \pm 0.1) \times 10^{-16}$	$(4.57 \pm 0.04) \times 10^{-2}$	$(9.9 \pm 0.2) \times 10^{-5}$
Wammer Ditch	$(3.13 \pm 0.03) \times 10^{-13}$	$(2.4 \pm 0.2) \times 10^{-16}$	$(4.04 \pm 0.07) \times 10^{-2}$	$(5.7 \pm 0.4) \times 10^{-5}$
Seven-mile Creek	$(4.65 \pm 0.09) \times 10^{-13}$	$(1.9 \pm 0.2) \times 10^{-16}$	$(4.32 \pm 0.05) \times 10^{-2}$	$(3.4 \pm 0.3) \times 10^{-5}$
WRRF Pre-Cl	$(2.1 \pm 0.3) \times 10^{-13}$	$(1.7 \pm 0.1) \times 10^{-16}$	$(3.0 \pm 0.5) \times 10^{-2}$	$(4.8 \pm 0.4) \times 10^{-5}$
WRRF Reuse	$(2.6 \pm 0.2) \times 10^{-13}$	$(1.6 \pm 0.2) \times 10^{-16}$	$(7.7 \pm 0.3) \times 10^{-2}$	$(1.0 \pm 0.1) \times 10^{-4}$
WRRF Post-Cl	$(3.0 \pm 0.4) \times 10^{-13}$	$(2.0 \pm 0.2) \times 10^{-16}$	$(5.8 \pm 0.8) \times 10^{-2}$	$(4.2 \pm 0.3) \times 10^{-5}$
Kiwannis	$(4.06 \pm 0.097) \times 10^{-13}$	$(1.53 \pm 0.07) \times 10^{-16}$	$(4.4 \pm 0.1) \times 10^{-2}$	$(3.5 \pm 0.2) \times 10^{-5}$
North Yahara	$(4.32 \pm 0.097) \times 10^{-13}$	$(1.39 \pm 0.03) \times 10^{-15}$	$(3.08 \pm 0.07) \times 10^{-2}$	$(2.66 \pm 0.07) \times 10^{-4}$
Lake Mendota	$(1.9 \pm 0.2) \times 10^{-13}$	$(3.19 \pm 0.06) \times 10^{-16}$	$(2.8 \pm 0.3) \times 10^{-2}$	$(9.7 \pm 0.2) \times 10^{-6}$
Lake Wingra	$(3.2 \pm 0.1) \times 10^{-13}$	$(2.5 \pm 0.2) \times 10^{-16}$	$(3.2 \pm 0.1) \times 10^{-2}$	$(5.6 \pm 0.6) \times 10^{-5}$
Lake Kegonsa	$(5.32 \pm 0.06) \times 10^{-13}$	$(2.6 \pm 0.2) \times 10^{-16}$	$(5.25 \pm 0.06) \times 10^{-2}$	$(1.4 \pm 0.1) \times 10^{-4}$
South Yahara	$(2.7 \pm 0.2) \times 10^{-13}$	$(7 \pm 1) \times 10^{-17}$	$(2.8 \pm 0.2) \times 10^{-2}$	$(2.7 \pm 0.5) \times 10^{-5}$
Badfish Upstream	$(2.86 \pm 0.04) \times 10^{-13}$	$(2.42 \pm 0.08) \times 10^{-16}$	$(3.80 \pm 0.05) \times 10^{-2}$	$(4.3 \pm 0.1) \times 10^{-5}$
Ninesprings Pre-UV	$(3.80 \pm 0.06) \times 10^{-13}$	$(2.3 \pm 0.2) \times 10^{-16}$	$(3.42 \pm 0.06) \times 10^{-2}$	$(5.3 \pm 0.4) \times 10^{-5}$
Ninesprings Post-UV	$(4.3 \pm 0.1) \times 10^{-13}$	$(1.16 \pm 0.01) \times 10^{-16}$	$(3.9 \pm 0.1) \times 10^{-2}$	$(3.08 \pm 0.09) \times 10^{-5}$
Badfish Downstream	$(2.98 \pm 0.08) \times 10^{-13}$	$(5 \pm 1) \times 10^{-16}$	$(2.76 \pm 0.08) \times 10^{-2}$	$(1.1 \pm 0.2) \times 10^{-4}$
Confluence	$(1.8 \pm 0.4) \times 10^{-13}$	$(1.0 \pm 0.3) \times 10^{-16}$	$(2.4 \pm 0.9) \times 10^{-2}$	$(3.0 \pm 0.8) \times 10^{-5}$

Sand Creek	$(8 \pm 1) \times 10^{-13}$	$(2.02 \pm 0.02) \times 10^{-15}$	$(6 \pm 1) \times 10^{-3}$	$(5.83 \pm 0.06) \times 10^{-4}$
Meadowlands	$(6.00 \pm 0.07) \times 10^{-13}$	$(7.22 \pm 0.08) \times 10^{-16}$	$(1.10 \pm 0.01) \times 10^{-2}$	$(1.39 \pm 0.02) \times 10^{-4}$
River Inn	$(6.08 \pm 0.02) \times 10^{-13}$	$(6.45 \pm 0.02) \times 10^{-16}$	$(1.369 \pm 0.004) \times 10^{-2}$	$(1.251 \pm 0.004) \times 10^{-4}$
Munger Landing	$(6.4 \pm 0.4) \times 10^{-13}$	$(3.5 \pm 0.1) \times 10^{-16}$	$(1.7 \pm 0.1) \times 10^{-2}$	$(7.1 \pm 0.2) \times 10^{-5}$
East Detroit	$(6.3 \pm 0.1) \times 10^{-13}$	$(4.19 \pm 0.06) \times 10^{-16}$	$(1.55 \pm 0.04) \times 10^{-2}$	$(8.4 \pm 0.1) \times 10^{-5}$
WLSSD Pre-Cl; Mill Shutdown	$(3.97 \pm 0.09) \times 10^{-13}$	NA	$(1.07 \pm 0.02) \times 10^{-2}$	NA
WLSSD Post-Cl; Mill Shutdown	$(4.71 \pm 0.06) \times 10^{-13}$	NA	$(1.56 \pm 0.02) \times 10^{-2}$	NA
WLSSD Pre-Cl	$(1.26 \pm 0.05) \times 10^{-12}$	$(3.69 \pm 0.097) \times 10^{-16}$	$(2.04 \pm 0.08) \times 10^{-2}$	$(1.49 \pm 0.04) \times 10^{-4}$
WLSSD Post-Cl	$(1.22 \pm 0.01) \times 10^{-12}$	$(1.87 \pm 0.04) \times 10^{-16}$	$(1.96 \pm 0.02) \times 10^{-2}$	$(6.1 \pm 0.1) \times 10^{-4}$
Blatnik Bridge	$(5.2 \pm 0.3) \times 10^{-13}$	$(2.72 \pm 0.08) \times 10^{-16}$	$(1.8 \pm 0.1) \times 10^{-2}$	$(6.8 \pm 0.2) \times 10^{-5}$
Wisconsin Point	$(4.9 \pm 0.99) \times 10^{-14}$	$(1.08 \pm 0.02) \times 10^{-16}$	$(2.25 \pm 0.03) \times 10^{-2}$	$(1.437 \pm 0.009) \times 10^{-4}$
River Front Park	$(6.74 \pm 0.03) \times 10^{-13}$	$(2.58 \pm 0.03) \times 10^{-16}$	$(4.70 \pm 0.02) \times 10^{-2}$	$(1.89 \pm 0.02) \times 10^{-4}$
East River Parkway	$(4.67 \pm 0.03) \times 10^{-13}$	$(2.65 \pm 0.03) \times 10^{-16}$	$(3.20 \pm 0.02) \times 10^{-2}$	$(1.1 \pm 0.1) \times 10^{-5}$
Minnesota River	$(4.07 \pm 0.08) \times 10^{-13}$	$(8.7 \pm 0.4) \times 10^{-16}$	$(5.9 \pm 0.1) \times 10^{-2}$	$(2.4 \pm 0.1) \times 10^{-4}$
Metro WWTP Pre-Cl	$(6.91 \pm 0.03) \times 10^{-13}$	$(3.25 \pm 0.05) \times 10^{-15}$	$(8.27 \pm 0.04) \times 10^{-2}$	$(1.05 \pm 0.02) \times 10^{-3}$
Metro WWTP Post-Cl	$(5.2 \pm 0.1) \times 10^{-13}$	$(2.4 \pm 0.1) \times 10^{-15}$	$(7.0 \pm 0.2) \times 10^{-2}$	$(1.03 \pm 0.04) \times 10^{-3}$
Metro Downstream	$(5 \pm 1) \times 10^{-13}$	$(4.2 \pm 0.3) \times 10^{-16}$	$(3.7 \pm 0.6) \times 10^{-2}$	$(1.07 \pm 0.08) \times 10^{-4}$
Eagles Point Pre-UV	$(2.2 \pm 0.2) \times 10^{-13}$	$(7.6 \pm 0.1) \times 10^{-16}$	$(2.6 \pm 0.2) \times 10^{-2}$	$(2.49 \pm 0.05) \times 10^{-4}$
Eagles Point Post-UV	$(2.41 \pm 0.08) \times 10^{-13}$	$(1.01 \pm 0.05) \times 10^{-15}$	$(2.79 \pm 0.096) \times 10^{-2}$	$(4.0 \pm 0.2) \times 10^{-4}$
Eagles Point Downstream	$(4.81 \pm 0.06) \times 10^{-13}$	$(4.7 \pm 0.2) \times 10^{-16}$	$(3.74 \pm 0.05) \times 10^{-2}$	$(1.26 \pm 0.04) \times 10^{-4}$
Lake of the Isles	$(2.4 \pm 0.1) \times 10^{-13}$	$(7 \pm 1) \times 10^{-17}$	$(5.8 \pm 0.3) \times 10^{-2}$	$(5.3 \pm 0.9) \times 10^{-5}$
Vadnais Lake	$(2.88 \pm 0.03) \times 10^{-13}$	$(7.5 \pm 0.5) \times 10^{-17}$	$(4.65 \pm 0.05) \times 10^{-2}$	$(3.4 \pm 0.3) \times 10^{-5}$

Lake Phalen	$(2.4 \pm 0.3) \times 10^{-13}$	$(5.7 \pm 0.6) \times 10^{-17}$	$(7 \pm 1) \times 10^{-2}$	$(3.4 \pm 0.4) \times 10^{-6}$

Table D.10. Simple linear regressions between bulk DOM composition parameters and Φ_{1O2} and $\Phi_{\bullet OH}$ in the complete data set.

		$\Phi_{1O2} \times 10^2$	$\Phi_{\bullet OH} \times 10^5$
$SUVA_{254}$ (L mg-C^{-1} m^{-1})	equation	y = -0.59x + 4.7	y = 0.025x + 15
	r^2	7.1×10^{-2}	1.03×10^{-6}
	p	6.9×10^{-2}	0.99
E_2:E_3	equation	y = 0.42x + 0.24	y = -3.7x + 43
	r^2	0.19	0.11
	p	1.9×10^{-3}	2.5×10^{-2}
EDC (mmol e^- mg-C^{-1})	equation	y = -0.54x + 4.38	y = 2.8x + 10
	r^2	0.11	1.3×10^{-2}
	p	2.0×10^{-2}	0.46

Table D.11. Simple linear regressions between bulk DOM composition parameters and Φ_{1O2} and $\Phi_{\bullet OH}$ in the rural samples.

		$\Phi_{1O2} \times 10^2$	$\Phi_{\bullet OH} \times 10^5$
$SUVA_{254}$ (L mg-C^{-1} m^{-1})	equation	y = -0.56x + 3.0	y = 5.2x + 1.3
	r^2	0.78	0.19
	p	3.2×10^{-5}	0.12
E_2:E_3	equation	y = 0.41x - 0.96	y = -4.2x + 41
	r^2	0.77	0.23
	p	3.79×10^{-5}	7.9×10^{-2}
EDC (mmol e^- mg-C^{-1})	equation	y = -0.76x + 2.9	y = 3.09x + 7.34
	r^2	0.59	2.7×10^{-2}
	p	1.2×10^{-3}	0.57

Table D.12. Simple linear regressions between bulk DOM composition parameters and Φ_{1O2} and $\Phi_{\bullet OH}$ in the urban samples.

		$\Phi_{1O2} \times 10^2$	$\Phi_{\bullet OH} \times 10^5$
$SUVA_{254}$ (L mg-C^{-1} m^{-1})	equation	y = -0.79x + 6.4	y = 3.6x + 5.2
	r^2	0.18	8.3×10^{-2}
	p	3.4×10^{-1}	0.5314

E_2:E_3	equation	y = -0.0043 + 4.8	y = 1.9x + 29
	r^2	5.7 x 10^{-5}	0.35
	p	0.96	0.12
EDC (mmol e^- $mg\text{-}C^{-1}$)	equation	y = 1.60x + 6.3	y = 1.6x + 9.6
	r^2	0.13	3.8 x 10^{-2}
	p	0.39	0.88

Table D.13. Simple linear regressions between bulk DOM composition parameters and Φ_{1O2} and $\Phi_{\bullet OH}$ in the agricultural samples.

		Φ_{1O2} x 10^2	**$\Phi_{\bullet OH}$ x 10^5**
$SUVA_{254}$ (L $mg\text{-}C^{-1}$ m^{-1})	equation	y = 0.29x + 3.3	y = 0.41 + 6.7
	r^2	3.1 x 10^{-2}	2.4x 10^{-3}
	p	0.58	0.88
E_2:E_3	equation	y = 0.17x + 2.6	y = -0.21 + 9.4
	r^2	3.7 x 10^{-2}	2.2 x 10^{-3}
	p	0.54	0.89
EDC (mmol e^- $mg\text{-}C^{-1}$)	equation	y = -0.21x + 4.3	y = 1.8x + 5.3
	r^2	7.6 x 10^{-3}	2.1 x 10^{-2}
	p	0.78	0.65

Table D.14. Simple linear regressions between bulk DOM composition parameters and Φ_{1O2} and $\Phi_{\bullet OH}$ in the wastewater samples.

		Φ_{1O2} x 10^2	**$\Phi_{\bullet OH}$ x 10^5**
$SUVA_{254}$ (L $mg\text{-}C^{-1}$ m^{-1})	equation	y = -4.4x + 12	y = -19 + 61
	r^2	0.57	4.73 x 10^{-2}
	p	1.8 x 10^{-3}	0.50
E_2:E_3	equation	y = 0.46x + 0.57	y = -6.0x + 71
	r^2	0.16	0.13
	p	0.16	0.26
EDC (mmol e^- $mg\text{-}C^{-1}$)	equation	y = -1.0x + 6.6	y = -6.8x + 43
	r^2	0.41	4.2 x 10^{-2}
	p	1.29 x 10^{-2}	0.52

Table D.15. Multiple linear regressions for $\Phi_{^1O_2}$. $R^2 = 0.59$ and $p = 5.5 \times 10^{-8}$.

Coefficient	Estimate	p-value
Intercept	0.239	8.79×10^{-13}
[DOC] (mg-C L^{-1})	-1.69×10^{-3}	3.36×10^{-5}
[DIC] (mg-C L^{-1})	1.01×10^{-3}	2.66×10^{-5}
EDC (mmol e^- mg-C^{-1})	-1.90×10^{-2}	2.41×10^{-4}
$O:C_w$	0.117	2.94×10^{-2}

Table D.16. Multiple linear regressions for $\Phi_{^\bullet OH}$. $R^2 = 0.31$ and $p = 3.4 \times 10^{-4}$.

Coefficient	Estimate	p-value
Intercept	3.03×10^{-2}	4.53×10^{-8}
$E_2:E_3$	-1.11×10^{-3}	6.95×10^{-3}
O:Cw	-2.61×10^{-2}	2.09×10^{-3}

D.7 References

(1) Dittmar, T.; Koch, B.; Hertkorn, N.; Kattner. A. B. Simple and efficient method for the solid-phase extraction of dissolved organic matter (SPE-DOM) from seawater. *Limnol. Oceanogr.: Methods*, **2008**, *6*, 230–235.

(2) Raeke, J.; Lechtenfeld, O. J.; Wagner, M.; Herzsprung, P.; Reemtsma, T. Selectivity of solid phase extraction of freshwater dissolved organic matter and its effect on ultrahigh resolution mass spectra. *Environ. Sci. Process. Impacts* **2016**, *18* (7), 918–927.

(3) Maizel, A. C.; Li, J.; Remucal, C. K. Relationships between dissolved organic matter composition and photochemistry in lakes of diverse trophic status. *Environ. Sci. Technol.* **2017**, *51* (17), 9624–9632.

(4) Walpen, N.; Houska, J.; Salhi, E.; Sander, M.; von Gunten, U. Quantification of the electron donating capacity and UV absorbance of dissolved organic matter during ozonation of secondary wastewater effluent by an assay and an automated analyzer. *Water Res.* **2020**, *185*, 116235.

(5) Page, S. E.; Arnold, W. A.; McNeill, K. Terephthalate as a probe for photochemically generated hydroxyl radical. *J. Environ. Monit.* **2010**, *12* (9), 1658–1665.

(6) Berg, S. M.; Whiting, Q. T.; Herrli, J. A.; Winkels, R.; Wammer, K. H.; Remucal, C. K. The role of dissolved organic matter composition in determining photochemical reactivity at the molecular level. *Environ. Sci. Technol.* **2019**.